Analysis of multiprotein-complex components pulled-down with STRIPAK in *Sordaria macrospora*

Dissertation

for the award of the degree

„Doctor rerum naturalium“

of the Georg-August-Universität Göttingen

within the doctoral program *Microbiology and Biochemistry*

of the Göttingen Graduate Center for Neurosciences, Biophysics

and Molecular Biosciences (GGNB)

submitted by

Anika Groth, geb. Gibron

from Hannover

Göttingen, 2022

Thesis Advisory Committee

Prof. Dr. Stefanie Pöggeler, Department of Genetics of Eukaryotic Microorganisms, Institute of Microbiology and Genetics, Georg-August-Universität Göttingen

Prof. Dr. Heike Krebber, Department of Molecular Genetics, Institute of Microbiology and Genetics, Georg-August-Universität Göttingen

Prof. Dr. Kai Heimel, Department of Microbial Cell Biology, Institute of Microbiology and Genetics, Georg-August-Universität Göttingen

Dr. Oliver Valerius, Department of Molecular Microbiology and Genetics, Institute of Microbiology and Genetics, Georg-August-Universität Göttingen

Members of the Examination Board

1st Referee: Prof. Dr. Stefanie Pöggeler, Department of Genetics of Eukaryotic Microorganisms, Institute of Microbiology and Genetics, Georg-August-Universität Göttingen

2nd Referee: Prof. Dr. Heike Krebber, Department of Molecular Genetics, Institute of Microbiology and Genetics, Georg-August-Universität Göttingen

Further members of the Examination Board

Prof. Dr. Kai Heimel, Department of Microbial Cell Biology, Institute of Microbiology and Genetics, Georg-August-Universität Göttingen

Dr. Oliver Valerius, Department of Molecular Microbiology and Genetics, Institute of Microbiology and Genetics, Georg-August-Universität Göttingen

PD Dr. Michael Hoppert, Department of General Microbiology, Institute of Microbiology and Genetics, Georg-August-Universität Göttingen

Prof. Dr. Rolf Daniel, Department of Genomic and Applied Microbiology & Göttingen Genomics Laboratory, Institute of Microbiology and Genetics, Georg-August-Universität Göttingen

Date of oral examination: 29.03.2022

"The important thing is to never stop questioning."

Albert Einstein (1879 – 1955)

Publications based on this thesis

In this thesis, performed in the group of Prof. Dr. Stefanie Pöggeler in the Department of Genetics of Eukaryotic Microorganisms at the Institute of Microbiology and Genetics, Georg-August-Universität Göttingen, three different multiprotein-complex components pulled-down with STRIPAK in *Sordaria macrospora* were analyzed. Therefore, this thesis is composed of the elaboration of three subtopics. The results of two of them have been already published and the third project is prepared for submission.

Groth, A.; Schunke, C.; Reschka, E.J.; Pöggeler, S.; Nordzieke, D.E. (2021) Tracking Fungal Growth: Establishment of Arp1 as a Marker for Polarity Establishment and Active Hyphal Growth in Filamentous Ascomycetes. *J. Fungi*, **7**, 580. https://doi.org/10.3390/jof7070580

Groth, A.; Schmitt, K.; Valerius, O.; Herzog, B.; Pöggeler, S. (2021) Analysis of the Putative Nucleoporin POM33 in the Filamentous Fungus *Sordaria macrospora*. *J. Fungi*, **7**, 682. https://doi.org/10.3390/jof7090682

Table of contents

I. List of Figures and Tables

Figures

Tables

II. List of important abbreviations

ARF	ADP ribosylation factors
ARL	ARF-like
ARM	Armadillo
ARP1	actin-related protein 1
ArPIKfyve	associated regulator of PIKfyve
Arps	actin-related proteins
Atg	autophagy-related protein
BioID	proximity-dependent biotin identification
CaM	calmodulin-binding domain
CC	coiled-coil
CCM3	cerebral cavernous malformation 3
cDNA	complementary DNA
cER	cortical ER
CMT4J	Charcot-Marie-Tooth syndrome 4J
cryo-EM	cryogenic electron microscopy
CTTNBP2	cortactin-binding protein 2
CTTNBP2NL	CTTNBP2 N-terminal-like protein
CV	caveolin-binding domain
CWI	cell-wall integrity
DHC	dynein-heavy chain
DNA	desoxyribonucleic acid
EE	early endosomes
ER	endoplasmic reticulum
ERES	ER-exit sites
Fab1	fatty-acid biosynthesis protein 1
FAR	factor arrest
FGFR1OP2	fibroblast growth factor receptor 1 oncogene partner 2
FG-Nups	Nups harboring phenylalanine (F) and glycine (G)-rich repeats
FHA	forkhead-associated domain
Fig4	factor-induced gene 4
FYVE	Fab1-YOTB-Vac1p-EEA1
GCKIII	germinal center kinase III
GP210	glycoprotein 210
HEAT	huntingtin-elongation-A subunit-TOR
HOOK1/3	Hook-homolog proteins 1 and 3
ingls	infantile gliosis
INM	inner nuclear membrane
JIP	c-Jun N-terminal kinase-interacting protein

JNK	c-Jun N-terminal kinase
kDa	kilodalton
LC-MS	liquid chromatography-mass spectrometry
LE	late endosomes
MAPK	mitogen-activated protein kinase
MAPK4K	MAPK kinase kinase kinase 4
Mb	mega base
MDa	megadalton
MINK1	misshapen-like kinase 1
miRNA	micro RNA
MOB3	monopolar spindle one binder 3
mRNA	messenger RNA
MSTs	mammalian STE20-like protein kinases
MTOC	microtubule-organizing center
MTs	microtubules
MVBs	multivesicular bodies
Ndc1	nuclear division cycle 1
NE	nuclear envelope
NPC	nuclear-pore complex
NTRs	nuclear transport receptors
Nups	Nucleoporins
ONM	outer nuclear membrane
PAS	PIKfyve-ArPIKfyve-Sac3
Per33	pore and ER protein of 33 kDa
PIKfyve	FYVE finger-containing phosphoinositide kinase
PIPs	phosphoinositides
PM	plasma membrane
Poms	pore-membrane proteins
POM33	pore-membrane protein of 33 kDa
PP2A	protein phosphatase 2 A
PP2AA	structural alpha isoform of PP2A
PP2Ac	catalytic subunit of PP2A
PRO11	protoperithecium mutant 11
PRO22	protoperithecium mutant 22
PRO45	protoperithecium mutant 45
PtdIns	phosphatidylinositol
PtdIns(3)P	Phosphatidylinositol 3-phosphate
PtdIns(3,5)P_2	Phosphatidylinositol 3,5-bisphosphate
RER	rough ER
RNA	ribonucleic acid

rRNA	ribosomal RNA
RTN	reticulon
Sac3	Sac domain-containing protein 3
SCI1	STRIPAK-complex interactor 1
SER	smooth ER
SG2NA	S/G_2 nuclear autoantigen
SIKE	suppressor of IκB kinase-e (IKKε)
SIN	septation initiation network
SIP	SIN-inhibitory PP2A
SLMAP	sarcolemmal membrane-associated protein
Sm	*Sordaria macrospora*
SmGPI1	*S. macrospora* glycosyl-phosphatidylinositol-anchored protein 1
SmKINs	*S. macrospora* GCKIII kinases
SmPP2Ac1	*S. macrospora* catalytic subunit 1 of PP2A
SPB	spindle-pole bodies
SPK	Spitzenkörper
SRP	signal-recognition particle
STE20	sterile 20
STKs	serine/threonine protein kinases
STRIP1/2	striatin-interacting proteins 1 and 2
STRIPAK	striatin-interacting phosphatase and kinase
TGN	*trans*-Golgi network
TL	toll-like
TM-Nups	transmembrane Nups
TMD	transmembrane domain
TMEM	transmembrane protein
TNIK	TRAF2 and NCK-interacting protein kinase
TOR	target of rapamycin
TRAF3IP3	tumor necrosis factor receptor-associated factor 3-interacting protein 3
TRPML	transient receptor potential of Ca^{2+}-channels of the mucolipin subfamily
tRNA	transfer RNA
Tts1	tetra-spanning protein 1
VAC14	vacuolar-morphology protein 14
Vac7	vacuolar-segregation protein 7
Vps	vacuolar-protein sorting
VSC	vesicle-supply center
Y2H	yeast-two-hybrid

Summary

The striatin-interacting phosphatase and kinase (STRIPAK)-complex is highly conserved and can be found in fungi and animals. In the filamentous ascomycete *Sordaria macrospora* (Sm), the SmSTRIPAK plays an important role in hyphal fusion, sexual development, septation and growth. In previous studies, pulldown experiments of SmSTRIPAK-components as baits coupled to liquid chromatography-mass spectrometry (LC-MS) provided a variety of possible interaction partners. This work gives insights into three of these pulled-down proteins, namely: the actin-related protein 1 (ARP1), the pore-membrane protein of 33 kDa (POM33) and the vacuolar-morphology protein 14 (VAC14), which are all part of large and conserved individual multiprotein complexes themselves. ARP1 is the most abundant protein in dynactin and is involved in mediating retrograde transport of various cargos on microtubules via the dynein-dynactin complex. In this study, SmARP1 was shown to be important for proper hyphal growth and fungal development. Fluorescence microscopy revealed that its localization is a dynamic process and that SmARP1 localizes subapical to the Spitzenkörper (SPK) as well as in close association with nuclei. Due to these characteristics, SmARP1 was established as a marker protein for actively growing hyphae and cell polarity.

In the second project, the transmembrane protein POM33 as putative part of the nuclear-pore complex (NPC) was analyzed. Thereby it was shown that deletion of *Smpom33* has no impact on sexual development even under stress conditions. Additionally, fluorescence microscopic investigations showed that SmPOM33 localizes at the nuclear envelope (NE) and the endoplasmic reticulum (ER). After LC-MS analysis, proteins of the ER were identified as potential interactors. This led to the conclusion that SmPOM33 is rather an ER protein than a component of the NPC.

In the third project, VAC14 as scaffolding subunit of the Fab1p/PIKfyve-complex was investigated. Vac14p/ArPIKfyve localizes to the vacuolar membrane in yeast and to membranes of endolysosomes in mammals, respectively. There, it facilitates the turnover and synthesis of PtdIns(3,5)P_2 that functions in multiple processes including organelle morphology, acidification of endolysosomes and autophagy. The data presented here investigated VAC14 for the first time in a filamentous fungus. In *S. macrospora*, SmVAC14

co-localizes with the ER, Golgi, vacuolar membranes, early and late endosomes and the SmSTRIPAK-component SCI1. Moreover, the Δvac14 mutant showed deformed perithecia, impairment of ascospore formation, and altered vacuolar morphology. Furthermore, the Δvac14 mutant displayed an increased sensitivity to diverse types of stresses; however, autophagy was not affected.

This work revealed that the three proteins presumably interacting with components of the STRIPAK-complex analyzed here, likewise are part of separate multiprotein complexes, and ARP1 and VAC14 are also required for accurate sexual development in *S. macrospora*.

Zusammenfassung

Der STRIPAK (striatin-interacting phosphatase and kinase)-Komplex ist in Pilzen und Tieren hoch konserviert. In dem filamentösen Ascomyceten *Sordaria macrospora* (Sm) kommt dem SmSTRIPAK eine wichtige Rolle bei der Hyphenfusion, sexuellen Entwicklung, Septierung und dem Wachstum zu. Durch Pulldown-Experimente mit SmSTRIPAK-Komponenten als Köder, konnten massenspektrometrisch eine Vielzahl möglicher Interaktionspartner identifiziert werden. Diese Arbeit gibt Einblicke in drei mögliche Interaktionspartner des SmSTRIPAK-Komplexes: ARP1 (actin-related protein 1), POM33 (pore-membrane protein of 33 kDa) und VAC14 (vacuolar-morphology protein 14). Sie alle sind selbst Komponenten großer und konservierter individueller Multiproteinkomplexe. ARP1 ist das am häufigsten vorkommende Protein in Dynactin und ist an dem retrograden Transport verschiedener Frachten auf Mikrotubuli durch den Dynein-Dynactin-Komplex beteiligt. In dieser Studie konnte gezeigt werden, dass SmARP1 für das Hyphenwachstum und die Pilzentwicklung wichtig ist. Mittels Fluoreszenzmikroskopie konnte gezeigt werden, dass die zelluläre Lokalisierung dieses Proteins dynamisch ist und es teilweise mit Zellkernen assoziiert ist, sowie subapikal in der Nähe des Spitzenkörpers (SPK) lokalisiert. Aufgrund dieser Charakteristika wurde SmARP1 als Markerprotein für aktiv wachsende Hyphen und Zellpolarität etabliert.

Im zweiten Projekt wurde das Transmembranprotein POM33, welches in anderen Organismen mit dem Kernporenkomplex (NPC) assoziiert ist, analysiert. Dabei wurde gezeigt, dass die Eliminierung des *Smpom33* Gens selbst unter Stressbedingungen keine Auswirkungen auf die sexuelle Entwicklung von *S. macrospora* hat. Darüber hinaus zeigten fluoreszenzmikroskopische Untersuchungen, dass SmPOM33 an der Kernhülle sowie am endoplasmatischen Retikulum (ER) lokalisiert. Nach einer massenspektrometrischen Analyse wurden Proteine des ERs als potenzielle Interaktionspartner identifiziert. Demnach ist SmPOM33 eher ein ER-Protein als ein Bestandteil des NPCs.

Im dritten Projekt dieser Arbeit wurde das Protein VAC14 untersucht. Es ist die gerüstbildende Untereinheit des Fab1p/PIKfyve-Komplexes, der in Hefe an der Vakuolenmembran und in Säugetieren an den Membranen von Endolysosomen

lokalisiert ist. Er regelt den Umsatz und die Synthese von PtdIns(3,5)P_2, welches bei zahlreichen zellulären Prozessen wie Organellenmorphologie, Ansäuerung von Endolysosomen und Autophagie beteiligt ist. In dieser Studie wurde VAC14 zum ersten Mal in filamentösen Pilzen untersucht. Demnach kolokalisiert SmVAC14 mit dem ER, Golgi, vesikulären Membranen, frühen und späten Endosomen und der SmSTRIPAK-Komponente SCI1. Darüber hinaus zeigte die Δvac14 Mutante deformierte Perithezien, eine Beeinträchtigung der Ascosporenbildung sowie eine veränderte Vakuolenmorphologie. Des Weiteren ist eine Δvac14 Mutante sensitiver gegenüber verschiedenen Arten von Stress, ist jedoch nicht in dem Prozess der Autophagie beeinträchtigt.

Diese Arbeit zeigt, dass die drei hier analysierten Proteine selbst Teil separater Multiproteinkomplexe sind und dass sowohl ARP1 als auch VAC14 für die korrekte sexuelle Entwicklung in *S. macrospora* erforderlich sind.

1. Introduction

Basic research is an elementary field to collect knowledge for further scientific studies. This research area includes the use of model organisms like bacteria, viruses, fungi, plants or animals for biological and biomedical studies. In the field of genetics, model organisms serve to understand intracellular mechanisms in more detail so that general discoveries can be assigned to higher organisms including humans. With the filamentous fungus *Sordaria macrospora* (Sm), conserved processes like sexual development and meiosis as well as autophagy can be investigated. Moreover, function and involvement of signaling complexes, like the striatin-interacting phosphatase and kinase (STRIPAK)-complex, in cellular processes can be explored. Resulting findings can promote the invention of therapeutics and targeted drug design since dysfunction in homologous multiprotein complexes and signaling pathways can lead to developmental disorders and neurodegenerative diseases in humans.

1.1 *Sordaria macrospora* as fungal model organism

In addition to the kingdom of animalia and plantae, fungi constitute a separate large kingdom among eukaryotic organisms (Engh *et al.*, 2010). It is estimated that about 1.5 million fungal species exist in nature (Hawksworth, 2001). Due to their ability of producing secondary metabolites like antibiotics that can be used for pharmaceutical and food industries, fungi play an important role in research and applied science (Engh *et al.*, 2010). Fungi are true eukaryotes that can be either uni- or multicellular. The baker's yeast *Saccharomyces cerevisiae* represents the most prominent unicellular fungal model organism that is used as main model system in eukaryotic cell biology (Botstein and Fink, 1988; Engh *et al.*, 2010; Kück *et al.*, 2009). On the contrary, the use of multicellular model organisms like filamentous fungi is essential in scientific research because complex cellular processes and interactions are different from unicellular model fungi. Moreover, filamentous fungi are more closely related to mammals than to plants making them suitable model organisms to study molecular processes and mechanisms also found in higher eukaryotes (Pace, 2009; Van der Klei and Veenhuis, 2006). The most important characteristics of filamentous fungi is the extreme polarized growth of their hyphae accompanied by vesicle

transport towards the apex as well as their ability to produce multicellular structures to protect and disseminate sexual and asexual spores.

In its natural habitat, the coprophilic filamentous ascomycete *S. macrospora* colonizes the dung of herbivorous, and is closely related to the fungal models *Podospora anserina* and *Neurospora crassa*, all of which belong to the family of Sordariaceae (Kück *et al.*, 2009; Teichert *et al.*, 2014). Other than *P. anserina* and *N. crassa*, *S. macrospora* is a homothallic fungus, which means that it does not need a mating partner for sexual reproduction. The effect of recessive mutations leading to defective fruiting-body formation can be directly observed making *S. macrospora* a suitable model to study sexual development (Kück *et al.*, 2009; Pöggeler *et al.*, 2006; Teichert *et al.*, 2014; Teichert *et al.*, 2020). Another advantage is the lack of vegetative sporulation hence the existence of only one developmental program ensures that no contaminations or unwanted interactions between sexual and asexual development disturb experimental observations (Kück *et al.*, 2009; Teichert *et al.*, 2014; Teichert *et al.*, 2020).

Furthermore, the life cycle of *S. macrospora* is rather short and can be completed within seven days under laboratory conditions (Kück *et al.*, 2009) (Figure 1). It starts with a germinating ascospore generating a vegetative haploid mycelium consisting of interconnected multinucleate hyphae. The mycelium differentiates, after growth for 2-3 days, into ascogonia, the female gametangia. Subsequently, within 4 days ascogenous cells are enveloped by sterile hyphae to produce round protoperithecia, the unpigmented fruiting-body precursors, that vary in size from 30-90 μm in diameter. Inside the protoperithecia self-fertilization and tissue differentiation take place followed by the buildup of an outer melanized peridial layer resulting in the formation of melanin-pigmented large protoperithecia (Engh *et al.*, 2010; Kück *et al.*, 2009). In ascogenous hyphal tips, two nuclei pair up and a hook-like structure called crozier is formed. Subsequently, synchronous mitotic division takes place followed by the formation of two septa. In the resulting apical cell, the two nuclei fuse with each other and after this process of karyogamy, a diploid nucleus develops followed by meiosis and a post-meiotic mitosis. After 6-7 days, the pear-shaped mature fruiting bodies, the perithecia, are formed. These harbor approximately 200 asci, each containing 8 linear-arranged black ascospores which are discharged trough the apical pore (ostiolum) at the tip of the neck of the mature

fruiting body (Kück *et al.*, 2009; Pöggeler *et al.*, 2006). Thereafter, ascospores start to germinate and the life cycle can start again (Engh *et al.*, 2010; Esser, 1982; Kück *et al.*, 2009).

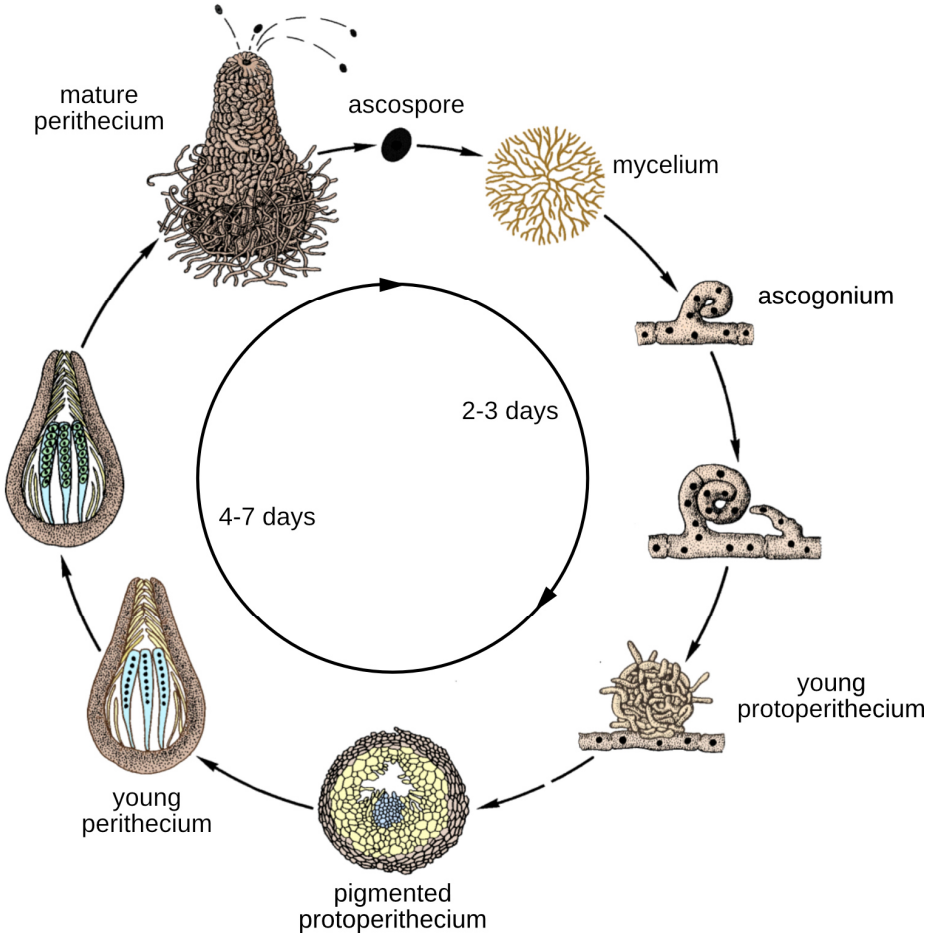

Figure 1: The life cycle of *S. macrospora*.
The life cycle starts with a germinating ascospore forming a vegetative mycelium that differentiates after 3 days into an ascogonium, the female gametangia. Development of protoperithecia, the fruiting-body precursors, into mature perithecia occurs within 4-7 days. Inside the pear-shaped mature fruiting-body, 8 linear-ordered black ascospores are incorporated per ascus. Mature ascospores are discharged through the ostiolum. Modified from Kück *et al.*, 2009.

Besides self-fertilization, consequent mutant testing, and its short life-cycle, there are other advantages to use *S. macrospora* as multicellular model organism. For instance, many molecular tools and genetic methods are available to analyze genes and proteins of this fungus. Additionally, *S. macrospora* is not harmful and can easily be manipulated and cultivated under laboratory conditions (Kück *et al.*, 2009). Moreover, next generation sequencing techniques facilitated whole sequencing of the haploid 39.8 Mb genome with 10.000 predicted genes distributed on seven chromosomes (Nowrousian *et al.*, 2010).

The development of the vegetative mycelium into diverse specialized tissues during sexual reproduction requires exact regulation. This is facilitated by several multiprotein complexes controlling important molecular pathways and mechanisms.

1.2 The STRIPAK-complex

The STRIPAK-complex was initially identified in mammals but its components are conserved among eukaryotes (Goudreault *et al.*, 2009). Name-giving for the striatin-interacting phosphatase and kinase (STRIPAK)-complex is the association of phosphatases and kinases with the scaffold protein striatin. By phosphorylation and dephosphorylation of multiple substrates, diverse signaling pathways influencing cell proliferation are regulated (Farrell and O'Farrell, 2014; Grallert *et al.*, 2015).

The scaffolding subunit of the STRIPAK-complex are striatins, which belong to protein phosphatase PP2A B-type regulatory subunits (Figure 2). More precisely, 4 protein families termed B, B′, B′′ and B′′′ constitute these B-type subunits and striatins represent the B′′′ family (Figure 2) (Sents *et al.*, 2013). Striatins were detected in rat brain, the dorsal part of the striatum as well as in the nervous system at motor neurons with presence in dendritic spines (Castets *et al.*, 1996; Goudreault *et al.*, 2009). In mammals, two paralogs of striatin (STRN1) exist, the S/G_2 nuclear autoantigen SG2NA (STRN3) and zinedin (STRN4) (Castets *et al.*, 1996; Castets *et al.*, 2000; Muro *et al.*, 1995). Interestingly, striatin and its paralogs are found in diverse cellular tissues including liver and cardiac muscle cells (Castets *et al.*, 2000; Moreno *et al.*, 2000).

The mammalian STRIPAK-complex consists of several subunits (Figure 2) including the protein phosphatase 2 A (PP2A), which is formed by each of the structural alpha isoform of PP2A (PP2AA) and the PP2A catalytic subunit (PP2Ac). The scaffolding heterotetramer of striatin, the striatin-interacting proteins 1 and 2 (STRIP1/2) as well as the sarcolemmal membrane-associated protein (SLMAP) and its paralog tumor necrosis factor receptor-associated factor 3-interacting protein 3 (TRAF3IP3). Moreover, the monopolar spindle one binder 3 (MOB3 also named MOB4 or phocein) as well as members of the mammalian sterile 20 (STE20)-like serine/threonine protein kinases germinal center kinase III (GCKIII) subfamily including MST3 (also named STK24), MST4 (also named STK26) and STK25 (also named YSK1 or SOK1) are subunits of the STRIPAK. In addition, cerebral cavernous

malformation 3 (CCM3) as well as the coiled-coil (CC) protein suppressor of IκB kinase-e (IKKε), SIKE, and its paralog fibroblast growth factor receptor 1 oncogene partner 2 (FGFR1OP2), and the cortactin-binding protein 2 (CTTNBP2) as well as its paralog CTTNBP2 N-terminal-like protein (CTTNBP2NL) are part of the mammalian STRIPAK-complex (Glatter *et al.*, 2009; Goudreault *et al.*, 2009; Jeong *et al.*, 2021; Kean *et al.*, 2011). It is suggested that two mutually exclusive STRIPAK-subcomplexes (I and II) are formed in mammals. Subcomplex I contains the striatin-assembly of SLMAP/TRAF3IP3-SIKE/FGFR1OP2. In contrast, subcomplex II lacks this connection and instead contains CTTNBP2/CTTNBP2NL (Goudreault *et al.*, 2009). For simplicity, only the composition of subcomplex I is shown in Figure 2.

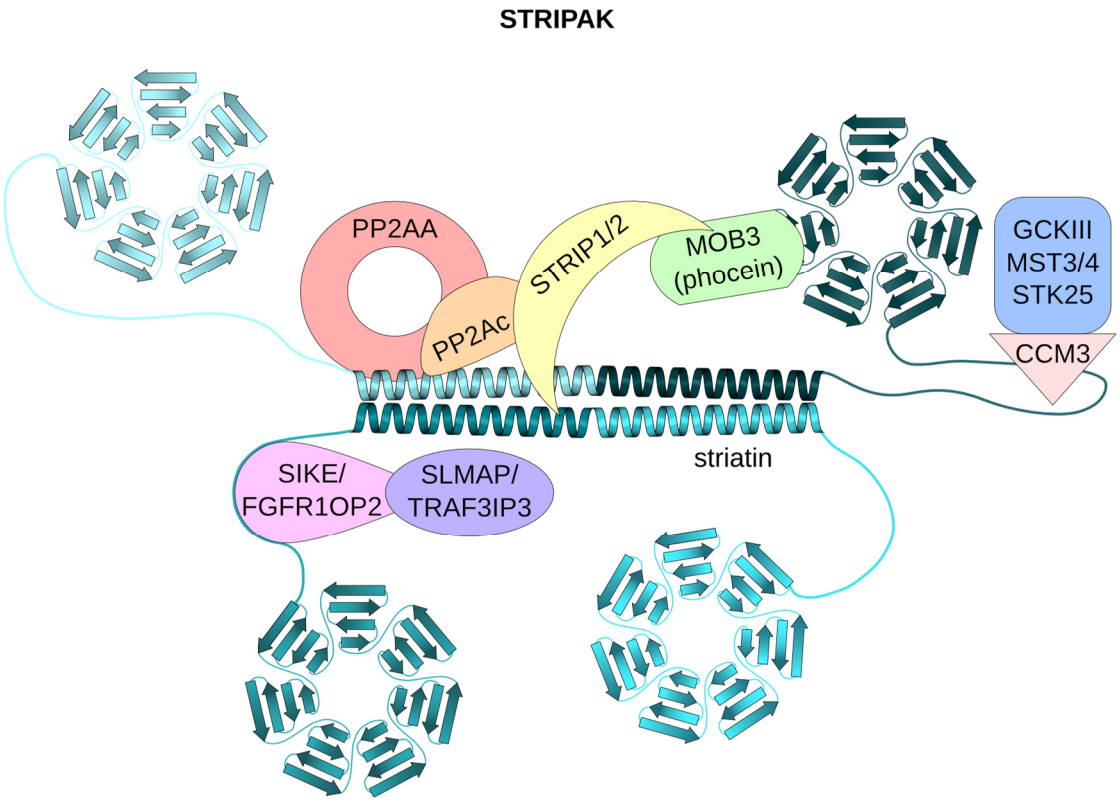

Figure 2: Structure of the mammalian STRIPAK-complex.
Schematic representation of the mammalian STRIPAK-subcomplex I. PP2AA (red): scaffolding subunit of phosphatase 2A (PP2A); PP2Ac (orange): catalytic subunit of PP2A; MOB3 (phocein) (green): monopolar spindle one binder 3; STRIP1/2 (yellow): striatin-interacting proteins 1 and 2; SLMAP/TRAF3IP3 (purple): sarcolemmal membrane-associated protein/tumor necrosis factor receptor-associated factor 3-interacting protein 3; SIKE/FGFR1OP2 (pink): suppressor of IKKε/ fibroblast growth factor receptor 1 oncogene partner 2; CCM3 (pale red): cerebral cavernous malformation 3; GCKIII (blue): germinal center kinases III including serine/threonine kinases MST3/4 and STK25. Interaction platforms of homotetrameric-striatin like N-terminal coiled-coils (cyan-shaded helices) and C-terminal WD40-repeats (cyan-shaded beta-propeller) are shown. Modified according to Jeong *et al.*, 2021 and Goudreault *et al.*, 2009.

In the following, the individual components of the mammalian STRIPAK-complex are presented with respect to their modular structure, function and localization.

As the core scaffolding regulatory subunit of STRIPAK-complexes, striatins consist of several functional domains including a caveolin-binding domain (CV), a CC motif, a Ca^{2+}-calmodulin-binding domain (CaM), and seven WD40-repeats (Benoist *et al.*, 2006; Castets *et al.*, 1996; Castets *et al.*, 2000). The CV domain can bind membranous calveolin, the CC domains function in heterotetramerization building up a platform for STRIPAK assembly. With their CaM domain striatins can interact with calmodulin in a Ca^{2+}-dependent manner, thereby functioning as Ca^{2+}-sensors to regulate their subcellular localization (Bartoli *et al.*, 1998; Benoist *et al.*, 2006; Castets *et al.*, 1996; Castets *et al.*, 2000; Gaillard *et al.*, 2001; Jeong *et al.*, 2021; Moreno *et al.*, 2000). The seven 40 amino-acids long WD-repeats (W: tryptophane, D: aspartic acid) are located at their C-terminus and form a 7-bladed beta-propeller that serve as basis for protein-protein interactions by bringing other substrates closely together in the STRIPAK (Hwang and Pallas, 2014; Neer *et al.*, 1994).

In mammals, the heterotrimeric serine/threonine protein phosphatase PP2A is composed of the scaffolding subunit PP2AA that consists of 15 huntingtin-elongation-A subunit-TOR (HEAT)-repeats providing surface for protein-protein interactions, a catalytic subunit PP2Ac and a regulatory subunit PP2AB (Cho and Xu, 2007). Two isoforms of PP2AA and PP2Ac exist in mammals, PP2AAα and PP2AAβ, and PP2Acα and PP2Acβ, respectively (Janssens *et al.*, 2008; Janssens and Goris, 2001; Sontag, 2001). The scaffolding and catalytic subunits, PP2AA and PP2Ac, form a core complex that associates with B-Type regulatory subunits like B'''-type striatins (Janssens *et al.*, 2008; Janssens and Goris, 2001).

Another core component of the STRIPAK-complex are the STRIP1/2 proteins that are composed of CC motifs and potential C-terminal transmembrane domains (TMDs) (Frost *et al.*, 2012). STRIPs were shown to interact with striatin and SLMAP. They are present in the Golgi and tether centrosomes to it for spindle assembly. Additionally, they are antagonistically involved in actin cytoskeleton organization (Bai *et al.*, 2011; Frost *et al.*, 2012; Goudreault *et al.*, 2009).

SLMAP is a STRIPAK-compound that consists of an N-terminal forkhead-associated domain (FHA), CC motifs and a C-terminal TMD (Frost *et al.*, 2012). The FHA domain

binds phosphopeptides of several regulatory proteins, such as the GCKII family members MST1 and MST2. Thereby, it mediates their recruitment to the STRIPAK-complex. With this interaction, the STRIPAK-complex is associated with Hippo signaling in mammals. The CC motifs of SLMAP are required for heterodimerization with SIKE (Byers *et al.*, 2009; Couzens *et al.*, 2013; Goudreault *et al.*, 2009; Tang *et al.*, 2019).

Diverse studies revealed that SLMAP localizes to centrosomes and that the TMD anchors the STRIPAK to membranes of the endoplasmic reticulum (ER), the nuclear envelope (NE) and mitochondria (Byers *et al.*, 2009; Frost *et al.*, 2012; Goudreault *et al.*, 2009). The SLMAP paralog TRAF3IP3 was shown to interact with striatins, MOB3, STRIP1/2, SLMAP, FGFR1OP2 and SIKE but it lacks the FHA domain and the TMD (Goudreault *et al.*, 2009). The TRAF3IP3 protein was shown to activate the c-Jun N-terminal kinase (JNK) signaling in mammals (Dadgostar *et al.*, 2003).

Additionally, MOB3 is a component of the STRIPAK containing a conserved MOB-Phocein domain, was shown to localize to the cytosol, membranes and the Golgi, interacts with striatins and is presumably involved in vesicular transport (Baillat *et al.*, 2001; Baillat *et al.*, 2002; Kück *et al.*, 2019).

Key developmental processes like cell-cycle control, organization of the cytoskeleton, cell growth and apoptosis are regulated by GCKs inducing specific signaling pathways (Sugden *et al.*, 2013).

In addition to the GCKIII-family members MST3/4 and STK25, members of other GCK subfamilies were also found to be known kinase components in STRIPAK-complexes.

They include GCKII-subfamily members MST1 (also named STK4) and MST2 (also named STK3), GCKIV-subfamily members misshapen-like kinase 1 (MINK1) and TRAF2 and NCK-interacting protein kinase (TNIK) as well as mitogen-activated protein kinase (MAPK) kinase kinase kinase 4 (MAPK4K) (Couzens *et al.*, 2013; Fuller *et al.*, 2021; Goudreault *et al.*, 2009; Hauri *et al.*, 2013; Hyodo *et al.*, 2012; Kim *et al.*, 2020; Ribeiro *et al.*, 2010; Tang *et al.*, 2019). The upstream kinases of the mammalian Hippo signaling pathway MST1 and MST2 were recently shown to be recruited to the STRIPAK-complex in a phosphorylation-dependent manner by a "2-arm" assembly via STRIP1 and SIKE-SLMAP (Tang *et al.*, 2019). In animals, organ size is controlled by GCKII members regulating cell proliferation and cytokinesis (Sugden *et al.*, 2013). Moreover, members of the GCKIII

subfamily are regulators of MAPK-cascades as well as apoptosis and associate with the Golgi, centrosomes and the nucleus to facilitate cell migration and polarity (Sugden *et al.*, 2013). Members of the GCKIV subfamily can activate the JNK and p38 pathways inducing cytoskeletal changes (Dan *et al.*, 2000; Fuller *et al.*, 2021).

The mammalian CCM3 protein associates with the GCKIII members MST3/4 and STK25 thus increasing MST4 activity and inducing the MAPK/ERK pathway even under oxidative stress to enhance cell growth (Fidalgo *et al.*, 2010; Goudreault *et al.*, 2009; Kück *et al.*, 2019; Ma *et al.*, 2007; Zhang *et al.*, 2012). However, the direct or indirect interactions of striatins with kinases via adaptor proteins have not been exclusively elucidated (Tang *et al.*, 2019).

The small CC proteins SIKE and its paralog FGFR1OP2 are components of the mammalian STRIPAK-subcomplex I and are involved in regulatory gene expression of toll-like (TL) receptors during immune response and oral-wound closure, respectively (Ito *et al.*, 2010; Lin *et al.*, 2010).

The two CTTNBP2 and CTTNBP2NL proteins are part of the mammalian STRIPAK-subcomplex II, contain CC domains and are reported to be connected to phosphorylation and regulation of actin cytoskeleton in neuronal cells (Goudreault *et al.*, 2009).

The diverse subcellular localizations of STRIPAK subunits suggest that this complex bridges multiple organelles such as NE, Golgi, mitochondria, spindle pole bodies (SPBs) or centromeres, and the plasma membrane (PM). Thus and by inducing signaling pathways, it facilitates communication between organelles in molecular processes such as sexual development and cell division (Frost *et al.*, 2012).

In fact, diverse studies showed that the STRIPAK-components are linked to numerous diverse biological functions like the assembly of the Golgi, cell-migration and -proliferation, Hippo signaling, cell-cycle control and remodeling of the cytoskeleton as well as autophagy and vesicular trafficking (Bazzi *et al.*, 2017; Frost *et al.*, 2012; Huang *et al.*, 2017; Kean *et al.*, 2011; Lant *et al.*, 2015; Madsen *et al.*, 2015; Pandey *et al.*, 2017; Ribeiro *et al.*, 2010; Zhang *et al.*, 2013; Zheng *et al.*, 2017).

Since the STRIPAK-complex is linked to various signaling pathways and kinase cascades, dysfunction of this large conserved multiprotein complex is associated with various human diseases. These include for example autism, type 2 diabetes, epilepsy and stroke,

neurodegeneration, Alzheimer's disease, and various types of cancer (Craig *et al.*, 1998; Hwang and Pallas, 2014; Janssens and Goris, 2001; Shi *et al.*, 2016).

Therefore, the elucidation of the connection of the STRIPAK-complex with multiple signaling pathways is an interesting field to understand the progression of several human diseases.

1.2.1 STRIPAK-complex orthologs in yeasts, fruit fly and filamentous fungi

Mammalian STRIPAK-complex orthologs were also identified in the fission yeast *Schizosaccharomyces pombe*, in the baker's yeast *S. cerevisiae*, as well as in the fruit fly *Drosophila melanogaster* and filamentous fungi like *S. macrospora*, *N. crassa* and *Aspergillus nidulans*. Their compositions are listed in Table 1.

Table 1: Composition of the human STRIPAK-complex and orthologs in yeasts, fruit fly and filamentous fungi.

subunit	*H. sapiens* (STRIPAK)	*S. pombe* (SIP)	*S. cerevisiae* (Far)	*D. melanogaster* (dSTRIPAK)	*A. nidulans* (AnSTRIPAK)	*N. crassa* (NcSTRIPAK)	*S. macrospora* (SmSTRIPAK)
PP2AA	PP2AAα/β	Paa1p	Tpd3p	Pp2A-29B	SipF	PP2A-A	SmPP2AA
PP2Ac	PP2Acα/β	Ppa3	Ppg1p	Mts	SipE	PPG-1	SmPP2Ac1
striatin	striatin (STRN1); SG2NA (STRN3); zinedin (STRN4)	Csc3p	Far8p	CKA	StrA	HAM-3	PRO11
SLMAP	SLMAP/TRAF3IP3 or CTTNBP2/CTTNBP2NL	Csc1p	Far9p/ Far10p	CG17494	SipD	HAM-4	PRO45
STRIP	STRIP1/2	Csc2p	Far11p	CG11526	SipC	HAM-2	PRO22
MOB	MOB3/MOB4/phocein	-	-	Mob4	SipA	MOB-3	SmMOB3
small CC	SIKE/FGFR1OP2	Csc4p	Far3p/ Far7p	FGOP2	SipB	NCU04324	SCI1
GCKIII	MST3 (STK24), MST4 (STK26), STK25 (YSK1/SOK1)	-	?	Hpo, Msn, GCKIII	?	?	SmKIN3, SmKIN24
CCM3	CCM3	-	-	CG5073	-	-	-
dual-targeted protein	-	-	-	-	-	NCU09375	SmGPI

Determinations according to (Castets *et al.*, 1996; Castets *et al.*, 2000; Glatter *et al.*, 2009; Goudreault *et al.*, 2009; Jeong *et al.*, 2021; Muro *et al.*, 1995) (for STRIPAK); (Hwang and Pallas, 2014; Singh *et al.*, 2011) (for SIP); (Goudreault *et al.*, 2009; Kemp and Sprague, 2003; Lai *et al.*, 2011; Lisa-Santamaría *et al.*, 2012) (for Far); (Chen *et al.*, 2002; Ribeiro *et al.*, 2010) (for dSTRIPAK); (Elramli *et al.*, 2019) (for AnSTRIPAK); (Dettmann *et al.*, 2013) (for NcSTRIPAK); (Beier *et al.*, 2016; Bernhards and Pöggeler, 2011; Bloemendal *et al.*, 2012; Frey *et al.*, 2015b; Kück *et al.*, 2016; Nordzieke *et al.*, 2015; Pöggeler and Kück, 2004; Radchenko *et al.*, 2018; Reschka *et al.*, 2018) (for SmSTRIPAK). Core-STRIPAK

components are indicated in light green and kinases (GCKIII) with their recruiter protein in dark green. STRIPAK-kinase homologs in *N. crassa* and *S. cerevisiae* are POD-6, SID-1, MST-1, and Sps1p, respectively but evidence is lacking if they are subunits of the STRIPAK.

In the following, the individual STRIPAK-complex orthologs of the mentioned organisms are briefly described with regard to their localization and function. In *S. pombe*, the septation initiation network (SIN)-inhibitory PP2A (SIP)-complex localizes to SPBs and was shown to be important for SIN-assembly to ensure correct septation and cytokinesis during mitotic events (Hwang and Pallas, 2014; Singh *et al.*, 2011).

In *S. cerevisiae*, the factor arrest (FAR)-complex is important for pheromone-mediated cell-cycle arrest, involved in autophagy and directly affects signaling of the serine/threonine kinase target of rapamycin (TOR). In TOR-signaling, the FAR-complex antagonizes complex 2 (TORC2) that functions in cell growth and actin polymerization via dephosphorylation of TORC2 substrates (Bartlett and Kim, 2014; Kemp and Sprague, 2003; Lisa-Santamaría *et al.*, 2012; Pracheil and Liu, 2013).

In *D. melanogaster* (d/D), the dSTRIPAK-complex was proposed to function in multicellular development, embryogenesis, plays a role in autophagy and further acts as negative regulator of Hippo signaling. The striatin-ortholog CKA is an essential component of the DJNK pathway that facilitates dorsal closure of the fly embryo and was also localized to autophagosomes (Chen *et al.*, 2002; Neal *et al.*, 2020; Neisch *et al.*, 2017; Ribeiro *et al.*, 2010).

In the filamentous fungus *A. nidulans* (An), the heptameric orthologous AnSTRIPAK-complex functions in fungal development, secondary metabolite production as well as in stress response by controlling the two MAPK-pathways MpkB and MpkC. The striatin StrA was shown to localize to the NE and the endomembrane system (Elramli *et al.*, 2019; Irniger *et al.*, 2016; Wang *et al.*, 2010). Moreover, assembly of the functional AnSTRIPAK was predicted by the primarily formation of the 3 subcomplexes SipA-StrA (MOB3-striatin), SipB-SipD (SIKE-SLMAP) and SipE-SipF-SipC (PP2Ac, PP2AA and STRIP1/2) interacting with striatin (Elramli *et al.*, 2019).

In *N. crassa* (Nc), the NcSTRIPAK-complex controls cell-cell recognition, cell fusion and fruiting-body formation. Furthermore, subunits of the complex localize to the NE where the NcSTRIPAK accumulates the cell-wall integrity (CWI) MAP kinase MAK-1 important

for the cell-wall stress pathway and cell-cell communication (Dettmann *et al.*, 2013; Kück *et al.*, 2019). Additionally, the NcSTRIPAK is connected with the MAP kinase MAK-2 that affects MAK-1 localization at the nucleus (Dettmann *et al.*, 2013). Homologous GCK family members connected to NcSTRIPAK are POD-6, SID-1 and MST-1 but it remains unclear if they are subunits of the NcSTRIPAK.

1.2.2 The SmSTRIPAK-complex of *S. macrospora*

In *S. macrospora* (Sm), the SmSTRIPAK-complex was identified by complementation analysis of sterile pro mutants arrested in the developmental stage of protoperithecia (Pöggeler and Kück, 2004). In a first analysis, the mutant pro11 that is impaired in sexual development was identified. This mutant has a nonsense mutation in the *pro11* gene (STOP codon at amino-acid position 546) resulting in a truncated PRO11 protein that lacks several WD40-repeats. Mutation and deletion of the *pro11* gene results in a sterile phenotype lacking hyphal fusion. Interestingly, complementation of the pro11 mutant with mouse striatin cDNA rescued the sterile phenotype (Pöggeler and Kück, 2004). Accordingly, PRO11 is involved in fruiting-body development, and hyphal fusion as well as in septation in ascogonia (Bloemendal *et al.*, 2012; Pöggeler and Kück, 2004; Radchenko *et al.*, 2018). Further characterization of PRO11 revealed high homology and structural similarity to mammalian striatin family members and also to the *D. melanogaster* CKA protein (Pöggeler and Kück, 2004). The *S. macrospora* human striatin homolog PRO11 contains seven C-terminal WD40-repeats, a putative Ca^{2+}-CaM-binding site, a putative caveolin-binding site and a N-terminal CC motif (Kück *et al.*, 2019; Pöggeler and Kück, 2004). PRO11 is the major scaffolding unit of the SmSTRIPAK-complex that is composed of the scaffolding and catalytic subunits of PP2A, SmPP2AA and SmPP2Ac1, respectively, the STRIP1/2 homolog PRO22, and the MOB3 (phocein) homolog SmMOB3 (Table 1). Moreover, the GCKIII kinases SmKIN3 and SmKIN24 are recruited to PRO11 (Beier *et al.*, 2016; Bernhards and Pöggeler, 2011; Bloemendal *et al.*, 2012; Frey *et al.*, 2015b; Radchenko *et al.*, 2018). Furthermore, the SLMAP homolog PRO45 and the putative SIKE homolog and CC protein STRIPAK-complex interactor 1 (SCI1) were identified as core subunits of the SmSTRIPAK (Nordzieke *et al.*, 2015; Reschka *et al.*, 2018). Additionally, the dual-targeted protein glycosyl-phosphatidylinositol-anchored protein 1 (SmGPI1) was

identified to genetically interact with the SmSTRIPAK-compound SmMOB3 (Frey *et al.*, 2015a). Analyses of knockout mutants of the individual SmSTRIPAK-components showed that they exhibited severe defects in vegetative growth, sexual development as well as hyphal fusion and septation (Kück *et al.*, 2016; Kück *et al.*, 2019; Teichert *et al.*, 2020). Furthermore, fluorescence microscopic investigations revealed diverse subcellular localizations of the single SmSTRIPAK-complex compounds within the hypha. Accordingly, PRO11 and the putative SIKE homolog SCI1 were found to localize around the nucleus and were further identified to physically interact with each other in yeast two-hybrid (Y2H) assays (Reschka *et al.*, 2018). In addition, SCI1 was found to directly interact with PRO45, which in turn interacts with SmMOB3 both showing localization in the NE, ER, and mitochondria (Nordzieke *et al.*, 2015; Reschka *et al.*, 2018). Thus, SmMOB3 might link the SmSTRIPAK to vesicular traffic and endocytosis by further interacting with PRO11 (Bernhards and Pöggeler, 2011; Bloemendal *et al.*, 2012). In addition, the SmMOB3-interacting protein SmGPI1 was localized in mitochondria, the PM and cell wall (Frey *et al.*, 2015a). Furthermore, the STRIP1/2 homolog PRO22 associates with the intermembrane system and tubular vacuoles, interacts with PRO11, and is a potential interactor of SmPP2Ac1 (Bloemendal *et al.*, 2010; Bloemendal *et al.*, 2012). The catalytic subunit of PP2A, SmPP2Ac1, was shown to physically interact with PRO22 and PP2AA in Y2H assays (Beier *et al.*, 2016). For the GCKIII members SmKIN3 and SmKIN24, a direct physical interaction with PRO11 was detected, indicating a connection between the SmSTRIPAK-complex and kinase-dependent signaling pathways. In this context, SmKIN3 was thought to link the SIN-pathway with SmSTRIPAK to induce septation and regulate cellular processes (Frey *et al.*, 2015b; Radchenko *et al.*, 2018).

In a recent study using cryogenic electron microscopy (cryo-EM), the structure of the human STRIPAK was identified showing that STRN3 forms a heterotetramer via its CC motifs to provide a platform for the interaction with one copy each of PP2AA and PP2Ac, STRIP1 and MOB4 (Jeong *et al.*, 2021). This structure, modified in Figure 2, can be used as a template for the SmSTRIPAK with all hitherto known components (Figure 3). All studies of subunit-interactions were included in this figure according to Beier *et al.*, 2016; Bernhards and Pöggeler, 2011; Bloemendal *et al.*, 2012; Frey *et al.*, 2015b; Kück *et al.*, 2016; Nordzieke *et al.*, 2015; Pöggeler and Kück, 2004; Radchenko *et al.*, 2018; Reschka *et al.*, 2018.

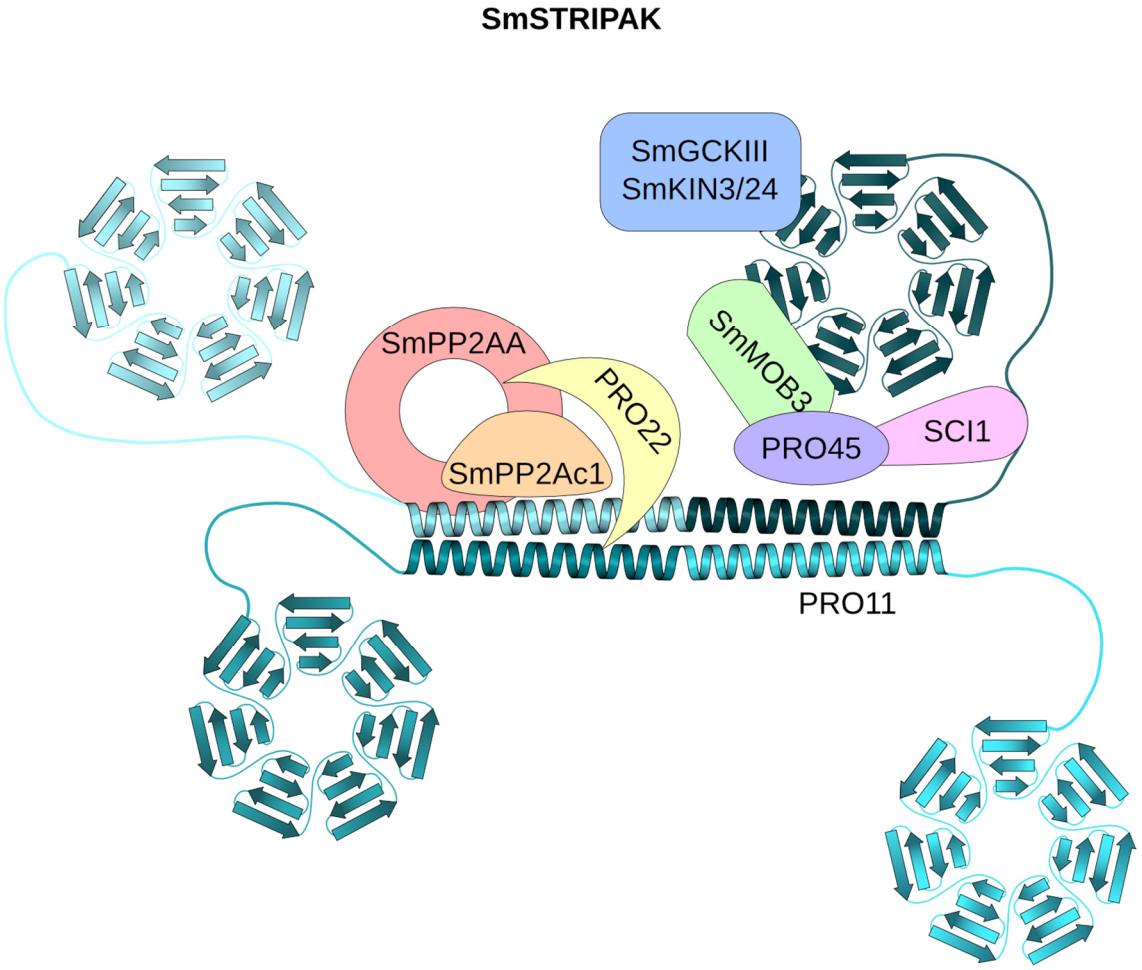

Figure 3: Structure of the *S. macrospora* SmSTRIPAK-complex.
Schematic representation of the SmSTRIPAK-complex of *S. macrospora* (Groth *et al.*, 2021). Human striatin homolog PRO11 forms a tetramer providing surface for protein-protein interactions harboring CC domains (cyan-shaded helices) and WD40-repeats (cyan-shaded beta-propeller). SmPP2AA (red): scaffolding subunit of phosphatase PP2A; SmPP2Ac1 (orange): catalytic subunit of PP2A; SmMOB3 (green); PRO22 (yellow): STRIP1/2 homolog; PRO45 (purple): SLMAP homolog; SCI1 (pink): putative SIKE homolog; SmKIN3/24 (blue): recruited GCKIII kinases.

1.3 The pulled-down proteins ARP1, POM33 and VAC14

In pulldown experiments coupled to liquid chromatography-mass spectrometry (LC-MS) analysis with the SmSTRIPAK-components PRO11 or SCI1 as bait, numerous proteins were pulled down including the cytoskeletal actin-related protein ARP1, the putative nucleoporin and ER pore-membrane protein POM33 and the vacuolar-morphology protein VAC14 which are all part of individual conserved multiprotein complexes themselves (Reschka *et al.*, 2018). In the following section, these proteins are introduced one by one.

1.3.1 The cytoskeletal protein ARP1

The cytoskeleton is a dynamic network helping cells in diverse functions. These include maintenance of the cell shape and mechanical support, cell migration via contraction as well as involvement in signaling pathways, endocytosis, chromosome-segregation and intracellular transport of several vesicles and organelles (Alberts, 2008; Fletcher and Mullins, 2010; Herrmann *et al.*, 2007). Besides microtubules (MTs), actin and intermediate filaments are also involved in cytoskeleton assembly. The motor proteins acting on actin filaments are myosins that enable sliding of filaments in muscle cells due to contraction as well as short-distance transport of vesicles and organelles in the cytoplasm. As part of the eukaryotic cytoskeleton, MTs are polarized ever-changing structures made of 13 protofilaments of α- and β-tubulin heterodimers. They form large structures of 25 nm in diameter with the plus end localized at the cell periphery and the minus end at the microtubule-organizing center (MTOC or centrosomes) (Keating and Borisy, 1999; Wolf and Böhm, 1997). Moreover, dynamic microtubules play an important role in creating cell polarity. In eukaryotes, polar tip growth can be found in neurons, root hairs, pollen tubes and at the apex of extremely polarized fungal hyphae (Fischer *et al.*, 2008; Riquelme, 2013). The microtubule cytoskeleton mediates long-distance movement via the molecular motors dyneins together with dynactin (minus-end directed) and kinesins (plus-end directed). For simplicity, only dynein and dynactin will be described in more detail here. Human cytoplasmic dynein-1 (referred to as dynein) is a large 1.4 MDa multiprotein complex (Zhang *et al.*, 2017). It interacts with dynactin to form the dynein-dynactin complex. This multiprotein-complex association enables retrograde long-distance transport of various cargoes. These include autophagosomes, endosomes, Golgi vesicles and nuclei as well as RNA, proteins and viruses (Reck-Peterson *et al.*, 2018).

In the human 1.1 MDa dynactin complex, the actin-related protein 1 (Arp1) is the most abundant protein (Bingham and Schroer, 1999; Gill *et al.*, 1991; Schafer *et al.*, 1994; Schroer and Sheetz, 1991). Because Arp1 has been isolated from cells only as a component of dynactin, understanding the role of Arp1 depends on knowledge of the function of dynactin as a co-factor of the microtubular motor cytoplasmic dynein-1 (Gill *et al.*, 1991; Schafer and Schroer, 1999; Schroer and Sheetz, 1991). Arps define a superfamily and are

highly conserved in eukaryotes including yeast and filamentous fungi. They play roles in vesicle motility, mitosis, dynamics of actin filaments and modulation of the chromatin structure. They are predominantly assembled with other proteins in stable complexes (Schafer and Schroer, 1999). Notably, members of the Arp family show sequence similarity but not identity to actin and were grouped into different subfamilies according to their amino-acid sequence (Schroer *et al*., 1994). Among the several Arps known, Arp1 (also referred to ACT5 in *S. cerevisiae* and Ro-4 in *N. crassa*) is most similar to actin with the ability to polymerize into filaments in an ATP-dependent manner (Bingham and Schroer, 1999). In mammals, the related Arp1 isoforms α-, β-, and γ-centractin exist with α-centractin being the most prominent one (Clark *et al*., 1994).

Besides Arp1, mammalian dynactin is composed of 11 different polypeptides (23 subunits in total) (Carter *et al*., 2016). The central 37 nm Arp1-filament, containing 8-10 Arp1 monomers, contains additionally one copy of β-actin and is capped by the F-actin capping protein CAPZ at the barbed-end and by Arp11 at the pointed-end of the complex. Arp11 itself interacts with the three proteins p25, p27 and p62 to form the pointed-end complex. Moreover, a shoulder domain sits on the barbed-end of the Arp1 filament that is composed of two copies of $p150^{glued}$, four copies of p50 dynamitin and two copies of p24. The N-terminus of $p150^{glued}$ forms a flexible elongation harboring two CC motifs interrupted by a globular domain and a CAP-Gly domain for interaction with MTs at the very end of the N-terminus (Waterman-Storer *et al*., 1995). The structure of the human dynein-dynactin complex is shown in Figure 4.

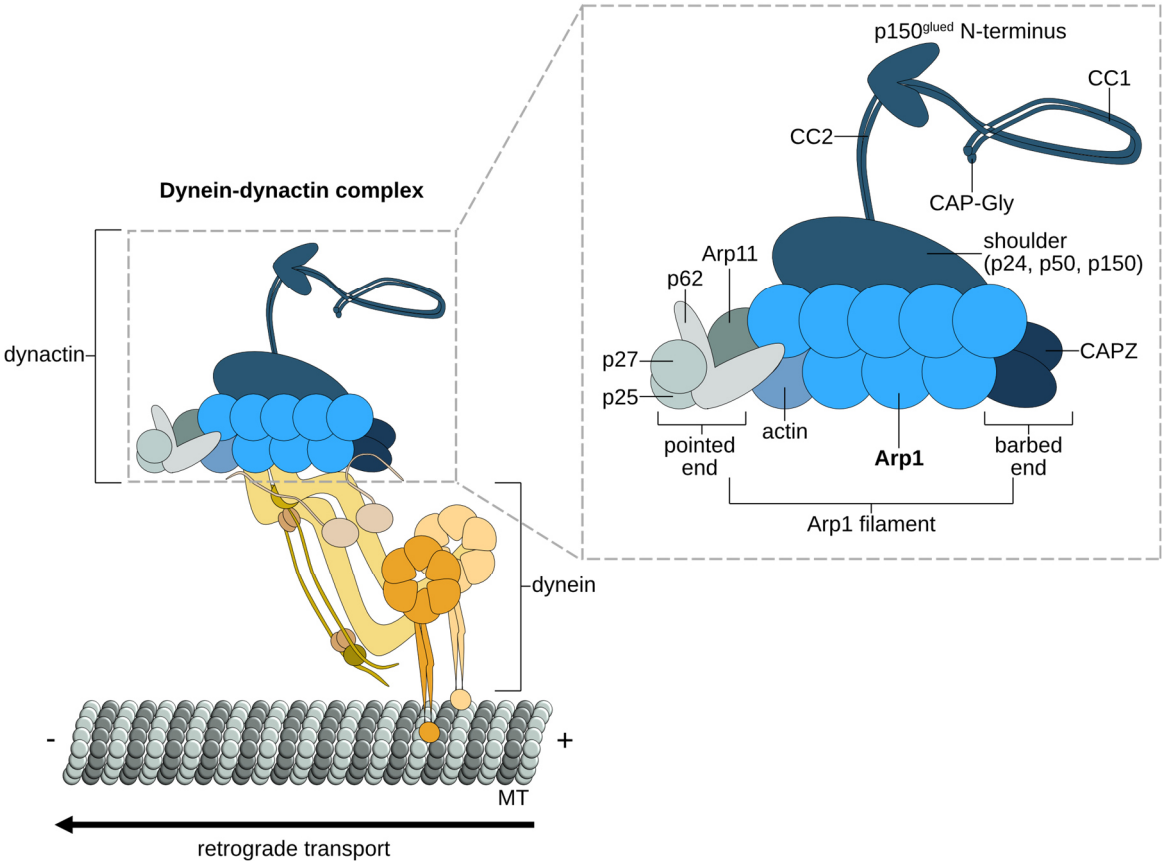

Figure 4: Structure of the human dynein-dynactin complex.
Schematic representation of the dynein-dynactin complex in mammals that mediates retrograde transport of diverse cargoes on microtubules (MT) from the plus (+) to the minus (-) end. Close-up of the dynactin complex is indicated at the right margin. The core component is the Arp1 filament consisting of 8-10 copies of Arp1 (light blue), and one copy of actin (pale blue). The pointed end complex consists of Arp11 (dark green), p62 (grey), p27 and p25 (pale green). The filament is capped at the barbed end by CAPZ (dark blue). The shoulder domain (dark cyan) is composed of p24, p50 and p150. The N-terminus of p150^{glued} forms an extension including coiled-coil motifs (CC1 and CC2) and a CAP-Gly end that can interact with microtubules. Based on Reck-Peterson *et al.*, 2018.

In fungi, the arrangement of the cytoskeleton establishes and maintains polarity providing a continuous and indefinite flow of outward- and inward-bound traffic at the hyphal tip during growth (Riquelme *et al.*, 2003). MTs of filamentous fungi also show bidirectional polarity with the plus end located in the apical region of the hyphae. In *Ustilago maydis* and *A. nidulans*, cytoplasmic dynein is recruited to the plus ends of MTs in a kinesin-dependent manner generating a dynein-loading zone close to the hyphal tip (Lenz *et al.*, 2006; Mouriño-Pérez *et al.*, 2006; Schuster *et al.*, 2011; Steinberg *et al.*, 2017; Zhang *et al.*, 2003). This active polar growth enables diverse functions including sensing and exploring of the environment, interacting with own fungal colonies or mating partners and hosts as

well as generating a hyphal network via branching and fusion of fungal cells (Lichius and Lord, 2014; Mela *et al.*, 2020).

In this regard, recruitment of the small Rho-family GTPase Cdc42 at new polarity sites is followed by regulation of multiple downstream effectors and is crucial for polarity establishment (Harris, 2011; Miller *et al.*, 2020; Momany, 2002; Park and Bi, 2007; Pruyne and Bretscher, 2000; Wendland and Philippsen, 2001; Woods and Lew, 2019). Moreover, the Spitzenkörper (SPK) is associated with hyphal polarity. It is a molecular structure near the hyphal tip consisting of accumulated vesicles. It functions as a vesicle-supply center (VSC) via microtubule- and actin-dependent vesicle transport (Harris *et al.*, 2005; Momany, 2002; Riquelme *et al.*, 2018; Steinberg *et al.*, 2017; Zheng *et al.*, 2020).

In filamentous fungi, transport of early endosomes (EEs) via motor proteins along MTs supports normal polarized hyphal growth (Peñalva, 2010; Shaw *et al.*, 2011; Steinberg, 2014). Surprisingly, studies in *U. maydis* revealed that on moving EEs entire polysomes assemble translating mRNAs "on the run" (Higuchi *et al.*, 2014). Furthermore, peroxisomes and nuclei were also described as cargos for dyneins and kinesins in filamentous fungi (Egan *et al.*, 2012). Of note, while deletions of the dynactin CAP-Gly component retain normal growth phenotypes in *A. nidulans*, incorrect distribution of nuclei was observed in *S. cerevisiae* (Kardon *et al.*, 2009; Yao *et al.*, 2012). Together these studies in filamentous fungi show that vesicular transport of diverse substrates as well as polarity establishment via the microtubule-cytoskeleton are important processes for various cellular functions. Due to the fact that similarities can be found in the transport mechanism between the hyphae of filamentous fungi and the neurons of metazoans, studies in filamentous fungi can be used to understand the basis of neuronal diseases like Parkinson disease-like Perry syndrome and Charcot-Marie-Tooth disease (Lasser *et al.*, 2018; Lipka *et al.*, 2013).

1.3.2 The putative nucleoporin POM33

The nucleus is surrounded by a double lipid bilayer consisting of the inner nuclear membrane (INM) and the outer nuclear membrane (ONM). At the sites of nuclear pores, the INM merges into the ONM, which is continuous with the ER and forms the nuclear envelope. (De Magistris and Antonin, 2018). The ER consists of peripheral sheet-like

cisternae followed by a network of ER tubules that are interconnected (Wang and Rapoport, 2019). Its morphology can be divided into the rough ER (RER) and the smooth ER (SER). The RER has membrane-bound ribosomes, whereas the SER is lacking them (Shibata *et al.*, 2006). The ER network is highly dynamic. Its tubules fuse and divide continuously, forming three-way junctions (Baumann and Walz, 2001; Du *et al.*, 2004; Lee and Chen, 1988; Wang and Rapoport, 2019).

At the sites of nuclear pores, where the INM fuses with the ONM, nuclear-pore complexes (NPCs) are incorporated. NPCs are large multiprotein complexes that form channels to mediate the exchange of diverse molecules between the nucleus and the cytoplasm (Hampoelz *et al.*, 2019). They are conserved from yeast to mammals and consist of about 1000 protein subunits of around 30 different nucleoporins (Nups). The large assemblies of NPCs can have a weight up to 120 MDa and can be present thousandfold (Beck and Hurt, 2017; Doye and Hurt, 1997; Dultz and Ellenberg, 2010; Hampoelz *et al.*, 2019; Lin *et al.*, 2016; Rout *et al.*, 2000; Schwartz, 2005; Schwartz, 2016). The biogenesis of NPCs can occur either postmitotic or *de novo*. During postmitotic NPC assembly, the NE reforms from the cortical ER (cER), which is located closely to the PM, into a pore that is stabilized by transmembrane (TM)-Nups, so-called pore-membrane proteins (Poms), or transmembrane proteins (TMEMs), so that other Nups can be recruited. During *de novo* NPC assembly, the double-membrane system of the NE fuses to form a pore (Antonin *et al.*, 2008; Doucet *et al.*, 2010; Doucet and Hetzer, 2010; Hetzer *et al.*, 2005). For example, in *S. cerevisiae* NPCs stay intact during the process of closed mitosis, whereas in the filamentous fungus *A. nidulans* a core NPC structure remains in the NE from which peripheral Nups detach during partially open mitosis (De Souza *et al.*, 2004; Liu *et al.*, 2009; Makhnevych *et al.*, 2003; Osmani *et al.*, 2006). As highly complex molecular machines, NPCs share principle structural elements including the cytoplasmic, inner, transmembrane, and nucleoplasmic ring (Figure 5). Moreover, at the cytoplasmic site, NPCs consist of filaments and at the nucleoplasmic site of the nuclear basket. The channel center of NPCs contains a network of Nups that harbor phenylalanine (F) and glycine (G)-rich repeats (FG-Nups) (Dickmanns *et al.*, 2015; Fahrenkrog and Aebi, 2003; Hurt and Beck, 2015; Schwartz, 2016; Von Appen and Beck, 2016). A schematic representation of the structural organization of human and yeast NPCs is shown in Figure 5.

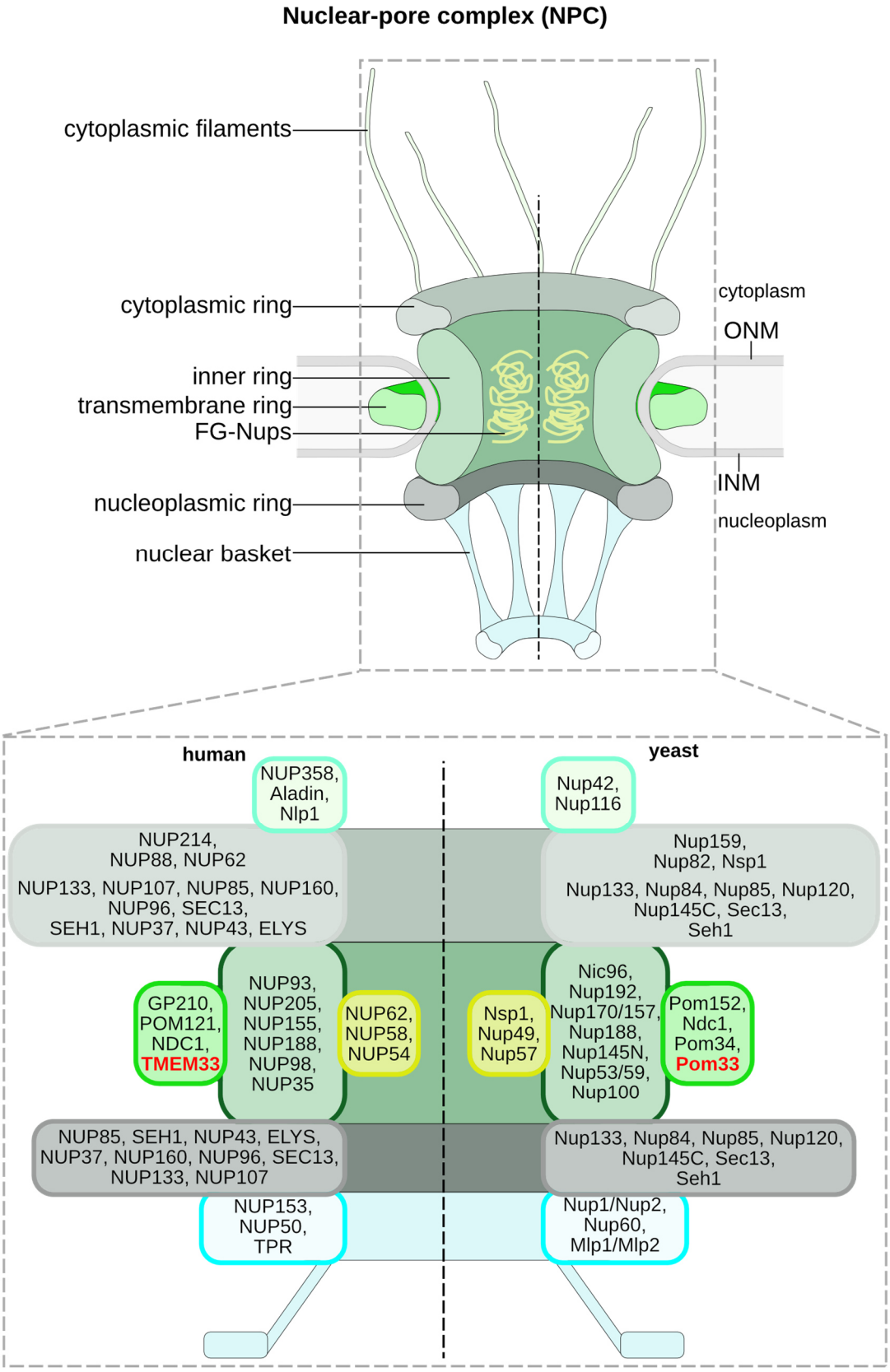

Figure 5: Structure of the nuclear-pore complex.
Schematic representation of the localization and structural organization of the nuclear-pore complex (NPC). Close-up of the NPC is indicated at the bottom margin. It is composed of cytoplasmic filaments (aquamarine), the cytoplasmic ring (light grey), the inner ring (dark green),

the transmembrane ring, which is composed of pore-membrane proteins (Poms) (light green), the nucleoplasmic ring (dark grey), FG-Nups (F: Phenylalanine; G: Glycine) (yellow), and the nuclear basket (cyan). The NPC is conserved from yeast to human and is assembled by the formation of diverse subcomplexes of nucleoporins (Nups) and joining proteins, here shown as color-coded outlined boxes in the zoom-in. The human transmembrane protein of 33 kDa (TMEM33) and the yeast homolog Pom33 are highlighted in red. ONM: outer nuclear membrane, INM: inner nuclear membrane. Modified according to Beck and Hurt, 2017; Donnaloja *et al.*, 2019.

As channels in the nuclear membrane, NPCs mediate bidirectional transport of diverse macromolecules. The import comprises nuclear proteins including polymerases, histones and transcription factors whereas nuclear RNAs (rRNA, mRNA, tRNA and miRNA) are exported from the nucleoplasm into the cytoplasm through NPCs (Beck and Hurt, 2017). Besides import and export, NPCs also facilitate the shuttling of proteins and RNAs that are involved in signaling, turnover and biogenesis as well as passive diffusion of small molecules (~40 kDa). Larger molecules are ferried through the pore via nuclear transport receptors (NTRs) like karyopherin-α and -β, which are bound by FG-Nups to facilitate nucleocytoplasmic transport (Bayliss *et al.*, 2000; Beck and Hurt, 2017; Kapinos *et al.*, 2017). Interestingly, Nups can also be mobile changing their localization from NPCs to the nucleoplasm where they are involved in chromatin interaction. In this regard, mutations of mammalian Nups are connected with cardiological diseases, cancer and amyotrophic lateral sclerosis (Donnaloja *et al.*, 2019; Liang *et al.*, 2013). Taken together, NPCs are large multiprotein assemblies associated with processes in the cytoplasm like translational control or cytoskeleton organization, and in the nucleus including DNA repair, chromatin organization or regulation of gene expression (Beck and Hurt, 2017).

In the following, the class of TM-Nups is discussed in detail. The nucleoporins of this class function predominantly in anchoring NPCs in the nuclear pore. Moreover, they also play roles in nucleocytoplasmic traffic though NPCs, are involved in the formation of new nuclear pores via mediating the fusion of the INM with the ONM, and maintain the NPC's structural organization (Brown *et al.*, 2021). In yeast, Pom152p, Pom34p, the highly conserved protein nuclear division cycle 1 (Ndc1), and the recently identified Pom33p or its paralog pore and ER protein of 33 kDa (Per33p) are components of the pore membrane domain of NPCs (Figure 5) (Chadrin *et al.*, 2010; Chial *et al.*, 1998; Rout *et al.*, 2000; Wozniak *et al.*, 1994). Deletion mutants of either *pom152* or *pom34* are viable and show no defects in protein import or export of mRNAs throughout the NPC (Belanger *et al.*, 2005; Brown *et*

al., 2021; Madrid *et al.*, 2006; Rout *et al.*, 2000; Wozniak *et al.*, 1994). Furthermore, Pom152p directly binds to Pom34p and Ndc1p and to Nup170p/157p to link the transmembrane ring with the inner NPC ring (Brown *et al.*, 2021; Kim *et al.*, 2018; Makio *et al.*, 2009). In contrast to this, deletions of *ndc1* or its *S. pombe* ortholog *cut11* result in lethality (Chial *et al.*, 1998; Mansfeld *et al.*, 2006; West *et al.*, 1998; Winey *et al.*, 1993). The recently identified protein Pom33p was shown to be involved in proper distribution of NPCs at the NE as well as in their assembly and stabilization (Chadrin *et al.*, 2010). Further studies revealed that the binding of Pom33p with the karyopherin Kap123p is important for NPC localization. Notably, the yeast Pom33p paralog Per33p can also associate with NPCs but was mainly localized at the ER and NE (Floch *et al.*, 2015). In *S. pombe*, the Pom33p ortholog tetra-spanning protein 1 (Tts1p), was shown to maintain the cER network and remodels the NE during mitosis by modulating the distribution of NPCs (Zhang and Oliferenko, 2014). In human, TM-Nups comprise the homolog of yeast Ndc1p, NDC1, as well as POM121, the glycoprotein 210 (GP210), and TMEM33 (Figure 5) (Chadrin *et al.*, 2010; Cohen *et al.*, 2003; Funakoshi *et al.*, 2007; Stavru *et al.*, 2006). Of interest, Ndc1 is conserved from yeast to human and also in filamentous fungi and plants (Stavru *et al.*, 2006). It was identified to be the only essential TM-Nup known so far to be involved in *de novo* NPC assembly (Chial *et al.*, 1998; Mansfeld *et al.*, 2006; Stavru *et al.*, 2006). Moreover, Ndc1 and Pom121 were shown to form subcomplexes to initiate pore formation *in vitro* (Panatala *et al.*, 2019). Human GP210 was found to be essential for transport of cargos into the nuclear lumen (Mudumbi *et al.*, 2020). The TMEM33 nucleoporin has not yet been shown to localize to NPCs but was enriched at the NE and the ER where it functions as potential structural regulator of ER membranes (Chadrin *et al.*, 2010; Floch *et al.*, 2015; Urade *et al.*, 2014). Taken together, besides the three known TM-Nups, a fourth conserved member, Pom33p/Tts1p/TMEM33, was identified to join this group and had been analyzed in yeast and mammals.

1.3.3 The vacuolar-morphology protein VAC14

Organelle identity is defined by the lipid composition of their membranes. These contain phosphorylated phosphoinositides (PIPs), which are produced at the cytosolic phase of eukaryotic cells (Di Paolo and Camilli, 2006; Lemmon, 2008). PIPs mediate organelle-

specific membrane signaling pathways and trafficking events. Additionally, they play a role in remodeling of the cytoskeleton, cell growth and nuclear processes like DNA repair or regulation of transcription (Di Paolo and Camilli, 2006). Due to reversible phosphorylation at position 3, 4 or 5 of the phosphatidylinositol (PtdIns) headgroups, seven different PIP-derivatives are known so far including PtdIns(3)P, PtdIns(4)P, PtdIns(5)P, PtdIns(3,4)P_2, PtdIns(3,5)P_2, PtdIns(4,5)P_2 (often referred to as PIP_2) and PtdIns(3,4,5)P_3 (often referred to as PIP_3). All these phospholipids are minor components of distinct cellular membranes where they recruit effector proteins to facilitate signal transduction and transport through activation of channels or transporters (Di Paolo and Camilli, 2006; Lemmon, 2008; Suh and Hille, 2008).

While PtdIns(3,4)P_2, PIP_2 and PIP_3 are predominantly localized to the PM, and PtdIns(4)P is enriched at the Golgi-complex, PtdIns(3)P is present on EEs and autophagosomes to regulate their maturation (Di Paolo and Camilli, 2006; Gillooly *et al.*, 2000; Stauffer *et al.*, 1998). In the following, the two phosphatidylinositols PtdIns(3)P and PtdIns(3,5)P_2 are described in more detail.

PtdIns(3)P is generated by the vacuolar-protein sorting (Vps) protein Vps34, which is a member of class III phosphatidylinositol 3-kinases and important for autophagy (Backer, 2008; Voigt *et al.*, 2014). Furthermore, PtdIns(3)P is involved in membrane fusion and receptor trafficking, and is a precursor for the generation of PtdIns(3,5)P_2 (Dove *et al.*, 1997; Joly *et al.*, 1995; Jones and Clague, 1995; Lindmo and Stenmark, 2006). The headgroup of PtdIns(3)P is recognized by binding partners containing a FYVE-finger domain that is named after the following four proteins: Fab1p, YOTB, Vac1p and EEA1, in which this motif was first identified (Stenmark *et al.*, 2002).

PtdIns(3,5)P_2 is produced in the endomembrane system, localizing mainly to late endosomes (LEs) and lysosomes but also in a smaller amount to EEs (Di Paolo and Camilli, 2006; Dove *et al.*, 2009). It controls diverse cellular functions including morphology of organelles, retrograde trafficking to the *trans*-Golgi network (TGN), ion transport, membrane recycling, cargo sorting into multi-vesicular bodies (MVBs), acidification of endolysosomes/vacuoles, stress response and autophagy (De Lartigue *et al.*, 2009; Dove *et al.*, 1997; Dove *et al.*, 2009; Efe *et al.*, 2005; Shisheva, 2008). In yeast and mammalian cells, PtdIns(3,5)P_2 is only present with <0.1 % and <0.05 % , respectively, whereas PtdIns(3)P

comprises 2.5 % and 0.2 %, respectively (Bonangelino *et al.*, 2002; Duex *et al.*, 2006a; Zhang *et al.*, 2007). Although PtdIns(3,5)P_2 is a minor PIP, its dysregulation in human can cause severe developmental and neurological defects like Charcot-Marie-Tooth syndrome 4J (CMT4J) and amyotrophic lateral sclerosis (Chow *et al.*, 2007; Chow *et al.*, 2009; Zhang *et al.*, 2007; Zhang *et al.*, 2008).

The turnover and synthesis of PtdIns(3,5)P_2 is regulated exclusively by a highly conserved multiprotein complex that is present in eukaryotes (Bonangelino *et al.*, 2002; Dove *et al.*, 2002; Duex *et al.*, 2006b; Rudge *et al.*, 2004; Sbrissa *et al.*, 2004; Zhang *et al.*, 2007).

The complex that mediates PtdIns(3,5)P_2 homeostasis is known as the Fab1p-complex in yeast, and as the PIKfyve- or PAS-complex, as abbreviation for PIKfyve-ArPIKfyve-Sac3, in mammals. In the following, the composition of the complex with the nomenclature in yeast and mammals is explained (Figure 6).

Accordingly, the Fab1p/PIKfyve-complex consists of the PtdIns(3)P 5-kinase fatty-acid biosynthesis protein 1 (Fab1p) in yeast or its ortholog FYVE finger-containing phosphoinositide kinase (PIKfyve) in mammals. The Fab1p kinase antagonizing PtdIns(3,5)P_2 phosphatase factor-induced gene 4 (Fig4p) or its mammalian ortholog Sac domain-containing protein 3 (Sac3). Moreover, the complex nucleating subunit vacuole morphology and inheritance protein 14 (Vac14p) or its mammalian ortholog associated regulator of PIKfyve (ArPIKfyve or often referred to as VAC14) are components of the Fab1p/PIKfyve-complex (Botelho *et al.*, 2008; Duex *et al.*, 2006a; Duex *et al.*, 2006b; Gary *et al.*, 1998; Ikonomov *et al.*, 2009b; Jin *et al.*, 2008; Lees *et al.*, 2020; Sbrissa *et al.*, 2008; Schulze *et al.*, 2014). Human VAC14 was recently described to form a pentamer (Lees *et al.*, 2020). In yeast, the Fab1p-complex additionally contains the major Fab1p activator vacuolar-segregation protein 7 (Vac7p) and its negative regulator autophagy-related protein 18 (Atg18p) (Bonangelino *et al.*, 1997; Efe *et al.*, 2007; Gary *et al.*, 2002). Due to its cellular function, the Fab1p/PIKfyve-complex is localized to the membranes of vacuoles in yeast or to EEs and LEs as well as to MVBs and lysosomes in mammals ((Bonangelino *et al.*, 2002; Dove *et al.*, 2002; Duex *et al.*, 2006b; Ikonomov *et al.*, 2006; Ikonomov *et al.*, 2009a; Rudge *et al.*, 2004; Rutherford *et al.*, 2006). The schematic composition and localization of the yeast Fab1p-complex and mammalian PIKfyve- or PAS-complex is represented in Figure 6.

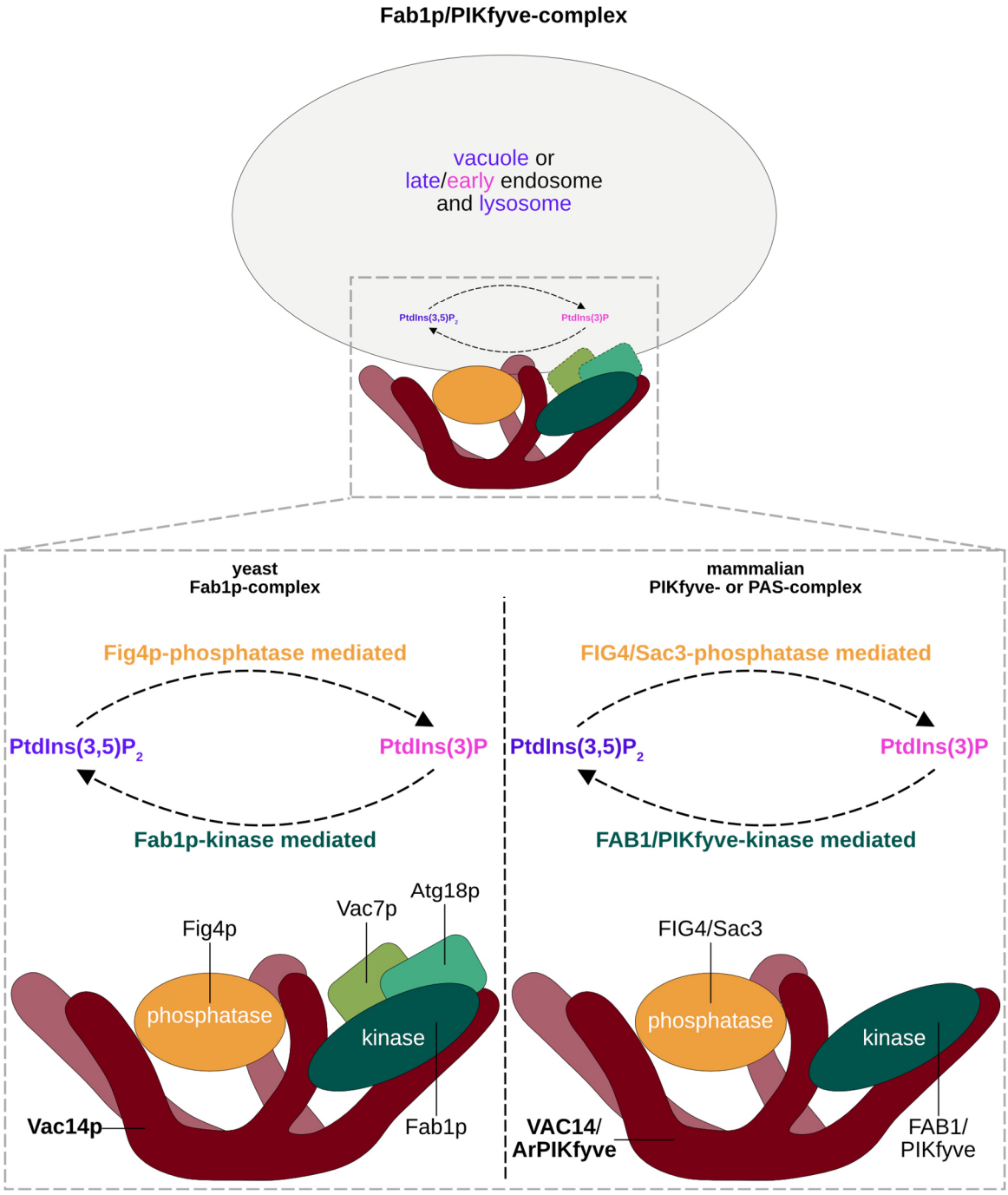

Figure 6: Structure of the Fab1p/PIKfyve-complex.
Schematic representation of the localization, function and structural organization of the Fab1p/PIKfyve-complex in yeast an mammals. Close-up of the complexes is indicated at the bottom margin. In yeast, the Fab1p-complex is located at vacuolar membranes and is composed of the PtdIns(3)P 5-kinase Fab1p (dark green), its activator Vac7p (light green) and negative regulator Atg18p (pale green), the PtdIns(3,5)P_2 phosphatase Fig4p (orange) and the scaffolding core Vac14p (dark red). In mammals, the PIKfyve- or PAS-complex localizes to early or late endosomes and lysosomes and contains the Fab1p kinase, Fig4p phosphatase and Vac14p orthologs PIKfyve (dark green), Sac3 (orange) and ArPIKfyve (dark red), respectively. The complex functions in the turnover and synthesis of PtdIns(3,5)P_2 from PtdIns(3)P at vacuolar/endolysosomal membranes. Based on Lees *et al.*, 2020.

In yeast, Vac14p was described to function as both activator and osmoregulator of Fab1p to maintain and regulate steady-state levels of PtdIns(3,5)P_2 (Bonangelino *et al.*, 2002). Moreover, mutants of *vac7*, *fab1* and *vac14* share same phenotypic effects including abnormal low or even undetectable levels of PtdIns(3,5)P_2 and defective vacuolar morphology and acidification (Bonangelino *et al.*, 2002; Duex *et al.*, 2006a; Duex *et al.*, 2006b; Gary *et al.*, 1998). In addition, Δatg18 and Δfig4 cells harbor also swollen vacuoles and low PtdIns(3,5)P_2 levels, supposedly because of defective vesicle recycling from the vacuole (Botelho *et al.*, 2008; Dove *et al.*, 2004). Furthermore, Vac14p was shown to regulate sorting of proteins into and via MVBs (Dove *et al.*, 2002).

Similarly to yeast Vac14p, the mammalian Vac14/ArPIKfyve ortholog acts as PIKfyve activator thus controlling PtdIns(3,5)P_2 accumulation (Sbrissa *et al.*, 2004). In addition, lack of or overexpression of Vac14^{wt} or the PIKfyve-binding deficient point mutant Vac14^{L156R} lead to enlarged, less acidified vacuolar structures accompanied by decreased levels of PtdIns(3,5)P_2 in mammals (Jin *et al.*, 2008; Sbrissa *et al.*, 2004; Schulze *et al.*, 2014; Zhang *et al.*, 2007). Moreover, proteins involved in endolysosomal and autophagic pathways had been identified as potential interactors of mammalian Vac14 (Schulze *et al.*, 2014).

In contrast to mammals, the Vac14p/Fab1p pathway in yeast appears to be a mechanism for adaption to sudden changes in the environmental osmolarity (Bonangelino *et al.*, 2002; Dove *et al.*, 1997). In mammals, the Vac14/PIKfyve pathway evolved rather to perform specific functions including MVB function and biogenesis since steady-state levels of PtdIns(3,5)P_2 did not increase upon hyperosmotic stress (Jones *et al.*, 1999; McEwen *et al.*, 1999). Taken together, the function of Vac14/ArPIKfyve is important for regulating the morphology of endolysosomes and vacuoles by scaffolding the Fab1p/PIKfyve-complex, which is important for proper development in yeast and mammals.

1.4 Aims of this study

Due to its diverse cellular roles and its association with serious diseases in mammals, the STRIPAK-complex has received much attention in the last years (Jeong *et al.*, 2021; Kück *et al.*, 2019). To date, not all of its interactors or effectors are known. Several potential candidates have been identified previously via pulldown experiments with the *S. macrospora* SmSTRIPAK-complex (Reschka *et al.*, 2018). In this study, the three SmSTRIPAK-dependent pulled-down proteins SmARP1, SmPOM33 and SmVAC14 should be analyzed. For this purpose, various experiments will be conducted to get a general picture of their cellular functions and subcellular localizations in *S. macrospora.*

To investigate the function of the associated genes, *S. macrospora* knockout strains should be generated. The ability of sexual development of the resulting loss-of-function mutants will be compared to the wildtype and complementation strains. Accordingly, phenotypic and quantitative analysis will be performed. In addition, stress tests should be conducted to gain further insight into the associated function of the encoded protein and connected signaling pathways. Furthermore, each protein should be fused to a fluorescent tag to allow for subcellular localization studies in *S. macrospora*. For this, *S. macrospora* strains will be transformed with the recombinant plasmids to ectopically express the fusion proteins, which in the following will be investigated by fluorescence microscopy with the help of organelle-marker proteins and dyes. Moreover, for one of the analyzed proteins, SmPOM33, pulldown experiments coupled to LC-MS analysis will be carried out to find possible interaction partners and to gain a deeper understanding of the identity of the protein.

The work on the proteins ARP1 and POM33 have been published during the time of my doctoral research and are attached in the following.

Studies regarding the third protein, VAC14, were prepared as manuscript for submission.

2. Article I: Tracking Fungal Growth: Establishment of Arp1 as a Marker for Polarity Establishment and Active Hyphal Growth in Filamentous Ascomycetes

This article represents the first subtopic of this thesis. It was authored by A. Groth, C. Schunke, E.J. Reschka, S. Pöggeler and D.E. Nordzieke. The article was published online in the Journal of Fungi (JoF) in July 2021. The full article including Supplementary information can also be found online at:
https://doi.org/10.3390/jof7070580.

Author contribution

As first author of the paper, A. Groth was involved in the methodology, validation, investigation and writing of the original draft preparation. Further, she performed experiments with *S. macrospora,* created the corresponding figures and edited as well as revised the manuscript.

Journal of Fungi

MDPI

Article

Tracking Fungal Growth: Establishment of Arp1 as a Marker for Polarity Establishment and Active Hyphal Growth in Filamentous Ascomycetes

Anika Groth [1], Carolin Schunke [1,2], Eva Johanna Reschka [1], Stefanie Pöggeler [1,*] and Daniela Elisabeth Nordzieke [1,*]

[1] Institute of Microbiology and Genetics, Genetics of Eukaryotic Microorganisms, Georg-August-University of Göttingen, Grisebachstr. 8, 37077 Göttingen, Germany; anika.gibron@stud.uni-goettingen.de (A.G.); carolin.schunke@bzh.uni-heidelberg.de (C.S.); evareschka@gmx.net (E.J.R.)
[2] Biochemistry Center, Heidelberg University, Im Neuenheimer Feld 328, 69120 Heidelberg, Germany
* Correspondence: spoegge@gwdg.de (S.P.); dnordzi@gwdg.de (D.E.N.)

Abstract: Polar growth is a key characteristic of all filamentous fungi. It allows these eukaryotes to not only effectively explore organic matter but also interact within its own colony, mating partners, and hosts. Therefore, a detailed understanding of the dynamics in polar growth establishment and maintenance is crucial for several fields of fungal research. We developed a new marker protein, the actin-related protein 1 (Arp1) fused to red and green fluorescent proteins, which allows for the tracking of polar axis establishment and active hyphal growth in microscopy approaches. To exclude a probable redundancy with known polarity markers, we compared the localizations of the Spitzenkörper (SPK) and Arp1 using an FM4-64 staining approach. As we show in applications with the coprophilous fungus *Sordaria macrospora* and the hemibiotrophic plant pathogen *Colletotrichum graminicola*, the monitoring of Arp1 can be used for detailed studies of hyphal growth dynamics and ascospore germination, the interpretation of chemotropic growth processes, and the tracking of elongating penetration pegs into plant material. Since the Arp1 marker showed the same dynamics in both fungi tested, we believe this marker can be broadly applied in fungal research to study the manifold polar growth processes determining fungal life.

Keywords: Arp1; polarity; microscopy; *Sordaria macrospora*; *Colletotrichum graminicola*; chemotropism

Citation: Groth, A.; Schunke, C.; Reschka, E.J.; Pöggeler, S.; Nordzieke, D.E. Tracking Fungal Growth: Establishment of Arp1 as a Marker for Polarity Establishment and Active Hyphal Growth in Filamentous Ascomycetes. *J. Fungi* **2021**, *7*, 580. https://doi.org/10.3390/jof7070580

Academic Editor: Aaron Neiman

Received: 6 April 2021
Accepted: 18 July 2021
Published: 20 July 2021

1. Introduction

Polar tip growth as a form of cell extension is widespread in eukaryotes and can be found in neurons, root hairs, pollen tubes, and at the apex of fungal hyphae [1,2]. In fungi, polar growth allows for not only radial growth but also hyphal network formation by branching followed by the targeted fusion of fungal cells [3,4]. Furthermore, the apical growth direction can be adapted by the sensing of light, physical contact, electrical currents, and chemicals, including nutrients, pheromones, and host-derived signals [5,6]. For plant-interacting symbionts and pathogens, the penetration peg formation and elongation outgoing from appressoria, hyphopodia (or so-called expressoria recently identified in *Epichloë festucae*) requires strict polar growth [7–11].

Before apical growth can start, cell polarity that enables the asymmetrical transport of cellular components for cell wall and plasma membrane extension must be established [1,12–14]. The recruitment of Rho-GTPase Cdc42 to the new polarity site is crucial for this process [13,15–18]. After Cdc42 accumulation, factors such as the septins and homologs of the yeast formin Bni1 are located on the new polar axis followed by the formation of actin or septin rings, respectively [19–24]. As work on *Neurospora crassa* has shown, a second Rho-GTPase, Rac1, is recruited to the polar site and regulates chemotropic growth processes, including germling and hyphal fusion [25]. A prominent molecular structure

correlated to hyphal polarity is the Spitzenkörper (SPK), a dark-phase structure close to the hyphal tip. Actin cables and microtubules (MTs), which are surrounded by vesicles either bound for fusion with the plasma membrane at the hyphal apex or endocytic vesicles involved in the recycling of membranes and proteins, are central to the SPK [11,13,26–28].

At a polar growing hypha, outward- and inward-bound traffic meet. This requires specific transportation systems for the coordination of stable polar growth [29]. Though actin and their motor protein myosin mediate short-distance transport from the SPK to the plasma membrane, long distance transport to the SPK takes places along MTs [1]. In filamentous fungi, MTs are polar structures that show a bidirectional polarity inside mature hyphae and clear plus-end polarity in the apical region [30–32]. Conserved among the eukaryotic kingdoms of life, the minus-end directed transport along MTs is dependent on the interaction of the multisubunit complexes dynein and dynactin [33]. Though dynein is the motor sitting on the MTs, different cargos are linked to the motor by dynactin. Dynactin is composed of a projecting sidearm, which interacts with the dynein motor, and a 37 nm minifilament, which binds to the cargo [33,34]. Eight monomers of actin-related protein 1, Arp1, the protein of its class that is able to form filaments, are central to the minifilament [35–37]. As was shown for *Ustilago maydis* and *Aspergillus nidulans*, cytoplasmic dynein is recruited to the plus-ends of MTs in a kinesin-dependent manner, resulting in the formation of a dynein loading zone close to the hyphal tip [38–41]. Together, dynein and dynactin allow for endoplasmic reticulum (ER)-to-Golgi vesicle trafficking, the minus-end directed transport of organelles, late and early endosomes, protein complexes, and lipid droplets, as well as the centripetal movement of virus capsids and ER–Golgi transport complexes [32–34,42,43].

In our study, we investigated the localization dynamics of the dominant dynactin component Arp1 using protein fusion constructs with the red and green fluorescence tags of TagRFP-T and mNeonGreen (mNG), respectively. As the monitoring of Arp1 in the coprophilous fungus *Sordaria macrospora* and the hemibiotrophic plant pathogen *Colletotrichum graminicola* has shown, Arp1 fusion proteins localize to tips of expanding hyphae and the sites of polar growth establishment, whereas they are absent from non-growing hyphae and future germling fusion sites. Furthermore, dynamic dot-like localization close to nuclei has indicated a role in nuclear transport and sorting. To test for the probable applicability of fluorescent Arp1 as a polarity marker, we monitored its localization during several polar growth processes, such as vegetative polar growth, ascospore germination, chemotropic growth, and penetration hyphae elongation. We additionally compared the localization of Arp1 and the SPK by co-staining with FM4-64. As our results showed, the usage of the Arp1 marker protein allows for dynamic growth processes to be followed in saprophytic and pathogenic fungal species, and it enables an improved assessment of chemotropic growth analyses. Since the Arp1 marker protein has overlapping but not identical localization characteristics compared with the SPK, we believe it will be a valuable extension to existing marker proteins.

2. Materials and Methods

2.1. Strains, Media and Growth Conditions

For the cloning and propagation of recombinant plasmids, *Escherichia coli* strain MACH1 (Thermo Fisher Scientific, Waltham, MA, USA) was used in standard culture conditions [44]. To generate recombinant plasmids via homologous recombination in yeast, positive transformants of *Saccharomyces cerevisiae* strain PJ69-4A were selected for uracil prototrophy [45,46].

S. macrospora wild-type strain DSM977 was transformed with recombinant plasmids according to the standard protocol [47]. Positive transformants were selected on media containing nourseothricin-dihydrogen sulphate (50 µg/mL, nat) (Jena Bioscience GmBH, Jena, Germany) and/or hygromycin B (110 U/mL, hyg) (Merck, Kenilworth, NJ, USA). *S. macrospora* strains were grown on liquid or solid biomalt maize medium (BMM) under continuous light conditions at 27 °C [48–50]. Crosses of *S. macrospora* strains were

performed as described previously [51]. After incubation for 7–10 d, plates were topped with an agar-plate containing nourseothricin and hygromycin B to select positive single-spore isolates.

The wild-type CgM2 strain (M1.001) of *C. graminicola* (Ces.) G. W. Wilson (teleomorph *Glomerella graminicola*) was used in this study [52]. For the generation of falcate conidia, *C. graminicola* was grown on oat meal agar (OMA) for 14–21 d at 23 °C [10]. Oval conidia, used as the basis for *C. graminicola* transformation and experimental procedures, were obtained in shaking cultures in a liquid complete medium with 0.5 M of sucrose (CMS) for two days (80 rpm and 23 °C), followed by 5–8 days of incubation in darkness [53]. For the selection of successful transformants and growth analyses, a complete medium (CM) containing nourseothricin-dihydrogen sulphate (150 µg/mL, nat; Jena Bioscience GmBH, Jena, Germany) or geneticin disulphate (G418, 400 µg/mL, gen; Carl Roth GmbH & Co. KG, Karlsruhe, Germany) was used when appropriate.

Details about all used strains are given in Table 1.

2.2. Multiple Sequence Alignment of Fungal Arp1

Multiple sequence alignments of protein sequences and neighbor joining phylogenetic analysis were performed with MAFFT version 7 [54]. A bootstrap analysis was conducted with 1000 iterations to test the tree for statistical significance. The tree was displayed with Archaeopteryx.js [55].

2.3. Construction of Plasmids

Plasmids were generated via homologous recombination in *S. cerevisiae* [45], as described previously [56], or the NEBuilder HiFi DNA Assembly Cloning Kit (New England Biolabs, Ipswich, MA, USA) according to the instruction manual. Information on all primer sequences and plasmids is provided in Tables S1 and S2, respectively.

For the construction of the pArp1-KO knockout plasmid, the Golden Gate cloning system according to Dahlmann et al., 2020, was used [57]. The 5′-(1311 bp) and 3′-(1791 bp) flanking regions of the *Smarp1* gene were amplified from *S. macrospora* wt gDNA with the Arp1-ko-5f/Arp1-ko-5r and Arp1-ko-3f/Arp1-ko-3r primer pairs, respectively. Together with the donor vector pGG-hph and the destination vector pDest-Amp, the fragments were cloned via the Golden Gate procedure [57].

To generate the pSmarp1 plasmid, a fragment (5028 bp) containing the native promotor, coding sequence and native terminator of *Smarp1* was amplified from *S. macrospora* wt gDNA with the Arp1-nat-5f/Arp1-nat-3r primer pair. The fragment was cloned into the *Xho*I-linearized pRS-nat vector [58] via homologous recombination using the PJ69-4A yeast strain [45].

The fragment containing the native promoter and coding sequence of *Smarp1* was amplified from *S. macrospora* wt gDNA using the Arp1_promotor_f/Arp1-Neo_r primer pair for the generation of the pSmarp1-mNG plasmid. The amplification of *mNG* was done with the Neo_f/Neo_TtrpC_r primer combination using the pmn-xyl plasmid [59]. The terminator of the anthranilate synthase gene *trpC* of *Aspergillus nidulans*, *TtrpC*, was amplified from the p1783-1 plasmid [60] with the TtrpC_f/TtrpC_pRS_r primer pair. The three PCR products were cloned into *Xho*I-linearized vector pRS-nat [58] via homologous recombination in the PJ69-4A yeast strain [45]. To construct the pSmarp1-TagRFP-T_nat/_hyg plasmids, the *Smarp1* promoter and coding sequence was amplified with the Arp1_5′f/Arp1_RFP_r primer pair from *S. macrospora* wt gDNA. The TagRFP-T sequence and the *A. nidulans TtrpC* were amplified using the primer pairs of RFP-f/RFP-r-trpC from pTagRFP-T_nat [61] and TrpC_F/pRS426GFPrev from p1783-1 [60], respectively. The *S. cerevisiae* strain PJ69-4A was transformed with the three amplicons and *Xho*I-linearized pRS-hyg [62] or pRS-nat [58] to generate recombinant plasmids via homologous recombination [45,46].

For the generation of the pCgarp1-TagRFP-T plasmid, three fragments were amplified for the assembly with pJet1.2 (Thermo Fisher Scientific, Waltham, MA, USA) using the NEBuilder HiFi DNA Assembly Cloning Kit (New England Biolabs). *Cgarp1*, including the

1 kb 5′ region, was amplified from CgM2 gDNA using the 5′CgArp1_pJet_fw/CgArp1_rev oligonucleotides. The coding sequence of TagRFP-T, including the *TtrpC* terminator of *A. nidulans*, was obtained from pSmarp1-TagRFP-T (TagRFP-T_CgArp1_fw/TtrpC_r). The neomycin phosphotransferase *nptII* resistance cassette, was amplified from the pII99 plasmid [63] using nptII_TtrpC_fw/PtrpC_pJet_rev. For further subcloning, *Eco*RV restriction sites were integrated in the oligonucleotide sequences of 5′CgArp1_pJet_fw and nptII_TtrpC_fw. Outgoing from pCgarp1-TagRFP-T, the pJet_gen plasmid harboring the *nptII*-resistance cassette was generated via hydrolysis with *Eco*RV and subsequent ligation of the plasmid backbone.

Primers were synthesized by Sigma-Aldrich Chemie GmbH (Taufkirchen, Germany). The DNA sequencing of the plasmids was performed by Seqlab Sequence Service Laboratories GmbH (Göttingen, Germany).

2.4. Generation of the Smarp1 Deletion Strain ΔSmarp1

To delete the *S. macrospora arp1* gene, the pArp1-KO knockout plasmid was used as a template to amplify the 4568 bp deletion cassette with the GG_KO_fw/GG_KO_rv primer pair containing the 5′- and 3′- flanking regions of *Smarp1* and the *hph* cassette. After the PCR clean-up of the amplicon, the *S. macrospora* ΔSmku70 strain was transformed with the deletion cassette to replace the *Smarp1* ORF with the *hph*-cassette. Primary transformants were crossed with the spore-color mutant fus1-1 (S23442) [64], and single-spore isolates (ssi) of ΔSmarp1 carrying hygromycin resistance were selected [51]. The verification of the absence of the *Smarp1* gene and the integration of the *hph*-cassette at the desired locus were performed with the Arp1-v5f/h3 (1578 bp) and Arp1-v5f/Arp1-vORF5-r (2170 bp) primer pairs, respectively. To check the presence of the *Smku70* gene in ΔSmarp1 after crossing, the Smku70-v1-f/ku70-ko-v3f(R) (2851 bp) primer pair was used. The deletion of ΔSmarp1 was verified via Southern hybridization hydrolyzing the gDNA of *S. macrospora* wt, ΔSmku70, and ΔSmarp1 with *Eco*RV. After electrophoresis, a capillary blot with a nylon membrane was performed at RT overnight. The 1791-bp 3′-probe was amplified from *S. macrospora* wt gDNA with the Arp1-ko-3f/Arp1-ko-3r primer pair. The labeling of probes for Southern blot experiments was done using the Amersham AlkPhos Direct Labelling and Detection Kit (GE Healthcare, Amersham RPN3680, Boston, MA, USA). Detection was performed according to the manufacturer's manual. Signals were visualized on X-ray films (Amersham Hyperfilm TM ECL; GE Healthcare, Boston, MA, USA) using an "Optimax X-ray film processor" (PROTEC GmbH & Co. KG, Oberstenfeld, Germany).

The complementation of ΔSmarp1 was performed by transformation with the pSmarp1-TagRFP-T_nat plasmid or its untagged Arp1 version, pSmarp1, resulting in the ΔSmarp1::Smarp1-TagRFP-T or ΔSmarp1::Smarp1 strains, respectively. Positive primary transformants were selected on BMM supplemented with nourseothricin and hygromycin. Crosses were performed as described previously [51].

Table 1. Strains used in this study.

Name of Strain	Genotype	Reference
Sordaria macrospora		
DSM997	*S. macrospora* wild-type (wt)	DSMZ
S23442	mutation in *fus1-1* gene, brownish ascospores, fertile	[64]
fus::RH2B	ectopic integration of pRH2B into S23442; hyg^R, pt, *Pgpd::hh2b::tdTomato::TtrpC*	[65]
wt::TagRFP-T	ectopic integration of ptRFP_nat into DSM997; nat^R, ssi, *Pccg1::TagRFP-T::TtrpC*	[61]
wt::GG-C-F-mNG	ectopic integration of pGG-C-F-mNG in DSM997; nat^R, ssi, *Pgpd::mNG::3xFLAG::TtrpC*	[59]

Table 1. *Cont.*

Name of Strain	Genotype	Reference
ΔSmku70	ΔSmku70::nat^R, fertile	[66]
Sm::Smarp1-TagRFP-T	ectopic integration of pSmarp1-TagRFP-T in DSM997; hyg^R, ssi, *Smarp1P::Smarp1::TagRFP-T::TtrpC*	this study
Sm::Smarp1-mNG	ectopic integration of pSmarp1-mNG in DSM997; nat^R, ssi, *Smarp1P::Smarp1::mNG::TtrpC*	this study
ΔSmarp1	ΔSmarp1::hyg^R, sterile	this study
ΔSmarp1::Smarp1	ectopic integration of pSmarp1 in ΔSmarp1; hyg^R, nat^R, ssi, *Smarp1P::Smarp1::Smarp1T*	this study
ΔSmarp1::Smarp1-TagRFP-T	ectopic integration of pSmarp1-TagRFP-T in ΔSmarp1; hyg^R, nat^R, ssi, *Smarp1P::Smarp1::TagRFP-T::TtrpC*	this study
Colletotrichum graminicola		
CgM2	*C. graminicola* wild-type (wt); also referred to as M1.001	[67]
CgM2::Smarp1-mNG	ectopic integration of pSmarp1-mNG in CgM2; nat^R, ssi, *Smarp1P::Smarp1::mNG::TtrpC*	this study
CgM2::Cgarp1-TagRFP-T	ectopic integration of pCgarp1-TagRFP-T in CgM2; gen^R, ssi, *Cgarp1P::Cgarp1::TagRFP-T::TtrpC*	this study

nat^R: nourseothricin resistant; hyg^R: hygromycin resistant; gen^R: geneticin disulphate resistant; ssi: single-spore isolate; pt: primary transformant; *P*: promotor region; *TtrpC*: terminator of the anthranilate synthase gene of *A. nidulans*; *Pccg1*: promoter of the *clock controlled gene 1* of *N. crassa*; *Pgpd*: promoter of the glyceraldehyde-3-phosphate dehydrogenase gene of *A. nidulans*; *mNG*: gene for green fluorescence protein monomeric NeonGreen (mNG) of *Branchiostoma lanceolatum*; *tdTomato*: gene encoding red fluorescence protein tdTomato from *Discosoma* species; *TagRFP-T*: gene for red fluorescence protein TagRFP-T of *Entacmaea quadricolor*; *hh2b*: gene for histone 2b.

2.5. Generation of S. macrospora Strains for Fluorescence Microscopy

Strains were generated by transforming wt *S. macrospora*, as described previously [47]. The ectopic integration of the pSmarp1-TagRFP-T and pSmarp1-mNG plasmids led to the selection of positive transformants on BMM supplemented with nourseothricin-dihydrogen sulphate (50 μg/mL) and/or hygromycin B (110 U/mL) (Merck, Kenilworth, NJ, USA). Primary transformants were grown over 7–9 d at 27 °C to obtain single-spore isolates, as described previously [51].

2.6. Generation of C. graminicola Strains

The pCgarp1-TagRFP-T and pSmarp1-mNG plasmids were linearized using *Not*I and *Nde*I, respectively, prior to transformation in CgM2. Protoplasts were obtained from oval conidia by cell wall digestion using a lysis enzyme of *Trichoderma harzianum*, as described previously [10]. To obtain homokaryotic transformants, colonies that had developed on CM plates supplemented with 400 μg/mL geneticin disulphate (pCgarp1-TagRFP-T) or 150 μg/mL nourseothricin-dihydrogen sulphate (pSmarp1-mNG) were allowed to conidiate on OMA. After single-spore isolation using the generated falcate conidia, resistant transformants were tested for the expression of the red or green fluorescent Arp1 fusion proteins by fluorescence microscopy.

2.7. Fluorescence Microscopy

Microscopic documentation was performed with the AxioImager M1 microscope (Zeiss, Jena, Germany) with differential interference contrast (DIC) and specific filter

sets for the detection of the fluorescent signals. Image capturing was performed with a Photometrix CoolSNAP HQ camera (Roper Scientific, Photometrics, Tucson, AZ, USA), and images were processed using ZEISS ZEN Digital Imaging (version 2.3; Zeiss). To detect the mNG signal, a 49002 Chroma filter set (exciter ET470/40x, ET525/50m, beam splitter T495lpxr) was used, and for tdTomato/TagRFP-T/FM4-64 signals, a 49005 Chroma filter set (exciter ET545/30x, emitter ET620/60 m and beam splitter T570LP) was used. For each experiment, at least three biological replicates were analyzed more than three times.

For the investigation of *S. macrospora* hyphae, the strains were grown for 24 h on BMM-covered glass slides and 2 mL of liquid BMM on top under continuous light at 27 °C. For FM4-64 (Thermo Fisher Scientific, Waltham, MA, USA) staining, the Sm::Smarp1-mNG strain was grown on solid BMM supplemented with 1.5% agarose (Biozym Scientific GmbH, Hessisch Oldendorf, Germany) at 27 °C under continuous light conditions for 24 h. Then, 100 µL of an FM4-64 solution (1 µg/mL in distilled water) was applied to the mycelium on the agar-piece and incubated for 15 min at 37 °C. For nuclei staining, DAPI (AppliChem, Darmstadt, Germany) was dissolved in distilled water to a stock solution of 1 mg/mL and further diluted with methanol to a concentration of 1 µg/mL. Incubation took place in the dark at 37 °C for 2–3 min. For time lapse studies of growing hyphae, *S. macrospora* strains were grown on BMM or Sordaria Westergaard (SWG) fructification medium [48–50] supplemented with 1.5% agarose (Biozym Scientific GmbH, Hessisch Oldendorf, Germany) under continuous light conditions for 24 h at 27 °C. For the analysis of SmArp1-mNG localization during ascospore germination, the wt::Smarp1-mNG x fus::RH2B strain was grown on BMM over 7–9 d, and discarded spores were washed down with 0.02% Tween 20. Ascospores were then plated on BMM containing 1.5% agarose, and pieces were cut out and analyzed under the fluorescence microscope after 3–4 h. Recording interval of 5 s over 20 min were used for time lapse studies. To analyze Arp1-mNG localization at nuclei, the ratio of Arp1-mNG localization close to a nucleus to the total number of nuclei was estimated for the 36 single pictures, thus resulting in Video S2.

The recording of *C. graminicola* hyphae expressing the Arp1 of *S. macrospora* C-terminally fused to mNG was performed after incubation for 3 d at 23 °C on CM covered with cellophane. The staining of these hyphae with FM4-64 (Thermo Fisher Scientific, Waltham, MA, USA) was done by the application of 100 µL of a 1 µg/mL working solution on the growing mycelium, followed by incubation for 15 min at 37 °C. For the analysis of Cgarp1-TagRFP-T localization during early germination and germling fusion, 50 µL of oval conidia (c = 5×10^7/mL) were spread on water agar (1% agarose, 1% Serva agar, and 25 mM $NaNO_3$). Incubation took place for 2 h (monitoring of young germlings) or 6 h (monitoring of CAT fusions and older germlings) at 23 °C. For time lapse studies of young germlings, a recording interval of 5 min was used. To track Cgarp1-TagRFP-T localization during plant penetration, a heat-inactivated onion epidermis covering water agar (1% agarose and 1% Serva agar) was inoculated with 10 µL drops containing 10^3 oval conidia in 0.01% Tween for 29 h at 23 °C [68]. Different layers of an infected onion epidermis were recorded at a fixed distance of 0.5 µm. All experiments were performed with a minimum of three independent replicates.

2.8. Analysis of Chemotropic Growth Using the Arp1-TagRFP-T Marker

The application of Cgarp1-TagRFP-T for the analysis of chemotropic growth was performed by confronting germlings derived from *C. graminicola* oval conidia (c = 5×10^5/mL) with a growing gradient of 50 mM glucose using a 3D-printed device, as described previously [69]. After 6 h of incubation at 23 °C with a minimum of 40 germlings/experiment, whether the tips of fungal germlings were growing to the established glucose gradient or to the solvent control (water) was determined. To allow for the discrimination of active growing germlings and to include non-germinated conidia with an established polar axis in the analysis, the localization of the Arp1-TagRFP-T maker was also tracked. In the final analysis, only germlings and conidia with a clear Arp1-TagRFP-T localization at the tip or a distinct cellular site were evaluated, respectively. In the case that one germling showed

Arp1-TagRFP-T localization at two tips, only individuals with a preferred growth direction were included into the analysis. From the obtained numbers, the chemotropic growth rate was calculated as described previously [69]. All experiments were performed with a minimum of five independent replicates. For statistical analyses, the t-test for equal variances was used for all displayed experiments.

2.9. Protein Sample Preparation and Western Blot Hybridization

S. macrospora strains were cultivated in liquid BMM and grown for 3 d at 27 °C to extract proteins from fungal mycelium. After harvesting, drying, and grinding the mycelium in liquid nitrogen, 520 µL of lysis buffer (10 mM Tris-HCl pH 7.5, 150 mM NaCl, 0.5 mM EDTA pH 8.0, 1 mM PMSF, 2 mM DTT, 0.5% NP-40, 1× protease inhibitor cocktail IV (1 tbl/50 mL, 04693132001, Mannheim, Germany), and 1× PhosSTOP™ (1 tbl/10 mL, Roche, Mannheim, Germany))/g mycelium powder were added. Together with about 200 µL of glass beads (Ø 0.25–0.5 mm; Roth GmbH, Karlsruhe, Germany), cells were lysed in the TissueLyser (Qiagen, Hilden, Germany) at 30 Hrz for 2 min. Subsequently, cells were separated from debris by centrifugation at 10,000 rpm for 15 min at 4 °C and were prepared for Western Blot analysis by adding 4× NuPAGE® LDS-SB (Thermo Fisher Scientific, Waltham, MA, USA) and 1 M DTT to the crude extract. After heating of the samples for 10 min at 70 °C, 25 µL were loaded on a 12% SDS gel. As a protein standard, the Nippon Genetics Co. Europe blue star pre-stained protein marker (NIPPON Genetics Europe, Düren, Germany) was used.

Blotting was performed using the AmershamTM ProtranTM Nitrocellulose Blotting Membrane (GE Healthcare, Little Chalfont, UK) with 1× transfer buffer and a Mini Trans-Blot® Cell device, as described by the manufacturer (Bio-Rad Laboratories, Hercules, CA, USA) [70]. The nitrocellulose membrane was blocked with 5% (*w*/*v*) skim milk powder in 1× Tris-buffered saline supplemented with 0.05% Tween 20® (TBST) for 1 h at RT. To detect antigen–antibody reactions, a primary TagRFP-T (rabbit) -antibody (1:12,500, BioCat (Evrogen, Moscow, Russia), AB233-ev) solved in 5% skim milk/TBST was used. After removing the primary antibody, the membrane was washed three times with 1× TBST for 15 min, and a horse-radish peroxidase (HRP)-coupled secondary anti rabbit-antibody (1:5000, Thermo Fisher Scientific, Waltham, MA, USA) was applied to the membrane for 1 h at RT. To detect the HRP-coupled antibodies, the ImmobilonTM Western HRP Substrate kit (Merck, Kenilworth, NJ, USA) was used. Signals were visualized on X-ray films (Amersham Hyperfilm TM ECL, Marlborough, MA, USA) using an "Optimax X-ray film processor" (PROTEC GmbH & Co. KG, Oberstenfeld, Germany).

2.10. Phenotypic Analysis

To define growth behavior and sexual development, *S. macrospora* strains were grown on solid SWG medium over 10 d and documented with a VHX-500F Digital Microscope (Keyence, Osaka, Japan). For growth-rate determination, six replicates each of *S. macrospora* wt strain, Sm::Smarp1-TagRFP-T and Sm::Smarp1-mNG, were grown in 30-cm race tubes filled with solid SWG medium over 7 d under continuous light at 27 °C. After 3 d, the growth front was marked every day at the same time to determine the growth velocity in cm/day.

For the determination of the *C. graminicola* growth rate, defined mycelial plugs of CgM2, CgM2::Arp1-TagRFP-T, and CgM2::SmArp1-mNG from pre-cultures were transferred to fresh CM plates without selection. After 3 d, the growth area was recorded using an Epson Perfection V600 Photo scanner in four subsequent days. The optical evaluation of the growth area was done using the measuring tool of Fiji [71] on scaled images. The growth rate of four replicates was determined by the difference of the growth area of two subsequent days in cm^2.

3. Results

3.1. Arp1 Deletion in S. macrospora Results in a Severe Growth Defect That Can Only Partially Be Complemented

As part of the dynactin protein complex, Arp1 is highly conserved among eukaryotes. As the performed multiple sequence alignment revealed, the Arp1 protein showed a high amino-acid identify among the clades of Ascomycota, Basidiomycota, and Mucormycota in saprophytic and pathogenic species (Table 2 and Figures S1 and S2). To characterize Arp1 in *S. macrospora*, the ΔSmarp1 deletion strain was generated by the homologous recombination of an hph-deletion cassette flanked by upstream and downstream regions of Smarp1 (Figure S3a). The resulting ΔSmarp1 strain was verified via PCR (Figure S3b) and Southern blot analysis (Figure S3c). To investigate the sexual development of the deletion strain, together with the complementation strains compared to the wt *S. macrospora*, the growth behavior was analyzed over 10 d (Figure S4a). The life cycle of wt *S. macrospora* starts with a germinating ascospore that differentiates into a vegetative mycelium. After three more days, the female gametangia (ascogonia) are produced, and one day later, the unpigmented fruiting-body precursors (protoperithecia) are formed. These develop into melanized protoperithecia, and after self-fertilization, karyogamy, meiosis, and a post-meiotic-mitosis, they mature into pear-shaped perithecia. The developmental stages of pigmented protoperithecia and pigmented mature fruiting-bodies could be observed in the wt strains after 5–10 d (Figure S4a). In contrast, the ΔSmarp1 strain was arrested in the formation of perithecia and displayed a slow growth velocity even after 10 d of incubation (Figure S4a). This severe phenotype was only partially complemented by the ectopic integration of Smarp1 with and without a fluorescence tag, although Western Blot analyses verified the expression of SmARP1-TagRFP-T in the investigated strain (Figure S4b).

Table 2. Pair-wise comparison of fungal Arp1 orthologs. Amino-acid identity is given in % from the Clustal Omega matrix of the alignment depicted in Figure S1.

	Sm	Nc	Cg	Fo	Mo	An	Ro	Ml	Cc	Sco	Cn	Um	Pc	Sp	Ca	Sc
Sm	100	100	93	92	88	78	74	74	70	73	71	74	74	51	56	50
Nc		100	92	91	88	78	74	74	70	73	71	71	74	51	56	50
Cg			100	94	87	79	74	74	69	73	71	73	76	52	57	51
Fo				100	87	78	74	74	70	74	72	74	75	51	57	50
Mo					100	78	74	75	69	70	70	73	74	51	59	52
An						100	73	74	68	72	71	71	71	50	58	51
Ro							100	99	77	81	79	81	82	54	60	50
Ml								100	77	82	78	82	81	54	60	50
Cc									100	87	80	78	74	49	54	48
Sco										100	83	82	77	52	58	51
Cn											100	80	74	52	59	50
Um												100	78	55	60	52
Pc													100	56	58	51
Sp														100	47	44
Ca															100	53
Sc																100

Abbreviations: Sm, *Sordaria macrospora*; Nc, *Neurospora crassa*; Cg, *Colletotricum graminicola*; Fo, *Fusarium oxysporum* f. sp. *Lycopersici*; Mo, *Magnaporthe oryzae*; An, *Aspergillus nidulans*; Sc, *Saccharomyces cerevisiae*; Ca, *Candida albicans*; Pc, *Pneumocystis carinii*, Sp, *Schizzosaccharomyces pombe*; Cn, *Cryptococcus neoformans* var. *grubii*; Um, *Ustilago maydis*; Cc, *Coprinopsis cinerea*; Sco, *Schizophyllum commune*; Ro, *Rhizopus oryzae*; Ml, *Mucor lusitanicus*.

3.2. SmArp1 Localization Is a Dynamic Process at Growing Hyphal Tips and in Proximity to the Nucleus

Fluorescence microscopy was performed to determine the cellular localization of SmArp1-TagRFP-T. The fusion construct predominantly localizes as subapical structures in the tips of growing hyphae (Figure 1a). The application of a higher imaging contrast allowed for the further determination of dot-like structures apart from hyphal tips (Figure 1a). To confirm that the SmArp1 localization was independent of the used fluorophore, we replaced TagRFP-T by a C-terminal fused mNG, a monomeric green fluorescent protein derived from the lancelet *Branchiostoma lanceolatum* [59]. SmArp1-mNG localized dynamically to growing hyphal tips (Figure S5 and Video S1). To exclude probable side effects on *S. macrospora* due to the expressed fusion constructs, growth rates were determined using race tubes. No difference in growth was seen in Sm::Smarp1-TagRFP-T (3.5 ± 0.29 cm) or Sm::Smarp1-mNG (3.1 ± 0.31 cm) compared to the wild-type strain (3.4 ± 0.27 cm). The co-staining of Sm::SmArp1-TagRFP-T with DAPI (Figure 1b) and co-expression experiments with a red fluorescent histone marker (RH2B tdTomato) were performed to address the dot-like localization pattern (Figure 1c). Both experiments showed that SmArp1-TagRFP-T localized to small dots close to nuclei that moved retrograde from the tip to the inner hypha (Figure 1c and Video S2). Moreover, the evaluation of the 36 single pictures of Video S2 revealed that 6–46% of nuclei showed a close-by SmArp1-mNG localization, emphasizing that the association of Arp1 to nuclei is a highly dynamic process.

3.3. Dynamic Localization of Arp1 in C. graminicola

To follow the hypothesis that Arp1 fused to a fluorescent protein can be used as a universal marker for active growing hyphae in fungi, we chose to transform the pSmarp1-mNG plasmid into the wild-type CgM2 strain of the plant pathogen *C. graminicola*. Comparable to *S. macrospora*, the expression of Smarp1-mNG resulted in a subapical localization at the hyphal tip (Figure 2a), indicating a conserved localization among ascomycetous fungi. For the detailed investigation of localization during *C. graminicola* development and pathogenicity, CgM2 was transformed with the *C. graminicola* arp1 gene (Cgarp1) fused to TagRFP-T under the control of its native promoter. The resulting CgM2::Cgarp1-TagRFP-T strain showed a highly dynamic CgArp1 localization to growing tips of germlings. Hyphae arrested in growth completely lost tip localization (Figure 2b). At the same time, new Cgarp1-TagRFP-T patches appeared on new branching sites, following the new polar axis and indicating the current growth direction (Figure 2b and Video S3). Similar to findings for *S. macrospora*, the expression of both Arp1 fusion proteins did not result in aberrant growth patterns of *C. graminicola* transformants (CgM2: 9.9 ± 1.7 cm^2; CgM2::Smarp1-mNG: 9.8 ± 2.2 cm^2; CgM2::Cgarp1-TagRFP-T: 9.2 ± 1.6 cm^2).

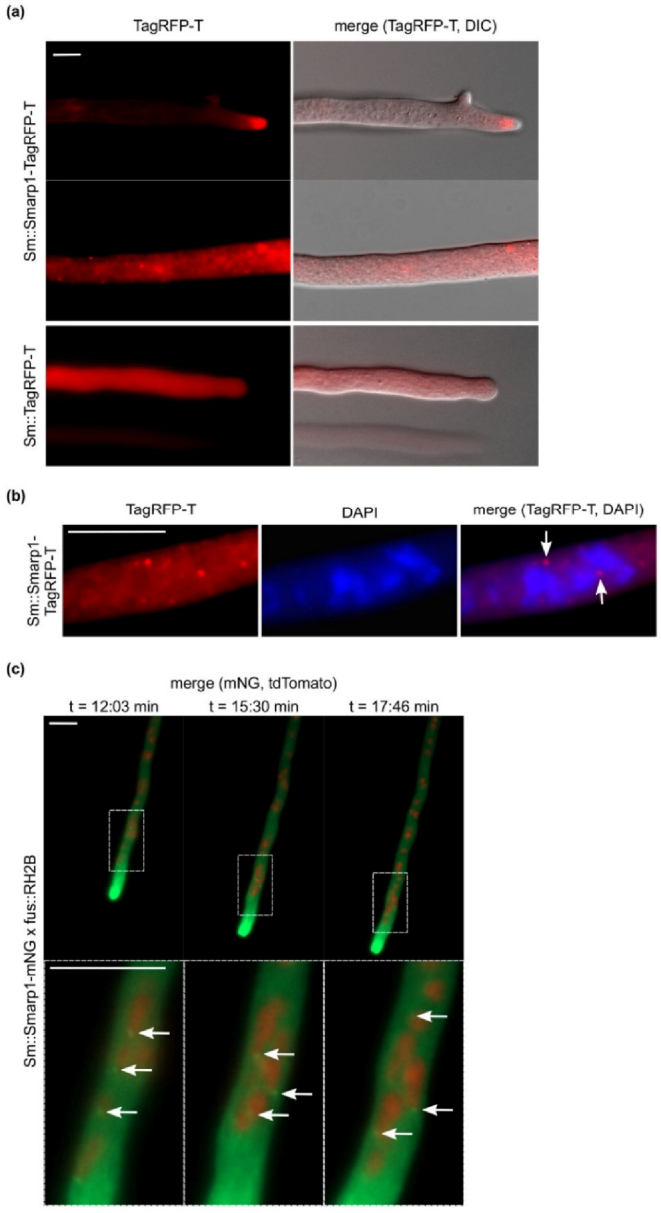

Figure 1. The localization of Arp1 in *S. macrospora* and the heterologous expression of pSmarp1-TagRFP-T or pSmarp1-mNG in wild-type *S. macrospora* hyphae: a recording of hyphae from growing strains on BMM-covered glass slides (**a**,**b**) or on BMM agar supplemented with agarose (**c**) after incubation for 24 h at 27 °C. (**a**) SmArp1-TagRFP-T shows subapical localization at the hyphal tip and as puncta-like structures in the hyphae. TagRFP-T expression served as the control. (**b**) The nuclear localization of SmArp1-TagRFP-T is marked by arrows. Nuclei were stained with DAPI. (**c**) Selected images of Video S2 showing the dynamic localization of SmArp1-mNG in growing hyphae after 24 h of incubation on BMM agar at 27 °C. The nuclear localization of SmArp1-mNG is indicated by arrows. Nuclei are labeled by histone 2B with tdTomato (RH2B), size bar = 10 μm.

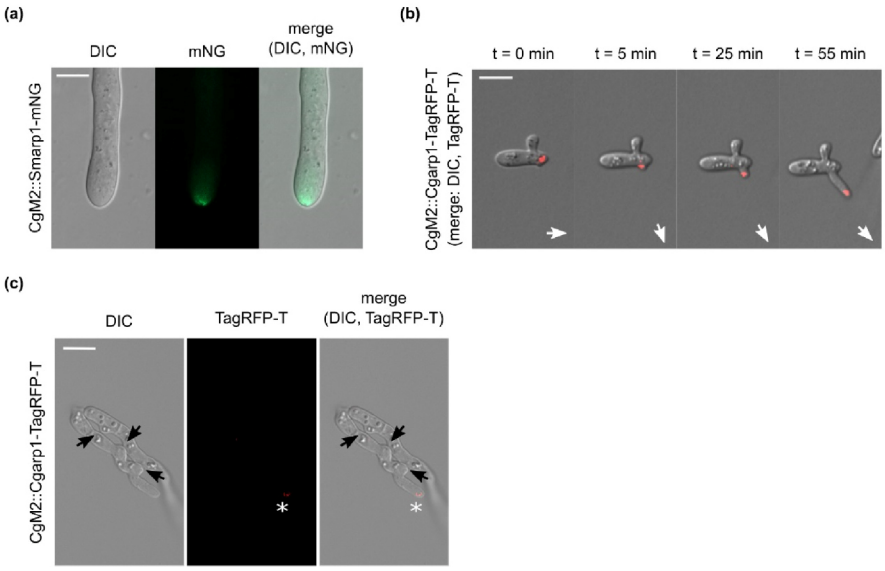

Figure 2. The localization of Arp1 in *C. graminicola*: (**a**) the heterologous expression of pSmarp1-mNG in wild-type *C. graminicola* CgM2 hyphae. Recording of hyphae from growing colonies on CM covered with cellophane after incubation for 3 d at 23 °C: (**b**) selected images of Video S3 showing the dynamic localization of CgArp1-TagRFP-T in growing germlings after 2 h of incubation on water agar at 23 °C. Recording interval = 5 min; polar growth axis is indicated by white arrows. (**c**) Arp1-RFP-T localization in *C. graminicola* germlings attempting for germling fusion. Germlings derived from oval conidia incubated for 6 h at 23 °C on water agar (50 µL, c = 5×10^7/mL). The localization of Arp1-TagRFP-T at the tip is indicated with *. Probable future fusion sites are indicated with black arrows; size bar = 10 µm.

3.4. Absence of CgArp1 localization to C. graminicola future fusion points

Germling fusion is a highly dynamic process resulting in the formation of conidial anastomosis tubes (CATs) that link germinating conidia during early colony development [72]. This process includes the recognition of a probable fusion partner by a so-far unknown signal and the stepwise growth towards the counterpart in the chemotropic phase of the process [73]. Due to the observed correlation between CgArp1 localization to the polar sites of the fungal cell, we speculated about a probable localization in chemotropically active germlings during the CAT formation process. However, we were never able to monitor a clear localization of CgArp1 during germling interactions (Figure 2c), indicating a fundamental difference between growing hyphae and the fusion of CATs.

3.5. Arp1 Localizes Subapical to SPK

The SPK, a highly organized structure at the hyphal apex that is mostly composed of secretory vesicles, is broadly used to determine active hyphal growth, growth direction, germination, and branching site selection [28,74–77]. To compare the localization of Arp1 and the SPK, we stained *S. macrospora* strains expressing SmArp1-mNG with the red fluorescent, membrane-selective dye FM4-64 [78,79]. As depicted in Figure 3, staining with FM4-64 predominantly visualized the SPK (a dense structure at the hyphal apex) and, to a lesser extent, intracellular membranes. The overlay with SmArp1-mNG revealed that Arp1 localizes just behind the SPK, verifying its subapical localization. An analogous experiment with CgM2::Smarp1-mNG showed the same cellular localization (Figure S6).

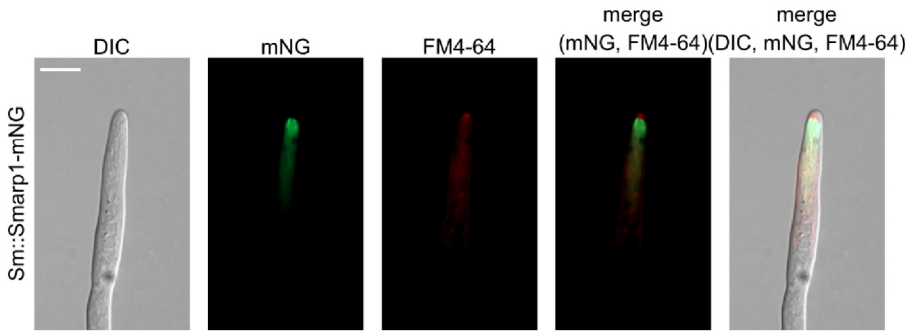

Figure 3. The localization of SmArp1-mNG together with FM4-64-stained hyphae in *S. macrospora*. The expression of pSmarp1-mNG in wild-type *S. macrospora* hyphae stained with FM4-64 (1 µg/mL in distilled water) and incubated for 15 min at 37 °C. The recording of hyphae was performed after growing on solid agarose-BMM for 24 h at 27 °C under continuous light conditions; scale bar = 10 µm.

3.6. S. macrospora Arp1 Shows Dynamic Localization during Ascospore Germination

Based on the localization of Arp1 in actively growing hyphae, its association with the nucleus, and its subapical localization, we assumed that it could serve as a complementing marker protein in the highly polar processes of fungal development and pathogenicity. To visualize the localization of Arp1 during the ascospore germination of *S. macrospora*, Smarp1-mNG and nuclei marked with tdTomato (RH2B) fused to histone 2B were recorded in a wild-type background (Video S4). After meiosis and a post-meiotic mitosis, the asci of *S. macrospora* were found to contain eight nuclei that were surrounded by the spore wall. Subsequently, iterate mitoses led to multiple nuclei in each ascospore. During germination, spores form one germination vesicle at one side of the ascospore. While the size of the germination vesicles increases, multiple nuclei of the ascospore are released to the vesicle. Finally, hyphae start growing form the germination vesicle [80].

During this highly dynamic germination process, we tracked SmArp1-mNG localization to four different sites and structures of the germination vesicle and the emerging hypha (Figure 4). First, Arp1 fluorescent signals appeared close to nuclei. Moreover, SmArp1-mNG localized at the growing hyphal tip, moving as dot-like structures in anterograde and retrograde directions. Third, a quickly emerging and disseminating fluorescent filamentous signal appeared in the germination vesicle. Additionally, a probable microtubule organization center (MTOC) was found to dominate the germination vesicle.

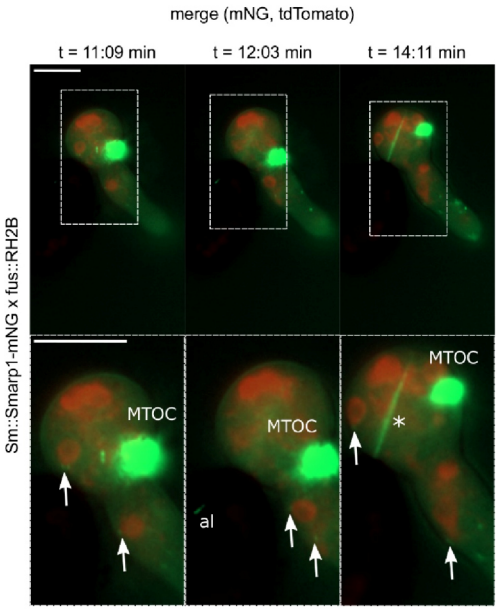

Figure 4. The dynamic localization of SmArp1-mNG in germinating *S. macrospora* ascospores. Selected images of Video S4, which tracks the germination of *S. macrospora* ascospores expressing *Smarp1-mNG* and red fluorescent histone 2B (RH2B tdTomato) on BMM-agar supplemented with agarose after incubation for 3–4 h at 27 °C. Arrows = localization of SmArp1-mNG close to nuclei; MTOC= putative microtubule organization center; al = SmArp1-mNG localization inside the ascospore; asterisk = SmArp1-mNG localization in fast appearing and dispersing linear structures; size bars = 10 μm; recording interval = 5 s.

3.7. Analysis of Chemotropic Growth Is Improved by the Usage of the Arp1-TagRFP-T Marker

Chemotropic growth to nutrient sources, mating partners, and hosts is a fundamental process in fungi [6]. However, the assessment of the chemoattractive signal as well as cellular factors involved in signal recognition is not trivial. Recently, we established a new, easily applicable method using a 3D-printed device based on the chemotropic assay developed by Turrà et al., 2015 [69,81]. In our approach, growing *C. graminicola* germlings are confronted with a signal gradient that can be sensed over time, resulting in growth re-direction. Using a hyphal tip projection angle to a theoretical vertical line, whether a germling is growing towards the signal gradient (1–179°), is repelled by it (181–359°), or shows a neutral orientation (0°/360° and 180° [69]) can be determined. The application of this method results in *C. graminicola* germlings with a strong chemotropic growth rate when 50 mM of glucose is used as chemoattractant, whereas the growth direction of germlings is uniform in control experiments with water, as depicted by a chemotropic rate of about 50% [69].

Despite its significance, this evaluation mode does not differentiate between germlings showing active growth re-direction due to signal sensing and germlings that stopped their growth during incubation time and are not actively sensing. Furthermore, in these experiments, we often observed germlings that grew bi-directionally, which could not be included in the evaluation since a clear readout was missing (Figure 5a).

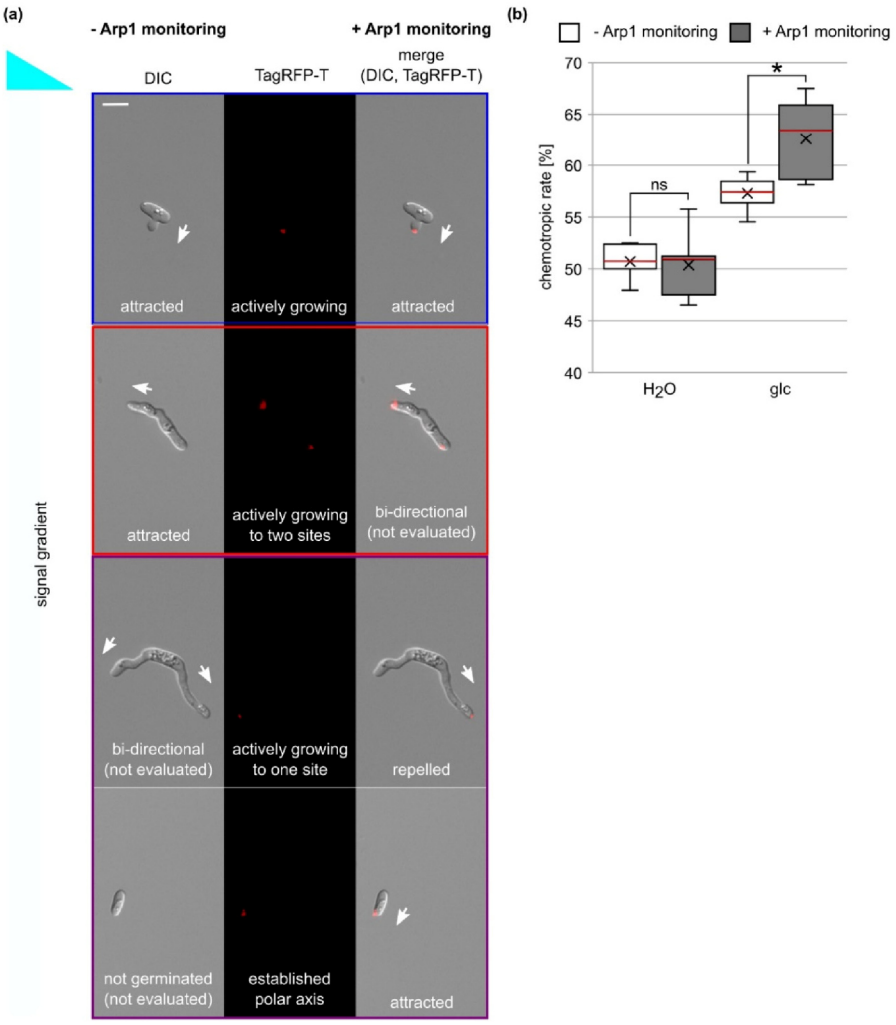

Figure 5. Enhanced evaluation of *C. graminicola* chemotropic growth by the application of the Arp1 marker: (**a**) the evaluation of growth direction of germlings based on microscopic analyses without (−) and with (+) Arp1 monitoring. The tip localization of Arp1-TagRFP-T was used as an indication for active growth or established polar axis. Blue box = same evaluation of results in (−) and (+); red box = different evaluation results in (−) and (+); violet box = germlings or non-germinated conidia that can be included in the (+) evaluation in contrast to (−); size bar = 10 µm. (**b**) The chemotropic rates of germlings to gradients of water (H_2O) and 50 mM glucose (glc) after incubation for 6 h at 23 °C obtained from experiments without (−) and with (+) the monitoring of the fluorescent Arp1 marker. Chemotropic rate: <50% = repulsion; = 50% = no growth reaction; >50% = attraction; meridian is indicated in red; average is indicated by x; $n \geq 5$; *, $p < 0.05$; ns = not significant.

Due to correlation between Arp1 tip localization and active growth or polarity axis establishment, we tested whether the usage of the Arp1 localization marker allowed us to improve the readout quality of the chemotropic assay. As depicted in Figure 5a, the localization of CgArp1-TagRFP-T to the tip often, but not always, corresponded to growth direction. In the case of bi-directional growing germlings, it allowed us to determine the current growth direction solely indicated by CgArp1-TagRFP-T localization to one hyphal tip. Interestingly, we also found that non-germinating conidia displayed a clear CgArp1-

RFP-T localization to one cellular site or displayed a rather scattered localization of Arp1. Anticipating the clear targeted localization to mark the current polar axis, we were also able to include those conidia into the evaluation (Figure 5a and Figure S7, and Videos S5 and S6). To test whether the integration of the CgArp1-TagRFP-T marker changed the determined chemotropic rate, we used this strain in experiments with a 50 mM glucose gradient and experiments with no-signal control (Figure 5b). For five replicates in which at least 40 germlings were evaluated for their dominant growth direction, we monitored DIC and TagRFP-T channel information and saved them for further analysis. In a first evaluation, we referred to the information obtained from DIC channel and analyzed chemotropic growth as described earlier [69]. This quantification resulted in chemotropic rates of 50.7% ± 1.7% (water control) and 57.3 % ± 1.6 % (50 mM glucose). In a second step, we used the same microscopic pictures for a renewed evaluation, and we integrated the information gained from the Arp1 monitoring. The exclusive integration of germlings or conidia with a clear CgArp1-TagRFP-T signal in the tip or a distinct cellular site resulted in a significant increase of the chemotropic rate to 50 mM glucose (62.6% ± 3.7%; $p = 0.01$), whereas no significant changes were observed in the control experiments (50.4% ± 3.3%; $p = 0.86$). From these results, we conclude that application of the Arp1 marker can be used to increase sensitivity to analyses of chemotropic growth.

3.8. Tracking of Penetration Hyphae into Plant Tissue by Monitoring of Arp1 Localization in C. graminicola

For plant pathogens such as *C. graminicola*, the penetration of plant tissue by appressoria emerging from conidia or hyphae-derived hyphopodia marks an early step of infection. Both appressoria and hyphopodia are specialized structures that are able to build up high turgor pressure [10]. Just prior to the penetration of a plant cell, the polarity of the penetration structure shifts to a predetermined breaking point. There, a penetration pore opens and the penetration peg emerges. In a second phase, the peg develops into a penetration hypha that pushes deeper into the plant tissue [9,82]. Since a distinct signaling network regulates penetration hyphae elongation [83,84], the tracking of its path into plant tissue might help to gain important insights about the role of certain molecular players. To test whether the Arp1 marker enables such an approach, we incubated oval conidia of CgM2::Cgarp1-TagRPF-T on a heat-inactivated onion epidermis. Using stack imaging, we were able to follow the penetration hyphae from its site of emergence into plant tissue. In addition to some dot-like, dynamic CgArp1-TagRFP-T localization patches, we observed a bright fluorescent signal at the subapical tip region, indicating the current growth direction (Figure 6 and Video S7).

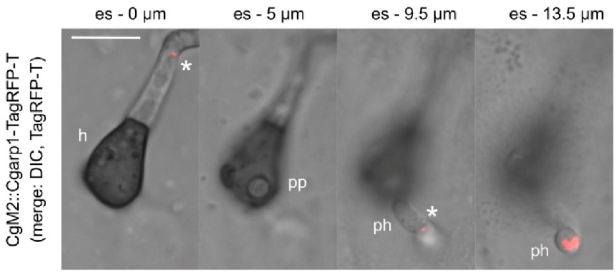

Figure 6. The visualization of penetration hyphae dynamics during onion epidermis perforation: 10^3 oval conidia of *C. graminicola* CgM2::Cgarp1-TagRFP-T were inoculated on a heat-inactivated onion epidermis overlaying water agar for 29 h at 23 °C. Different layers were recorded at a fixed distance of 0.5 µm originating from the epidermal surface (es). In the selected images of Video S7, size bar = 10 µm; h = hyphopodium; pp = penetration pore; ph = penetration hyphae; * non-tip localization of Arp1-TagRFP-T.

4. Discussion

In most fungi, MTs are organized by the nuclear membrane-embedded spindle pole body (SPB), also referred to as the MTOC, and found as part of intranuclear spindles and tracks within the cytoplasm [85,86]. Consequently, we monitored fluorescently labelled dynactin complex component Arp1 at distinct sites in the filaments of germlings and mature hyphae of two ascomycetous fungi, *S. macrospora* and *C. graminicola*. Highly prominent and independent of the used fluorophore, a dynamic localization of Arp1 to the subapical part of the hyphal tip was found to be correlated with an active growth of hyphae (Figures 1 and 2). A similar localization was reported for *A. nidulans* expressing a GFP-tagged version of the dynein heavy chain *nudA* [87]. Additionally in axons and migrating fibroblasts during wound healing, Arp1 is enriched in the leading edge of polar growing cells [88,89]. Since the accumulation of dynactin and polarity establishment in axons and fibroblasts are simultaneous processes, it has been proposed that the dynein/dynactin complex is involved in microtubule orientation and transport rather than being a passive motor running along microtubule rails [90]. Additionally, in the corn-smut fungus *Ustilago maydis*, such a dependence of microtubule motility on the motor dynein was proposed [91], indicating a conservation of this interaction.

This hypothesis is consistent with the observed drastic reduced growth in ΔSmarp1, a phenotype previously reported for Δro-4, an arp1 deletion mutant generated in *N. crassa* (Figure S4) [92]. Additionally, our Arp1 localization studies in the conidia and germlings of *C. graminicola* support a role for Arp1 in transport along MTs, as well as an active role in MT organization (Figure 2). In *C. graminicola*, we observed a shift of Arp1-TagRFP-T accumulation to a new branching site before actual growth had begun.

Likewise, in the use of the Arp1-TagRPF-T marker in chemotropic growth analyses, we observed that several conidia that had not yet been germinated showed a strong and distinct localization of Arp1 to one distinct cellular site, different to dormant conidia with a uniform Arp1 localization (Figure 5 and Figure S7). Similar observations have been made for the cell end marker tea from *A. nidulans*, which appears at the future germination site prior to germ tube formation. *Tea* deletion mutant analysis showed a rather uncontrolled germination pattern at multiple sites, indicating a misfunction in polarity establishment and microtubule organization [93]. Direct evidence for dynein and dynactin in microtubule organization in filamentous fungi was derived from a study by Riquelme and co-workers (2000) in which functional dynein or dynactin complexes were correlated with fast hyphal expansion, stable polar growth, and SPK assembly [94]. To characterize the localization of Arp1 in regard to the SPK, we stained hyphae of *S. macrospora* and *C. graminicola* expressing green fluorescent Arp1 with the membrane-selective dye FM4-64. Interestingly, Arp1 was found to localize just behind the SPK in both fungi and seems to be embedded within this vesicle organization's center. These observations are consistent with the role of dynein/dynactin in the retrograde transport of endosomal vesicles from the hyphal apex [38,41,95]. However, Arp1 and the SPK are involved in overlapping but not identical cellular functions, whereas the SPK is absent from very young germlings and correlates with germling length in *N. crassa* [96], so we also monitored fluorescent Arp1 in very young germlings of *C. graminicola* (Figure 2). Furthermore, whereas the SPK is visible at protrusions marking future cellular fusion points in *N. crassa* [97], we were not able to monitor fluorescent Arp1 at these cellular sites. This finding is in line with previous studies providing evidence that MTs are dispensable for germling communication and fusion in *N. crassa* [98]. Instead, actin patches and cables associated with endocytic vesicles and exocytosis, respectively, are enriched at germling protrusions in that fungus [98–100].

In addition to the importance of MTs for polarity establishment and growth, they also provide a basis for the transport of various cellular components [34]. Among others, they organize nuclear distribution along the hyphae [43,101]. In this study, we observed dynamic dot-like Arp1 patches in the mature hyphae of *S. macrospora*, which are associated with nuclei and nuclear movement in both hyphae (Figure 1) and germinating *S. macrospora* ascospores (Figure 4). Our findings are supported by an early study of Plamann and

coworkers, in which *N. crassa* deletion mutants of dynein and dynactin components were investigated [43]. Phenotypes of both mutants defective in either the heavy chain of cytoplasmatic dynein (ro-1) or arp1 showed defects in polar growth, as well as evenly nuclear distribution along the fungal hyphae. Intriguingly, both deletion mutants showed a segmented accumulation of nuclei leaving other hyphal segments nuclei-free [43]. In *A. nidulans*, the coiled-coil protein ApsB is attached to the nuclei in an Arp1-like fashion during their transport along MTs and has been shown to regulate nuclear migration [101–103]. However, instead of localizing to the poles of the mitotic spindle, as with ApsB [102], fluorescent Arp1-mNG seemed to localize to the dynamic spindle itself in some cases, as well as to a probable MTOC in the germination vesicle (Figure 4). Though the localization of the dynein/dynactin complex to the spindle has been shown by various studies [104], such a dense Arp1 accumulation has not been monitored to date. However, one might speculate that this dense structure in the germination vesicle is potentially involved in the organized sorting of nuclei into the emerging hyphae and might be ascospore-specific. Intriguingly, this structure does not leave the vesicle, indicating that it might be a specific cellular structure required for ascospore germination. To investigate processes regarding ascospore germination in greater depth, further investigations are required.

5. Conclusions

Polar growth is critical for filamentous fungi and takes part in manifold processes determining fungal development and pathogenicity. Through detailed localization studies of the two filamentous fungi *S. macrospora* and *C. graminicola*, Arp1, we have provided evidence that the central component of dynactin marks sites of polarity establishment and active polar growth in filamentous fungi. Additionally, Arp1 attaches to nuclei and forms a so-far unknown structure that is probably involved in organelle sorting in germinating ascospores. Though fluorescently-tagged Arp1 shares some characteristics with established polarity markers, its localization shows some unique patterns, which makes this new marker valuable for the investigation of polar growth processes including chemotropic growth, plant penetration, and ascospore germination.

Supplementary Materials: The following are available online at https://www.mdpi.com/article/10.3390/jof7070580/s1: Figure S1: CLUSTAL Omega (1.2.4) multiple sequence alignment of fungal ARP1 orthologs; Figure S2: Phylogenetic tree of Arp1 orthologs from fungi; Figure S3: Verification of *S. macrospora Smarp1* deletion by PCR and Southern blot analysis; Figure S4: Growth of *S. macrospora* ΔSmarp1 and complementing strains and corresponding expression controls via Western blot analysis; Figure S5: Localization of SmArp1-mNG and free mNG in *S. macrospora*; Figure S6: Localization of Arp1 and FM4-64 in *C. graminicola*. Heterologous expression of pSmarp1-mNG in *C. graminicola* wild-type CgM2 hyphae; Figure S7: Localization of Arp1 in unpolarized, non-germinated oval conidia of *C. graminicola*; Table S1: Oligonucleotides used in this study; Table S2: Plasmids used in this study; Video S1: Dynamic localization of SmArp1-mNG to growing hyphal tips; Video S2: Nuclear localization of SmArp1-mNG. Heterologous expression of *pSmarp1-mNG* in *S. macrospora* wild-type hyphae; Video S3: Dynamic localization of CgArp1-TagRFP-T in growing *C. graminicola* germlings; Video S4: Dynamic localization of SmArp1-mNG in *S. macrospora* germinating ascospores; Video S5: Establishment of a polar Arp1-TagRFP-T localization prior to germination of *C. graminicola*; Video S6: Tracking of Arp1-RFP-T during the germination of *C. graminicola* oval conidia; Video S7: Visualization of *C. graminicola* penetration hyphae dynamics during onion epidermis perforation.

Author Contributions: Conceptualization, D.E.N. and S.P.; methodology, A.G., C.S., E.J.R., and D.E.N.; validation, D.E.N., A.G., and S.P.; investigation, A.G. and D.E.N.; resources, D.E.N. and S.P.; writing—original draft preparation, A.G. and D.E.N.; writing—review and editing, A.G., C.S., E.J.R., S.P., and D.E.N.; supervision, D.E.N. and S.P.; funding acquisition, D.E.N. and S.P. All authors have read and agreed to the published version of the manuscript.

Funding: This work was funded by the Deutsche Forschungsgemeinschaft (Bonn-Bad Godesberg, projects NO 1230/3-1 (447175909) and PO 523/9-1 (429272002)). We acknowledge support by the Open Access Publication Funds of the Göttingen University.

Institutional Review Board Statement: Not applicable.

Informed Consent Statement: Not applicable.

Data Availability Statement: The data presented in this study are available on request from the corresponding author.

Acknowledgments: We are grateful to Gertrud Stahlhut and Gabriele Beyer for excellent technical assistance. We also thank Anja Raschke, Institute for Agricultural and Nutritional Sciences, Martin-Luther-University Halle-Wittenberg, for sharing the protocol for *C. graminicola* onion epidermis infection.

Conflicts of Interest: The authors declare no conflict of interest. The funders had no role in the design of the study, the conducted analyses, the interpretation of data, the writing of the manuscript, or in the decision to publish the results.

References

1. Riquelme, M. Tip growth in filamentous fungi: A road trip to the apex. *Annu. Rev. Microbiol.* **2013**, *67*, 587–609. [CrossRef] [PubMed]
2. Fischer, R.; Zekert, N.; Takeshita, N. Polarized growth in fungi-interplay between the cytoskeleton, positional markers and membrane domains. *Mol. Microbiol.* **2008**, *68*, 813–826. [CrossRef]
3. Mela, A.P.; Rico-Ramírez, A.M.; Glass, N.L. Syncytia in Fungi. *Cells* **2020**, *9*, 2255. [CrossRef]
4. Lichius, A.; Lord, K.M. Chemoattractive mechanisms in filamentous fungi. *Open Mycol. J.* **2014**, *8*, 28–57. [CrossRef]
5. Brand, A.; Gow, N.A. Mechanisms of hypha orientation of fungi. *Curr. Opin. Microbiol.* **2009**, *12*, 350–357. [CrossRef] [PubMed]
6. Turrà, D.; Nordzieke, D.; Vitale, S.; El Ghalid, M.; Di Pietro, A. Hyphal chemotropism in fungal pathogenicity. *Semin. Cell Dev. Biol.* **2016**, *57*, 69–75. [CrossRef] [PubMed]
7. Becker, M.; Becker, Y.; Green, K.; Scott, B. The endophytic symbiont *Epichloe festucae* establishes an epiphyllous net on the surface of *Lolium perenne* leaves by development of an expressorium, an appressorium-like leaf exit structure. *New Phytol.* **2016**, *211*, 240–254. [CrossRef]
8. Zhao, Y.L.; Zhou, T.T.; Guo, H.S. Hyphopodium-specific VdNoxB/VdPls1-Dependent ROS-Ca^{2+} signaling is required for plant infection by *Verticillium dahliae*. *PLoS Pathog.* **2016**, *12*, e1005793. [CrossRef]
9. Ryder, L.S.; Talbot, N.J. Regulation of appressorium development in pathogenic fungi. *Curr. Opin. Plant Biol.* **2015**, *26*, 8–13. [CrossRef]
10. Werner, S.; Sugui, J.A.; Steinberg, G.; Deising, H.B. A chitin synthase with a myosin-like motor domain is essential for hyphal growth, appressorium differentiation, and pathogenicity of the maize anthracnose fungus *Colletotrichum graminicola*. *Mol. Plant Microbe Interact.* **2007**, *20*, 1555–1567. [CrossRef]
11. Riquelme, M.; Aguirre, J.; Bartnicki-García, S.; Braus, G.H.; Feldbrügge, M.; Fleig, U.; Hansberg, W.; Herrera-Estrella, A.; Kamper, J.; Kück, U.; et al. Fungal morphogenesis, from the polarized growth of hyphae to complex reproduction and infection structures. *Microbiol. Mol. Biol. Rev.* **2018**, *82*, e00068-17. [CrossRef]
12. Higuchi, Y.; Shoji, J.Y.; Arioka, M.; Kitamoto, K. Endocytosis is crucial for cell polarity and apical membrane recycling in the filamentous fungus *Aspergillus oryzae*. *Eukaryot. Cell* **2009**, *8*, 37–46. [CrossRef]
13. Momany, M. Polarity in filamentous fungi: Establishment, maintenance and new axes. *Curr. Opin. Microbiol.* **2002**, *5*, 580–585. [CrossRef]
14. Riquelme, M.; Martínez-Núñez, L. Hyphal ontogeny in Neurospora crassa: A model organism for all seasons. *F1000Research* **2016**, *5*, 2801. [CrossRef] [PubMed]
15. Wendland, J.; Philippsen, P. Cell polarity and hyphal morphogenesis are controlled by multiple rho-protein modules in the filamentous ascomycete *Ashbya gossypii*. *Genetics* **2001**, *157*, 601–610. [CrossRef] [PubMed]
16. Woods, B.; Lew, D.J. Polarity establishment by Cdc42: Key roles for positive feedback and differential mobility. *Small GTPases* **2019**, *10*, 130–137. [CrossRef] [PubMed]
17. Miller, K.E.; Kang, P.J.; Park, H.-O. Regulation of Cdc42 for polarized growth in budding yeast. *Microb. Cell* **2020**, *7*, 175. [CrossRef] [PubMed]
18. Harris, S.D. Cdc42/Rho GTPases in fungi: Variations on a common theme. *Mol. Microbiol.* **2011**, *79*, 1123–1127. [CrossRef]
19. Drees, B.L.; Sundin, B.; Brazeau, E.; Caviston, J.P.; Chen, G.C.; Guo, W.; Kozminski, K.G.; Lau, M.W.; Moskow, J.J.; Tong, A.; et al. A protein interaction map for cell polarity development. *J. Cell Biol.* **2001**, *154*, 549–571. [CrossRef] [PubMed]
20. Martin, S.G.; Arkowitz, R.A. Cell polarization in budding and fission yeasts. *FEMS Microbiol. Rev.* **2014**, *38*, 228–253. [CrossRef]
21. Sharpless, K.E.; Harris, S.D. Functional characterization and localization of the *Aspergillus nidulans* formin SEPA. *Mol. Biol. Cell* **2002**, *13*, 469–479. [CrossRef] [PubMed]
22. Lichius, A.; Yáñez-Gutiérrez, M.E.; Read, N.D.; Castro-Longoria, E. Comparative live-cell imaging analyses of SPA-2, BUD-6 and BNI-1 in *Neurospora crassa* reveal novel features of the filamentous fungal polarisome. *PLoS ONE* **2012**, *7*, e30372. [CrossRef]
23. Giesbert, S.; Siegmund, U.; Schumacher, J.; Kokkelink, L.; Tudzynski, P. Functional analysis of BcBem1 and its interaction partners in *Botrytis cinerea*: Impact on differentiation and virulence. *PLoS ONE* **2014**, *9*, e95172. [CrossRef] [PubMed]

24. Harris, S.D.; Hamer, L.; Sharpless, K.E.; Hamer, J.E. The *Aspergillus nidulans* sepA gene encodes an FH1/2 protein involved in cytokinesis and the maintenance of cellular polarity. *EMBO J.* **1997**, *16*, 3474–3483. [CrossRef] [PubMed]
25. Lichius, A.; Goryachev, A.B.; Fricker, M.D.; Obara, B.; Castro-Longoria, E.; Read, N.D. CDC-42 and RAC-1 regulate opposite chemotropisms in *Neurospora crassa*. *J. Cell Sci.* **2014**, *127*, 1953–1965. [CrossRef] [PubMed]
26. Zheng, P.; Nguyen, T.A.; Wong, J.Y.; Lee, M.; Nguyen, T.A.; Fan, J.S.; Yang, D.; Jedd, G. Spitzenkörper assembly mechanisms reveal conserved features of fungal and metazoan polarity scaffolds. *Nat. Commun.* **2020**, *11*, 2830. [CrossRef] [PubMed]
27. Steinberg, G. Hyphal growth: A tale of motors, lipids, and the Spitzenkörper. *Eukaryot. Cell* **2007**, *6*, 351–360. [CrossRef] [PubMed]
28. Harris, S.D.; Read, N.D.; Roberson, R.W.; Shaw, B.; Seiler, S.; Plamann, M.; Momany, M. Polarisome meets Spitzenkörper: Microscopy, genetics, and genomics converge. *Eukaryot. Cell* **2005**, *4*, 225–229. [CrossRef]
29. Wendland, J.; Walther, A. *Ashbya gossypii*: A model for fungal developmental biology. *Nat. Rev. Microbiol.* **2005**, *3*, 421–429. [CrossRef] [PubMed]
30. Mouriño-Pérez, R.R.; Roberson, R.W.; Bartnicki-García, S. Microtubule dynamics and organization during hyphal growth and branching in *Neurospora crassa*. *Fungal Genet. Biol.* **2006**, *43*, 389–400. [CrossRef] [PubMed]
31. Konzack, S.; Rischitor, P.E.; Enke, C.; Fischer, R. The role of the kinesin motor KipA in microtubule organization and polarized growth of *Aspergillus nidulans*. *Mol. Biol. Cell* **2005**, *16*, 497–506. [CrossRef]
32. Steinberg, G.; Peñalva, M.A.; Riquelme, M.; Wösten, H.A.; Harris, S.D. Cell biology of hyphal growth. *Microbiol. Spectr.* **2017**, *5*, FUNK-0034-2016. [CrossRef]
33. Holleran, E.A.; Ligon, L.A.; Tokito, M.; Stankewich, M.C.; Morrow, J.S.; Holzbaur, E.L. βIII spectrin binds to the Arp1 subunit of dynactin. *J. Biol. Chem.* **2001**, *276*, 36598–36605. [CrossRef] [PubMed]
34. Reck-Peterson, S.L.; Redwine, W.B.; Vale, R.D.; Carter, A.P. The cytoplasmic dynein transport machinery and its many cargoes. *Nat. Rev. Mol. Cell Biol.* **2018**, *19*, 382–398. [CrossRef] [PubMed]
35. Eckley, D.M.; Schroer, T.A. Interactions between the evolutionarily conserved, actin-related protein, Arp11, actin, and Arp1. *Mol. Biol. Cell* **2003**, *14*, 2645–2654. [CrossRef] [PubMed]
36. Christopher, L.; Fletcher, L.; Dykstra, C. Cloning and Identification of Arp1, an Actin-Related Protein from *Pneumocystis carinii*. *J. Eukaryot. Microbiol.* **1995**, *42*, 142–149. [CrossRef]
37. Schafer, D.; Gill, S.R.; Cooper, J.; Heuser, J.; Schroer, T. Ultrastructural analysis of the dynactin complex: An actin-related protein is a component of a filament that resembles F-actin. *J. Cell Biol.* **1994**, *126*, 403–412. [CrossRef] [PubMed]
38. Lenz, J.H.; Schuchardt, I.; Straube, A.; Steinberg, G. A dynein loading zone for retrograde endosome motility at microtubule plus-ends. *EMBO J.* **2006**, *25*, 2275–2286. [CrossRef]
39. Egan, M.J.; Tan, K.; Reck-Peterson, S.L. Lis1 is an initiation factor for dynein-driven organelle transport. *J. Cell Biol.* **2012**, *197*, 971–982. [CrossRef]
40. Zhang, J.; Li, S.; Fischer, R.; Xiang, X. Accumulation of cytoplasmic dynein and dynactin at microtubule plus ends in *Aspergillus nidulans* is kinesin dependent. *Mol. Biol. Cell* **2003**, *14*, 1479–1488. [CrossRef] [PubMed]
41. Schuster, M.; Kilaru, S.; Ashwin, P.; Lin, C.; Severs, N.J.; Steinberg, G. Controlled and stochastic retention concentrates dynein at microtubule ends to keep endosomes on track. *EMBO J.* **2011**, *30*, 652–664. [CrossRef] [PubMed]
42. Eckley, D.M.; Gill, S.R.; Melkonian, K.A.; Bingham, J.B.; Goodson, H.V.; Heuser, J.E.; Schroer, T.A. Analysis of dynactin subcomplexes reveals a novel actin-related protein associated with the arp1 minifilament pointed end. *J. Cell Biol.* **1999**, *147*, 307–320. [CrossRef] [PubMed]
43. Plamann, M.; Minke, P.F.; Tinsley, J.H.; Bruno, K.S. Cytoplasmic dynein and actin-related protein Arp1 are required for normal nuclear distribution in filamentous fungi. *J. Cell Biol.* **1994**, *127*, 139–149. [CrossRef] [PubMed]
44. Sambrook, J.; Fritsch, E.; Maniatis, T. (Eds.) *Molecular Cloning: A Laboratory Manual*; Cold Spring Harbor Laboratory Press: Cold Spring Harbor, NY, USA, 2001.
45. Colot, H.V.; Park, G.; Turner, G.E.; Ringelberg, C.; Crew, C.M.; Litvinkova, L.; Weiss, R.L.; Borkovich, K.A.; Dunlap, J.C. A high-throughput gene knockout procedure for *Neurospora* reveals functions for multiple transcription factors. *Proc. Natl. Acad. Sci. USA* **2006**, *103*, 10352–10357. [CrossRef]
46. James, P.; Halladay, J.; Craig, E.A. Genomic libraries and a host strain designed for highly efficient two-hybrid selection in yeast. *Genetics* **1996**, *144*, 1425–1436. [CrossRef]
47. Walz, M.; Kück, U. Transformation of *Sordaria macrospora* to hygromycin B resistance: Characterization of transformants by electrophoretic karyotyping and tetrad analysis. *Curr. Genet.* **1995**, *29*, 88–95. [CrossRef]
48. Elleuche, S.; Pöggeler, S. Visualization of peroxisomes via SKL-tagged DsRed protein in *Sordaria macrospora*. *Fungal Genet. Rep.* **2008**, *55*, 9–12. [CrossRef]
49. Esser, K. *Cryptogams—Cyanobacteria, Algae, Fungi, Lichens*; Cambridge University Press: London, UK, 1982.
50. Nowrousian, M.; Ringelberg, C.; Dunlap, J.C.; Loros, J.J.; Kück, U. Cross-species microarray hybridization to identify developmentally regulated genes in the filamentous fungus *Sordaria macrospora*. *Mol. Genet. Genom.* **2005**, *273*, 137–149. [CrossRef]
51. Bernhards, Y.; Pöggeler, S. The phocein homologue SmMOB3 is essential for vegetative cell fusion and sexual development in the filamentous ascomycete *Sordaria macrospora*. *Curr. Genet.* **2011**, *57*, 133–149. [CrossRef]
52. O'Connell, R.J.; Thon, M.R.; Hacquard, S.; Amyotte, S.G.; Kleemann, J.; Torres, M.F.; Damm, U.; Buiate, E.A.; Epstein, L.; Alkan, N.; et al. Lifestyle transitions in plant pathogenic *Colletotrichum* fungi deciphered by genome and transcriptome analyses. *Nat. Genet.* **2012**, *44*, 1060–1065. [CrossRef]

53. Nordzieke, D.E.; Sanken, A.; Antelo, L.; Raschke, A.; Deising, H.B.; Pöggeler, S. Specialized infection strategies of falcate and oval conidia of *Colletotrichum graminicola*. *Fungal Genet. Biol.* **2019**, *133*, 103276. [CrossRef]
54. Katoh, K.; Rozewicki, J.; Yamada, K.D. MAFFT online service: Multiple sequence alignment, interactive sequence choice and visualization. *Brief. Bioinform.* **2019**, *20*, 1160–1166. [CrossRef]
55. Han, M.V.; Zmasek, C.M. phyloXML: XML for evolutionary biology and comparative genomics. *BMC Bioinform.* **2009**, *10*, 1–6. [CrossRef]
56. Reschka, E.J.; Nordzieke, S.; Valerius, O.; Braus, G.H.; Pöggeler, S. A novel STRIPAK complex component mediates hyphal fusion and fruiting-body development in filamentous fungi. *Mol. Microbiol.* **2018**, *110*, 513–532. [CrossRef]
57. Dahlmann, T.A.; Terfehr, D.; Becker, K.; Teichert, I. Golden Gate vectors for efficient gene fusion and gene deletion in diverse filamentous fungi. *Curr. Genet.* **2021**, *67*, 317–330. [CrossRef]
58. Klix, V.; Nowrousian, M.; Ringelberg, C.; Loros, J.J.; Dunlap, J.C.; Pöggeler, S. Functional characterization of MAT1-1-specific mating-type genes in the homothallic ascomycete *Sordaria macrospora* provides new insights into essential and nonessential sexual regulators. *Eukaryot. Cell* **2010**, *9*, 894–905. [CrossRef] [PubMed]
59. Werner, A.; Otte, K.L.; Stahlhut, G.; Pöggeler, S. Establishment of the monomeric yellow-green fluorescent protein mNeonGreen for life cell imaging in mycelial fungi. *AMB Express* **2020**, *10*, 222. [CrossRef] [PubMed]
60. Pöggeler, S.; Masloff, S.; Hoff, B.; Mayrhofer, S.; Kück, U. Versatile EGFP reporter plasmids for cellular localization of recombinant gene products in filamentous fungi. *Curr. Genet.* **2003**, *43*, 54–61. [CrossRef]
61. Werner, A.; Otte, K.; Stahlhut, G.; Hanke, L.M.; Pöggeler, S. The glyoxysomal protease LON2 is involved in fruiting-body development, ascosporogenesis and stress resistance in *Sordaria macrospora*. *J. Fungi* **2021**, *7*, 82. [CrossRef]
62. Bloemendal, S.; Bernhards, Y.; Bartho, K.; Dettmann, A.; Voigt, O.; Teichert, I.; Seiler, S.; Wolters, D.A.; Pöggeler, S.; Kück, U. A homologue of the human STRIPAK complex controls sexual development in fungi. *Mol. Microbiol.* **2012**, *84*, 310–323. [CrossRef] [PubMed]
63. Shibayama, M.; Ooi, K.; Johnson, R.; Scott, B.; Itoh, Y. Suppression of tandem-multimer formation during genetic transformation of the mycotoxin-producing fungus *Penicillium paxilli* by disrupting an orthologue of *Aspergillus nidulans* uvsC. *Curr. Genet.* **2002**, *42*, 59–65. [CrossRef]
64. Nowrousian, M.; Teichert, I.; Masloff, S.; Kück, U. Whole-genome sequencing of *Sordaria macrospora* mutants identifies developmental genes. *G3 Genes Genomes Genet.* **2012**, *2*, 261–270.
65. Nordzieke, S.; Zobel, T.; Franzel, B.; Wolters, D.A.; Kück, U.; Teichert, I. A fungal sarcolemmal membrane-associated protein (SLMAP) homolog plays a fundamental role in development and localizes to the nuclear envelope, endoplasmic reticulum, and mitochondria. *Eukaryot. Cell* **2015**, *14*, 345–358. [CrossRef] [PubMed]
66. Pöggeler, S.; Kück, U. Highly efficient generation of signal transduction knockout mutants using a fungal strain deficient in the mammalian *ku70* ortholog. *Gene* **2006**, *378*, 1–10. [CrossRef] [PubMed]
67. Forgey, W.M.; Blanco, M.H.; Loegering, W.Q. Differences in pathological capabilities and host specificity of *Colletotrichum graminicola* on *Zea mays*. *Plant Dis. Rep.* **1978**, *62*, 573–576.
68. Horbach, R.; Graf, A.; Weihmann, F.; Antelo, L.; Mathea, S.; Liermann, J.C.; Opatz, T.; Thines, E.; Aguirre, J.; Deising, H.B. Sfp-type 4′-phosphopantetheinyl transferase is indispensable for fungal pathogenicity. *Plant Cell* **2009**, *21*, 3379–3396. [CrossRef] [PubMed]
69. Schunke, C.; Pöggeler, S.; Nordzieke, D.E. A 3D printed device for easy and reliable quantification of fungal chemotropic growth. *Front. Microbiol.* **2020**, *11*, 584525. [CrossRef]
70. Towbin, H.; Staehelin, T.; Gordon, J. Electrophoretic transfer of proteins from polyacrylamide gels to nitrocellulose sheets: Procedure and some applications. *Proc. Natl. Acad. Sci. USA* **1979**, *76*, 4350–4354. [CrossRef] [PubMed]
71. Schindelin, J.; Arganda-Carreras, I.; Frise, E.; Kaynig, V.; Longair, M.; Pietzsch, T.; Preibisch, S.; Rueden, C.; Saalfeld, S.; Schmid, B. Fiji: An open-source platform for biological-image analysis. *Nat. Methods* **2012**, *9*, 676–682. [CrossRef]
72. Fleissner, A.; Herzog, S. Signal exchange and integration during self-fusion in filamentous fungi. *Semin. Cell Dev. Biol.* **2016**, *57*, 76–83. [CrossRef]
73. Read, N.D.; Goryachev, A.B.; Lichius, A. The mechanistic basis of self-fusion between conidial anastomosis tubes during fungal colony initiation. *Fungal Biol. Rev.* **2012**, *26*, 1–11. [CrossRef]
74. Grove, S.N.; Bracker, C.E. Protoplasmic organization of hyphal tips among fungi: Vesicles and Spitzenkörper. *J. Bacteriol.* **1970**, *104*, 989–1009. [CrossRef] [PubMed]
75. Löpez-Franco, R.; Bracker, C.E. Diversity and dynamics of the Spitzenkörper in growing hyphal tips of higher fungi. *J. Bacteriol.* **1996**, *195*, 90–111.
76. Virag, A.; Harris, S.D. The Spitzenkörper: A molecular perspective. *Mycol. Res.* **2006**, *110*, 4–13. [CrossRef]
77. Riquelme, M.; Reynaga-Peña, C.G.; Gierz, G.; Bartnicki-García, S. What determines growth direction in fungal hyphae? *Fungal Genet. Biol.* **1998**, *24*, 101–109. [CrossRef]
78. Peñalva, M.A. Tracing the endocytic pathway of *Aspergillus nidulans* with FM4-64. *Fungal Genet. Biol.* **2005**, *42*, 963–975. [CrossRef]
79. Fischer-Parton, S.; Parton, R.; Hickey, P.; Dijksterhuis, J.; Atkinson, H.; Read, N. Confocal microscopy of FM4-64 as a tool for analysing endocytosis and vesicle trafficking in living fungal hyphae. *J. Microsc.* **2000**, *198*, 246–259. [CrossRef]
80. Teichert, I. Nuclear dynamics during ascospore germination in *Sordaria macrospora*. *Fungal Genet. Biol.* **2017**, *98*, 20–22. [CrossRef] [PubMed]

81. Turrà, D.; El Ghalid, M.; Rossi, F.; Di Pietro, A. Fungal pathogen uses sex pheromone receptor for chemotropic sensing of host plant signals. *Nature* **2015**, *527*, 521–524. [CrossRef]
82. Mendgen, K.; Hahn, M.; Deising, H. Morphogenesis and mechanisms of penetration by plant pathogenic fungi. *Annu. Rev. Phytopathol.* **1996**, *34*, 367–386. [CrossRef] [PubMed]
83. Ryder, L.S.; Dagdas, Y.F.; Mentlak, T.A.; Kershaw, M.J.; Thornton, C.R.; Schuster, M.; Chen, J.; Wang, Z.; Talbot, N.J. NADPH oxidases regulate septin-mediated cytoskeletal remodeling during plant infection by the rice blast fungus. *Proc. Natl. Acad. Sci. USA* **2013**, *110*, 3179–3184. [CrossRef] [PubMed]
84. Brun, S.; Malagnac, F.; Bidard, F.; Lalucque, H.; Silar, P. Functions and regulation of the Nox family in the filamentous fungus *Podospora anserina*: A new role in cellulose degradation. *Mol. Microbiol.* **2009**, *74*, 480–496. [CrossRef] [PubMed]
85. Oakley, B.R.; Oakley, C.E.; Yoon, Y.; Jung, M.K. γ-Tubulin is a component of the spindle pole body that is essential for microtubule function in *Aspergillus nidulans*. *Cell* **1990**, *61*, 1289–1301. [CrossRef]
86. Takeshita, N.; Manck, R.; Grün, N.; de Vega, S.H.; Fischer, R. Interdependence of the actin and the microtubule cytoskeleton during fungal growth. *Curr. Opin. Microbiol.* **2014**, *20*, 34–41. [CrossRef]
87. Xiang, X.; Han, G.; Winkelmann, D.A.; Zuo, W.; Morris, N.R. Dynamics of cytoplasmic dynein in living cells and the effect of a mutation in the dynactin complex actin-related protein Arp1. *Curr. Biol.* **2000**, *10*, 603–606. [CrossRef]
88. Baas, P.W.; Lin, S. Hooks and comets: The story of microtubule polarity orientation in the neuron. *Dev. Neurobiol.* **2011**, *71*, 403–418. [CrossRef]
89. Dujardin, D.L.; Barnhart, L.E.; Stehman, S.A.; Gomes, E.R.; Gundersen, G.G.; Vallee, R.B. A role for cytoplasmic dynein and LIS1 in directed cell movement. *J. Cell Biol.* **2003**, *163*, 1205–1211. [CrossRef]
90. Baas, P.W.; Vidya, N.C.; Myers, K.A. Axonal transport of microtubules: The long and short of it. *Traffic* **2006**, *7*, 490–498. [CrossRef]
91. Fink, G.; Steinberg, G. Dynein-dependent motility of microtubules and nucleation sites supports polarization of the tubulin array in the fungus *Ustilago maydis*. *Mol. Biol. Cell* **2006**, *17*, 3242–3253. [CrossRef] [PubMed]
92. Minke, P.; Lee, I.; Tinsley, J.; Plamann, M. A *Neurospora crassa* Arp1 mutation affecting cytoplasmic dynein and dynactin localization. *Mol. Gen. Genet. MGG* **2000**, *264*, 433–440. [CrossRef] [PubMed]
93. Takeshita, N.; Fischer, R. On the role of microtubules, cell end markers, and septal microtubule organizing centres on site selection for polar growth in *Aspergillus nidulans*. *Fungal Biol.* **2011**, *115*, 506–517. [CrossRef] [PubMed]
94. Riquelme, M.; Gierz, G.; Bartnicki-García, S. Dynein and dynactin deficiencies affect the formation and function of the Spitzenkörper and distort hyphal morphogenesis of *Neurospora crassa*. *Microbiology* **2000**, *146*, 1743–1752. [CrossRef]
95. Steinberg, G. On the move: Endosomes in fungal growth and pathogenicity. *Nat. Rev. Microbiol.* **2007**, *5*, 309–316. [CrossRef]
96. Araujo-Palomares, C.L.; Castro-Longoria, E.; Riquelme, M. Ontogeny of the Spitzenkörper in germlings of *Neurospora crassa*. *Fungal Genet. Biol.* **2007**, *44*, 492–503. [CrossRef]
97. Hickey, P.C.; Jacobson, D.; Read, N.D.; Glass, N.L. Live-cell imaging of vegetative hyphal fusion in *Neurospora crassa*. *Fungal Genet. Biol.* **2002**, *37*, 109–119. [CrossRef]
98. Roca, M.G.; Kuo, H.C.; Lichius, A.; Freitag, M.; Read, N.D. Nuclear dynamics, mitosis, and the cytoskeleton during the early stages of colony initiation in *Neurospora crassa*. *Eukaryot. Cell* **2010**, *9*, 1171–1183. [CrossRef] [PubMed]
99. Berepiki, A.; Lichius, A.; Shoji, J.Y.; Tilsner, J.; Read, N.D. F-actin dynamics in *Neurospora crassa*. *Eukaryot. Cell* **2010**, *9*, 547–557. [CrossRef] [PubMed]
100. Fischer, M.S.; Glass, N.L. Communicate and fuse: How filamentous fungi establish and maintain an interconnected mycelial network. *Front. Microbiol.* **2019**, *10*, 619. [CrossRef] [PubMed]
101. Suelmann, R.; Sievers, N.; Fischer, R. Nuclear traffic in fungal hyphae: In vivo study of nuclear migration and positioning in *Aspergillus nidulans*. *Mol. Microbiol.* **1997**, *25*, 757–769. [CrossRef] [PubMed]
102. Veith, D.; Scherr, N.; Efimov, V.P.; Fischer, R. Role of the spindle-pole-body protein ApsB and the cortex protein ApsA in microtubule organization and nuclear migration in *Aspergillus nidulans*. *J. Cell Sci.* **2005**, *118*, 3705–3716. [CrossRef]
103. Fischer, R.; Timberlake, W.E. *Aspergillus nidulans apsA* (anucleate primary sterigmata) encodes a coiled-coil protein required for nuclear positioning and completion of asexual development. *J. Cell Biol.* **1995**, *128*, 485–498. [CrossRef] [PubMed]
104. Steuer, E.R.; Wordeman, L.; Schroer, T.A.; Sheetz, M.P. Localization of cytoplasmic dynein to mitotic spindles and kinetochores. *Nature* **1990**, *345*, 266–268. [CrossRef] [PubMed]

3. Article II: Analysis of the Putative Nucleoporin POM33 in the Filamentous Fungus *Sordaria macrospora*

This article represents the second subtopic of this thesis. It was authored by A. Groth, K. Schmitt, O. Valerius, B. Herzog and S. Pöggeler. The article was published online in the Journal of Fungi (JoF) in August 2021. The full article together with the Supplementary information and datasets can be found online at:
https://doi.org/10.3390/jof7090682.

Author contribution

As first author of the paper, A. Groth was involved in the design of the experimental procedures, performed the depicted experiments and analyzed the data. Additionally, she created all the figures and wrote, edited as well as revised the manuscript.

Journal of *Fungi*

MDPI

Article

Analysis of the Putative Nucleoporin POM33 in the Filamentous Fungus *Sordaria macrospora*

Anika Groth [1], Kerstin Schmitt [2], Oliver Valerius [2], Britta Herzog [1] and Stefanie Pöggeler [1,*]

[1] Department of Genetics of Eukaryotic Microorganisms, Institute of Microbiology and Genetics, Georg-August-University of Göttingen, Grisebachstr. 8, 37077 Göttingen, Germany; anika.gibron@uni-goettingen.de (A.G.); bherzog@gwdg.de (B.H.)
[2] Department of Molecular Microbiology and Genetics, Service Unit LCMS Protein Analytics, Institute of Microbiology and Genetics, Georg-August-University of Göttingen, Grisebachstr. 8, 37077 Göttingen, Germany; kschmit1@gwdg.de (K.S.); ovaleri@gwdg.de (O.V.)
* Correspondence: spoegge@gwdg.de; Tel.: +49-551-391-3930

Abstract: In the filamentous fungus *Sordaria macrospora* (Sm), the STRIPAK complex is required for vegetative growth, fruiting-body development and hyphal fusion. The SmSTRIPAK core consists of the striatin homolog PRO11, the scaffolding subunit of phosphatase PP2A, SmPP2AA, and its catalytic subunit SmPP2Ac1. Among other STRIPAK proteins, the recently identified coiled-coil protein SCI1 was demonstrated to co-localize around the nucleus. Pulldown experiments with SCI identified the transmembrane nucleoporin (TM Nup) SmPOM33 as a potential nuclear-anchor of SmSTRIPAK. Localization studies revealed that SmPOM33 partially localizes to the nuclear envelope (NE), but mainly to the endoplasmic reticulum (ER). We succeeded to generate a Δpom33 deletion mutant by homologous recombination in a new *S. macrospora* Δku80 recipient strain, which is defective in non-homologous end joining. Deletion of *Smpom33* did neither impair vegetative growth nor sexual development. In pulldown experiments of SmPOM33 followed by LC/MS analysis, ER-membrane proteins involved in ER morphology, protein translocation, glycosylation, sterol biosynthesis and Ca^{2+}-transport were significantly enriched. Data are available via ProteomeXchange with identifier PXD026253. Although no SmSTRIPAK components were identified as putative interaction partners, it cannot be excluded that SmPOM33 is involved in temporarily anchoring the SmSTRIPAK to the NE or other sites in the cell.

Keywords: STRIPAK complex; POM33; transmembrane nucleoporins; nuclear envelope; endoplasmic reticulum; *Sordaria macrospora*

Citation: Groth, A.; Schmitt, K.; Valerius, O.; Herzog, B.; Pöggeler, S. Analysis of the Putative Nucleoporin POM33 in the Filamentous Fungus *Sordaria macrospora*. *J. Fungi* **2021**, *7*, 682. https://doi.org/10.3390/jof7090682

Academic Editor: Javier Arroyo

Received: 31 May 2021
Accepted: 17 August 2021
Published: 24 August 2021

1. Introduction

The striatin-interacting phosphatase and kinase (STRIPAK) complex is a conserved multiprotein complex involved in diverse cell-signaling pathways like cell growth and -fusion, vesicular traffic, endocytosis and even apoptosis in animals and fungi [1,2]. The main components of STRIPAK complexes are striatin scaffolding proteins [3]. The coprophilic ascomycete *Sordaria macrospora* (Sm) is a fungal model organism to study complex fruiting-body development [4,5]. In *S. macrospora*, SmSTRIPAK plays an important role in vegetative growth, hyphal fusion and sexual development. The major scaffold protein of the SmSTRIPAK complex is the human striatin homolog PRO11 [6–8]. In addition, the SmSTRIPAK complex consists of the STRIP1/2 homolog PRO22, SmMOB3, the scaffolding subunit of phosphatase PP2A, SmPP2AA, and its catalytic subunit SmPP2Ac1 as well as recruited GCKIII kinases SmKIN24 and SmKIN3 [6,9–13]. Moreover, the SLMAP homolog PRO45 and the coiled-coil protein SCI1 were identified as key subunits of the SmSTRIPAK [9,14]. Recently, the cryo-EM structure of the human STRIPAK core was determined. There, the coiled-coil domains of striatin form a homotetrameric platform for the interaction with one copy of PP2AA and PP2Ac, STRIP1 and MOB4 [15]. A similar structure can be

assumed for SmSTRIPAK (Figure 1). Fluorescence microscopic investigations revealed that SCI1 and PRO11 both co-localize around the nucleus [14]. In addition, the STRIPAK components SLMAP homolog PRO45 and SmMOB3 were localized to the nuclear envelope (NE), endoplasmic reticulum (ER), and mitochondria [9].

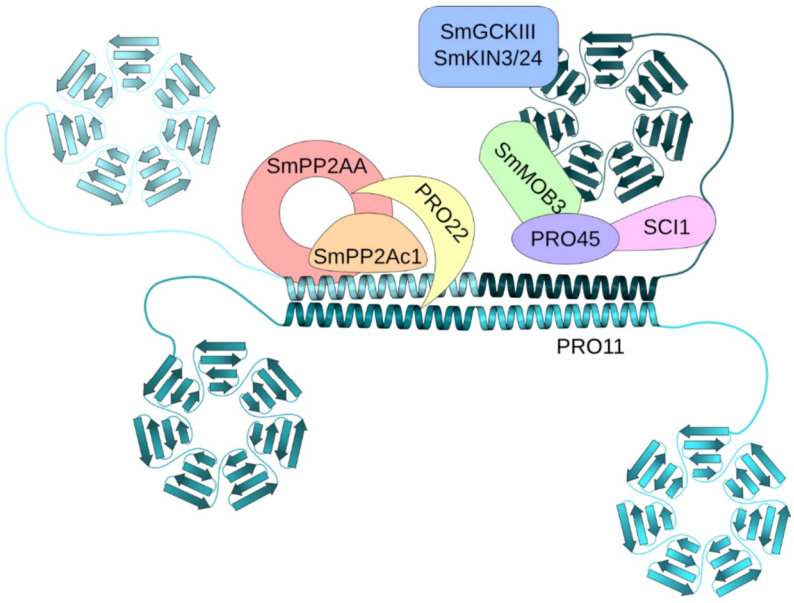

Figure 1. Schematic illustration of the SmSTRIPAK complex. According to structural data of the human STRIPAK complex [15] and data from *S. macrospora* [6–14], the SmSTRIPAK complex consists of a tetramer of the scaffolding human striatin homolog PRO11 harboring an N-terminal coiled-coil domain (cyan-shaded helices) and C-terminal WD40 repeats (cyan-shaded beta-propeller). Further components are the STRIP1/2 homolog PRO22 (yellow), SmMOB3 (green), the scaffolding subunit of phosphatase PP2A, SmPP2AA (red), and its catalytic subunit SmPP2Ac1 (orange) and recruited GCKIII kinases SmKIN3/24 (blue). Moreover, the SLMAP homolog PRO45 (purple) and the coiled-coil protein SCI1 (pink) are key subunits of the SmSTRIPAK.

In pulldown experiments coupled to LC/MS analysis, the putative TM Nup SmPOM33 had previously been identified as putative interaction partner of the SmSTRIPAK component SCI1 [14]. Together with this result and the observation that SCI1 and other STRIPAK components co-localize around the nucleus, we addressed the question if SmPOM33 might be anchoring the SmSTRIPAK to the nucleus. The nucleus is surrounded by a double-lipid bilayer comprising the inner nuclear membrane (INM) that merges into the outer nuclear membrane (ONM) at sites of nuclear pores and is continuous with the endoplasmic reticulum forming the nuclear envelope [16]. The ER plays an important role in many cellular processes, like protein synthesis and modification, lipid synthesis and Ca^{2+}-regulation, homeostasis and secretion [17]. It consists of peripheral sheet-like cisternae and a network of interconnected ER tubules [18]. Its morphology is divided into the rough ER (RER) with membrane-bound ribosomes and the ribosome-absent smooth ER (SER) [19]. The tubules of the ER undergo continuous fusion and partitioning events to establish three-way junctions showing that the ER network is highly dynamic [17,18,20,21]. At the fusion sites of the INM and the ONM, nuclear-pore complexes (NPCs) are incorporated. NPCs are large protein complexes that form channels to mediate nucleocytoplasmic exchange [22]. The assembly of NPCs-consisting proteins, termed nucleoporins (Nups), can occur postmitotic or *de novo*. In case of postmitotic NPC biogenesis, the NE reforms

from cortical ER (cER) into a pore that is stabilized by pore membrane proteins (Poms) so that Nups are recruited [23–26]. During *de novo* NPC assembly, the pore is formed by fusion of the double membrane system of the NE. For this process, the conserved protein Ndc1 is the only essential transmembrane Nup (TM Nup) so far known [27–29]. Besides Ndc1, three other TM Nups Pom33/Tts1/TMEM33 assist in NPC assembly [30–32].

In this study, we performed fluorescence microscopy, generated a *Smpom33* deletion mutant ΔSmpom33 and did pulldown experiments coupled to LC/MS analysis to examine if we can pull down SCI1 or other SmSTRIPAK components vice versa. We showed that SmPOM33 localizes at the ER and NE. Pulldown experiments with a tagged version of SmPOM33 identified no SmSTRIPAK components but revealed ER-membrane proteins involved in ER morphology, protein translocation, glycosylation, sterol biosynthesis and Ca^{2+}-transport as putative interaction partners.

2. Materials and Methods

2.1. Strains, Media and Growth Conditions

All strains used in this study are presented in Table 1. For cloning and propagation of recombinant plasmids, *Escherichia coli* MACH1 (Thermo Fisher Scientific, C862003, Waltham, MA, USA) was used in standard culture conditions [33]. To generate recombinant plasmids, homologous recombination (HR) was performed using *Saccharomyces cerevisiae* strain PJ69-4A [34,35] and positive clones were selected for uracil prototrophy. *S. macrospora* strains were transformed with the recombinant plasmids (Table S1 in Supplementary Materials) as described in the standard protocol [36,37]. Positive transformants were selected on media containing nourseothricin-dihydrogen sulfate (50 µg/mL, nat) (Jena Bioscience GmbH, AB-102XL, Jena, Germany) and/ or hygromycin B (110 U/mL, hyg) (Merck, 4400051-10MU, Kenilworth, NJ, USA). *S. macrospora* strains were grown on liquid or solid biomalt maize medium (BMM) or Sordaria Westergaard (SWG) fructification medium at 27 °C under continuous light conditions [38–40]. Crosses of different *S. macrospora* strains were performed as described previously [13]. For phenotypic analysis under different stress conditions, the temperature was changed to 16 °C and 37 °C or SWG medium was supplemented with 0.1 M NaCl, 0.01% H_2O_2, 100 µg/mL Calcofluor White (CFW), 0.2 µg/mL Tunicamycin (TM) or 1.5 mM DTT. For microscopic analyses, *S. macrospora* strains were grown under continuous light at 27 °C on solid SWG or selective BMM medium covered with Cellophane or on BMM-agar slides. For the agar slides, two sterile toothpicks were placed in an empty petri dish, a glass slide was laid on top and covered with fresh BMM media (2% agar and 50 mL clear liquid BMM). After inoculating the BMM-covered slide with a piece of fungal mycelia from an agar plate, liquid BMM was poured carefully into the petri dish slightly covering the slide to increase the humidity. Dishes were incubated at 27 °C over night. Dependent on the developmental stage analyzed, the growth period differed between 24 h or 2–10 days.

Table 1. Strains used and generated in this study.

Strain	Genotype	References
	Escherichia coli	
MACH1	Δ*recA1398*, *endA1*, *tonA*, *Φ80ΔlacM15*, Δ*lacX74*, *hsdR*, (rK-mK+)	Invitrogen
	Saccharomyces cerevisiae	
PJ69-4A	*MATa*, *trp1-901*, *leu2-3*, *112*, *ura3-52*, *his3-200*, *gal4Δ*, *gal80Δ*, *LYS2::GAL1-HIS3*, *GAL2-ADE2*, *met2::GAL7-lacZ*	[35]
	Sordaria macrospora	
DSM997	wild type (wt)	DSMZ
S23442	mutation in *fus1-1* gene, brownish ascospores, fertile	[41]
Δku70	Δku70::nat^R, fertile	[42]
Δsci1	Δsci1::hyg^R, ssi, sterile	[14]

Table 1. *Cont.*

Strain	Genotype	References
Δsci1::nca1-TagRFP-T^{ect}	ectopic integration of p5′nca1-TagRFP-T _nat into Δsci1; *hyg*^{R}, *nat*^{R} pt, sterile, *Pnca1::nca1::TagRFP-T::TtrpC*	Reschka and Pöggeler (unpublished)
wt::egfp^{ect}	ectopic integration of p1783-1 into DSM997; *hyg*^{R}, ssi, fertile, *Pgpd::egfp::TtrpC*	[43]
wt::TagRFP-T^{ect}	ectopic integration of pTagRFP-T_nat into DSM997; *nat*^{R}, ssi, fertile, *Pccg1::TagRFP-T::TtrpC*	[44]
wt::GH2A^{ect}	ectopic integration of pGH2A into DSM997; *hyg*^{R}, pt, fertile, *Pgpd::hh2a::egfp::TtrpC*	Reschka and Pöggeler (unpublished)
fus::RH2B^{ect}	ectopic integration of pRH2B in S23442; *hyg*^{R}, pt, fertile, *Pgpd::hh2b::tdTomato::TtrpC*	Reschka and Pöggeler (unpublished)
wt::nca1-TagRFP-T^{ect}	ectopic integration of p5′nca1-TagRFP-T_hyg into DSM997; *hyg*^{R}, pt, fertile, *Pnca1::nca1::TagRFP-T::TtrpC*	Werner and Pöggeler (unpublished)
Δku80	Δku80::hyg^R, ssi, fertile	This study
Δpom33	Δpom33::nat^R, ssi, fertile	This study
wt::pom33-TagRFP-T^{ect}	ectopic integration of p5′pom33-TagRFP-T_nat into DSM997; *nat*^{R}, ssi, fertile, *Ppom33::pom33:: TagRFP-T::TtrpC*	This study
wt::pom33-TagRFP-T^{ect}	ectopic integration of p5′pom33-TagRFP-T_hyg into DSM997; *hyg*^{R}, pt, fertile, *Ppom33::pom33:: TagRFP-T::TtrpC*	This study
wt::pom33-egfp^{ect}	ectopic integration of p5′pom33-egfp into DSM997; *nat*^{R}, ssi, fertile, *Ppom33::pom33::egfpt::TtrpC*	This study
wt::pom33-TagRFP-T^{ect} + pom152-egfp^{ect}	ectopic integration of p5′pom33-TagRFP-T_hyg and pSmPOM152GFP into DSM997; *hyg*^{R}, *nat*^{R}, pt, fertile, *Ppom33::pom33:: TagRFP-T::TtrpC; Pccg1::pom152::egfp::TtrpC*	This study
wt::pom33-TagRFP-T^{ect} + sci1-egfp^{ect}	ectopic integration of p5′pom33-TagRFP-T_hyg and p5′sci1gfp_nat into DSM997; *hyg*^{R}, *nat*^{R}, pt, fertile, *Ppom33::pom33:: TagRFP-T::TtrpC; Psci1::sci1::egfp::TtrpC*	This study
Δpom33::pom33-TagRFP-T^{ect}	ectopic integration of p5′pom33-TagRFP-T_hyg into Δpom33; *hyg*^{R}, *nat*^{R} ssi, fertile, *Ppom33::pom33:: TagRFP-T::TtrpC*	This study
Δpom33::RH2B^{ect}	ectopic integration of pRH2B into Δpom33; *hyg*^{R}, *nat*^{R} pt, fertile, *Pgpd::hh2b::tdTomato::TtrpC*	This study
Δpom33:: nca1-TagRFP-T^{ect}	ectopic integration of p5′nca1-TagRFP-T_hyg into Δpom33; *hyg*^{R}, *nat*^{R} pt, fertile, *Pnca1::nca1::TagRFP-T::TtrpC*	This study
Δpom33::sci1-egfp^{ect}	ectopic integration of p5′sci1-egfp_hyg into Δpom33; *hyg*^{R}, *nat*^{R} pt, fertile, *Psci1::sci1::egfp::TtrpC*	This study
Δpom33::pro11-egfp^{ect}	ectopic integration of pPRO11-GFP_hyg into Δpom33; *hyg*^{R}, *nat*^{R} pt, fertile, *Pccg1::HA::pro11::egfp::TtrpC*	This study

nat^R: nourseothricin resistant, *hyg*^{R}: hygromycin resistant, *Pccg1*: promotor of the *clock controlled gene 1* of *Neurospora crassa*, *Pgpd*: promotor of the glyceraldehyde-3-phosphate dehydrogenase gene of *Aspergillus nidulans*, *TtrpC*: terminator of the anthranilate synthase gene of *A. nidulans*, ssi: single-spore isolate, pt: primary transformant, *egfp*: gene for green fluorescent protein enhanced green fluorescent protein (eGFP) of *Aequoria victoria*, *TagRFP-T*: gene for red fluorescent protein TagRFP-T of *Entacmaea quadricolor*, *tdTomato*: gene for red fluorescence protein tdTomato from *Discosoma* species. *P*: promoter, *T*: terminator.

2.2. Generation of Plasmids

All plasmids and primers (Sigma-Aldrich Chemie GmbH Taufkirchen, Germany) used in this study are shown in Tables S1 and S2 in Supplementary Materials. Plasmids were constructed via HR in *S. cerevisiae* [34] or the Golden Gate (GG) cloning system [45]. For p5′sci1-egfp_hyg, the *S. macrospora sci1* native promotor and ORF and the *trpC* terminator (*TtrpC*) of *Aspergillus nidulans* were amplified from plasmid p5′sci1gfp_nat [14] with the primer pair 5′sci1-f/pRS426GFPrev. The fragment was cloned into *Xho*I-linearized

vector pRS-hyg [6] via HR in the *S. cerevisiae* strain PJ69-4A [35]. To generate the plasmid p5′pom33-egfp, plasmid p5′sci1gfp_nat [14] served as template and was hydrolyzed with *Bgl*II to cut out the *sci1* promoter and ORF. The *S. macrospora pom33* promoter (*Ppom33*) and the *pom33* ORF were amplified from *S. macrospora* wildtype (DSM997) (wt) gDNA using primer pair Smpom33-f/Smpom33-egfp-r. The resulting fragment was integrated into *Bgl*II-digested p5′sci1gfp_nat via HR in *S. cerevisiae*. For plasmids p5′pom33-TagRFP-T_hyg/_nat, a fragment comprised of the *pom33* promoter and *pom33* ORF was amplified with primer pair Smpom33-f/Smpom33-RFP-r from wt gDNA and a fragment comprised of *TagRFP-T* and the *TtrpC* terminator of *A. nidulans* was amplified with primer pair RFP-f/pRS426GFPrev from pTagRFP-T_nat [44]. Both fragments were integrated into *Xho*I-linearized pRS-nat [46] or pRS-hyg [6] via HR in *S. cerevisiae*.

For the construction of the plasmid pRSku80::hph, the primer pair ku80-5f/ku80-5-hyg-r was used to amplify the 5′ flanking region (1021 bp) of the *ku80* gene. For amplification of the *ku80* 3′ flanking region (1010 bp) primer pair ku80-3-hyg-f/ku80-3r was used. The flanking regions were amplified from *S. macrospora* gDNA and contained an 29-bp overhang to pRS426 vector [47] and the *hph*-cassette, respectively. The *hph*-resistance cassette (1385 bp) was amplified from plasmid pCB1003 [48] with primer hph-f and hph-r. The three PCR fragments were transformed with an *Xho*I-linearized pRS426 vector into the *S. cerevisiae* for HR.

To generate the knockout-plasmid pPom33-KO, the Golden Gate cloning system according to [45] was used. The 5′ (726 bp) and 3′ (1021 bp) flanking regions of the *pom33* gene were amplified from *S. macrospora* wt gDNA with primer pairs Pom33-GG-ko-5f/Pom33-GG-ko-5r and Pom33-GG-ko-3f/Pom33-GG-ko-3r, respectively. Together with donor vector pGG-nat1 and the destination vector pDest-Amp, the fragments were cloned via the Golden Gate procedure [45].

DNA sequencing of the plasmids was performed by Seqlab Sequence Service Laboratories GmbH (Göttingen, Germany).

2.3. Generation of the Knockout Strains Δ*ku80* and Δ*pom33*

For the deletion of the *S. macrospora ku80* gene, the deletion cassette was amplified from pRSku80::hph with primer pair ku80-5f/ku80-3r and transformed into the nourseothricin resistant *S. macrospora* strain Δku70 [42]. To eliminate the Δku70 background hygromycin/nourseothricin resistant strains were crossed with the spore color mutant fus1-1 (S23442) [41]. Single-spore isolates were selected on BMM medium supplemented with hygromycin. The single-spore mutant was named Δku80 and the deletion of *ku80* was verified by PCR and Southern blot analyses. To verify the presence of the *hph*-cassette at the desired gene locus, primer pair ku80-ko-v5f/tC1 (1181 bp) and h3/ku80-r (1152 bp), respectively, were used. Absence of the *ku80* gene in the generated Δku80 strain was verified with primer pairs ku80-ko-v5f/ku80-1r (1581 bp) and ku80-1f/ku80-1r (484 bp). For Southern hybridization, 30 µg of wt and Δku80 gDNA were digested with *Aat*II and *Bgl*II. Electrophoresis of digested gDNA was performed on an 0.8% agarose (Biozym Scientific GmbH, Hessisch Oldendorf, Germany) gel. A capillary blot with nylon membrane (GE Healthcare, Amersham RPN303B, Boston, MA, USA) was performed at room temperature (RT) overnight. The corresponding probes for the 5′- and 3′- flanking regions were PCR amplified with primer pair ku80-ko-v5f/ku80-ko-v5r and ku80-ko-v3f/ku80-r, respectively.

To delete the *S. macrospora pom33* gene, the knockout plasmid pPom33-KO was used as template to amplify the 2645 bp deletion cassette with the primer pair GG_KO_fw/GG_KO_rv, containing the 5′- and 3′- flanking regions of *pom33* and the *nat* cassette. After PCR-clean-up of the amplicon, the *S. macrospora* Δku80 strain was transformed with the deletion cassette to replace the *pom33* ORF with the *nat*-cassette. Primary transformants were crossed with the color-spore mutant fus1-1 [41] and single-spore isolates of Δpom33 carrying nourseothricin resistance were selected [13]. Verification of the absence of the *pom33* gene and integration of the *nat*-cassette at the desired locus was performed with

primer pairs Pom33-v2f/tC1 (948 bp) and Smpom33-vORF3-f/Pom33-v2r (1339 bp), respectively. To check the presence of the *hph*-cassette in Δku80 and the *ku80* gene in Δpom33 after crossing, primer pairs ku80-ko-v5f/tC1 (1176 bp) and ku80-ko-v5f/ku80-1r (1580 bp), respectively, were used. Deletion of *Smpom33* was further verified via Southern hybridization. For this, 30 µg of wt and Δpom33 gDNA were hydrolyzed with *Pst*I and separation of digested gDNA was done on an 0.8% agarose (Biozym Scientific GmbH, Hessisch Oldendorf, Germany) gel. A capillary blot with nylon membrane (GE Healthcare, Amersham RPN303B, Boston, MA, USA) was performed at RT overnight. The 726-bp *pom33* probe was amplified from *S. macrospora* wt gDNA with primer pair Pom33-GG-ko-5f/Pom33-GG-ko-5r.

Labeling of probes for Southern blot experiments was done using the Amersham AlkPhos Direct Labelling and Detection Kit (GE Healthcare, Amersham RPN3680, Boston, MA, USA). Detection was performed according to the manufacturer's manual. Signals were visualized on X-ray films (Amersham Hyperfilm™ ECL, Marlborough, MA, USA) using an "Optimax X-ray film processor" (PROTEC GmbH & Co. KG, Oberstenfeld, Germany).

2.4. Light and Fluorescence Microscopy

To investigate vegetative hyphae and sexual structures, *S. macrospora* strains were grown on solid SWG medium covered with a piece of cellophane (0.5 cm × 0.5 cm) over 2 to 9 days and documented with an AxioImage M1 microscope (Zeiss, Jena, Germany) using differential-interference contrast (DIC) or a VHX-500F Digital Microscope (Keyence, Neu-Isenburg, Germany). Images were captured with a Photometrix CoolSNAP HQ camera (Roper Scientific, Photometrics, Tucson, AZ, USA). Image processing was done using ZEISS ZEN Digital Imaging (version 2.3; Zeiss, Jena, Germany) and the Affinity Publisher software (version 1.9.2.1035, Serif (Europe) Ltd., Nottingham, UK, https://affinity.serif.com/de/publisher/; accessed on 1 March 2021).

For fluorescence microscopic analyses, *S. macrospora* strains were grown on selective BMM medium on top of cellophane sheets or on BMM-covered glass slides for 24 h at 27 °C. For the detection of the EGFP signal Chroma filter set 49002 (exciter ET470/40x, ET525/50m, beamsplitter T495lpxr) and for TagRFP-T/tdTomato Chroma filter set 49005 (exciter ET545/30x, emitter ET620/60m and beamsplitter T570LP) was used.

2.5. Protein Sample Preparation and Western Blot Hybridization

To extract proteins from fungal mycelium, *S. macrospora* strains were cultivated in liquid BMM medium and grown for 3 days at 27 °C. The mycelium was harvested, dried and grounded in liquid nitrogen. After adding 520 µL lysis buffer (10 mM Tris-HCl pH 7.5, 150 mM NaCl, 0.5 mM EDTA pH 8.0, 1 mM PMSF, 2 mM DTT, 0.5% NP-40, 1× protease inhibitor cocktail IV (1tbl/50 mL, 04693132001, Mannheim, Germany), 1× PhosSTOP™ (1tbl/10 mL, Roche, 04906837001, Mannheim, Germany)) /g mycelium powder and ~200 µL glass beads (Ø 0.25–0.5 mm, Roth GmbH, A553.1, Karlsruhe, Germany), cells were lysed in the Tissue Lyser (Qiagen, Hilden, Germany) by 30 Hrz for 2 min. Subsequently, cells were separated from debris by centrifugation at 10,000 rpm for 15 min at 4 °C and were prepared for Western Blot analysis by adding 20 µL 4× NuPAGE® LDS-SB (Thermo Fisher Scientific, NP0007, Waltham, MA, USA) and 4 µL 1 M DTT to 56 µL crude extract and subsequent heating for 10 min at 70 °C. A total of 25 µL of the samples were loaded on a 12% SDS gel. As a protein standard 5 µL of the Nippon Genetics Co. Europe blue star pre-stained protein marker (NIPPON Genetics Europe, MWP03, Düren, Germany) was used.

After separating the proteins they were transferred from the SDS-PAGE gel onto an Amersham™ Protran™ Nitrocellulose Blotting Membrane (GE Healthcare, RPN203B, Little Chalfont, UK) using 1× transfer buffer and a Mini Trans-Blot® Cell device as described by the manufacturer (Bio-Rad Laboratories, Hercules, CA, USA) [49].

The nitrocellulose membrane was blocked with 5% (*w*/*v*) skim milk powder in 1× Tris-buffered saline supplemented with 0.05% Tween 20® (TBST) for 1 h at RT. To detect antigen–antibody reaction, a primary EGFP (rat)- (1:4000, ChromoTek GmbH, 3h9-

100, Planegg-Martinsried, Germany) or TagRFP-T (rabbit) -antibody (1:12,500, BioCat (Evrogen, Moscow, Russia), AB233-ev) solved in 5% skim milk/TBST was used and the membrane was incubated with the antibody solution over night at 4 °C. After removing the primary antibody, the membrane was washed three times with 1× TBST for 15 min and a horse-radish peroxidase (HRP) coupled secondary anti rat- or rabbit-antibody (1:5500, Thermo Fisher Scientific, 62-9520, Waltham, MA, USA; 1:5000, Thermo Fisher Scientific, G-21234, Waltham, MA, USA) was applied to the membrane for 1 h at room temperature. Enhanced chemiluminescence reaction was used to detect the HRP coupled antibodies using the Immobilon™ Western HRP Substrate kit (Merck, WBKLS0500, Kenilworth, NJ, USA). Signals were visualized on X-ray films (Amersham Hyperfilm™ ECL, Marlborough, MA, USA) using an "Optimax X-ray film processor" (PROTEC GmbH & Co. KG, Oberstenfeld, Germany).

2.6. Pulldown Experiments, LC/MS and Data Analysis

2.6.1. Pulldown Experiments

In pulldown experiments, first three biological and in the second experiment additionally one technical replicate of the *S. macrospora* strains Δpom33::pom33-TagRFP-T^{ect} and as control wt::TagRFP-T^{ect} were used. Protein sample preparation was performed as described above but without NP-40 in the lysis buffer and with the first centrifugation step at 10,000 g for 20 min at 4 °C followed by a second centrifugation of the lysate at 10,000 g for 10 min at 4 °C. Here, the lysate of *S. macrospora* wt was used to dilute the control samples 1:1. For the pulldown, 1 mL of the lysate was incubated with 2 µL of primary TagRFP-T (rabbit) antibody (BioCat (Evrogen, Moscow, Russia), AB233-ev) for 2 h at 4 °C on a rotation wheel. Preparation of 50 µL Dynabeads™ Protein G (Thermo Fisher Scientific, 10003D, Waltham, MA, USA) per ml lysate was performed by 30 s of vortexing and removing the supernatant after applying the magnet. The lysate-antibody solution was added to the beads and samples were rotated for 1 h at 4 °C. After applying the magnet and removing the supernatant, beads were washed twice with dilution buffer (lysis buffer without NP-40 and DTT). Beads were separated from the antibody-protein complex by adding 50 µL of 4× NuPAGE® LDS-SB (Thermo Fisher Scientific, NP0007, Waltham, MA, USA) to get a 1× dilution and 5 µL 1 M DTT followed by heating for 10 min at 70 °C. A total of 25 µL of the control and samples were loaded on a 12% SDS gel and sample lanes were separated by lanes loaded with 5 µL of the Nippon Genetics Co. Europe blue star pre-stained protein marker (NIPPON Genetics Europe, MWP03, Düren, Germany). After separation of the proteins by SDS-PAGE, the gel was shaken for 30 min in fixing solution (10% acetic acid and 40% ethanol). Subsequently, the gel was washed with H_2O for 10 min. Sample and control lanes were cut with a fresh scalpel into 4 small pieces and covered with ~200 µL HPLC-H_2O for storing at 4 °C overnight in 1.5 mL Protein LoBind Tubes (0030108116, Eppendorf, Hamburg, Germany).

2.6.2. Trypsin In-Gel Digest of Proteins and C18 Stage Tip Purification

Protein in-gel digestion with trypsin was performed according to [50]. After removing the water, 30 µL acetonitrile were added to the gel pieces and samples were incubated for 10 min at RT. Acetonitrile was taken off and gel pieces were dried for 10 min in the SpeedVac concentrator (Eppendorf concentrator 5301, Hamburg, Germany) at 50 °C. Further, 150 µL 10 mM DTT (in 100 mM NH_4HCO_3) was added and samples were incubated for 1 h at 56 °C. The DTT was removed and samples were incubated for 45 min at RT in the dark after 150 µL of 55 mM iodoacetamide (in 100 mM NH_4HCO_3) was added. To remove iodoacetamide, gel pieces were washed with 150 µL 100 mM NH_4HCO_3 and shaken for 10 min at RT. Next, the solution was discarded and 150 µL acetonitrile was added. Samples were shaken again for 10 min at RT before the solution was removed. The washing procedure was repeated once with 100 mM NH_4HCO_3 and acetonitrile. The gel pieces were dried for 10 min in the SpeedVac concentrator (Eppendorf concentrator 5301, Hamburg, Germany) and subsequently covered with sufficient trypsin digestion

buffer (according to manufacturer's information; SERVA Electrophoresis GmbH, 37283.01, Heidelberg, Germany). The samples were incubated on ice for 45 min and the excessive digestion buffer was removed. Gel pieces were covered with 25 mM NH_4HCO_3 pH 8.0 and incubated over night at 37 °C. After centrifugation at 13,000 rpm for 1 min at RT, the supernatant was transferred to a fresh 1.5 mL Protein LoBind Tube (0030108116, Eppendorf, Hamburg, Germany). Extraction of peptides was achieved by adding 20 mM NH_4HCO_3, shaking for 10 min at RT, centrifugation for 1 min at 13,000 rpm and subsequent addition 50% acetonitrile/ 5% formic acid to the gel pieces, shaking for 20 min at RT and centrifugation. The extraction with acetonitrile/ formic acid was repeated twice and all supernatants were collected and dried completely in the SpeedVac concentrator (Eppendorf concentrator 5301, Hamburg, Germany). For further purification, the peptide pellet was resolved in 20 µL fresh sample buffer (2% acetonitrile, 0.1% formic acid).

The C18 stage tip purification was performed as described previously [51]. The stage tips were equilibrated by the use of 100 µL methanol with 0.1% formic acid, followed by 100 µL 70% acetonitrile with 0.1% formic acid and two times 100 µL H_2O with 0.1% formic acid. After adding the single solvent, the stage tips were centrifuged with the help of an adaptor in 2 mL reaction tubes at 13,000 rpm for 2 min and the flow through was discarded each time. The peptide samples were loaded on the C18 column, incubated for 5 min and centrifuged for 5 min at 4000 rpm. For a better yield, the flow through was reloaded and centrifuged under same conditions before the flow through was discarded. The column was washed twice with 100 µL H_2O with 0.1% formic acid followed by centrifugation at 10,000 rpm for 2 min. To elute the peptides 60 µL 70% acetonitrile with 0.1% formic acid were added to the column and centrifuged at 4000 rpm for 5 min. The peptide solution was dried completely in the SpeedVac concentrator (Eppendorf concentrator 5301, Hamburg, Germany) and the pellet was resolved in 20 µL of sample buffer for LC/MS analysis.

2.6.3. Liquid Chromatography—Mass Spectrometry (LC/MS) Analysis

For peptide separation, 2 µL of each sample were subjected to reverse phase liquid chromatography using an RSLCnano Ultimate 3000 system (Thermo Fisher Scientific, Waltham, MA, USA). Peptides were loaded on an Acclaim PepMap 100 pre-column (100 µm × 2 cm, C18, 5 µm, 100 Å; Thermo Fisher Scientific, Waltham, MA, USA) with 0.07% trifluoroacetic acid at a flow rate of 20 µL/min for 3 min. To separate the peptides analytically, an Acclaim PepMap RSLC column (75 µm × 50 cm, C18, 2 µm, 100 Å; Thermo Fisher Scientific, Waltham, MA, USA) with a flow rate of 300 nL/min was used. The solvent composition was gradually changed within 94 min from 96% Solvent A (0.1% formic acid) and 4% Solvent B (80% acetonitrile, 0.1% formic acid) to 10% Solvent B within 2 min, to 30% Solvent B within the next 58 min, to 45% Solvent B within the following 22 min, and to 90% Solvent B within the last 12 min of the gradient. All solvents and acids were prepared to have Optima grade for LC/MS (Thermo Fisher Scientific, Waltham, MA, USA). Nano-electrospray (nESI) using the Nanospray Flex Ion Source (Thermo Fisher Scientific, Waltham, MA, USA) at 1.5 kV (liquid junction) was used to on-line ionize eluting peptides, which were subsequently transferred into a Q Exactive HF mass spectrometer (Thermo Fisher Scientific, Waltham, MA, USA). At a resolution of 30,000, full scans in a mass range of 300 to 1650 m/z were recorded followed by data-dependent top 10 HCD fragmentation at a resolution of 15,000 (dynamic exclusion enabled). LC/MS method programming and data acquisition was performed using the XCalibur 4.0 software (Thermo Fisher Scientific, Waltham, MA, USA). Measurements were performed at the Service Unit LC/MS Protein Analytics of the Göttingen Center for Molecular Biosciences (GZMB) at the University of Göttingen, Germany.

2.7. Data Acquisition and Analysis

For protein identification, the LC/MS data were analyzed with the MaxQuant 1.6.0.16 software (Max-Planck-Institute of Biochemistry, Munich, Germany) [52]. The *S. macrospora*-specific peptide database Smacrospora_v03 [53], including the peptide sequence of free

TagRFP-T, was used for database search with the Andromeda algorithm and the program's default parameters. As the digestion mode trypsin/P was used and maximum missed cleavage sites were set to two. As fixed modifications carbamidomethylation of cysteins was considered and acetylation of the N-terminus and oxidation of methionine were set as variable modifications. Label free quantification (LFQ) was activated with a minimal ratio count of two to analyze the raw data. The decoy mode was revert with a false discovery rate of 0.01. Data evaluation and statistical analysis was performed with the Perseus 1.6.0.7 software (Max-Planck-Institute of Biochemistry, Munich, Germany) [54] and the online program Venny2.1 [55]. The protocol of the data processing is given in Table S5 in Supplementary Materials. BLAST searches of the best hits of identified proteins were conducted using the *Saccharomyces* Genome Database (SGD) (https://www.yeastgenome.org/blast-sgd; accessed on 12 April 2021) [56] and the UniProtKB BLAST tool (https://www.uniprot.org/blast/; accessed on 12 April 2021) [57] for fungi and *Homo sapiens*.

2.8. Protein Domain Analysis

Protein domains and position of the N- and C-terminus either in the lumen or the cytoplasm were predicted using the program InterProScan (https://www.ebi.ac.uk/interpro/search/sequence/; accessed on 15 March 2021) [58]. The coiled-coil motifs were predicted using NPS@: COILED-COILS PREDICTION (https://npsa.lyon.inserm.fr/cgi-bin/npsa_automat.pl?page=/NPSA/npsa_lupas.html; accessed on 15 March 2021) [59] and helices with the program NetSurfP—2.0 (https://services.healthtech.dtu.dk/service.php?NetSurfP-2.0; accessed on 15 March 2021) [60]. Design of the schematic illustration was performed in same relation to the amino acids indicated in the figure.

3. Results

3.1. S. macrospora POM33 Belongs to the Pom33/TMEM33 Protein Family

In LC/MS analysis with *S. macrospora* STRIPAK complex protein SCI1 as bait, a protein encoded by SMAC_00774 had previously been identified as putative interaction partner and predicted to be a POM33 homolog via BLASTP analysis [14]. The 1219-bp coding region of the *pom33* gene from *S. macrospora* is interrupted by 3 introns and encodes a putative 286 aa transmembrane membrane protein of 33 kDa. In *S. cerevisiae*, *S. pombe* and *H. sapiens*, four transmembrane nucleoporins (TM Nups) are known so far, among them Pom33p in *S. cerevisiae*, TMEM33 in *H. sapiens* and Tts1p in *S. pombe* (Figure S1A in Supplementary Materials) [61]. BLASTP analysis with the SmPOM33 protein sequence revealed 31.71% sequence identity with the *H. sapiens* transmembrane protein 33 (TMEM33, NP_060596.2, e-value: 6e−07), 31.37% with *S. cerevisiae* nucleoporin Pom33 (Pom33p, NP_013077.1, e-value: 6e−46), 18.61% with its paralog Per33p (Pore and ER protein of 33 kDa) (Per33p, NP_013165.1, e-value: 1e−10), and 28.36% to the *S. pombe* tetra-spanning protein 1 (Tts1p, NP_596818.1, e-value: 4e−35). SmPOM33 is predicted to contain 4 transmembrane domains (TMD), one coiled-coil (CC) motif and 3 amphiphatic α-helices (Figure S1B in Supplementary Materials). Using the InterProScan program N- and C-terminus of SmPOM33 were predicted to point to the cytoplasm.

3.2. SmPOM33 Localizes at the Nuclear Envelope and the ER

To determine the cellular localization of *S. macrospora* POM33, fluorescence microscopy was performed. SmPOM33 was C-terminally fused with either EGFP or TagRFP-T, to confirm the localization of POM33 independent of the tag. Both fusion constructs (POM33-EGFP and POM33-TagRFP-T) displayed a donut-like localization presumably around the nucleus that differs from the localization of free EGFP or TagRFP-T (Figures 2 and S2 in Supplementary Materials). For localization of free EGFP or TagRFP-T, *S. macrospora* wt was transformed with plasmid p1783-1 [62] or pTagRFP-T_nat [44], respectively. To verify the localization of POM33 around the nucleus, we crossed the wildtype (wt) strain expressing POM33-EGFP with a fus1-1 (fus) strain expressing the histone 2B (H2B) fused to tdTomato

(Figure 2A). The merged fluorescence image revealed the localization of POM33-EGFP as a fading ring around the red-labeled nucleus. To determine if POM33 also localizes to the endoplasmic reticulum (ER), *S. macrospora* wt strains expressing POM33-EGFP and the SERCA-type Ca^{2+}-ATPase NCA1 tagged to TagRFP-T as a reporter protein for the ER and the NE, were crossed (Figure 2B). The resulting yellow fluorescence signal in the merged picture showed co-localization of POM33-EGFP with NCA1-TagRFP-T at the ER in the hyphae. To confirm the localization of POM33 around the nucleus independent of the fluorescence tag, a wt strain expressing POM33-TagRFP-T was crossed with a wt strain expressing histone 2A (H2A) fused to EGFP (Figure 2C). Here, the fluorescence signal of POM33-TagRFP-T was visible in ring-like structures around the green-labeled nuclei, supporting the localization of POM33 around the nucleus. Further, microscopic investigation of co-transformed wt strain expressing POM33-TagRFP-T and the TM Nup of the nuclear pore complex (NPC) POM152 C-terminally fused to EGFP, revealed partial co-localization of the fusion constructs with a more faded one of POM33-TagRFP-T as described above for POM33-EGFP (Figure 2D). To verify expression of POM33-TagRFP-T and POM33-EGFP, we performed Western blot experiments (Figure S3 in Supplementary Materials).

3.3. Deletion of pom33 Displays no Distinct Phenotype Compared to the Wildtype

For construction of knock-out strains of *S. macrospora* we usually use a Δku70 strain, which is impaired in the repair of DNA double-strand breaks and has been shown to be an ideal recipient strain for gene targeting experiments [42]. Primary transformants of *S. macrospora* are often heterokaryotic, therefore, we isolated single-spore isolates to segregate the wt and mutant alleles of *Smpom33* gene in a Δku70 background. Strains that were homokaryotic for the desired *Smpom33* deletion and carried the *ku70*-deletion were further crossed against color-spore mutant fus1-1. However, by conventional genetic analysis, we never succeeded in isolating hygromycin resistant spores without the Δku70 (nourseothricin-resistant) background, indicating that *Smpom33* and *ku70* are coupled genes. Non-homologous end joining involves the binding of the Ku heterodimer (Ku70/Ku80) at the ends of a DNA double-strand break (DSB) [63]. It has been previously demonstrated that homologous recombination in fungi is equally increased in Δku80 strains [64,65]. Therefore, we decided to generate a *S. macrospora* Δku80 deletion mutant. A BLAST search revealed that *SMAC_00164* encodes the homolog of the *N. crassa* KU80 protein. Deletion of the *ku80* gene was performed by homologous recombination of a *hph* deletion cassette in the Δku70 strain. After isolation of single-spore isolates and subsequent crosses to the spore-color mutant fus1-1, we succeeded in isolating a *hyg* resistant Δku80 strain without the Δku70 background. Deletion of the *ku80* gene was confirmed by PCR and Southern blot analysis (Figure S4 in Supplementary Materials). Similar to the Δku70 strain no impairment in vegetative growth or sexual development could be observed in the Δku80 strain, making it an ideal recipient strain for homologous recombination in *S. macrospora* as well (Figure S5 in Supplementary Materials).

We then used the Δku80 deletion strain to generate a Δpom33 deletion mutant of *S. macrospora*. To construct the Δpom33 strain, homologous recombination of a *nat* deletion cassette flanked by upstream and downstream regions of *pom33* was performed. Deletion of *pom33* was confirmed by PCR and Southern blot analysis (Figure S6 in Supplementary Materials). To examine the role of POM33 during sexual development, the life cycle of the deletion strain and a complementation strain, ectopically expressing the genomic version of *pom33* fused to *TagRFP-T* (Δpom33::pom33-TagRFP-T^{ect}), were microscopically investigated together with the Δsci1 strain compared to the wt (Figure 3).

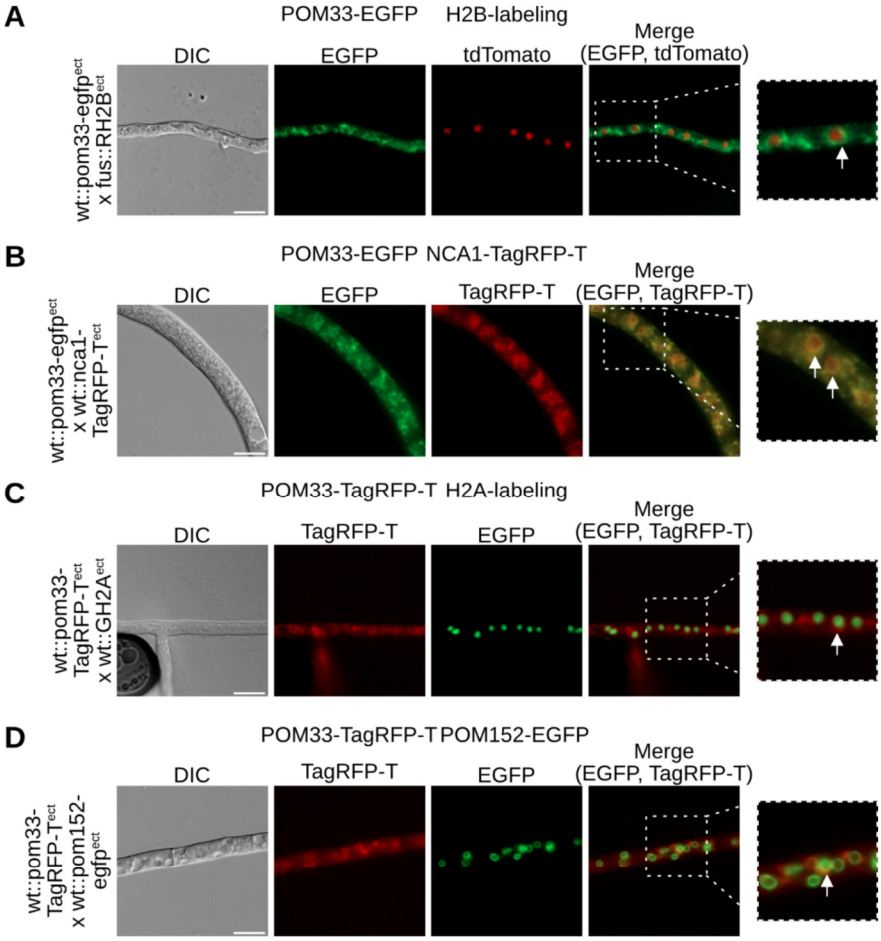

Figure 2. Co-localization of POM33 and marker proteins in *S. macrospora* wt using different fluorescence tags. *S. macrospora* wt expressing either POM33-EGFP or POM33-TagRFP-T was crossed with *S. macrospora* strains expressing marker proteins for the nucleus, endoplasmic reticulum (ER) and the nuclear envelope or the wt strain was co-transformed. Fluorescence microscopy was performed to visualize co-localization of the fusion proteins. (**A**) *S. macrospora* wt expressing POM33-EGFP was crossed with the fus1-1 strain expressing histone 2B labeled with tdTomato (RH2B). White arrow indicates localization of POM33-EGFP around the nucleus. (**B**) *S. macrospora* wt strains expressing POM33-EGFP and NCA1-TagRFP-T were crossed and co-localization of both proteins resulted in a yellow fluorescence signal is shown by the white arrows in the merged zoom-in picture. (**C**) *S. macrospora* wt expressing POM33-TagRFP-T and histone 2A tagged with EGFP (GH2A) were crossed to show localization of POM33 around the nucleus, independent of the fluorescence tag (white arrow in the merged zoom-in). (**D**) Partial co-localization of POM33-TagRFP-T with POM152-EGFP in *S. macrospora* wt (indicated by the white arrow). Scale bars = 10 µm. DIC, differential interference contrast. Detailed two-fold enlargements of the merge pictures are indicated with a dashed frame and shown at the right margin.

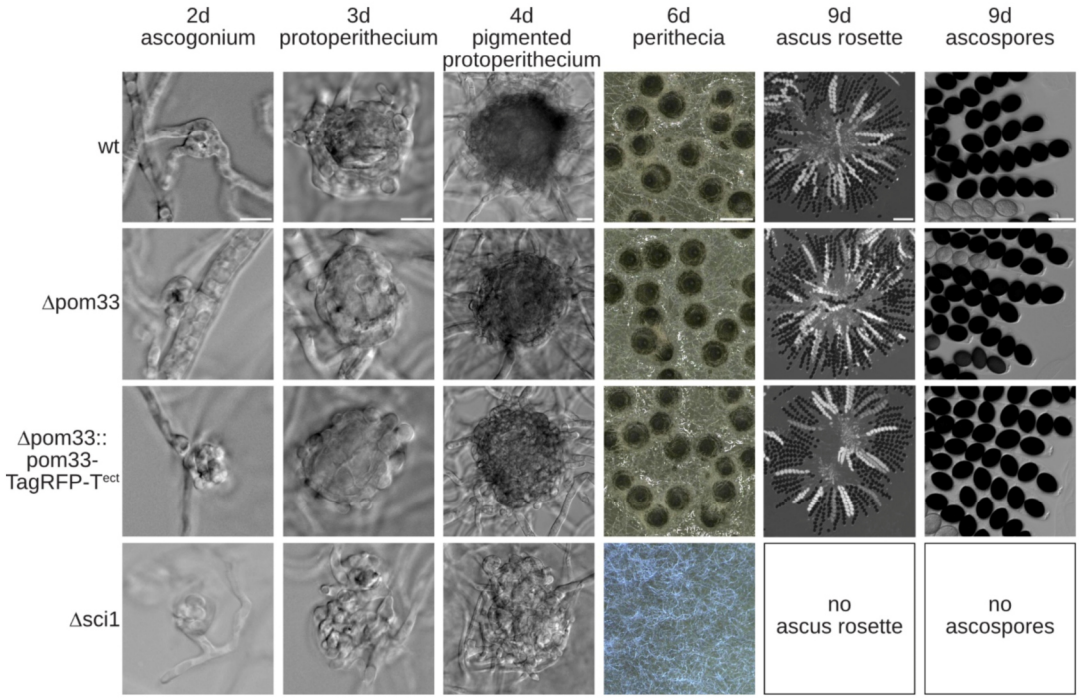

Figure 3. Sexual development in the wt, Δpom33, the complementation strain and Δsci1. Microscopic investigation of wt, Δpom33, the complementation strain (Δpom33::pom33-TagRFP-T^{ect}) and Δsci1 grown over cellophane on SWG agar plates at 27 °C. Photographs were taken at indicated days. Scale bars from left to right: 10 µm; 10 µm; 10 µm; 0.5 mm; 100 µm and 25 µm.

The wt, Δpom33 and the complemented strain completed the life cycle within 9 days and produced ascospores. The life cycle of *S. macrospora* starts with a germinating ascospore developing a vegetative mycelium. After 2–3 days, female gametangia (ascogonia) and after 3–4 days unpigmented fruiting-body precursors (protoperithecia) were produced that could be observed in all strains, respectively. These protoperithecia developed into melanin-pigmented large protoperithecia and after self-fertilization, karyogamy, meiosis and a postmeiotic-mitosis in the maturing perithecia, eight linear-arranged ascospores are present per ascus. Thus, the deletion mutant Δpom33 displayed no obvious phenotype in comparison to the wt (Figure 3). In contrast, STRIPAK deletion strain Δsci1 is impaired in sexual development and incapable of producing perithecia within 7 days (Figure 3). The Δsci1 strain arrests in the sexual developmental stage of protoperithecia, has a reduced growth rate and is unable to undergo hyphal fusions [14]. These defects were not observed in the Δpom33 strain (Figure 3).

3.4. The Mutant Δpom33 Exhibits no Sensitivity against a Series of Stress Conditions

Since there were no obvious developmental defects of Δpom33 visible in comparison to the wt and the complemented strain, we tested sexual development under different stress conditions. Here, sexual development of all three strains including the *sci1* deletion mutant, Δsci1, was investigated after 8 days on medium containing 0.1 M NaCl, mimicking osmotic stress, or under oxidative-stress conditions by supplementing the media with 0.01% H_2O_2. Moreover, growth under cell wall stress (100 µg/mL CFW) or under ER-stress conditions (1.5 mM DTT, 0.25 µg/mL TM) as well as temperature sensitivity (16 °C, 37 °C) was analyzed. All strains except Δsci1 were able to form perithecia under osmotic-,

oxidative-, cell wall- and ER-stress conditions displaying normal sexual development (Figure 4A). Furthermore, all strains were sensitive to cold and heat stress conditions and unable to produce mature fruiting-bodies (Figure 4B). In addition, no obvious difference in the number of discharged ascospores after 10 days could be observed except for Δsci1 (Figure 4B). These results showed that sexual development of *S. macrospora* is independent of POM33 function.

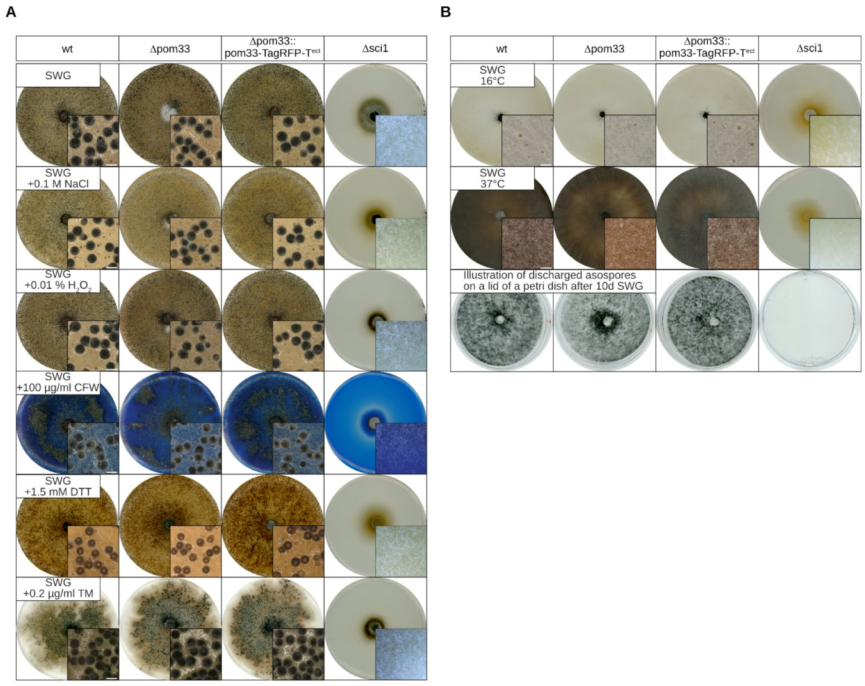

Figure 4. Sexual development in the wt, Δpom33, the complementation strain and Δsci1 on different stress media. (**A**) The wt, deletion mutant (Δpom33) and the complementation strain (Δpom33::pom33-TagRFP-T^{ect}) as well as the Δsci1 strain were grown in presence of different stress conditions, such as osmotic- (0.1 M NaCl), oxidative- (0.01% H_2O_2), cell wall- (100 µg/mL CFW), or ER stress (1.5 mM DTT, 0.2 µg/mL TM) by adding the different components to SWG medium. (**B**) Strains from (**A**) were grown on SWG media at 16 °C and 37 °C to perform temperature stress. After 10 days the lids of petri dishes with discharged ascospores were documented. Here, the spores were already germinated. Pictures of the agar plates and microscopic images of perithecia as shown in the small boxes on the bottom right sides were taken after 8 days. Scale bar of microscopic images: 0.5 mm.

3.5. Proteins of the ER Are Putative Interaction Partners of POM33

To analyze putative interaction partners of POM33-TagRFP-T, total protein extracts from Δpom33::pom33-TagRFP-T^{ect} strains and the control strain wt::TagRFP-T^{ect} were enriched in TagRFP-T pulldown experiments, trypsin digested and resulting peptides were analyzed by LC/MS. Data were evaluated in a semiquantitative method with label-free quantification (LFQ) based on signal intensities using the MaxQuant and Perseus programs [52,54]. Putative interaction candidates were illustrated in a volcano plot, where the difference in LFQ intensities versus the significance is graphed using a false discovery rate (FDR) of 0.01 and an S0 of 0.1 (Figure 5). To get reliable interaction partners, missing values were replaced four times with imputed values and proteins that were significant in all four repetitions are presented in Table S4 in Supplementary Materials.

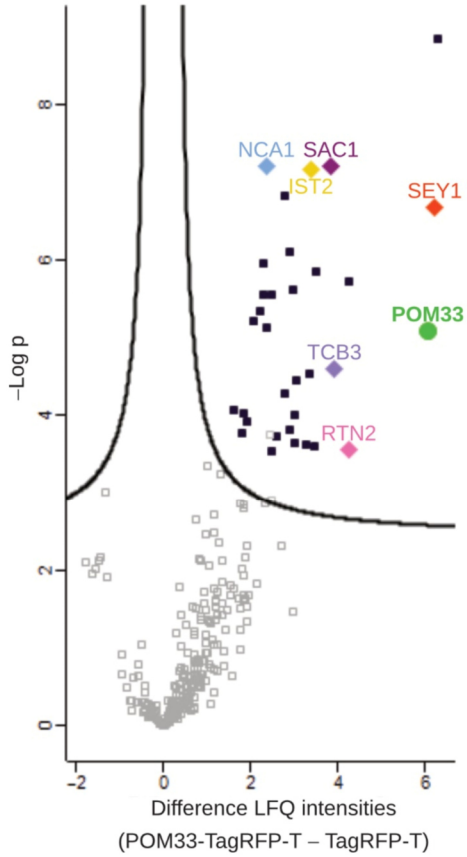

Figure 5. Volcano plot of putative interacting proteins from POM33-TagRFP-T pulldowns. For the pulldowns, in the first experiment three biological replicates of Δpom33::pom33-TagRFP-T^{ect} and wt::TagRFP-T^{ect} as control and for the second experiment three biological plus one technical replicate each of the sample and control strain were grown in liquid BMM media over 3 days at 27 °C under continuous light. Protein extracts of the strains were subjected to TagRFP-T-trap pulldown, trypsin digested and resulting peptides were analyzed by LC/MS. The result of two independent experiments is shown. In the volcano plot, the difference of LFQ intensities of POM33-TagRFPT in comparison to free TagRFP-T is plotted on the x-axis versus -Log *p*-values on the y-axis using a false discovery rate of 0.01 and an S0 of 0.1. The cutoff curve indicates proteins that were significantly enriched with POM33-TagRFP-T. Missing values were replaced four times with imputed values to get reliable interaction candidates. Proteins that were significant in all four repetitions are visible in the upper right part and are marked by dark blue squares (see also Table S4 in Supplementary Materials). They include NCA1 (light blue diamond), RTN2 (pink diamond), SEY1 (red diamond), TCB3 (purple diamond), IST2 (yellow diamond) and SAC1 (magenta diamond) as putative POM33 (neon green circle) interaction partners.

Homologous proteins in *S. cerevisiae* were identified using the *S. cerevisiae* Genome Database (SGD) (https://www.yeastgenome.org/blast-sgd; accessed on 12 April 2021) [56] and for proteins in *N. crassa* or *H. sapiens*, the UniProtKB BLAST tool (https://www.uniprot.org/blast/ accessed on 12 April 2021) [57] for fungi and *H. sapiens* was used. Nearly all proteins identified as putative POM33 interaction partners are predicted to locate at the ER-membrane where they have functions in metabolic processes, cation transport or cellu-

lar trafficking (Table S4 in Supplementary Materials). Among the best hits, proteins having functions in ER-shaping and -organization were identified, namely SEY1 (SMAC_08906), a reticulon-like protein (SMAC_00989), a putative tricalbin (SMAC_02980) and TMEM16-like protein (SMAC_00943). Interestingly, the ER-marker and calcium-transporting ATPase SmNCA1 (SMAC_04583) was also ascertained as putative interaction candidate of POM33. Besides, proteins involved in lipid metabolism, like a cyclopropane-fatty-acyl-phospholipid synthase (SMAC_02133), or the putative phosphatidyl inositol 4-phosphatase SAC1 (SMAC_01583) were determined. Moreover, a fatty acid desaturase (SMAC_03650), an acyl-CoA desaturase 1 (SMAC_01733) and a very-long-chain 3-oxoacyl-CoA reductase (SMAC_01146) which play roles in fatty acid biosynthesis were identified. Additionally, several proteins participating in sterol biosynthesis were among the 33 high confidence interactors, like a sterol 24-C methyltransferase (SMAC_01214), cytochrome P450 51 (SMAC_05737), a squalene monooxygenase (SMAC_00934), a C-3 sterol dehydrogenase/C-4 decarboxylase (SMAC_04350), a C-4 methylsterol oxidase (SMAC_00952), a squalene synthase (SMAC_07413) and cytochrome P450 4A5 (SMAC_05894). Furthermore, proteins that are important for protein glycosylation were detected, like dolichyl-diphosphooligosaccharide-protein glycosyltransferase subunit 1 (SMAC_05819), a dolichyl-phosphate-mannose-protein mannosyltransferase (SMAC_02375), a dolichyl-diphosphooligosaccharide-protein glycosyltransferase subunit WBP1 (SMAC_01348) and two other dolichyl-phosphate-mannose-protein mannosyltransferases (SMAC_06805, SMAC_08483). Proteins that translocate proteins to the ER were also found, like signal recognition particle (SRP) receptor subunit beta (SMAC_09603), transport protein SEC61 subunit alpha (SMAC_05120) and a translocation complex component (putative SEC63) (SMAC_02255). The putative interaction partners of POM33 validated the result of the localization study. To examine whether the ER-morphology changed due to deletion of *Smpom33*, we transformed the Δpom33 mutant with the *Tag-RFP-T* tagged ER-marker gene *Smnca1*. However, we did not observe any difference in ER-morphology when comparing the localization of NCA1-TagRFP-T in Δpom33, Δsci1 and the wt (Figure S7 in Supplementary Materials).

As these results revealed, no SmSTRIPAK-component was found to be significantly enriched in the POM33 pulldown experiments. In addition, fluorescence microscopic co-localization studies using POM33-TagRFP-T and SCI1-EGFP indicated no obvious co-localization of the two proteins (Figure S8 in Supplementary Materials). SCI1 and the striatin protein PRO11 were shown to localize around the nucleus and at cytoplasmic structures [14]. Therefore, we analyzed their localization in the Δpom33 deletion background together with red-labeled histone 2B using fluorescence microscopy (Figure S9 in Supplementary Materials). The expression of the proteins was verified by Western blot analysis (Figure S9 in Supplementary Materials). Due to the fact that SCI1-EGFP and PRO11-EGFP signals revealed no change in localization in comparison to the wt, we conclude that localization of the two SmSTRIPAK-components SCI1 and PRO11 did not depend on SmPOM33.

4. Discussion

In *S. macrospora*, the striatin homolog PRO11, SCI1 and other core components of the SmSTRIPAK have been to some extend localized around the nucleus [9,14]. A protein similar to the nucleoporin POM33 had previously been identified as a putative interactor of the *S. macrospora* SmSTRIPAK component SCI1 [14], leading to the hypothesis that it might be a putative anchor of the SmSTRIPAK to the nucleus. In this study, we determined the subcellular localization of SmPOM33 and identified its putative interaction candidates via pulldown experiments coupled to LC/MS analysis. Furthermore, we successfully established the Δku80 deletion strain as a useful tool for the generation of *S. macrospora* knockout strains.

Fluorescence microscopic investigations revealed SmPOM33 localization around the nucleus, at the NE and the ER using labeled histones or NE/ER marker proteins (Figure 2A–C). The homolog of the *N. crassa* SERCA-type Ca^{2+}-ATPase NCA-1, SmNCA1,

was used as marker protein for the ER and the NE (Figure 2B). This calcium pump was chosen as marker because fluorescence microscopy of *N. crassa* NCA1-GFP showed co-localization with GRP-78, a protein that facilitates protein folding in the ER [66], and DPM, a dolichol-phosphate mannosyltransferase located in the ER [67,68]. Since SmNCA1 and SmPOM33 displayed co-localization, whereas the TM Nup SmPOM152 and SmPOM33 could only partially be co-localized, SmPOM33 might rather be a NE/ER protein than an NPC component (Figure 2D). In fact, *S. cerevisiae* ScPom33p was shown to localize to the inner (INM) and outer (ONM) nuclear membrane of the NE with minor fractions at the ER, whereas its paralog ScPer33p was shown to be associated with NPCs but could mainly be localized at the ER and the NE [30,69]. More precisely, ScPom33p behaves as a dynamic TM Nup, because it exchanges between the NPC and the ER using ScNdc1p and a subunit of the translocon localizing to the cortical and perinuclear ER, ScSec61p, as controls in photobleaching experiments [30]. Moreover, the authors illustrated that ScPom33p contributes to NPC assembly, distribution and stabilization. In contrast, the mammalian ortholog of ScPom33p/ScPer33p, HsTMEM33, was not demonstrated to localize at the NPC but together with Calnexin and an ER-Tracker its subcellular location was determined at the ER with enrichment at the NE [30,69,70]. Similarly, in *S. pombe* Tts1p localizes to the tubular ER network and the NE with partially enrichment at NPCs [31,71].

Our results showed that deletion of *Smpom33* has no defect in sexual development under normal or stress conditions (Figures 3 and 4). Contrary to this, deletion of *sci1* displays a severe defect in sexual development and growth demonstrating that SmPOM33 likely acts independently of the SmSTRIPAK. Similarly, *S. cerevisiae* Δpom33 is viable with no growth defect at any temperature but shows a clustering-phenotype in which NPC-distribution along the NE is altered [30]. This clustering-phenotype could also be observed in yeast Δrtn1 and Δypo1 mutants that are impaired in NPC biogenesis [72,73]. Moreover, no detectable phenotype was visible upon HsTMEM33-depletion [30]. These observations suggest a redundancy between transmembrane Nups. However, HsTMEM33 protein expression was increased by ER stress induced by thapsigargin and tunicamycin implementing a role in the unfolded protein response (UPR) pathway [70]. Here, we could not observe any phenotype of Δpom33 under ER-stress conditions after application of DTT or tunicamycin in comparison to the wt (Figure 4).

Our pulldown experiments coupled to LC/MS analysis revealed mainly ER-membrane proteins as putative interaction partners of SmPOM33 (Figure 6 and Table S4 in Supplementary Materials).

With the chosen thresholds, 33 candidates were found whereby the SmPOM152 was filtered out as it was only identified in two of the seven SmPOM33-TagRFP-T samples and therefore not covered as being significant. This result matched the observation that SmPOM33 only partially co-localized with POM152 (Figure 2D). On the other hand, a reticulon-like protein homologous to *S. cerevisiae* Rtn2p and the ER-shaping and organization component SEY1 was identified with high significance.

Formation and maintenance of highly curved ER tubules is facilitated by ER-membrane proteins like members of the reticulon (RTN) family and the DP1/Yop1p family. RTN and DP1 protein families are involved in ER tubule shaping and stabilization by inserting their wedge-shaped hairpin C-terminal region (~200 amino acids) into the outer leaflet of the lipid bilayer to deform the ER membrane [74–77]. Noteworthy, the homolog of the yeast Yop1p, SMAC_06633, was also identified in our pulldown analysis with SmPOM33 but was not enriched with high significance in the tested samples (Figure 6). In yeast and mammals, RTNs are absent from ER sheets and peripheral ER and restricted to the tubular ER network [75]. In addition, several studies suggested that RTNs and DP1/Yop1p are involved in NE assembly and *de novo* nuclear-pore formation and stability due to their membrane-shaping properties [73,78,79]. The mammalian reticulon Rtn4a/NogoA is required for the generation and maintenance of tubular ER in vitro [75]. Affinity chromatography revealed that HsTMEM33 co-localizes with Rtn4C at ER sheets and partially at ER tubules and suppresses the membrane-shaping activity of reticulons, thus regulating

the tubular ER structure [32]. The *S. pombe* Tts1p co-localizes with Rtn1p and Yop1p at curved ER membranes and at the NE and plays a role in remodeling the NE during mitosis by modulating NPC distribution [31,71]. To sustain the highly curved ER domains, Ttsp1 functionally interacts with the ER-shaping proteins Rtn1p and Yop1p via its C-terminal α-helix [31,71]. For SmPOM33 also, C-terminal α-helices were predicted and an RTN2 homolog (SMAC_00989) was identified in the pulldowns. These findings hint to a possible interaction between the SmPOM33 helices and RTN2. The cooperation between TMDs and C-terminal helices in maintaining ER morphology has been reported for the dynamin-like GTPase atlastin/Sey1p [80–82]. In the study presented here, the homolog of Sey1p, SMAC_08906, was identified as a putative interactor of SmPOM33 (Table S4 in Supplementary Materials and Figure 5). Studies from [80] showed that mammalian atlastins localize to tubular ER and interact with tubule-shaping proteins. The atlastins functional ortholog in *S. cerevisiae*, Sey1p, mediates the fusion of two ER tubules at three-way junctions [80,83].

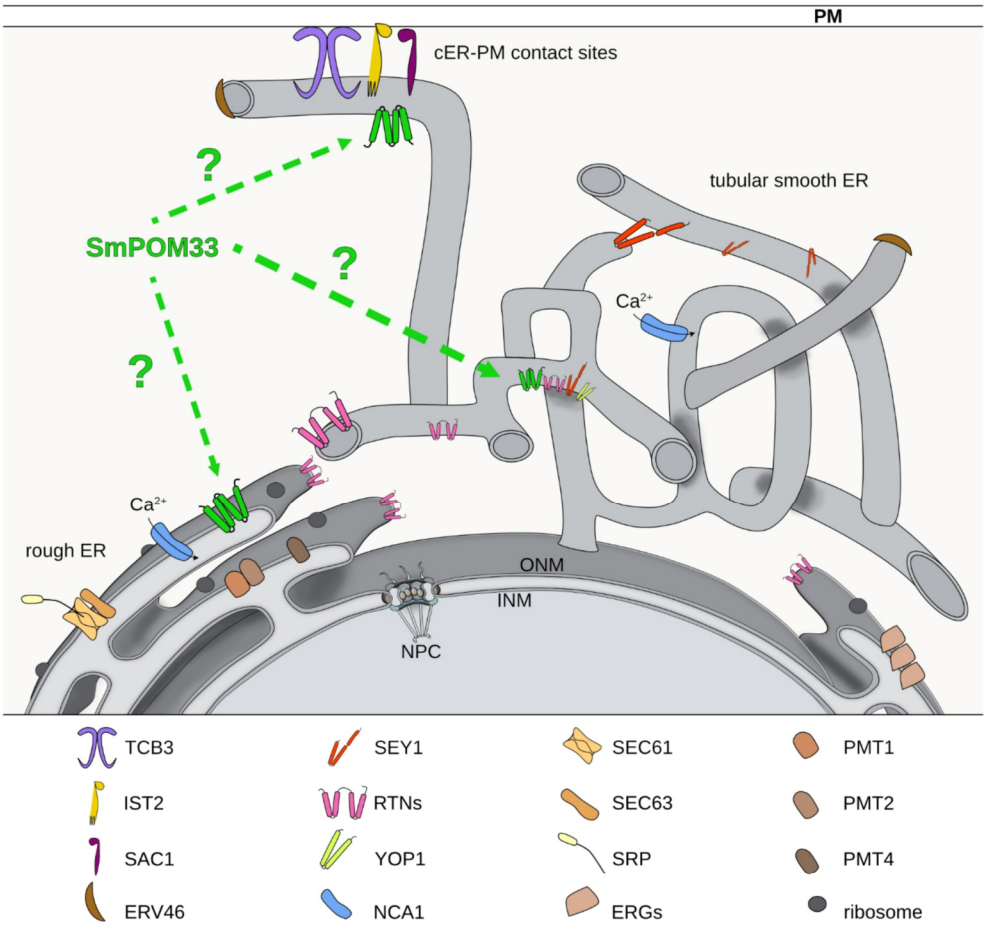

Figure 6. Schematic illustration of putative SmPOM33 localization and its potential interaction partners. Shown are the putative localization of SmPOM33 and the discussed proteins identified via pulldown experiments coupled to LC/MS analysis (Table S4 in Supplementary Materials). Putative interactions partners of SmPOM33 are located at the ER-membrane of the rough or tubular smooth ER. NPC: nuclear pore complex, INM: inner nuclear membrane, ONM: outer nuclear membrane, PM: plasma membrane, cER: cortical ER.

Additionally, to these ER-shaping candidates, SmNCA1 (SMAC_04583) occurred among the best hits (Figures 5 and 6). This result hint to a possible interaction of the Ca^{2+}-ATPase NCA1 with SmPOM33, which matched with their co-localization in fluorescence microscopy (Figure 2B). In *S. cerevisiae*, the P-type Ca^{2+}-ATPase Pmr1p, transports calcium and manganese into the Golgi [84–86].

Furthermore, *S. macrospora* homologs of *S. cerevisiae* tricalbin Tcb3p (SMAC_02980), the phosphatidylinositol phosphate phosphatase Sac1p (SMAC_01583) and the cER protein Ist2p (SMAC_000943) were identified (Figures 5 and 6). In yeast, together tricalbins and Ist2p are involved in tethering cER to the plasma membrane (PM) at cER-PM contact sites. They control the access of the phosphatydil-inositol-4-phosphatase Sac1p to its substrate phosphatidylinositol-4-phosphate (PI4P) thus regulating PI4P levels [87]. Thereby, contributing to cellular lipid fluxes, shaping of the cER and PM integrity [88,89]. Interestingly, a recent global phosphoproteom study of SmSTRIPAK mutants revealed that the tricalbin homolog SMAC_02980 is differential phosphorylated at T1203 in STRIPAK mutants making this SmPOM33 interactor a putative STRIPAK target [90]. In *S. cerevisiae*, the SmPOM33 homolog Per33p showed a positive genetic interaction with Tcb3p suggesting a regulatory connection between both proteins [91].

Additionally, putative homologs of SEC61 (SMAC_05120) and SEC63 (SMAC_02255) together with the SRP receptor beta subunit (SMAC_09603) were enriched in the SmPOM33 pulldown (Table S4 in Supplementary Materials). The Sec61 complex mediates SRP-dependent protein import into the ER and by interaction with the Sec63 complex is required for SRP-independent protein import [92,93]. Moreover, three putative protein O-mannosyltransferases homologous to yeast PMT1 (SMAC_06805), PMT2 (SMAC_02375), and PMT4 (SMAC_08483) were found to be enriched in the LC/MS analysis of SmPOM33 pulldowns. In *S. cerevisiae*, Pmts are located in the ER membrane where they function in protein O-glycosylation [94–96]. Besides these ER membrane proteins, a homolog of the *S. cerevisiae* COPII-coated vesicle protein ERV46 (SAMC_04901) was identified. In fact, specialized regions of the smooth tubular ER, called ER exit sites (ERES), play a unique role in the assembly of COPII-coated vesicles which mediate trafficking from ER to the Golgi [97]. Besides, several *S. macrospora* homologs of the ergosterol-biosynthesis pathway were also enriched in the pulldown experiments, namely ERG6 (SMAC_01214), ERG11 (SMAC_05737 or SMAC_05894), ERG1 (SMAC_00934), ERG26 (SMAC_04350), ERG25 (SMAC_00952) and ERG9 (SMAC_07413). Of interest, in *N. crassa* the knockout of *erg2* or *erg1* leads to cell fusion defects of hyphae [98,99]. This phenotype of dysfunctional hyphal fusion was also described for mutants of SmSTRIPAK components like in Δsci1 [14].

The results of the pulldown using SmPOM33 as bait revealed no SmSTRIPAK-component as putative interaction partner. Therefore, it seems that SmPOM33 is not anchoring the SmSTRIPAK to the nucleus. This suggestion is highlighted by the fact, that using PRO11 and SmMOB3 as bait, the nucleoporin NIC96 of the NPC was identified and might be the candidate responsible for nucleus-anchoring of the SmSTRIPAK [14]. Furthermore, SCI1 and PRO11 were co-localized with the nucleoporin SmPOM152 [14] that only partially co-localized with SmPOM33. Interestingly, SmSEY1 (SMAC_08906) was significantly enriched in PRO11 pulldowns [14].

The results of our fluorescence microscopic localization studies and pulldown experiments coupled to LC/MS analysis indicate that similar to the human homolog HsTMEM33, SmPOM33 is rather an ER/NE protein than a component of the NPC. HsTMEM33 is absent from the NPC and abundant at the ER and NE [30,69]. Targeting of ScPom33p to the NPC is facilitated by the nuclear import factor Kap123 that directly interacts with the amphipathic α-helices within the C-terminal domain of ScPom33p [69]. Accordingly, proper NPC localization of ScPom33p is dependent on its lipid binding ability and Kap123 binding. Interestingly, the CTD of ScPom33p is not very conserved in SmPOM33, revealing that SmPOM33 possesses no binding site for the direct interaction with nuclear import factors. This fact is underlined by the results of the LC/MS analysis, where mainly ER-

membrane proteins were identified and no component of NPCs or any nuclear import factor like Kap123.

5. Conclusions

In conclusion, the pulldown and LC/MS analysis of SmPOM33 revealed potential interactions partners that are localized at the ER-membrane in the nuclear envelope or at cER-PM contact sites possessing different cellular functions (Figure 6). Therefore, SmPOM33 is rather an ER-protein than a component of the NPC. To confirm this assumption, further future studies are required to verify direct physical or genetic interaction with the identified candidates and the impact of the STRIPAK complex on ER morphology and organization. These include the identification of the conditions under which SmPOM33 is functional, the exact localization of SmPOM33 by super-resolution microscopy or immune EM.

Supplementary Materials: The following are available online at https://www.mdpi.com/article/10.3390/jof7090682/s1, Table S1: list of plasmids, Table S2: primers used in this study, Table S3: Perseus 1.6.0.7 workflow, Figure S1: transmembrane nucleoporins and domain organization of POM33 orthologs and paralogues in human and fungi, Figure S2: localization of free TagRFP-T and EGFP, Figure S3: fluorescence microscopy of POM33-TagRFP-T/-EGFP and expression controls via Western blot analysis, Figure S4: verification of *Smku80* deletion by PCR and Southern blot analyses, Figure S5: sexual development and vegetative growth rates in the Δku80 and wt strain, Figure S6: verification of *Smpom33* deletion by PCR and Southern blot analyses, Figure S7: localization of the ER-marker NCA1-TagRFP-T in the *S. macrospora* wt, Δpom33 and Δsci1 strain, Figure S8: co-localization of POM33 and SCI1 in *S. macrospora* wt, Figure S9: localization of SCI1 and PRO11 in Δpom33 and Western blot analysis.

Author Contributions: A.G. and S.P. made the experimental design; A.G., K.S., O.V. and B.H. performed experiments and analyzed data; A.G. and S.P. wrote the manuscript. All authors have read and agreed to the published version of the manuscript.

Funding: This research was funded by the Deutsche Forschungsgemeinschaft (DFG, German Research Foundation), Po 523/9-1 Project number 429272002, VA 352/2-2, and INST 186/1230-1 FUGG. We further acknowledge support by the Open Access Publication Funds of the Göttingen University.

Institutional Review Board Statement: Not applicable.

Informed Consent Statement: Not applicable.

Data Availability Statement: The mass spectrometry proteomics data have been deposited to the ProteomeXchange Consortium via the PRIDE [100] partner repository with the dataset identifier PXD026253.

Acknowledgments: We gratefully acknowledge Gertrud Stahlhut for her excellent technical support and Daniela Nordzieke for critically reading the manuscript.

Conflicts of Interest: The authors declare no conflict of interest. The funders had no role in the design of the study; in the collection, analyses, or interpretation of data; in the writing of the manuscript, or in the decision to publish the results.

References

1. Hwang, J.; Pallas, D.C. STRIPAK complexes: Structure, biological function, and involvement in human diseases. *Int. J. Biochem. Cell Biol.* **2014**, *47*, 118–148. [CrossRef]
2. Shi, Z.; Jiao, S.; Zhou, Z. STRIPAK complexes in cell signaling and cancer. *Oncogene* **2016**, *35*, 4549–4557. [CrossRef]
3. Benoist, M.; Gaillard, S.; Castets, F. The striatin family: A new signaling platform in dendritic spines. *J. Physiol. Paris* **2006**, *99*, 146–153. [CrossRef]
4. Teichert, I.; Nowrousian, M.; Pöggeler, S.; Kück, U. The filamentous fungus *Sordaria macrospora* as a genetic model to study fruiting body development. *Adv. Genet.* **2014**, *87*, 199–244.
5. Teichert, I.; Pöggeler, S.; Nowrousian, M. *Sordaria macrospora*: 25 years as a model organism for studying the molecular mechanisms of fruiting body development. *Appl. Microbiol. Biotechnol.* **2020**, *104*, 3691–3704. [CrossRef] [PubMed]

6. Bloemendal, S.; Bernhards, Y.; Bartho, K.; Dettmann, A.; Voigt, O.; Teichert, I.; Seiler, S.; Wolters, D.A.; Pöggeler, S.; Kück, U. A homologue of the human STRIPAK complex controls sexual development in fungi. *Mol. Microbiol.* **2012**, *84*, 310–323. [CrossRef] [PubMed]
7. Pöggeler, S.; Kück, U. A WD40 repeat protein regulates fungal cell differentiation and can be replaced functionally by the mammalian homologue striatin. *Eukaryot. Cell* **2004**, *3*, 232–240. [CrossRef]
8. Kück, U.; Beier, A.M.; Teichert, I. The composition and function of the striatin-interacting phosphatases and kinases (STRIPAK) complex in fungi. *Fungal Genet. Biol.* **2016**, *90*, 31–38. [CrossRef] [PubMed]
9. Nordzieke, S.; Zobel, T.; Franzel, B.; Wolters, D.A.; Kück, U.; Teichert, I. A fungal sarcolemmal membrane-associated protein (SLMAP) homolog plays a fundamental role in development and localizes to the nuclear envelope, endoplasmic reticulum, and mitochondria. *Eukaryot. Cell* **2015**, *14*, 345–358. [CrossRef] [PubMed]
10. Beier, A.; Teichert, I.; Krisp, C.; Wolters, D.A.; Kück, U. Catalytic Subunit 1 of Protein Phosphatase 2A Is a Subunit of the STRIPAK Complex and Governs Fungal Sexual Development. *mBio* **2016**, *7*, 1–11. [CrossRef] [PubMed]
11. Frey, S.; Reschka, E.J.; Pöggeler, S. Germinal Center Kinases SmKIN3 and SmKIN24 Are Associated with the *Sordaria macrospora* Striatin-Interacting Phosphatase and Kinase (STRIPAK) Complex. *PLoS ONE* **2015**, *10*, e0139163. [CrossRef] [PubMed]
12. Radchenko, D.; Teichert, I.; Pöggeler, S.; Kück, U. A Hippo pathway-related GCK controls both sexual and vegetative developmental processes in the fungus *Sordaria macrospora*. *Genetics* **2018**, *210*, 137–153. [CrossRef] [PubMed]
13. Bernhards, Y.; Pöggeler, S. The phocein homologue SmMOB3 is essential for vegetative cell fusion and sexual development in the filamentous ascomycete *Sordaria macrospora*. *Curr Genet.* **2011**, *57*, 133–149. [CrossRef]
14. Reschka, E.J.; Nordzieke, S.; Valerius, O.; Braus, G.H.; Pöggeler, S. A novel STRIPAK complex component mediates hyphal fusion and fruiting-body development in filamentous fungi. *Mol. Microbiol.* **2018**, *110*, 513–532. [CrossRef]
15. Jeong, B.C.; Bae, S.J.; Ni, L.; Zhang, X.; Bai, X.C.; Luo, X. Cryo-EM structure of the Hippo signaling integrator human STRIPAK. *Nat. Struct. Mol. Biol.* **2021**, *28*, 290–299. [CrossRef]
16. De Magistris, P.; Antonin, W. The dynamic nature of the nuclear envelope. *Curr. Biol.* **2018**, *28*, R487–R497. [CrossRef]
17. Baumann, O.; Walz, B. Endoplasmic reticulum of animal cells and its organization into structural and functional domains. *Int. Rev. Cytol.* **2001**, *205*, 149–214.
18. Wang, N.; Rapoport, T.A. Reconstituting the reticular ER network–mechanistic implications and open questions. *J. Cell Sci.* **2019**, *132*, 1–7. [CrossRef]
19. Shibata, Y.; Voeltz, G.K.; Rapoport, T.A. Rough sheets and smooth tubules. *Cell* **2006**, *126*, 435–439. [CrossRef]
20. Lee, C.; Chen, L.B. Dynamic behavior of endoplasmic reticulum in living cells. *Cell* **1988**, *54*, 37–46. [CrossRef]
21. Du, Y.; Ferro-Novick, S.; Novick, P. Dynamics and inheritance of the endoplasmic reticulum. *J. Cell Sci.* **2004**, *117*, 2871–2878. [CrossRef]
22. Hampoelz, B.; Andres-Pons, A.; Kastritis, P.; Beck, M. Structure and assembly of the nuclear pore complex. *Annu. Rev. Biophys.* **2019**, *48*, 515–536. [CrossRef] [PubMed]
23. Hetzer, M.W.; Walther, T.C.; Mattaj, I.W. Pushing the envelope: Structure, function, and dynamics of the nuclear periphery. *Annu. Rev. Cell Dev. Biol.* **2005**, *21*, 347–380. [CrossRef]
24. Antonin, W.; Ellenberg, J.; Dultz, E. Nuclear pore complex assembly through the cell cycle: Regulation and membrane organization. *FEBS Lett.* **2008**, *582*, 2004–2016. [CrossRef]
25. Doucet, C.M.; Hetzer, M.W. Nuclear pore biogenesis into an intact nuclear envelope. *Chromosoma* **2010**, *119*, 469–477. [CrossRef] [PubMed]
26. Doucet, C.M.; Talamas, J.A.; Hetzer, M.W. Cell cycle-dependent differences in nuclear pore complex assembly in metazoa. *Cell* **2010**, *141*, 1030–1041. [CrossRef]
27. Chial, H.J.; Rout, M.P.; Giddings Jr, T.H.; Winey, M. *Saccharomyces cerevisiae* Ndc1p is a shared component of nuclear pore complexes and spindle pole bodies. *J. Cell Biol.* **1998**, *143*, 1789–1800. [CrossRef]
28. Mansfeld, J.; Güttinger, S.; Hawryluk-Gara, L.A.; Panté, N.; Mall, M.; Galy, V.; Haselmann, U.; Mühlhäusser, P.; Wozniak, R.W.; Mattaj, I.W.; et al. The conserved transmembrane nucleoporin NDC1 is required for nuclear pore complex assembly in vertebrate cells. *Mol. Cell* **2006**, *22*, 93–103. [CrossRef]
29. Stavru, F.; Hülsmann, B.B.; Spang, A.; Hartmann, E.; Cordes, V.C.; Görlich, D. NDC1: A crucial membrane-integral nucleoporin of metazoan nuclear pore complexes. *J. Cell Biol.* **2006**, *173*, 509–519. [CrossRef]
30. Chadrin, A.; Hess, B.; San Roman, M.; Gatti, X.; Lombard, B.; Loew, D.; Barral, Y.; Palancade, B.; Doye, V. Pom33, a novel transmembrane nucleoporin required for proper nuclear pore complex distribution. *J. Cell Biol.* **2010**, *189*, 795–811. [CrossRef]
31. Zhang, D.; Oliferenko, S. Tts1, the fission yeast homologue of the TMEM33 family, functions in NE remodeling during mitosis. *Mol. Biol. Cell* **2014**, *25*, 2970–2983. [CrossRef]
32. Urade, T.; Yamamoto, Y.; Zhang, X.; Ku, Y.; Sakisaka, T. Identification and characterization of TMEM33 as a reticulon-binding protein. *Kobe J. Med. Sci.* **2014**, *60*, E57–E65.
33. Sambrook, J.; Fritsch, E.; Maniatis, T. *Molecular Cloning: A Laboratory Manual*; Cold Spring Harbor Laboratory Press: Cold Spring Harbor, NY, USA, 2001.
34. Colot, H.V.; Park, G.; Turner, G.E.; Ringelberg, C.; Crew, C.M.; Litvinkova, L.; Weiss, R.L.; Borkovich, K.A.; Dunlap, J.C. A high-throughput gene knockout procedure for Neurospora reveals functions for multiple transcription factors. *Proc. Natl. Acad. Sci. USA* **2006**, *103*, 10352–10357. [CrossRef]

35. James, P.; Halladay, J.; Craig, E.A. Genomic libraries and a host strain designed for highly efficient two-hybrid selection in yeast. *Genetics* **1996**, *144*, 1425–1436. [CrossRef]
36. Walz, M.; Kuck, U. Transformation of *Sordaria macrospora* to hygromycin B resistance: Characterization of transformants by electrophoretic karyotyping and tetrad analysis. *Curr. Genet.* **1995**, *29*, 88–95. [CrossRef]
37. Kück, U.; Hoff, B. Application of the nourseothricin acetyltransferase gene (nat1) as dominant marker for the transformation of filamentous fungi. *Fungal Genet. Newsl.* **2006**, *53*, 9–11. [CrossRef]
38. Elleuche, S.; Pöggeler, S. Visualization of peroxisomes via SKL-tagged DsRed protein in *Sordaria macrospora*. *Fungal Genet. Rep.* **2008**, *55*, 9–12. [CrossRef]
39. Esser, K. *Cryptogams: Cyanobacteria, Algae, Fungi, Lichens*; Cambridge University Press: Cambridge, UK, 1982.
40. Nowrousian, M.; Ringelberg, C.; Dunlap, J.C.; Loros, J.J.; Kück, U. Cross-species microarray hybridization to identify developmentally regulated genes in the filamentous fungus *Sordaria macrospora*. *Mol. Genet. Genom.* **2005**, *273*, 137–149. [CrossRef]
41. Nowrousian, M.; Teichert, I.; Masloff, S.; Kück, U. Whole-Genome Sequencing of *Sordaria macrospora* Mutants Identifies Developmental Genes. *G3* **2012**, *2*, 261–270. [CrossRef]
42. Pöggeler, S.; Kück, U. Highly efficient generation of signal transduction knockout mutants using a fungal strain deficient in the mammalian *ku70* ortholog. *Gene* **2006**, *378*, 1–10. [CrossRef] [PubMed]
43. Voigt, O.; Pöggeler, S. Autophagy genes *Smatg8* and *Smatg4* are required for fruiting-body development, vegetative growth and ascospore germination in the filamentous ascomycete *Sordaria macrospora*. *Autophagy* **2013**, *9*, 33–49. [CrossRef]
44. Werner, A.; Otte, K.; Stahlhut, G.; Hanke, L.M.; Pöggeler, S. The Glyoxysomal Protease LON2 Is Involved in Fruiting-Body Development, Ascosporogenesis and Stress Resistance in *Sordaria macrospora*. *J. Fungi* **2021**, *7*, 82. [CrossRef]
45. Dahlmann, T.A.; Terfehr, D.; Becker, K.; Teichert, I. Golden Gate vectors for efficient gene fusion and gene deletion in diverse filamentous fungi. *Curr. Genet.* **2021**, *67*, 317–330. [CrossRef]
46. Klix, V.; Nowrousian, M.; Ringelberg, C.; Loros, J.J.; Dunlap, J.C.; Pöggeler, S. Functional characterization of MAT1-1-specific mating-type genes in the homothallic ascomycete *Sordaria macrospora* provides new insights into essential and nonessential sexual regulators. *Eukaryot. Cell* **2010**, *9*, 894–905. [CrossRef]
47. Christianson, T.W.; Sikorski, R.S.; Dante, M.; Shero, J.H.; Hieter, P. Multifunctional yeast high-copy-number shuttle vectors. *Gene* **1992**, *110*, 119–122. [CrossRef]
48. Carroll, A.M.; Sweigard, J.A.; Valent, B. Improved vectors for selecting resistance to hygromycin. *Fungal Genet. Rep.* **1994**, *41*, 22. [CrossRef]
49. Towbin, H.; Staehelin, T.; Gordon, J. Electrophoretic transfer of proteins from polyacrylamide gels to nitrocellulose sheets: Procedure and some applications. *Proc. Natl. Acad. Sci. USA* **1979**, *76*, 4350–4354. [CrossRef]
50. Shevchenko, A.; Wilm, M.; Vorm, O.; Mann, M. Mass spectrometric sequencing of proteins silver-stained polyacrylamide gels. *Anal. Chem.* **1996**, *68*, 850–858. [CrossRef]
51. Rappsilber, J.; Ishihama, Y.; Mann, M. Stop and go extraction tips for matrix-assisted laser desorption/ionization, nanoelectrospray, and LC/MS sample pretreatment in proteomics. *Anal. Chem.* **2003**, *75*, 663–670. [CrossRef]
52. Cox, J.; Mann, M. MaxQuant enables high peptide identification rates, individualized p.p.b.-range mass accuracies and proteome-wide protein quantification. *Nat. Biotechnol.* **2008**, *26*, 1367–1372. [CrossRef]
53. Blank-Landeshammer, B.; Teichert, I.; Märker, R.; Nowrousian, M.; Kück, U.; Sickmann, A. Combination of Proteogenomics with peptide *de novo* sequencing identifies new genes and hidden posttranscriptional modifications. *MBio* **2019**, *10*, 1–17. [CrossRef]
54. Tyanova, S.; Temu, T.; Sinitcyn, P.; Carlson, A.; Hein, M.Y.; Geiger, T.; Mann, M.; Cox, J. The Perseus computational platform for comprehensive analysis of (prote)omics data. *Nat. Methods* **2016**, *13*, 731–740. [CrossRef]
55. Oliveros, J.C. VENNY. An Interactive Tool for Comparing Lists with Venn Diagrams (2007–2015). Available online: https://bioinfogp.cnb.csic.es/tools/venny/index.html (accessed on 12 April 2021).
56. Cherry, J.M.; Adler, C.; Ball, C.; Chervitz, S.A.; Dwight, S.S.; Hester, E.T.; Jia, Y.; Juvik, G.; Roe, T.; Schroeder, M.; et al. SGD: Saccharomyces Genome Database. *Nucleic Acids Res.* **1998**, *26*, 73–79. [CrossRef]
57. UniProt Consortium. UniProt: The universal protein knowledgebase in 2021. *Nucleic Acids Res.* **2021**, *49*, D480–D489. [CrossRef]
58. Blum, M.; Chang, H.Y.; Chuguransky, S.; Grego, T.; Kandasaamy, S.; Mitchell, A.; Nuka, G.; Paysan-Lafosse, T.; Qureshi, M.; Raj, S.; et al. The InterPro protein families and domains database: 20 years on. *Nucleic Acids Res.* **2021**, *49*, D344–D354. [CrossRef] [PubMed]
59. Combet, C.; Blanchet, C.; Geourjon, C.; Deleage, G. NPS@: Network protein sequence analysis. *Trends Biochem. Sci.* **2000**, *25*, 147–150. [CrossRef]
60. Klausen, M.S.; Jespersen, M.C.; Nielsen, H.; Jensen, K.K.; Jurtz, V.I.; Sonderby, C.K.; Sommer, M.O.A.; Winther, O.; Nielsen, M.; Petersen, B.; et al. NetSurfP-2.0: Improved prediction of protein structural features by integrated deep learning. *Proteins* **2019**, *87*, 520–527. [CrossRef]
61. Asakawa, H.; Yang, H.J.; Yamamoto, T.G.; Ohtsuki, C.; Chikashige, Y.; Sakata-Sogawa, K.; Tokunaga, M.; Iwamoto, M.; Hiraoka, Y.; Haraguchi, T. Characterization of nuclear pore complex components in fission yeast *Schizosaccharomyces pombe*. *Nucleus* **2014**, *5*, 149–162. [CrossRef] [PubMed]
62. Pöggeler, S.; Masloff, S.; Hoff, B.; Mayrhofer, S.; Kück, U. Versatile EGFP reporter plasmids for cellular localization of recombinant gene products in filamentous fungi. *Curr. Genet.* **2003**, *43*, 54–61. [CrossRef] [PubMed]

63. Fell, V.L.; Schild-Poulter, C. The Ku heterodimer: Function in DNA repair and beyond. *Mutat. Res. Rev. Mutat. Res.* **2015**, *763*, 15–29. [CrossRef] [PubMed]
64. Da Silva Ferreira, M.E.; Kress, M.R.; Savoldi, M.; Goldman, M.H.S.; Härtl, A.; Heinekamp, T.; Brakhage, A.A.; Goldman, G.H. The akuBKU80 mutant deficient for nonhomologous end joining is a powerful tool for analyzing pathogenicity in Aspergillus fumigatus. *Eukaryot. Cell* **2006**, *5*, 207–211. [CrossRef]
65. Ninomiya, Y.; Suzuki, K.; Ishii, C.; Inoue, H. Highly efficient gene replacements in Neurospora strains deficient for nonhomologous end-joining. *Proc. Natl. Acad. Sci. USA* **2004**, *101*, 12248–12253. [CrossRef]
66. Monnerjahn, C.; Techel, D.; Meyer, U.; Rensing, L. The grp78 promoter of *Neurospora crassa*: Constitutive, stress and differentiation-dependent protein-binding patterns. *Curr. Genet.* **2001**, *39*, 319–326. [CrossRef] [PubMed]
67. Orlean, P.; Albright, C.; Robbins, P.W. Cloning and sequencing of the yeast gene for dolichol phosphate mannose synthase, an essential protein. *J. Biol. Chem.* **1988**, *263*, 17499–17507. [CrossRef]
68. Bowman, B.J.; Draskovic, M.; Freitag, M.; Bowman, E.J. Structure and distribution of organelles and cellular location of calcium transporters in *Neurospora crassa*. *Eukaryot. Cell* **2009**, *8*, 1845–1855. [CrossRef]
69. Floch, A.G.; Tareste, D.; Fuchs, P.F.; Chadrin, A.; Naciri, I.; Leger, T.; Schlenstedt, G.; Palancade, B.; Doye, V. Nuclear pore targeting of the yeast Pom33 nucleoporin depends on karyopherin and lipid binding. *J. Cell Sci.* **2015**, *128*, 305–316. [CrossRef]
70. Sakabe, I.; Hu, R.; Jin, L.; Clarke, R.; Kasid, U.N. TMEM33: A new stress-inducible endoplasmic reticulum transmembrane protein and modulator of the unfolded protein response signaling. *Breast Cancer Res. Treat.* **2015**, *153*, 285–297. [CrossRef]
71. Zhang, D.; Vjestica, A.; Oliferenko, S. The cortical ER network limits the permissive zone for actomyosin ring assembly. *Curr. Biol.* **2010**, *20*, 1029–1034. [CrossRef]
72. Doye, V.; Hurt, E. From nucleoporins to nuclear pore complexes. *Curr. Opin. Cell Biol.* **1997**, *9*, 401–411. [CrossRef]
73. Dawson, T.R.; Lazarus, M.D.; Hetzer, M.W.; Wente, S.R. ER membrane-bending proteins are necessary for *de novo* nuclear pore formation. *J. Cell Biol.* **2009**, *184*, 659–675. [CrossRef]
74. Oertle, T.; Klinger, M.; Stuermer, C.A.; Schwab, M.E. A reticular rhapsody: Phylogenic evolution and nomenclature of the RTN/Nogo gene family. *FASEB J.* **2003**, *17*, 1238–1247. [CrossRef]
75. Voeltz, G.K.; Prinz, W.A.; Shibata, Y.; Rist, J.M.; Rapoport, T.A. A class of membrane proteins shaping the tubular endoplasmic reticulum. *Cell* **2006**, *124*, 573–586. [CrossRef]
76. Hu, J.; Shibata, Y.; Voss, C.; Shemesh, T.; Li, Z.; Coughlin, M.; Kozlov, M.M.; Rapoport, T.A.; Prinz, W.A. Membrane proteins of the endoplasmic reticulum induce high-curvature tubules. *Science* **2008**, *319*, 1247–1250. [CrossRef] [PubMed]
77. Shibata, Y.; Voss, C.; Rist, J.M.; Hu, J.; Rapoport, T.A.; Prinz, W.A.; Voeltz, G.K. The reticulon and DP1/Yop1p proteins form immobile oligomers in the tubular endoplasmic reticulum. *J. Biol. Chem.* **2008**, *283*, 18892–18904. [CrossRef]
78. Anderson, D.J.; Hetzer, M.W. Reshaping of the endoplasmic reticulum limits the rate for nuclear envelope formation. *J. Cell Biol.* **2008**, *182*, 911–924. [CrossRef] [PubMed]
79. Kiseleva, E.; Morozova, K.N.; Voeltz, G.K.; Allen, T.D.; Goldberg, M.W. Reticulon 4a/NogoA locates to regions of high membrane curvature and may have a role in nuclear envelope growth. *J. Struct. Biol.* **2007**, *160*, 224–235. [CrossRef] [PubMed]
80. Hu, J.; Shibata, Y.; Zhu, P.P.; Voss, C.; Rismanchi, N.; Prinz, W.A.; Rapoport, T.A.; Blackstone, C. A class of dynamin-like GTPases involved in the generation of the tubular ER network. *Cell* **2009**, *138*, 549–561. [CrossRef]
81. Orso, G.; Pendin, D.; Liu, S.; Tosetto, J.; Moss, T.J.; Faust, J.E.; Micaroni, M.; Egorova, A.; Martinuzzi, A.; McNew, J.A. Homotypic fusion of ER membranes requires the dynamin-like GTPase atlastin. *Nature* **2009**, *460*, 978–983. [CrossRef]
82. Liu, T.Y.; Bian, X.; Sun, S.; Hu, X.; Klemm, R.W.; Prinz, W.A.; Rapoport, T.A.; Hu, J. Lipid interaction of the C terminus and association of the transmembrane segments facilitate atlastin-mediated homotypic endoplasmic reticulum fusion. *Proc. Natl. Acad. Sci. USA* **2012**, *109*, E2146–E2154. [CrossRef]
83. Chen, S.; Novick, P.; Ferro-Novick, S. ER structure and function. *Curr. Opin. Cell Biol.* **2013**, *25*, 428–433. [CrossRef]
84. Antebi, A.; Fink, G.R. The yeast Ca $^{(2+)}$-ATPase homologue, PMR1, is required for normal Golgi function and localizes in a novel Golgi-like distribution. *Mol. Biol. Cell* **1992**, *3*, 633–654. [CrossRef]
85. Dürr, G.; Strayle, J.; Plemper, R.; Elbs, S.; Klee, S.K.; Catty, P.; Wolf, D.H.; Rudolph, H.K. The medial-Golgi ion pump Pmr1 supplies the yeast secretory pathway with Ca^{2+} and Mn^{2+} required for glycosylation, sorting, and endoplasmic reticulum-associated protein degradation. *Mol. Biol. Cell* **1998**, *9*, 1149–1162. [CrossRef]
86. Rudolph, H.K.; Antebi, A.; Fink, G.R.; Buckley, C.M.; Dorman, T.E.; LeVitre, J.; Davidow, L.S.; Mao, J.; Moir, D.T. The yeast secretory pathway is perturbed by mutations in PMR1, a member of a Ca^{2+} ATPase family. *Cell* **1989**, *58*, 133–145. [CrossRef]
87. Manford, A.G.; Stefan, C.J.; Yuan, H.L.; Macgurn, J.A.; Emr, S.D. ER-to-plasma membrane tethering proteins regulate cell signaling and ER morphology. *Dev. Cell* **2012**, *23*, 1129–1140. [CrossRef] [PubMed]
88. Hoffmann, P.C.; Bharat, T.A.M.; Wozny, M.R.; Boulanger, J.; Miller, E.A.; Kukulski, W. Tricalbins Contribute to Cellular Lipid Flux and Form Curved ER-PM Contacts that Are Bridged by Rod-Shaped Structures. *Dev. Cell* **2019**, *51*, 488–502.e8. [CrossRef] [PubMed]
89. Collado, J.; Kalemanov, M.; Campelo, F.; Bourgoint, C.; Thomas, F.; Loewith, R.; Martinez-Sanchez, A.; Baumeister, W.; Stefan, C.J.; Fernandez-Busnadiego, R. Tricalbin-Mediated Contact Sites Control ER Curvature to Maintain Plasma Membrane Integrity. *Dev. Cell* **2019**, *51*, 476.e477–487.e477. [CrossRef] [PubMed]

90. Stein, V.; Blank-Landeshammer, B.; Muntjes, K.; Marker, R.; Teichert, I.; Feldbrugge, M.; Sickmann, A.; Kück, U. The STRIPAK signaling complex regulates dephosphorylation of GUL1, an RNA-binding protein that shuttles on endosomes. *PLoS Genet.* **2020**, *16*, 1–32. [CrossRef]
91. Costanzo, M.; VanderSluis, B.; Koch, E.N.; Baryshnikova, A.; Pons, C.; Tan, G.; Wang, W.; Usaj, M.; Hanchard, J.; Lee, S.D.; et al. A global genetic interaction network maps a wiring diagram of cellular function. *Science* **2016**, *353*, 1–34. [CrossRef]
92. Deshaies, R.J.; Schekman, R. A yeast mutant defective at an early stage in import of secretory protein precursors into the endoplasmic reticulum. *J. Cell Biol.* **1987**, *105*, 633–645. [CrossRef]
93. Plath, K.; Wilkinson, B.M.; Stirling, C.J.; Rapoport, T.A. Interactions between Sec complex and prepro-alpha-factor during posttranslational protein transport into the endoplasmic reticulum. *Mol. Biol. Cell* **2004**, *15*, 1–10. [CrossRef]
94. Strahl-Bolsinger, S.; Immervoll, T.; Deutzmann, R.; Tanner, W. PMT1, the gene for a key enzyme of protein O-glycosylation in *Saccharomyces cerevisiae*. *Proc. Natl. Acad. Sci. USA* **1993**, *90*, 8164–8168. [CrossRef]
95. Gentzsch, M.; Tanner, W. The PMT gene family: Protein O-glycosylation in *Saccharomyces cerevisiae* is vital. *EMBO J.* **1996**, *15*, 5752–5759. [CrossRef]
96. Gentzsch, M.; Immervoll, T.; Tanner, W. Protein O-glycosylation in *Saccharomyces cerevisiae*: The protein O-mannosyltransferases Pmt1p and Pmt2p function as heterodimer. *FEBS Lett.* **1995**, *377*, 128–130. [CrossRef]
97. Watanabe, R.; Riezman, H. Differential ER exit in yeast and mammalian cells. *Curr. Opin. Cell Biol.* **2004**, *16*, 350–355. [CrossRef]
98. Weichert, M.; Lichius, A.; Priegnitz, B.E.; Brandt, U.; Gottschalk, J.; Nawrath, T.; Groenhagen, U.; Read, N.D.; Schulz, S.; Fleissner, A. Accumulation of specific sterol precursors targets a MAP kinase cascade mediating cell-cell recognition and fusion. *Proc. Natl. Acad. Sci. USA* **2016**, *113*, 11877–11882. [CrossRef] [PubMed]
99. Weichert, M.; Herzog, S.; Robson, S.A.; Brandt, R.; Priegnitz, B.E.; Brandt, U.; Schulz, S.; Fleissner, A. Plasma Membrane Fusion Is Specifically Impacted by the Molecular Structure of Membrane Sterols During Vegetative Development of *Neurospora crassa*. *Genetics* **2020**, *216*, 1103–1116. [CrossRef] [PubMed]
100. Perez-Riverol, Y.; Csordas, A.; Bai, J.; Bernal-Llinares, M.; Hewapathirana, S.; Kundu, D.J.; Inuganti, A.; Griss, J.; Mayer, G.; Eisenacher, M.; et al. The PRIDE database and related tools and resources in 2019: Improving support for quantification data. *Nucleic Acids Res.* **2019**, *47*, 442–450. [CrossRef] [PubMed]

4. Manuscript: The Vacuolar-Morphology Protein VAC14 Plays an Important Role in Sexual Development in the Filamentous Ascomycete *Sordaria macrospora*

This manuscript represents the third subtopic of this thesis and is being prepared for submission. Supplementary materials are included in the main part and created videos are available on the data drive attached in this thesis, which will be available online after publication.

Author contribution

As first author, A. Groth conceived and performed all experiments and analyzed the results and corresponding data. She also prepared the figures and wrote the manuscript.

Other contributions

E.J.R. created some of the plasmids and E.J.R. and S.A. generated *S. macrospora* strains relevant for this study. S.P. did the supervision, conceptualization, validation and reviewed the manuscript.

The Vacuolar Morphology Protein VAC14 Plays an Important Role in Sexual Development in the Filamentous Ascomycete *Sordaria macrospora*

Anika Groth [1], Eva Johanna Reschka [1], Svenja Ahlmann [1] and Stefanie Pöggeler [1,*]

[1] Department of Genetics of Eukaryotic Microorganisms, Institute of Microbiology and Genetics, Georg-August-University of Göttingen, Grisebachstr. 8, 37077 Göttingen, Germany; anika.gibron@uni-goettingen.de (A.G.); evareschka@gmx.net (E.J.R.); svenja.ahlmann@stud.uni-goettingen.de (S.A.)

[*] Correspondence: spoegge@gwdg.de; Tel.: +49-551-39-24051

Abstract

The multiprotein Fab1p/PIKfyve-complex regulating the abundance of the phospholipid phosphatidylinositol 3,5-bisphosphate (PtdIns(3,5)P_2) is highly conserved among eukaryotes. In yeast/mammals it is composed of the phosphatidylinositol 3-phosphate 5-kinase Fab1p/PIKfyve, the PtdIns(3,5)P_2 phosphatase Fig4p/Sac3 and the scaffolding subunit Vac14p/ArPIKfyve. The complex is located to vacuolar membranes in yeast and to endosomal membranes in mammals, where it controls the synthesis and turnover of PtdIns(3,5)P_2. In this study, we analyzed the role and function of the Fab1p/PIKfyve-complex scaffold protein SmVAC14 in the filamentous ascomycete *Sordaria macrospora* (Sm). We generated the *Smvac14* deletion strain Δvac14 and performed phenotypic analysis of the mutant. Furthermore, we conducted fluorescence-microscopic localization studies of fluorescently labeled SmVAC14 with other organelle-marker proteins. Our results revealed that SmVAC14 is important for maintaining vacuolar size and appearance as well as proper sexual development in *S. macrospora*. In addition, SmVAC14 plays an important role in stress response and its deletion has an impact on the localization of endosomal marker proteins. Accordingly, our results propose that the turnover of PtdIns(3,5)P_2 is of great significance for developmental processes in filamentous fungi.

Key words: VAC14, Fab1/PIKfyve-complex, sexual development, vacuolar morphology, *Sordaria macrospora*

1. Introduction

Developmental processes such as sexual development, cell-fusion, -migration and growth, as well as vesicular trafficking and organelle morphology are tightly regulated by conserved multiprotein kinase/phosphatase complexes. These include the Fab1p/PIKfyve-complex that mediates turnover and synthesis of phosphatidylinositol 3,5-bisphosphate (PtdIns(3,5)P_2) at vacuolar membranes in yeast or on early- and late endosomes as well as multivesicular bodies (MVBs) and lysosomes in mammalian cells (Dove *et al.*, 2002; Duex *et al.*, 2006b; Ikonomov *et al.*, 2009a; Jin *et al.*, 2008; Rudge *et al.*, 2004; Sbrissa *et al.*, 2007; Shisheva, 2008). It is composed of the phosphatidylinositol 3-phosphate (PtdIns(3)P) 5-kinase Fab1p/PIKfyve, its antagonizing PtdIns(3,5)P_2 phosphatase Fig4p/Sac3 and the scaffold protein Vac14p/ArPIKfyve (yeast/mammalian nomenclature) (Botelho *et al.*, 2008; Duex *et al.*, 2006a; Duex *et al.*, 2006b; Ikonomov *et al.*, 2009b; Jin *et al.*, 2008; Sbrissa *et al.*, 2008; Schulze *et al.*, 2014). In yeast, the complex additionally contains the Fab1p activator Vac7p and its inhibitor Atg18p (Bonangelino *et al.*, 1997; Duex *et al.*, 2006a; Duex *et al.*, 2006b; Efe *et al.*, 2007; Gary *et al.*, 2002). The low abundant phospholipid PtdIns(3,5)P_2 controls diverse cellular functions including morphology of organelles, retrograde trafficking to the *trans*-Golgi network, ion transport, membrane recycling, cargo sorting into MVBs, acidification of endolysosomes and autophagy (De Lartigue *et al.*, 2009; Dove *et al.*, 2009; Efe *et al.*, 2005; Rutherford *et al.*, 2006; Shisheva, 2008; Vicinanza *et al.*, 2008). In mammals, disturbance of the abundance and distribution of the phospholipid PtdIns(3,5)P_2 can cause severe developmental defects and neurodegeneration like Charcot-Marie-Tooth syndrome 4J and amyotrophic lateral sclerosis (Chow *et al.*, 2007; Chow *et al.*, 2009; Zhang *et al.*, 2007; Zhang *et al.*, 2008).

In yeast, Vac14p forms a stable subcomplex with the 5-phosphatase Fig4p that allows for the recruitment of the Fab1p kinase (Duex *et al.*, 2006b; Rudge *et al.*, 2004). In this regard, both Vac14p and Fig4p were shown to activate Fab1p to regulate steady-state and hyperosmotic elevated levels of PtdIns(3,5)P_2 (Bonangelino *et al.*, 2002; Duex *et al.*, 2006a; Duex *et al.*, 2006b; Gary *et al.*, 2002). Mutants of Fab1p-complex components show low levels of PtdIns(3,5)P_2 accompanied by enlarged less acidified vacuoles (Bonangelino *et al.*, 2002; Duex *et al.*, 2006a; Duex *et al.*, 2006b; Gary *et al.*, 1998).

Similar phenotypic effects could be observed in mammalian cells either lacking or overexpressing Vac14 (Jin *et al.*, 2008; Sbrissa *et al.*, 2004; Schulze *et al.*, 2014; Zhang *et al.*, 2007). With a previously performed affinity approach, mammalian Vac14 could be linked to proteins of the endosomal and autophagic pathways (Schulze *et al.*, 2014).

Interestingly, the VAC14 homolog of the coprophilic ascomycete *Sordaria macrospora* (Sm) had been recently identified in a pulldown with the striatin-interacting phosphatase and kinase (STRIPAK)-complex component SCI1 (Reschka *et al.*, 2018). The multiprotein STRIPAK-complex is conserved in animal and fungi and coordinates a number of signaling pathways and developmental processes including cell-growth, -polarity and -migration as well as vesicular trafficking, Golgi assembly, neural and sexual development, endocytosis, hyphal fusion, septation and vegetative growth (Beier *et al.*, 2016; Bernhards and Pöggeler, 2011; Bloemendal *et al.*, 2012; Frey *et al.*, 2015; Hwang and Pallas, 2014; Kück *et al.*, 2016; Kück *et al.*, 2019; Pöggeler and Kück, 2004; Shi *et al.*, 2016). *S. macrospora* is used as model organism to study conserved processes like fruiting-body formation, sexual development, meiosis and autophagy (Esser and Straub, 1958; Kück *et al.*, 2009; Pöggeler *et al.*, 2006; Teichert *et al.*, 2014; Teichert *et al.*, 2020). Both, autophagy and the SmSTRIPAK are important for proper fruiting-body formation and sexual development in *S. macrospora*. In this regard, we investigated the *S. macrospora* core scaffold protein SmVAC14 for the first time in a filamentous fungus. In this work, we generated and analyzed a *Smvac14* deletion mutant, Δvac14 and performed localization studies using fluorescence microscopy. We showed that SmVAC14 is a conserved protein that co-localizes with the SmSTRIPAK-component SCI1, to vacuolar membranes, the Golgi, early and late endosomes, and partially to the endoplasmic reticulum (ER). Moreover, *Smvac14* deletion caused enlarged, less acidified vacuoles, deformed perithecia and impaired ascospore formation. Additionally, hyperosmotic and oxidative stress as well as amino-acid starvation led to developmental defects in the Δvac14 mutant though autophagy is apparently not affected.

2. Material and Methods

2.1 Strains, Media and Growth Conditions

A list of all strains used and generated in this study is given in Table 1. For cloning and propagation of recombinant plasmids, *Escherichia coli* strain MACH1 (C862003, Thermo Fisher Scientific, Waltham, MA, USA) was used in standard culture conditions (Sambrook *et al.*, 2001). To generate recombinant plasmids via homologous recombination (HR), positive transformants of the yeast *Saccharomyces cerevisiae* strain PJ69-4A were selected for uracil prototrophy (Colot *et al.*, 2006; James *et al.*, 1996). *S. macrospora* strains were transformed with the recombinant plasmids according to the standard protocol (Kück and Hoff, 2006; Walz and Kück, 1995). Positive transformants were selected on media containing nourseothricin-dihydrogen sulphate (50 µg/mL, nat) (AB-102XL, Jena Bioscience GmbH, Jena, Germany) and/or hygromycin B (110 U/mL, hyg) (4400051-10MU, Merck, Kenilworth, NJ, USA). *S. macrospora* strains were grown on liquid or solid biomalt maize medium (BMM) or on solid Sordaria Westergaard (SWG) fructification medium under continuous light conditions at 27 °C (Elleuche and Pöggeler, 2009; Esser, 1982; Nowrousian *et al.*, 2005). To generate single spore isolates and strains expressing tagged proteins, *S. macrospora* strains were crossed as described previously (Bernhards and Pöggeler, 2011).

Table 1: List of strains used and generated in this study.

Strain	Genotype	Reference
Escherichia coli		
MACH1	Δ*recA1398*, *endA1*, *tonA*, *Φ80ΔlacM15*, Δ*lacX74*, *hsdR*, (rK-mK+)	Invitrogen
Saccharomyces cerevisiae		
PJ69-4A	*MATa*, *trp1-901*, *leu2-3*, *112*, *ura3-52*, *his3-200*, *gal4*Δ, *gal80*Δ, *LYS2::GAL1-HIS3*, *GAL2-ADE2*, *met2::GAL7-lacZ*	(James *et al.*, 1996)
Sordaria macrospora		
DSM997	wild type (wt)	DSMZ
S23442	mutation in *fus1-1* gene, brownish ascospores, fertile	(Nowrousian *et al.*, 2012)
Δku70	Δku70::*nat*^{R}, fertile	(Pöggeler and Kück, 2006)
Δsci1	Δsci1::*hyg*^{R}, ssi, sterile	(Reschka *et al.*, 2018)
fus::RH2B^{ect}	ectopic integration of pRH2B_hyg into S23442; *hyg*^{R}, pt, fertile; *Pgpd::hh2b::tdTomato::TtrpC*	Reschka and Pöggler, unpublished

wt::egfp^{ect}	ectopic integration of p1783-1 into DSM997; *hyg*^{R}, ssi, fertile; *Pgpd::egfp::TtrpC*	(Voigt and Pöggeler, 2013)
wt::TagRFP-T^{ect}	ectopic integration of pTagRFP-T into DSM997; *nat*^{R}, ssi, fertile; *Pccg1::TagRFP-T::TtrpC*	(Werner *et al.*, 2021)
wt::HA	ectopic integration of pHA_nat into DSM997; *nat*^{R}, ssi, fertile; *Pccg1::HA::TtrpC*	(Reschka *et al.*, 2018)
wt::nbr1-egfp^{ect}	ectopic integration of pnbr1-egfp into DSM997; *nat*^{R}, ssi, fertile; *Pnbr1::nbr1::egfp::TtrpC*	Werner, 2012
wt::pom33-egfp^{ect}	ectopic integration of p5'pom33-egfp into DSM997; *nat*^{R}, ssi, fertile; *Ppom33::pom33::egfp::TtrpC*	(Groth *et al.*, 2021)
wt::egfp-atg8^{ect}	ectopic integration of pegfp-atg8 into DSM997; *nat*^{R}, ssi, fertile; *Patg8::egfp::atg8::Tatg8*	This study
wt::egfp-Ztrab5^{ect}	ectopic integration of pHeGFPRab5_hyg into DSM997; *hyg*^{R}, pt, fertile; *PZttub2::egfp::Ztrab5::TZttub2*	This study
wt::egfp-Ztrab7^{ect}	ectopic integration of pHeGFPRab7_hyg into DSM997; *hyg*^{R}, pt, fertile; *PZttub2::egfp::Ztrab7::TZttub2*	This study
Δvac14	Δvac14::*hyg*^{R}, ssi, fertile	This study
Δvac14::RH2B^{ect}	ectopic integration of pRH2B_nat into Δvac14; *hyg*^{R}, *nat*^{R}, pt, fertile; *Pgpd::hh2b::tdTomato::TtrpC*	This study
Δvac14::egfp^{ect}	ectopic integration of pDS23 into Δvac14; *hyg*^{R}, *nat*^{R} ssi, fertile; *Pgpd::egfp::TtrpC*	This study
Δvac14::TagRFP-T^{ect}	ectopic integration of pTagRFP-T into Δvac14; *hyg*^{R}, *nat*^{R}, ssi, fertile; *Pccg1::TagRFP-T::TtrpC*	This study
Δvac14::5'vac14-TagRFP-T^{ect}	ectopic integration of p5'vac14-TagRFP-T into Δvac14; *hyg*^{R}, *nat*^{R}, ssi, fertile; *Pvac14::vac14::TagRFP-T::TtrpC*	This study
Δvac14::ccg1vac14-TagRFP-T^{ect}	ectopic integration of pccg1vac14-TagRFP-T_nat into Δvac14; *hyg*^{R}, *nat*^{R}, ssi, fertile; *Pccg1::vac14::TagRFP-T::TtrpC*	This study
Δvac14::egfp-Ztrab5^{ect}	ectopic integration of pegfp-Ztrab5_nat into Δvac14; *hyg*^{R}, *nat*^{R}, pt, fertile; *Ptub2::egfp::Ztrab5::Ttub2*	This study
Δvac14::egfp-Ztrab7^{ect}	ectopic integration of pegfp-Ztrab7_nat into Δvac14; *hyg*^{R}, *nat*^{R}, pt, fertile; *Ptub2::egfp::Ztrab7::Ttub2*	This study
Δvac14::nbr1-egfp^{ect}	ectopic integration of pnbr1-egfp into Δvac14; *hyg*^{R}, *nat*^{R}, ssi, fertile; *Pnbr1::nbr1::egfp::TtrpC*	This study
Δvac14::egfp-atg8^{ect}	ectopic integration of pegfp-atg8 into Δvac14; *hyg*^{R}, *nat*^{R}, ssi, fertile; *Patg8::egfp::atg8::Tatg8*	This study
Δvac14::TagRFP-T-vac14^{ect}	ectopic integration of pTagRFP-T-vac14 into Δvac14; *hyg*^{R}, *nat*^{R},pt**,** sterile; *Pvac14::TagRFP-T::vac14::Tvac14*	This study
wt::5'vac14-TagRFP-T^{ect}	ectopic integration of p5'vac14-TagRFP-T into DSM997; *nat*^{R}, pt, fertile; *Pvac14::vac14::TagRFP-T::TtrpC*	This study
wt::ccg1vac14-TagRFP-T^{ect}	ectopic integration of pccg1vac14-TagRFP-T_hyg into DSM997; *hyg*^{R}, ssi, fertile; *Pccg1::vac14::TagRFP-T::TtrpC*	This study
wt::vac14-TagRFP-T + sci1-egfp^{ect}	ectopic integration of pccg1vac14-TagRFP-T_hyg and p5'sci1-egfp into DSM997;	This study

	hyg^{R}, *nat*^{R}, ssi, fertile; *Pccg1::vac14::TagRFP-T::TtrpC;* *Psci1::sci1::egfp::TtrpC*	
wt::vac14-TagRFP-T + egfp-vma1^{ect}	ectopic integration of pccg1vac14-TagRFP-T_nat and pegfp-vma1 into DSM997; *hyg*^{R}, *nat*^{R}, pt, fertile; *Pccg1::vac14::TagRFP-T::TtrpC;* *Pvma1::egfp::vma1::Tvma1*	This study
wt::vac14-TagRFP-T + pom33-egfp^{ect}	crossing of strain wt::ccg1vac14-TagRFP-T^{ect} with wt::pom33-egfp^{ect} *hyg*^{R}, *nat*^{R}, ssi, fertile; *Pccg1::vac14::TagRFP-T::TtrpC;* *Ppom33::pom33::egfp::TtrpC*	This study
wt::vac14-egfp + TagRFP-T-ypt1^{ect}	ectopic integration of pvac14-egfp and pTagRFP-T-ypt1 into DSM997; *hyg*^{R}, *nat*^{R}, pt, fertile; *Pvac14::vac14::egfp::TtrpC;* *Pccg1::TagRFP-T::ypt1::TtrpC*	This study
wt::vac14-TagRFP-T + egfp-Ztrab5^{ect}	ectopic integration of pccg1vac14-TagRFP-T_hyg and pegfp-Ztrab5_nat into DSM997; *hyg*^{R}, *nat*^{R}, ssi, fertile; *Pccg1::vac14::TagRFP-T::TtrpC;* *Ptub2::egfp::rab5::Ttub2*	This study
wt::vac14-TagRFP-T + egfp-Ztrab7^{ect}	ectopic integration of pccg1vac14-TagRFP-T_hyg and pegfp-Ztrab7_nat into DSM997; *hyg*^{R}, *nat*^{R}, ssi, fertile; *Pccg1::vac14::TagRFP-T::TtrpC;* *Ptub2::egfp::rab7::Ttub2*	This study
wt::vac14-TagRFP-T + nbr1-egfp^{ect}	crossing of strain wt::ccg1vac14-TagRFP-T^{ect} with wt::nbr1-egfp^{ect} *hyg*^{R}, *nat*^{R}, ssi, fertile; *Pccg1::vac14::TagRFP-T::TtrpC;* *Pnbr1::nbr1::egfp::TtrpC*	This study
wt::vac14-TagRFP-T + egfp-atg8^{ect}	crossing of strain wt::ccg1vac14-TagRFP-T^{ect} with wt::egfp-atg8^{ect} *hyg*^{R}, *nat*^{R}, ssi, fertile; *Pccg1::vac14::TagRFP-T::TtrpC;* *Patg8::egfp::atg8::Tatg8*	This study

nat^{R}: nourseothricin resistant, *hyg*^{R}: hygromycin resistant, ssi: single-spore isolate, pt: primary transformant, ect: ectopically integrated, *P*: promoter, *T*: terminator, *Pgpd*: promoter of the glyceraldehyde-3-phosphate dehydrogenase gene from *Aspergillus nidulans*, *Pccg1*: promoter of the *clock-controlled gene 1* from *Neurospora crassa*, *TtrpC*: terminator of the anthranilate synthase gene from *A. nidulans*, *egfp*: gene for green fluorescence protein enhanced green fluorescent protein (EGFP) from *Aequorea victoria*, *TagRFP-T*: gene for red fluorescence protein TagRFP-T of *Entacmaea quadricolor*, *tdTomato*: gene for red fluorescence protein tdTomato from *Discosoma* species.

2.2 Phenotypic Analysis

For phenotypic analysis, three biological replicates each of the *S. macrospora* wt, Δvac14, Δvac14::5'vac14-TagRFP-T^{ect} and Δvac14::ccg1vac14-TagRFP-T^{ect} strains were grown on solid SWG medium over distinct days (d), according to the respective analysis, at 27 °C under continuous light conditions. Strains were documented with a VHX-550F Digital Microscope (Keyence, Neu-Isenburg, Germany). For quantification of perithecia, strains were grown for 7 d, and perithecia were counted 20-fold per 0.0625 cm^2. The experiment

was repeated three times. For phenotypic analysis of perithecia, cross-sections of agar plates were prepared. To assess ascus rosette maturation, an "inner" and "outer" area of the petri dish was defined using the diameter of a 50 mL falcon tube as spacer. For these analyses, the strains were grown for 8 d. Perithecia were prepared using dissecting needles and thin agar-slices were prepared with a scalpel and both were placed on a glass-slide for documentation. For determination of ascospore maturation, strains were grown for 9 d, ten perithecia per strain were cracked and the enclosed ascus rosettes were categorized. To determine the growth behavior and sexual development under different stress conditions, strains were grown over 10 d on SWG media supplemented with 0.1 M NaCl, 0.4 M sorbitol, 2.5 mM 3-amino-1,2,4-triazole (3-AT), 0.003 % SDS, 0.01 % H_2O_2 or without KNO_3. The experiment was repeated twice.

The determination of the growth rate/day was done in triplicate and strains were grown in 30-cm race tubes filled with the respective stress media. After 3 d of growth, the growth front was marked every day at the same time. This experiment was repeated three times. The experiment for analyzing sexual development two times.

2.3 Construction of Plasmids

All plasmids used and constructed in this study are shown in Table S1. Plasmids were generated via HR in *S. cerevisiae* (Colot *et al.*, 2006), or Golden Gate (GG) cloning (Dahlmann *et al.*, 2021). Information about the used primers (Sigma-Aldrich Chemie GmbH Taufkirchen, Germany) is provided in Table S2. For the generation of the pvac14-KO_V3w knockout plasmid, as 5'-flanking region, the first 1030 bp and as 3'-flanking region, the last 1030 bp of the *vac14* open reading frame (ORF) were amplified from *S. macrospora* wt genomic (g)DNA using the primer pairs Vac14-ko-5f_3w/Vac14-ko-5r_3w and Vac14-ko-3f_3/Vac14-ko-3r_3, respectively. Together with the donor vector pGG-hph and the destination vector pDest-Amp, the fragments were cloned via the GG procedure (Dahlmann *et al.*, 2021).

Plasmid p5'vac14-egfp was generated via HR in the *S. cerevisiae* strain PJ69-4A (Colot *et al.*, 2006). A fragment (4309 bp) consisting of the *S. macrospora vac14* native promoter (*Pvac14*) and the ORF was amplified from wt gDNA with primer pair Vac14-egfp-f/Vac14-egfp-r. A second fragment (1510 bp), comprising *egfp* and the *trpC* terminator (*TtrpC*) of *Aspergillus nidulans* was amplified from plasmid p1783-1 (Pöggeler *et al.*, 2003) with the

primer pair GFP-F/pRS426GFPrev. Both PCR fragments were integrated into the *Xho*I-linearized vector pRS-hyg (Bloemendal *et al.*, 2012).

For the construction of p5'vac14-TagRFP-T, a fragment of 4307 bp containing the *S. macrospora Pvac14* and *vac14* ORF was amplified from wt gDNA using the primer combination Vac14-egfp-f/Vac14-tRFP-r. Together with a fragment (1531 bp) comprised of *TagRFP-T* and the *TtrpC* of *A. nidulans* amplified from pTagRFP-T (Werner *et al.*, 2021) with the primers RFP-f and pRS426GFPrev, both fragments were integrated into *Xho*I-linearized pRS-nat (Klix *et al.*, 2010) via HR in the *S. cerevisiae* strain PJ69-4A (Colot *et al.*, 2006).

To construct the overexpression plasmids pccg1vac14-TagRFP-T_nat/_hyg, following three fragments were cloned into *Xho*I-linearized pRS-nat (Klix *et al.*, 2010) or pRS-hyg (Bloemendal *et al.*, 2012), respectively. The overexpression promoter of the *clock-controlled gene 1* (*Pccg1*) of *Neurospora crassa* (950 bp) was amplified with the primer combination pRSccg1/Pccg1-r from pHA_nat (Reschka *et al.*, 2018). The *S. macrospora vac14* ORF (3439 bp) was amplified from wt gDNA using the primer pair Vac14-ccg1-f/Vac14-tRFP-r and a fragment (1513 bp) consisting of *TagRFP-T* and the *TtrpC* of *A. nidulans* was amplified from pTagRFP-T (Werner *et al.*, 2021) with the primers RFP-f and pRS426GFPrev. Fusion of the three PCR products was performed via HR in *S. cerevisiae* (Colot *et al.*, 2006). For tagging SmVAC14 N-terminally with TagRFP-T, plasmid pTagRFP-T-vac14 was generated with the NEBuilder HiFi DNA Assembly Cloning Kit (New England Biolabs, Ipswich, MA, USA) according to the instruction manual. The promoter *Pvac14* (882 bp) was amplified from wt gDNA using the primer combination N-vac14_P-f/N-vac14_P-r, the *TagRFP-T* (746 bp) was amplified from pTagRFP-T (Werner *et al.*, 2021) with the primers N-tRFP-f and N-tRFP-r, and a fragment (4201 bp) consisting of the *vac14* ORF and terminator (*Tvac14*) was amplified from wt gDNA with primer combination N-vac14-f/N-vac14_T-r. The three fragments were cloned into *Eco*RV-linearized pJet_nat (Nordzieke, unpublished).

For the generation of the plasmids pegfp-Ztrab5/-Ztrab7_nat/hyg, primer pair Tub2Ztf/Tub2Ztr was used to amplify a fragment consisting of the constitutive *tub2* promoter of *Zymoseptoria tritici* (Zt) (*PZttub2*), *egfp*, the *Ztrab5*/*Ztrab7* coding region and the constitutive *Zttub2* terminator (*TZttub2*) from the plasmids pHeGFPRab5/-Rab7_hyg

(Kilaru *et al.*, 2015). The resulting fragments of 3763 bp and 3766 bp were integrated into *Xho*I-linearized pRS-nat (Klix *et al.*, 2010) or pRS-hyg (Bloemendal et al., 2012), respectively, via HR in the *S. cerevisiae* strain PJ69-4A (Colot *et al.*, 2006).

The plasmid pegfp-vma1, was constructed by amplifying the *S. macrospora vma1* native promoter (1058 bp) and ORF including the *vma1* terminator (4068 bp) with primer pairs Vma1P-f/Vma1P-EGFP-r and Vma1-EGFP-f/Vma1-r, respectively, from wt gDNA. The *egfp* fragment (717 bp) was amplified with the primers GFP-f and GFP-r from p1783-1 (Pöggeler *et al.*, 2003) and the fragments were cloned into *Xho*I-linearized pRS-hyg via HR in *S. cerevisiae* (Colot *et al.*, 2006).

Construction of the plasmid pTagRFP-T-ypt1 was performed by integrating the following three fragments into *Xho*I-linearized pRS-nat (Klix *et al.*, 2010) via HR in yeast (Colot *et al.*, 2006). A fragment of 1653 bp containing the *Pccg1* of *N. crassa* and *TagRFP-T* was amplified with the primer combination pRSccg1/RFP-r from pTagRFP-T (Werner *et al.*, 2021). The *S. macrospora ypt1* ORF (610 bp) was amplified from wt gDNA with the primer pair Ypt1-RFP_f/Rek_dsred_ypt1 bw and the *TtrpC* of *A. nidulans* (767 bp) was amplified from p1783-1 (Pöggeler *et al.*, 2003) with the primers TtrpC_F and pRS426GFPrev.

Sequencing of generated plasmid DNA was performed by Seqlab Sequence Service Laboratories GmbH (Göttingen, Germany).

2.4 Generation of the *S. macrospora* Knockout Strain Δvac14

For the partial-deletion of the *S. macrospora vac14* gene (Figure S1), the pvac14-KO_V3w knockout plasmid was used as template to amplify the 3526 bp deletion cassette with the primer pair GG_KO_fw/GG_KO_rv, containing the defined 5′- and 3′-flanking regions of *vac14* and the *hph* cassette. The *S. macrospora* Δku70 strain (Pöggeler and Kück, 2006) was transformed with the deletion cassette to replace the remaining 1379 bp of the *vac14* ORF with the *hph* cassette (Figure S1A). Crosses of primary transformants with the color-spore mutant fus1-1 were performed as described previously (Bernhards and Pöggeler, 2011; Nowrousian *et al.*, 2012). Single-spore isolates of Δvac14 carrying hyg resistance were selected and verification of the absence of the fragment of the *vac14* gene and integration of the *hph* cassette at the desired locus was performed with primer pairs Vac14-2v5f/ Vac14-2vORF5-r (3395 bp) and tC1_o/Vac14-2v3r (2555 bp), respectively (Figure S1B). To verify the presence of the *ku70* gene in Δvac14 after crossing, primer pair Smku70-v1-

f/ku70-ko-v3f(R) (2851 bp) was used (Figure S1B). For Southern hybridization, gDNA of the *S. macrospora* wt, Δku70 and Δvac14 strain was hydrolyzed with *Pst*I. A capillary blot using a nylon membrane (RPN303B, GE Healthcare, Boston, MA, USA) was performed overnight at RT. The 1030 bp 3'-probe was amplified from *S. macrospora* wt gDNA with the Vac14-ko-3f_3/Vac14-ko-3r_3 primer pair. Labeling of the probe was performed with the Amersham AlkPhos Direct Labelling and Detection Kit (RPN3680, GE Healthcare, Botson, MA, USA). Detection was done after the manufacturer's manual. Signals were visualized on X-ray films (Amersham Hyperfilm™ ECL, GE Healthcare, Botson, MA, USA) using an "Optimax X-ray film processor" (PROTEC GmbH & Co. KG, Oberstenfeld, Germany) (Figure S1C).

2.5 Light and Fluorescence Microscopy

To investigate vegetative hyphae and sexual structures, *S. macrospora* strains were grown on SWG-covered glass slides for 5 d or on solid SWG medium for 9 d under continuous light at 27 °C. The slides were prepared as described previously (Groth *et al.*, 2021), whereas SWG was used as solid medium and instead of liquid BMM water was poured into the petri dish to prevent desiccation of the growth medium. The documentation was performed with an AxioImage M1 microscope (Zeiss, Jena, Germany) using differential-interference contrast (DIC) or a VHX-500F Digital Microscope (Keyence, Neu Isenburg, Germany). Images were captured with a Photometrix CoolSNAP HQ camera (Roper Scientific, Photometrics, Tuscon, AZ, USA). Image processing was done using ZEISS ZEN Digital Imaging (version 2.3; Zeiss, Jena, Germany) and the Affinity Publisher software (version 1.10.1, Serif (Europe) Ltd., Nottingham, UK, https://affinity.serif.com/de/publisher/; accessed on 24.08.2021).

For fluorescence microscopic analyses, *S. macrospora* strains were grown for 24 h on BMM-agar slides, as described in (Groth *et al.*, 2021), for 72 h on solid SWG medium supplemented with 1.5 % agarose (Biozym Scientific GmbH, Hessisch Oldendorf, Germany), or for 24-72 h on SWG + 1.5 % agarose media supplemented with 0.1 M NaCl, 0.4 M sorbitol, 2.5 mM 3-AT, 0.003 % SDS, 0.01 % H_2O_2 or without KNO_3 at 27°C under continuous light conditions. To detect EGFP signals, Chroma filter set 49002 (exciter ET470/40x, ET525/50m, beamsplitter T495lpxr), for TagRFP-T/tdTomato/FM4-64-signals, Chroma filter set 49005 (exciter ET545/30x, emitter ET620/60m and beamsplitter T570LP)

and for CMAC, a 49000 (ET350/50x, emitter ET460/50m and beamsplitter T400LP) was used.

For FM4-64 (Thermo Fisher Scientific, Waltham, MA, USA) staining, *S. macrospora* strains were grown on solid SWG + 1.5 % agarose for 24 h at 27 °C. Staining was conducted by applying 100 µL of an FM4-64 solution (1 µg/mL in distilled water) to the mycelium on the agar-piece followed by incubation for 15 min at 37 °C.

For CMAC (Thermo Fisher Scientific, Waltham, MA, USA) staining, *S. macrospora* strains were grown on BMM-slides or over a piece of cellophane (0.5 cm x 0.5 cm) on solid SWG for 24 h or on solid SWG + 1.5 % agarose for 72 h at 27 °C. Then, the CMAC 10 mM stock solution was diluted 1:400 in distilled water and 100 µL of the CMAC solution was applied for 30 min at 37 °C to the mycelium.

With the transformation of plasmid pRH2B_nat (histone 2B fused with tdTomato) (Reschka *et al.*, 2018) into the Δvac14 deletion strain, nuclei could be visualized by fluorescence microscopy.

For time lapse studies of growing hyphae, *S. macrospora* strains were grown on BMM + 1.5 % agarose for 24 h at 27 °C, as described previously (Groth *et al.*, 2021). Recording intervals of 5 s over 20 min were used for time lapse studies.

2.6 Protein Sample Preparation and Western Blot Hybridization

For protein extraction from fungal mycelium, *S. macrospora* strains were cultivated in liquid BMM and were grown for 3 d at 27 °C. Then, the mycelium was harvested, dried, ground in liquid nitrogen and 520 µL of lysis buffer (10 mM Tris-HCl pH 7.5, 150 mM NaCl, 0.5 mM EDTA pH 8.0, 1 mM PMSF, 2 mM DTT, 0.5 % NP-40, 1x protease inhibitor cocktail IV (1tbl/50 mL, 04693132001, Mannheim, Germany), 1x PhosSTOP™ (1tbl/10 mL, 04906837001, Roche, Mannheim, Germany)) per g mycelium powder was added.

Cells were lysed in a Tissue Lyser (Qiagen, Hilden, Germany) by 30 Hrz for 2 min and prepared for Western Blot analysis by applying 4x NuPAGE® LDS-SB (NP0007, Thermo Fisher Scientific, Waltham, MA, USA) according to the manufacturer's manual. As protein standards, either the Nippon Genetics Co. Europe blue star pre-stained protein marker (MWP03, NIPPON Genetics Europe, Düren, Germany) or the PageRuler™ prestained protein ladder (26619, Thermo Fisher Scientific, Waltham, MA, USA) was used.

Proteins were separated by SDS-PAGE and transferred to a Amersham™ Protran™ Nitrocellulose Blotting Membrane (RPN203B, GE Healthcare, Little Chalfont, UK) using 1x transfer buffer and a Mini Trans-Blot® Cell device as described by the manufacturer (Bio-Rad Laboratories, Hercules, CA, USA) (Towbin *et al.*, 1979).

The nitrocellulose membrane, containing transferred proteins, was blocked with 5 % (w/v) skim milk powder in 1x Tris-buffered saline supplemented with 0.05 % Tween 20® (TBST) for 1 h at RT. Detection of antigen-antibody reaction was performed with a primary EGFP (rat)- (1:4000, 3h9-100, ChromoTek GmbH, Planegg-Martinsried, Germany) or TagRFP-T (rabbit) -antibody (1:12500, AB233-ev, BioCat (Evrogen, Moscow, Russia)) solved in 5 % skim milk/TBST. The membrane and antibody solution were incubated overnight at 4 °C. After the primary antibody was removed, the membrane was washed three times with 1x TBST for 15 min. A horse-radish peroxidase (HRP) coupled secondary anti rat- or rabbit-antibody (1:5500, 62-9520, Thermo Fisher Scientific, Waltham, MA, USA; 1:5000, G-21234, Thermo Fisher Scientific, Waltham, MA, USA) was applied to the membrane for 1 h at RT before the membrane was washed three times with 1x TBST for 15 min. Enhanced chemiluminescence reaction was used to detect the HRP-coupled antibodies using the Immobilon™ Western HRP Substrate kit (WBKLS0500, Merck, Kenilworth, NJ, USA). Signals were visualized on X-ray films (Amersham Hyperfilm™ ECL, GE Healthcare, Botson, MA, USA) using an "Optimax X-ray film processor" (PROTEC GmbH & Co. KG, Germany).

2.7 Protein Domain Determination

Protein domains were predicted using the program InterProScan (https://www.ebi.ac.uk/interpro/search/sequence/; accessed on 15.03.2021) (Blum *et al.*, 2021). The coiled-coil motifs were predicted using NPS@: COILED-COILS PREDICTION (https://npsa-prabi.ibcp.fr/cgi-bin/npsa_automat.pl?page=/NPSA/npsa_lupas.html; accessed on 15.03.2021) (Lupas *et al.*, 1991). Transmembrane domains (TMD) were predicted with the program HMMTOP (http://www.enzim.hu/hmmtop/html/submit.html; accessed on 15.03.2021) (Tusnády and Simon, 2001). Design of the schematic illustration was performed in same relation to the amino acids indicated in the figure using the Affinity Publisher software (version 1.10.1, Serif (Europe) Ltd., Nottingham, UK, https://affinity.serif.com/de/publisher/; accessed on 24.08.2021).

2.8 Multiple Sequence Alignment and Phylogenetic Analysis of Vac14

Protein sequences of Vac14 from fungi, animals and plants were obtained from BLASTP search using the public databases at NCBI (https://blast.ncbi.nlm.nih.gov/Blast.cgi?PAGE=Proteins; accessed on 24.08.2021) and were prepared with the online program MAFFT (version 7, https://mafft.cbrc.jp/alignment/server/; accessed on 24.08.2021) (Katoh *et al.*, 2019). The program GeneDoc (version 2.7.000; accessed on 24.08.2021) (Nicholas and Nicholas, 1997) and the Affinity Publisher software (version 1.10.1, Serif (Europe) Ltd., Nottingham, UK, https://affinity.serif.com/de/publisher/; accessed on 24.08.2021) were used to represent the alignment of protein sequences. Alignments of multiple protein sequences and neighbor joining phylogenetic analysis were performed with MAFFT (version 7, https://mafft.cbrc.jp/alignment/server/; accessed on 12.10.2021) (Katoh *et al.*, 2019). To test the tree for statistical significance, a bootstrap analysis was conducted with 1000 iterations. The tree was displayed with Phylo.io (version 1.0.k, http://phylo.io/; accessed on 12.10.21) (Robinson *et al.*, 2016) and edited with the Affinity Publisher software (version 1.10.1, Serif (Europe) Ltd., Nottingham, UK, https://affinity.serif.com/de/publisher/; accessed on 12.10.2021).

3. Results

3.1 The Vac14 Protein is Conserved Among Fungi, Plants and Animals

In previously performed LC-MS analysis with the SmSTRIPAK-complex component SCI1 as bait, a protein encoded by SMAC_08299 had been identified and predicted to be a VAC14 homolog via BLASTP analysis (Reschka *et al.*, 2018). Moreover, interactors of the endolysosomal and autophagic pathways were identified for mammalian VAC14 (Schulze *et al.*, 2014). Since the SmSTRIPAK-complex and the autophagic process are critical for *S. macrospora* sexual development, we investigated the SmVAC14 protein in more detail (Voigt and Pöggeler, 2013; Werner *et al.*, 2019). The 3384-bp coding region of the *S. macrospora vac14* gene is interrupted by 8 introns and encodes a protein of 892 aa with a molecular weight of 98 kDa (from the genome database Smacrospora_v03 from (Blank-Landeshammer *et al.*, 2019)). SmVAC14 is predicted to contain a Fab1- and a Fig4-binding domain, 3 transmembrane domains (TMD), 4 Coiled Coils (CC), and with up to 4 predicted Armadillo (ARM)-repeats it belongs to the ARM-repeat superfamily. The ARM-

superfamily also comprises HEAT (huntingtin-elongation-A subunit-TOR)-repeats but due to their degeneration and prediction problems of commonly used software (Andrade *et al.*, 2001), we focused on the prediction of ARM-repeats. Domain organization of VAC14 proteins in *S. macrospora*, *Neurospora crassa*, *Saccharomyces cerevisiae*, *Homo sapiens* and *Arabidopsis thaliana* are shown in Figure 1. Multiple sequence alignment with the SmVAC14 protein sequences using the online tool MAFFT (Katoh *et al.*, 2019) revealed 97 % sequence similarity with the *N. crassa* NcVAC14 protein (XP_011395167.1), 52 % with the *S. cerevisiae* Vac14p (NP_013490.3), 47 % with the *H. sapiens* HsVAC14/ArPIKfyve protein (NP_060522.3) and 50 % with the *A. thaliana* AtVac14 protein (NP_565275.1), respectively (Figure S2). Furthermore, multiple sequence alignment revealed that VAC14 is conserved in saprophytic and pathogenic species among the clades of Ascomycota and Basidiomycota showing 55-86 % sequence similarity to SmVAC14 (Figure S3 and Figure S4).

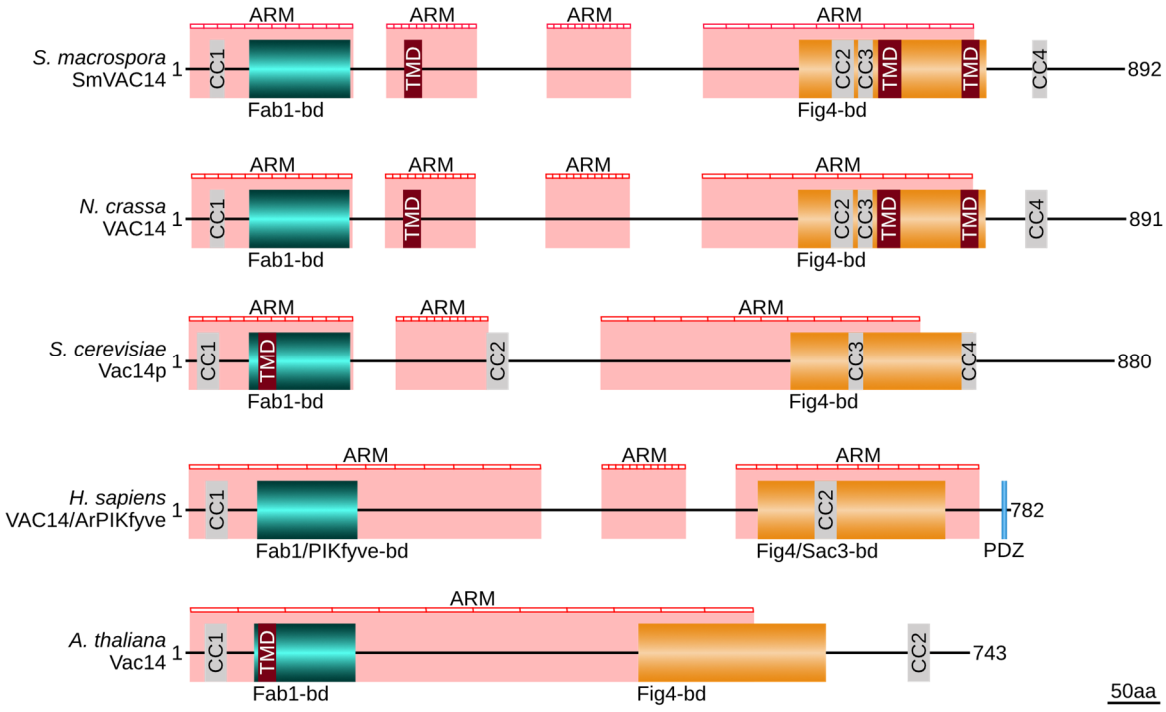

Figure 1: Domain organization of VAC14 proteins from fungi, animals and plants.
Domains for Fab1 and Fig4 binding and ARM-repeats were predicted using the program InterProScan (Blum *et al.*, 2021). Coiled-coil (CC) motifs (light grey) were predicted with NPS@: COILED-COILS PREDICTION (Lupas *et al.*, 1991) and transmembrane domains (TMD) (dark red) with HMMTOP (Tusnády and Simon, 2001). The N-terminal Fab1-binding domain (Fab1-bd) is shown in cyan, the C-terminal Fig4-bd in orange, and a PSD95-Discs-large-ZO-1 (PDZ)-recognition motif (Lemaire and McPherson, 2006) in light blue. Positions of presumable Armadillo (ARM)-repeats are indicated as striped red bars. Protein sequence of the *S. macrospora* SmVAC14

(SMAC_08299) was taken from the *S. macrospora*-specific peptide database Smacrospora_v03 (Blank-Landeshammer *et al.*, 2019). Accession numbers of the other proteins are as following: *N. crassa* VAC14 (XP_011395167.1), *S. cerevisiae* Vac14p (NP_013490.3), *H. sapiens* VAC14/ArPIKfyve (NP_060522.3) and *A. thaliana* Vac14 (NP_565275.1).

3.2 Deletion of *vac14* Results in Deformed Perithecia and an Impairment of Ascospore Formation

The *S. macrospora* Δvac14 partial-deletion mutant was generated using the Δku70 strain (Pöggeler and Kück, 2006). For the construction of the Δvac14 strain, homologous recombination of a *hph* deletion cassette flanked by the first and last 1000 bp of the *vac14* gene was performed resulting in a 1140-bp deletion of the *vac14* coding region. Partial deletion of *vac14* was confirmed by PCR and Southern blot analysis (Figure S1). To investigate the role of SmVAC14 during sexual development, the life cycle of the Δvac14 deletion strain and two complementation strains were microscopically examined and compared to the wt (Figure 2A). In the complementation strains, VAC14 is C-terminally tagged with TagRFP-T either under the control of the endogenous promotor (5′) (Δvac14::5′vac14-TagRFP-T^{ect}) or the overexpression promotor (ccg1) (Δvac14::ccg1vac14-TagRFP-T^{ect}). Further, phenotypic analyses were performed in which the morphology and number of perithecia and ascus rosette maturity was determined in the strains (Figure 2B-E).

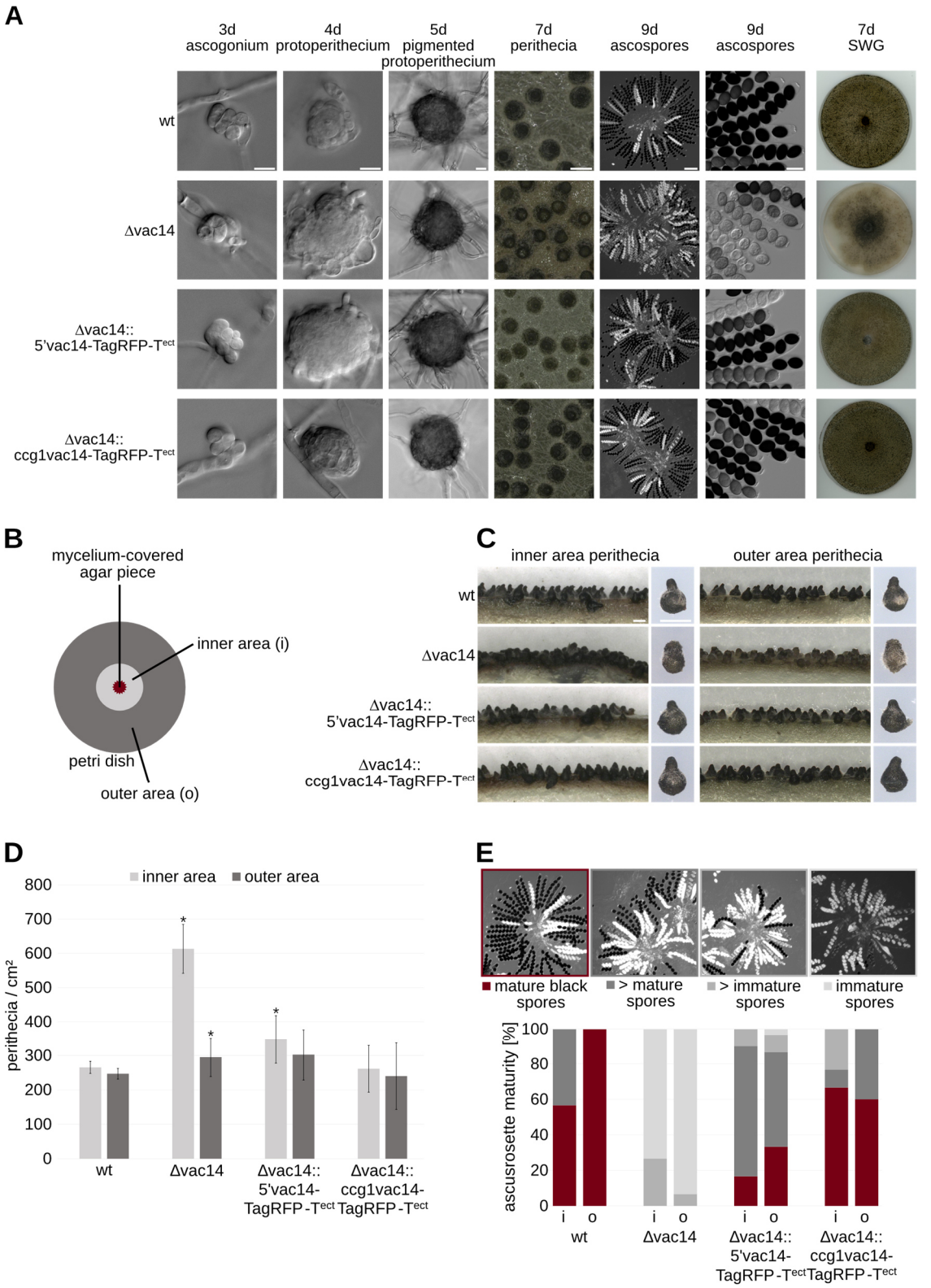

Figure 2: Phenotypic analysis of the *S. macrospora* wt, Δvac14 and complementation strains Δvac14::5'vac14-TagRFP-T^{ect} and Δvac14::ccg1vac14-TagRFP-T^{ect}.

A Microscopic investigation of sexual development. Strains were grown on SWG-slides or on solid SWG medium at 27 °C for indicated periods of 3 to 9 days. Scale bars from left to right: 10 µm; 10 µm; 10 µm; 0.5 mm; 100 Mm and 25 µm. **B** Schematic illustration of a petri dish divided in an inner (i) (dark grey) and outer (o) (light grey) area with the inoculum, mycelium-covered agar piece

(dark red), placed upside-down in the center. **C** Cross-sections of the strains from the defined inner and outer area and representative pictures of a single perithecium. Pictures were taken after strains were grown for 8 d on solid SWG-media. Scale bar: 0.5 mm. **D** Quantification of perithecia per cm^2 after 7 d of growth. Perithecia were counted 20 times in an area of 0.0625 cm^2 and the averages from three biological replicates from each strain of three independent experiments (n = 60) are shown. Counting was performed in the inner (i) (dark grey) and outer (o) (light grey) area, respectively. Significant differences to the wt of $p < 0.05$ according to Student's t-test are indicated by asterisks (*). **E** Ascus rosette maturation was determined after 9 d on solid SWG media. Ten perithecia of three biological replicates from each strain (n = 30) in the defined inner (i) and outer (o) area were cracked and categorized rosettes mature asci with 8 black spores (dark red), > rosettes of mostly asci with mature spores (dark grey), > rosettes of some asci with mature spores (middle grey), and rosettes of asci with immature spores (light grey). A representative picture of an ascus rosette of each category is shown above the diagram. Mature black spores of wt in the outer area were set to 100 %.

All strains completed the life cycle within 9 days including the production of ascospores. The *S. macrospora* life cycle begins with a germinating ascospore that develops into a vegetative mycelium. After 2-3 days, ascogonia, the female gametangia, were formed and after 3-4 days protoperithecia, unpigmented fruiting-body precursors, were produced. These stages could be observed in all strains whereby the Δvac14 strain displayed an enlarged protoperithecium compared to the wt (Figure 2A). After further development of the protoperithecia into melanin-pigmented protoperithecia, self-fertilization, karyogamy, meiosis and a postmeiotic-mitosis in the maturing perithecia took place. Subsequently, eight linear-arranged black ascospores are present per ascus. In Δvac14, the ascospores are predominantly immature compared to the wt. Additionally, after growth for 7 days on SWG medium, the Δvac14 deletion mutant exhibits an increased density of perithecia formed near the agar-piece in the center of the petri dish (Figure 2A). Due to this phenotype, we defined an "inner" and "outer" area of the petri-dish for further analysis (Figure 2B). Cross-sections were performed to analyze the morphology of the perithecia in the inner and outer area. This showed that the perithecia of the inner area of the Δvac14 strain appear more melanized and piled up. In addition, they appeared deformed and do not form a neck and a pear-shaped structure as seen in the wt or complementation strains (Figure 2C). To investigate the Δvac14 phenotype regarding perithecia production in more detail, numbers of perithecia per cm^2 in the defined areas were calculated after 7 days (Figure 2D). This analysis revealed a significantly higher amount (~2-fold) of perithecia in the inner area of the Δvac14 strain compared to the wt.

For further phenotypic analysis, ascus rosette maturation was analyzed in the defined areas in all strains (Figure 2E). For this, ascus rosettes were categorized into 4 stages according to their maturity revealing that Δvac14 perithecia contain an increased number of asci with immature spores compared to the wt.

3.3 Vacuolar Morphology is Altered in the Δvac14 Mutant

Since sexual development and growth behavior is impaired in the *S. macrospora* partial-deletion strain Δvac14, we microscopically investigated living hyphae to analyze vacuolar morphology. Our results revealed an atypical morphology and appearance of vacuoles (Figure 3). To visualize vacuolar membranes, we stained the *S. macrospora* wt and Δvac14 strain with the red fluorescent and membrane-selective dye FM4-64 (Fischer-Parton *et al.*, 2000; Peñalva, 2005) (Figure 3A). For further staining of the acidic lumen of vacuoles, we used the fluorescent compound 7-amino-4-chloromethyl-coumarin (CMAC) (Cole *et al.*, 1997; Cole *et al.*, 1998) (Figure 3B). These experiments revealed that the vacuoles of the Δvac14 mutant are extreme enlarged and, due to their fainter staining with CMAC, appear to be less acidified when compared to the wt. Moreover, we examined the localization of nuclei in both strains at growing hyphal tips using the histone 2B labeled with tdTomato (RH2B) (Figure 3C and Video S1 and Video S2). In the Δvac14 strain, enlarged, cellular space-consuming vacuoles at hyphal tips appear to displace nuclei to the periphery of the hyphae. This changed vacuolar morphology and distribution seemed to impair the growth rate of the Δvac14 mutant in comparison to the wt (Figure 3C).

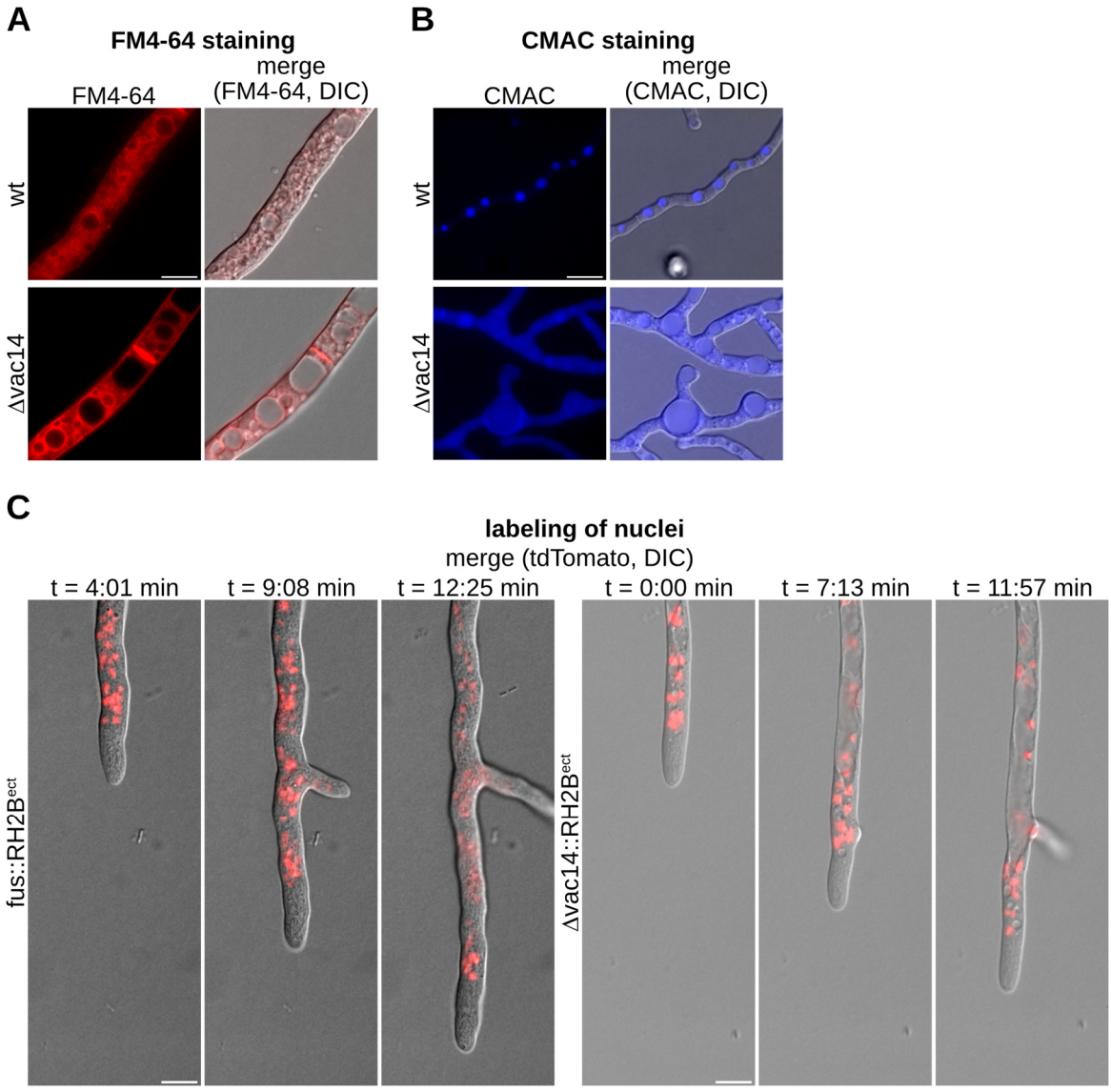

Figure 3: Vacuolar morphology of *S. macrospora* Δvac14 and wt.
A Vacuolar membranes of the hyphae were stained with FM4-64 (1 µg/mL in distilled water, and incubated for 15 min at 37 °C). Hyphae were recorded after growth on SWG + 1.5 % agarose medium for 24 h at 27 °C under continuous light. **B** The lumen of the vacuoles was stained with CMAC (1:400 of 10 mM stock solution, and incubated for 30 min at 37 °C). Hyphae were recorded after growth over a piece of cellophane (0.5 cm x 0.5 cm) on solid SWG medium for 24 h at 27 °C under continuous light. **C** Selected images of Video S1 and Video S2 showing localization of enlarged vacuoles and distribution of nuclei in growing hyphae of the wt (S1) and Δvac14 (S2) strain after 24 h on BMM + 1.5 % agarose medium at 27 °C. Nuclei were labeled by histone 2B fused to tdTomato (RH2B). Scale bar = 10 µm, DIC: differential interference contrast.

3.4 The Δvac14 Mutant is More Stress Sensitive than the Wt

Next, we analyzed the growth and developmental behavior of the Δvac14 mutant when confronted with various stress conditions (Figure 4). Sexual development of all strains was investigated after 10 days of growth on medium containing 0.1 M NaCl or 0.4 M sorbitol,

mimicking osmotic stress, applying 2.5 mM 3-AT to generate amino-acid starvation or by adding 0.01 % H_2O_2 for oxidative stress conditions (Figure 4A). The wt, complementation, and vac14-overexpression strains were able to grow and form perithecia under all stress conditions and revealed normal sexual development. On the contrary, the Δvac14 deletion strain displayed severe growth and developmental defects including decreased perithecia formation and slower growth rates (Figure 4A); though localization of VAC14-TagRFP-T was not altered under these stress conditions (Figure S5).

Additionally, we tested the growth velocity in cm per day of all strains on stress media (Figure 4B). The results revealed the most significant growth impairment of Δvac14 on media mimicking amino-acid starvation (2.5 mM 3-AT). Further, osmotic stress conditions (0.1 M NaCl or 0.4 M sorbitol) also prevent normal sexual development in the Δvac14 deletion mutant compared to the wt. Growth of Δvac14 on oxidative stress (0.01 % H_2O_2) lead to a comparable impaired growth rate as under normal conditions (SWG). The complementation strains Δvac14::5'vac14-TagRFP-T^{ect} and Δvac14::ccg1vac14-TagRFP-T^{ect} showed similar development and growth under these conditions like the wt. However, overexpression of VAC14-TagRFP-T restored the Δvac14 phenotype more efficiently. Limitation of nitrogen by omitting KNO_3 from the medium and cell-wall stress by adding 0.003 % SDS were also tested with no obvious effect concerning the development of the Δvac14 strain (Figure S6).

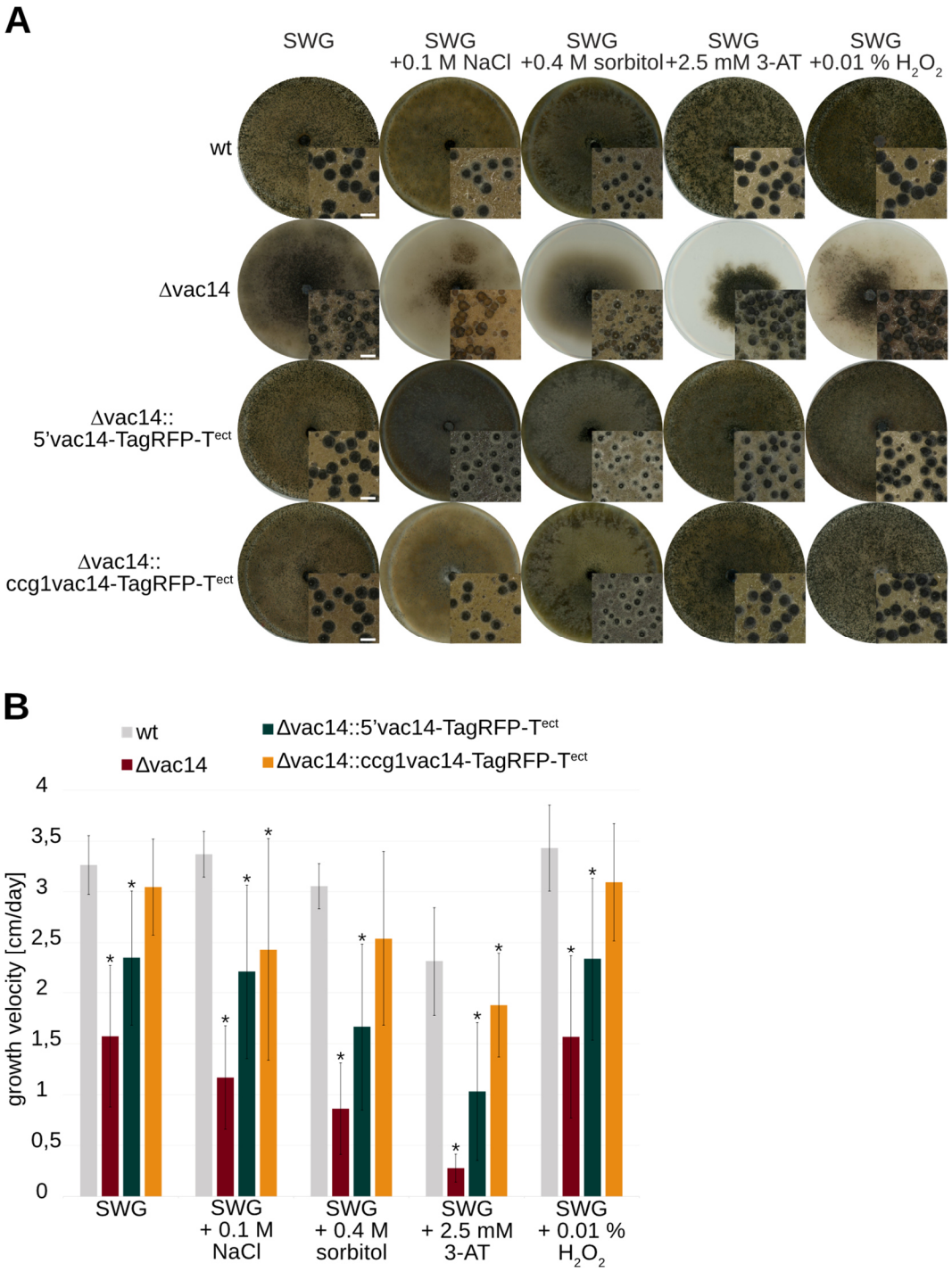

Figure 4: Sexual developmental and growth behavior of *S. macrospora* wt, Δvac14 and the complementation strains Δvac14::5'vac14-TagRFP-T^{ect} and Δvac14::ccg1vac14-TagRFP-T^{ect} on different stress media.

A Strains were grown in presence of various stress conditions, such as osmotic stress (0.1 M NaCl, 0.4 M sorbitol), under amino-acid starvation (2.5 mM 3-AT) or oxidative stress (0.01 % H_2O_2) by adding the components to SWG medium. Pictures of the agar plates and enlargement of perithecia by microscopic images were taken after 10 days. Scale bar of microscopic images: 0.5 mm. **B** For determination of growth rate per day, strains were grown in 30-cm race tubes filled with selected stress media. Three biological replicates of each strain were analyzed in three independent experiments (n = 9). Asterisks (*) indicate a significant difference to the wt strain, according to Student's t-test ($p < 0.05$).

3.5 SmVAC14 Co-localizes with the SmSTRIPAK-component SmSCI1 and Localizes to Vacuolar Membranes, the ER, the Golgi and to Early and Late Endosomes

Fluorescence microscopy was performed to determine the subcellular localization of the *S. macrospora* VAC14 protein. SmVAC14 was C-terminally fused with either one of the fluorescent tags EGFP and TagRFP-T, to confirm the localization of VAC14 independent of the tag (Figure 5). Due to the fact that the N-terminally tagged fusion protein TagRFP-T-VAC14 does not complement the Δvac14 phenotype (Figure S7), we performed the experiments with the C-terminally tagged protein version. Since the subcellular localization of VAC14 does not change whether it is expressed under the native (5') or the overexpression promotor of the *clock-controlled gene* 1 of *N. crassa* (ccg1) (Figure S8), but the latter version resulted in increased fluorescence, we used this variant for fluorescence microscopy. For localization of free EGFP or TagRFP-T as control, *S. macrospora* wt and Δvac14 strains were transformed with either plasmid p1783-1 (Pöggeler *et al.*, 2003) or pDS23 (Teichert *et al.*, 2012) or pTagRFP-T (Werner *et al.*, 2021) (Figure S9). To analyze putative co-localization of VAC14 with the SmSTRIPAK-complex, *S. macrospora* wt was transformed with the plasmids pccg1vac14-TagRFP-T_hyg and p5'sci1-egfp (Reschka *et al.*, 2018) to ectopically express the fusion proteins VAC14-TagRFP-T and SCI1-EGFP, respectively (Figure 5A). The resulting yellow fluorescence signal in the merged picture revealed partial co-localization of the fusion proteins. To determine if VAC14 localizes with the highly dynamic vacuolar compartment, we generated a *S. macrospora* wt strain expressing VAC14-TagRFP-T and the vacuolar ATPase catalytic subunit A, VMA1, tagged with EGFP as reporter protein for vacuolar membranes and vesicles (Figure 5B). Here, the merged picture revealed co-localization of VAC14-TagRFP-T with VMA1-EGFP at tubular shaped vacuoles and punctuated vesicular structures. Further, localization of VAC14 at the ER was tested using the recently identified *S. macrospora* ER-marker protein POM33 (Groth *et al.*, 2021). For this, *S. macrospora* wt strains expressing either VAC14-TagRFP-T or POM33-EGFP were crossed (Figure 5C). Here, the merged picture revealed partial co-localization of the fusion proteins whereby VAC14-TagRFP-T localized in dot-like structures at the ER and tubular filaments departing from them into the cytoplasm. In addition to this, we examined if VAC14 is linked to the secretory pathway by using the

Rab family GTPase YPT1, N-terminally fused to TagRFP-T, as marker protein for ER-to-Golgi vesicle trafficking (Figure 5D). Co-localization of VAC14-EGFP and TagRFP-T-YPT1 is shown in the merged picture by the yellow fluorescent signal at long filamentous structures spanning the cytoplasm and small vesicles. Furthermore, we investigated if SmVAC14 also showed localization to the endocytic pathway by performing co-localization studies with the early- and late-endosomal reporter proteins of *Z. tritici* ZtRAB5 and ZtRAB7, respectively (Figure 5E-F). Accordingly, VAC14-TagRFP-T partially co-localized with EGFP-ZtRAB5 at filamentous structures (Figure 5E). In contrast, VAC14-TagRFP-T showed distinct co-localization with EGFP-ZtRAB7 also at filamentous compartments and vesicles (Figure 5F).

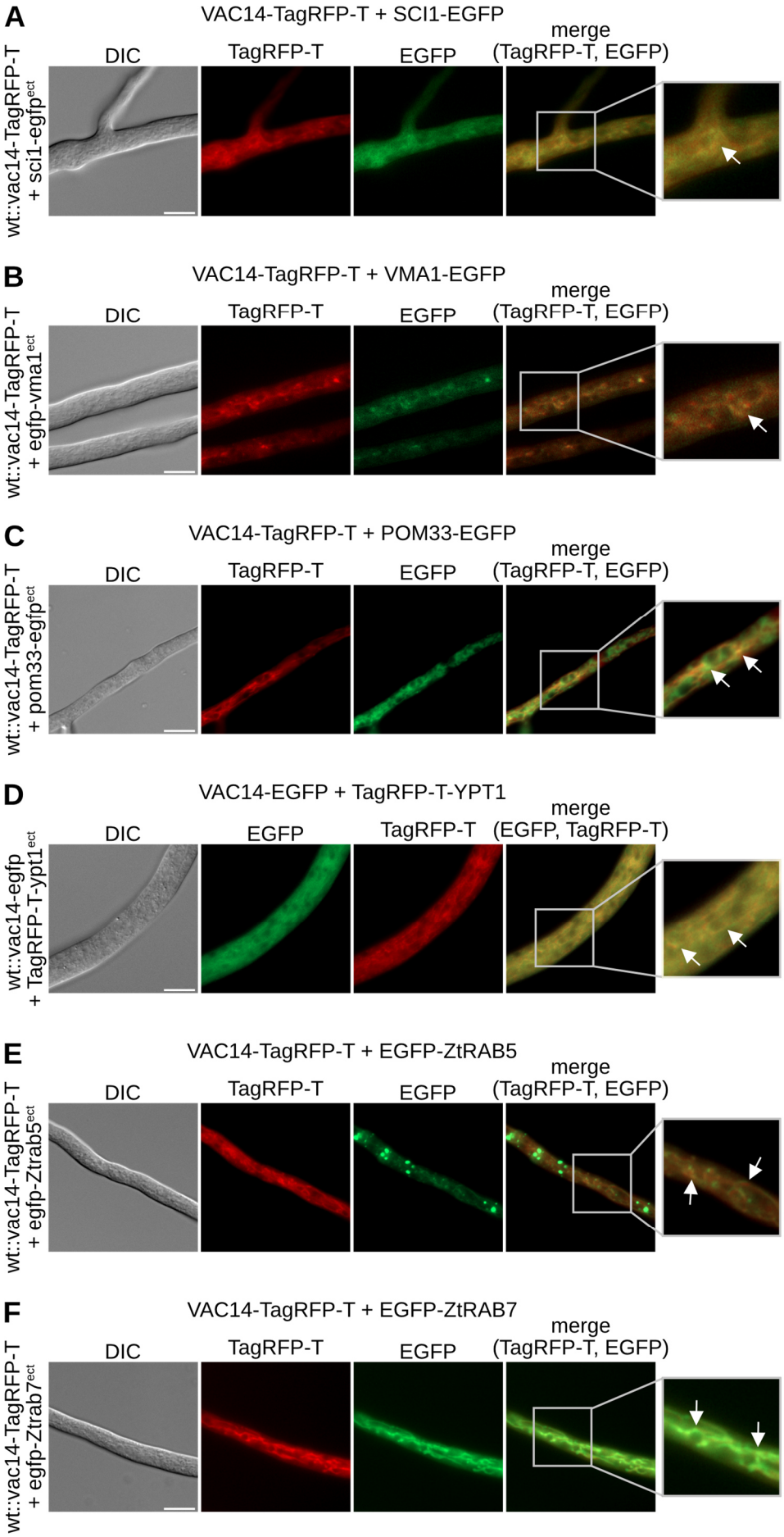
A
VAC14-TagRFP-T + SCI1-EGFP
DIC
TagRFP-T
EGFP
merge
(TagRFP-T, EGFP)
wt::vac14-TagRFP-T
+ sci1-egfp^ect
B
VAC14-TagRFP-T + VMA1-EGFP
DIC
TagRFP-T
EGFP
merge
(TagRFP-T, EGFP)
wt::vac14-TagRFP-T
+ egfp-vma1^ect
C
VAC14-TagRFP-T + POM33-EGFP
DIC
TagRFP-T
EGFP
merge
(TagRFP-T, EGFP)
wt::vac14-TagRFP-T
+ pom33-egfp^ect
D
VAC14-EGFP + TagRFP-T-YPT1
DIC
EGFP
TagRFP-T
merge
(EGFP, TagRFP-T)
wt::vac14-egfp
+ TagRFP-T-ypt1^ect
E
VAC14-TagRFP-T + EGFP-ZtRAB5
DIC
TagRFP-T
EGFP
merge
(TagRFP-T, EGFP)
wt::vac14-TagRFP-T
+ egfp-Ztrab5^ect
F
VAC14-TagRFP-T + EGFP-ZtRAB7
DIC
TagRFP-T
EGFP
merge
(TagRFP-T, EGFP)
wt::vac14-TagRFP-T
+ egfp-Ztrab7^ect

Figure 5: Co-localization of VAC14 and marker proteins in *S. macrospora* using different fluorescence tags.
S. macrospora wt was either co-transformed or strains expressing fluorescent proteins were crossed. Fluorescence microscopy was performed to visualize co-localization of the fusion proteins. **A** *S. macrospora* wt was co-transformed to express VAC14-TagRFP-T and the fluorescence-labeled SmSTRIPAK-component SCI1-EGFP. A white arrow indicates co-localization of both fusion constructs. **B** Co-transformed *S. macrospora* wt expressing VAC14-TagRFP-T and the tubular-vacuole marker VMA1 fused to EGFP. Co-localization of the fusion proteins is indicated by a white arrow. **C** *S. macrospora* wt strains expressing either VAC14-TagRFP-T or the ER-marker protein POM33-EGFP were crossed and partial co-localization of both fusion proteins is indicated by white arrows. **D** For co-localization at the Golgi, *S. macrospora* wt was co-transformed to express VAC14-EGFP together with TagRFP-T-YPT1. White arrows indicate co-localization. *S. macrospora* wt expressing VAC14-TagRFP-T together with the fluorescence-tagged *Z. tritici* early- and late endosomal markers EGFP-ZtRAB5 (**E**) and EGFP-ZtRAB7 (**F**), respectively. White arrows indicate co-localization of the fusion proteins. Scale bars = 10 μm, DIC: differential interference contrast. Detailed two-fold enlargements of the merge pictures are indicated by a frame and shown at the right margin.

3.6 Deletion of *vac14* has an Impact on the Endocytic Pathway

To further verify if the deletion of *S. macrospora vac14* has an impact on the endocytic pathway, we investigated the localization of the early endosomal marker EGFP-ZtRAB5 and the late endosomal marker EGFP-ZtRAB7 after 24 h and 72 h in the wt and the Δvac14 deletion strain, respectively (Figure 6). Vacuoles were stained with CMAC resulting in a bright blue fluorescence signal of the vacuolar lumen. In contrast to the wt, the early endosomal marker EGFP-ZtRAB5 localized already after 24 h inside vacuoles in Δvac14, whereas after 72 h no difference in the localization of the fusion construct could be observed comparing both strains (Figure 6A). The late endosomal marker EGFP-ZtRAB7 was present inside and around vacuoles after 24 h in both strains. However, after 72 h EGFP-ZtRAB7 localized exclusively in the lumen of vacuoles in the wt but showed an additional localization as a ring-like structure at the vacuolar membranes in Δvac14 (Figure 6C). Expression of both fusion proteins (EGFP-ZtRAB5: 56 kDa; EGFP-ZtRAB7: 49 kDa) was verified via Western blot analysis (Figure 6B and Figure 6D, respectively).

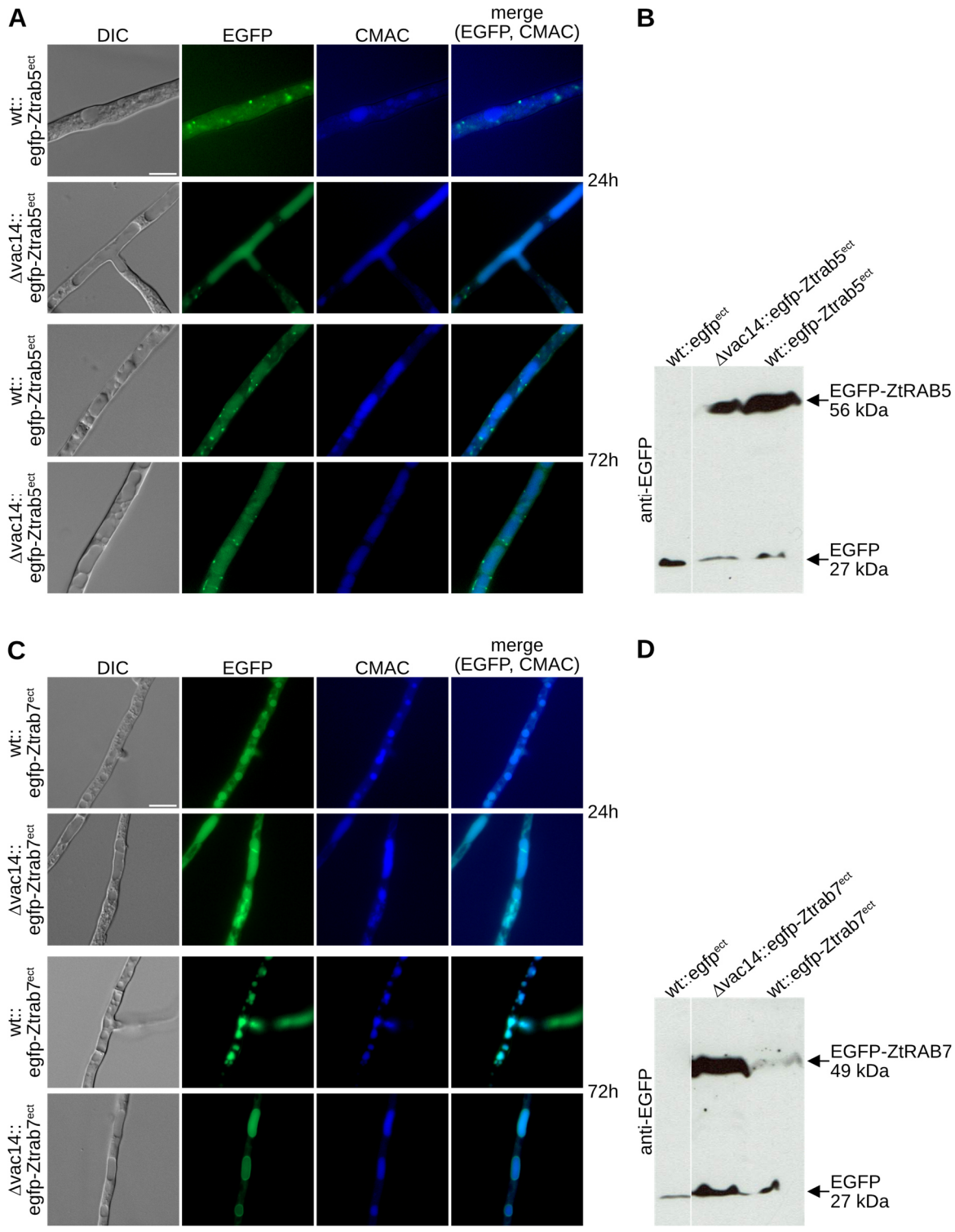

Figure 6: Localization of the early- and late-endosomal markers ZtRAB5 and ZtRAB7 in *S. macrospora* wt and Δvac14 strains.

S. macrospora wt and Δvac14 strains expressing the fluorescence-tagged *Z. tritici* early- and late endosomal markers EGFP-ZtRAB5 (**A**) and EGFP-ZtRAB7 (**C**) with corresponding Western blot analysis (**B**) and (**D**), respectively. Strains were grown on BMM-slides for 24 h or on SWG-slides for 72 h at 27 °C under continuous light. Vacuoles of the hyphae were stained with CMAC (1:400 of 10 mM stock solution) and incubated for 30 min at 37 °C. Scale bars = 10 µm, DIC: differential interference contrast.

3.7 Autophagy is not Affected by *vac14* Deletion

Since our results revealed a strong stress-sensitive phenotype for Δvac14 especially under amino-acid starvation conditions, we assumed that autophagy might be affected upon *Smvac14* deletion. In this context, it is also notably that deletion of *Smnbr1*, the autophagic receptor, also resulted in immature spore-formation (Werner *et al.*, 2019), which is similar to the phenotype of Δvac14. Moreover, human VAC14 was proposed to interact with endolysosomal and autophagic proteins (Schulze *et al.*, 2014). First, we investigated the localization of SmVAC14 with autophagic marker proteins. For this purpose, *S. macrospora* wt strains expressing VAC14-TagRFP-T together with either the EGFP-tagged autophagosomal-marker protein SmATG8 or the autophagic receptor SmNBR1, both fused to EGFP, were generated (Figure 7A and Figure 7B). To investigate the localization of these autophagy-marker proteins wt and Δvac14, were transformed with the plasmids pegfp-atg8 (Voigt and Pöggeler, 2013) and pnbr1-egfp (Werner *et al.*, 2019), respectively. VAC14-TagRFP-T localized inside as well as around vacuoles and at vacuolar compartments. The fusion proteins EGFP-ATG8 and NBR1-EGFP shown in Figure 7A and Figure 7B, respectively, were degraded in the vacuole leading to stable green fluorescence in the vacuolar lumen. To further test if autophagy is affected upon *vac14* deletion, we performed fluorescence microscopy of both marker proteins in Δvac14 and used Western-blot analysis for degradation analysis (Figure 7C-E). The results showed no alteration in the localizations of SmATG8 or SmNBR1 in the Δvac14 deletion background compared to the wt (Figure 7C and Figure 7E). Moreover, SmATG8 was degraded similarly in Δvac14 and wt, suggesting no effect of *vac14* deletion on autophagy.

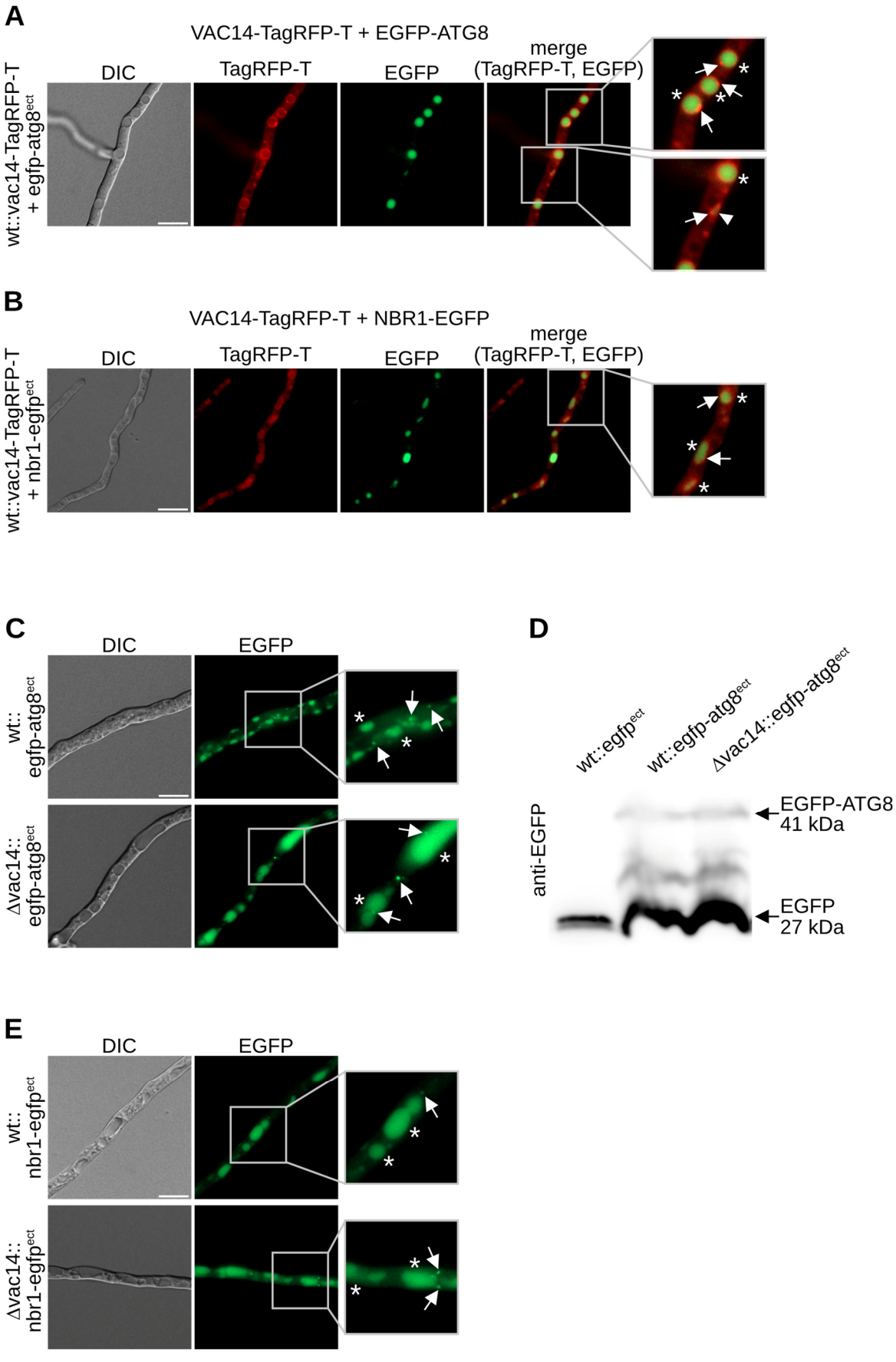
A
VAC14-TagRFP-T + EGFP-ATG8
DIC
TagRFP-T
EGFP
merge
(TagRFP-T, EGFP)
wt::vac14-TagRFP-T
+ egfp-atg8ect
B
VAC14-TagRFP-T + NBR1-EGFP
DIC
TagRFP-T
EGFP
merge
(TagRFP-T, EGFP)
wt::vac14-TagRFP-T
+ nbr1-egfpect
C
DIC
EGFP
wt::
egfp-atg8ect
Δvac14::
egfp-atg8ect
D
wt::egfpect
wt::egfp-atg8ect
Δvac14::egfp-atg8ect
anti-EGFP
EGFP-ATG8
41 kDa
EGFP
27 kDa
E
DIC
EGFP
wt::
nbr1-egfpect
Δvac14::
nbr1-egfpect

Figure 7: Co-localization of VAC14 with the autophagic marker proteins ATG8 and NBR1 in *S. macrospora* wt and localization in Δvac14.
Strains were grown on Co-transformed *S. macrospora* wt was used for fluorescence microscopy to visualize co-localization of fusion proteins (**A+B**). *S. macrospora* wt expressing VAC14-TagRFP-T together with the fluorescence-labeled autophagic marker EGFP-ATG8 (**A**) and the autophagy receptor NBR1-EGFP (**B**), respectively. After 72 h of growth the autophagic marker proteins displayed a localization inside of vacuoles marked by asterisks (*). White arrows indicate localization of VAC14-TagRFP-T around and at those vacuoles. An autophagosome is marked by a white rectangle. Detailed two-fold enlargements of the merge pictures are indicated by a frame and are shown at the right margin. *S. macrospora* wt and Δvac14 strains expressing the fluorescence-labeled autophagy-marker proteins EGFP-ATG8 and NBR1-EGFP (**C-E**). The autophagic markers show localization inside vacuoles marked by asterisks (*). White arrows indicate localization in small dots, presumably autophagosomes. Detailed two-fold enlargements of the merged pictures are indicated by a frame and shown at the right margin. **D** Western blot analysis for expression of EGFP-ATG8. The strain wt::egfp^{ect} served as control. Protein sizes are indicated. Degradation products of the fusion protein are visible. Scale bars = 10 μm, DIC: differential interference contrast.

4. Discussion

The Fab1p/PIKfyve-multiprotein complex controls the generation of the minor phosphorylated phosphatidylinositol PtdIns(3,5)P_2 and is comprised of the lipid and protein kinase Fab1p/PIKfyve, the lipid and protein phosphatase Fig4p/Sac3, and the scaffolding core Vac14p/ArPIKfyve. In yeast, additionally the Fab1p activator Vac7p and its inhibitor Atg18p are components of the Fab1p-complex (Bonangelino *et al.*, 1997; Botelho *et al.*, 2008; Duex *et al.*, 2006b; Efe *et al.*, 2007; Gary *et al.*, 2002; Ikonomov *et al.*, 2009a; Jin *et al.*, 2008; Sbrissa *et al.*, 2008; Schulze *et al.*, 2014). In our study we investigated the role of the Fab1p/PIKfyve scaffolding unit VAC14 of *S. macrospora*. We investigated the effect of *vac14* deletion and determined the subcellular localization of SmVAC14. Moreover, we analyzed the localization of endosomal and autophagy marker proteins in the Δvac14 mutant strain.

Protein domain prediction revealed that SmVAC14 is a conserved protein that besides a Fab1/PIKfyve- and a Fig4/Sac3-binding domain and multiple TMDs as well as CCs is predicted to be composed of several ARM-repeats (Figure 1). ARM- and HEAT-repeats are very similar evolutionary related motifs of tandemly repeated sequences of about 50 aa that provide surfaces for protein-protein interactions (Andrade *et al.*, 2001; Cingolani *et al.*, 1999; Malik *et al.*, 1997). However, HEAT-repeats are degenerated and therefore difficult to be predicted by available online programs including the one we used here (Andrade *et al.*, 2001). In our study, due to prediction challenges of HEAT-repeats, we restricted our

analysis only to ARM-repeats present in the Vac14 homologs. Accordingly, SmVAC14 together with Vac14 homologs in yeast in mammals can be classified as a member of the ARM-superfamily. However, yeast Vac14p was predicted to contain 17 HEAT-repeats, whereas up to 21 HEAT-repeats were predicted for the mammalian VAC14/ArPIKfyve homolog (Jin *et al.*, 2008). Therefore, it is suggested that HEAT-repeats span the whole Vac14p/ArPIKfyve protein to facilitate interactions with itself to form pentamers and with the other Fab1p/PIKfyve complex components (Jin *et al.*, 2008; Lees *et al.*, 2020). Based on the fact that the domain structure of SmVAC14 is similar to that of yeast, mammals and plants, a comparable function and localization is also probable. To analyze the function of SmVAC14, a Δvac14 deletion strain was generated and phenotypically investigated.

Accordingly, deletion of *Smvac14* caused deformed, less melanized perithecia and impaired ascospore formation (Figure 2). Interestingly, in mammals the point mutant $Vac14^{L156R}$, incapable of PIKfyve binding, induced the infantile gliosis (*ingls*) phenotype in mice characterized by less pigmentation and body size (Jin *et al.*, 2008). Besides these phenotypic features, the *S. macrospora* Δvac14 mutant also exhibited a high number of piled up perithecia around the inoculate agar-piece compared to the remaining outer area of the petri-dish (Figure 2C). Fertile pile-mutants were already described in *S. macrospora* showing defects in melanization of perithecia that are formed on top of each other, but so far these mutants have not been molecularly analyzed. Therefore, its not known which genes caused the "pile" phenotype (Engh *et al.*, 2007; Kück *et al.*, 2009; Teichert *et al.*, 2014). Our studies further showed that deletion of *Smvac14* resulted not only in impaired sexual development but also in enlarged, visually poorly acidified vacuoles already present in growing hyphal tips (Figure 2 and Figure 3). A similar effect has been described for Δfab1 and Δvac14 deletion stains in yeast and mammals. Enlarged vacuoles and lysosomes were reported to be accompanied by loss of or lower levels of PtdIns(3,5)P_2 (Gary *et al.*, 1998; Ikonomov *et al.*, 2001; Rusten *et al.*, 2006). PtdIns(3,5)P_2 was recently proposed to activate the vacuolar (V)-ATPase H+-pump thereby maintaining sufficient acidification of the vacuoles and their morphology and size (Li *et al.*, 2014). However, quantitative pH analysis revealed no defects in vacuolar acidification of *S. cerevisiae* Δfab1p and Δvac14p mutants since their pH were as acidic as wild-type cells (Ho *et al.*, 2015). Moreover, PtdIns(3,5)P_2 might not control the activity of the V-ATPase for steady-state conditions but

rather in response to salt stress for osmoregulation (Li *et al.*, 2014). Accordingly, regulation of the PtdIns(3,5)P_2 level at endolysosomal membranes is controlled by hyperosmotic stress (Bonangelino *et al.*, 2002; Jin *et al.*, 2017). Thus, disturbed osmotic regulation results in enlargement of vacuoles (Banerjee and Kane, 2020; Wilson *et al.*, 2018).

Accordingly, the *S. macrospora* Δvac14 strain revealed a strong stress-phenotype by being sensitive to hyperosmotic stress, amino-acid starvation, and oxidative-stress conditions, which led to developmental defects with concentrated perithecia formation only in a small area around the agar-piece (Figure 4). This observation is consistent with those in yeast, where Δfab1p, Δfig4p and Δvac14p mutants also reacted to hyperosmotic shock by increased PtdIns(3,5)P_2 levels that returned to its native quantity quickly after stressing the cells (Bonangelino *et al.*, 2002; Dove *et al.*, 1997; Duex *et al.*, 2006b).

For localization studies of SmVAC14, we performed fluorescence microscopy. Recently, pulldown experiments had identified SmVAC14 as potential interaction partner of SCI1 (Reschka *et al.*, 2018). Thus, connection between both proteins had been proposed, which is consistent with the co-localization of both proteins in our studies (Figure 5). In addition, a recent global phosphoproteomic study revealed that SmVAC14 is differentially phosphorylated at T455 and S429 in SmSTRIPAK mutants, suggesting another link between the scaffolding protein SmVAC14 and the SmSTRIPAK-complex (Märker *et al.*, 2020; Stein *et al.*, 2020). Interestingly, a recently performed proximity-dependent biotin identification (BioID) analysis with mammalian Vac14 and Fig4 revealed STRIPAK-components in proximity as potential interactors (Qiu *et al.*, 2021). Together with our co-localization result, these findings indicate a possible connection of VAC14 with the STRIPAK-complex.

Furthermore, fluorescence microscopy revealed that SmVAC14 localized at vacuolar membranes, the Golgi and with early and late endosomes (Figure 5). These results are concurrent with observations in yeast and mammals, where Vac14p/ArPIKfyve localizes to the membranes of vacuoles and to endolysosomes, respectively (Bonangelino *et al.*, 2002; Dove *et al.*, 2002; Jin *et al.*, 2008).

Further microscopic investigations showed that the enlarged vacuoles in the Δvac14 strain were enriched with the early and late endosomal marker proteins of RAB5 and RAB7, respectively (Figure 6), resulting in a mixture of early and late endosome/lysosome-like

vacuoles. These result are consistent with observation in Vac14^{wt} or PIKfyve-binding deficient Vac14^{L156R} overexpression mammalian cells, in which the enlarged vacuoles are positive for late endosomal markers Rab7, CD63, and Lamp2 (Schulze *et al.*, 2014; Schulze *et al.*, 2017). In contrast to this, highly enlarged vacuolar/endolysosomal compartments could not be detected when *Smvac14* was overexpressed in *S. macrospora* (Figure S8). However, our results lead to the assumption that maturation or fusion events in the endolysosmal pathway are altered upon *Smvac14* deletion.

Due to the fact, that proteins that are linked to lysosomal and autophagic membrane dynamics (Rab9, Rab7 activator TBC1D15, and Rab5-interacting protein Sun2) were identified as potential interaction partners of mammalian Vac14 (Schulze *et al.*, 2014; Schulze *et al.*, 2017), we investigated if autophagy might be affected in the *S. macrospora* Δvac14 deletion strain. For this, we first investigated the localization of SmVAC14 together with the autophagic marker proteins SmATG8 and SmNBR1 (Figure 7A and Figure 7B). Accordingly, SmVAC14 localized at membranes of vacuoles and autophagosomes. Then, we analyzed if the localization and protein degradation of these marker proteins is altered in the Δvac14 strain compared to the wt (Figure 7C-E). The results revealed that autophagy is probably not affected in Δvac14 since the expression control and localization of the autophagic-marker proteins SmATG8 and SmNBR1 is not altered compared to the wt. These observations are consistent with those of mammalian Vac14 overexpression mutants, where the autophagic flux was not affected by enlarged lysosomes, although LC3 accumulated in Western blot analysis of these mutants (Schulze *et al.*, 2014; Schulze *et al.*, 2017). In addition, in *ingls* mice, as well as in *Drosophila* and *Caenorhabditis elegans vac14* deletion mutants accumulation of autophagosomes was detected (De Lartigue *et al.*, 2009; Ferguson *et al.*, 2009; Ho *et al.*, 2012; Nicot *et al.*, 2006; Rusten *et al.*, 2007). To obtain an overview of the diverse functions of the Fab1/PIKfyve-complex and its potential connection with other regulatory complexes and signaling pathways in *S. macrospora*, more studies should be performed including the construction of knockout strains of other Fab1/PIKfyve-complex components, phenotypic analysis and interaction studies.

5. Conclusion

Organelle morphology is defined by the composition of lipids. PtdIns(3,5)P_2 is generated by the Fab1p/PIKfyve-complex localized at vacuoles and endosomes. Through detailed phenotypic analysis, we have shown that the Fab1p/PIKfyve scaffold protein SmVAC14 is important for controlling vacuolar size, proper sexual development, and stress responses in *S macrospora.* Furthermore, fluorescently-tagged SmVAC14 localizes to vacuolar membranes and co-localizes to diverse organelles including the Golgi, ER and endosomes as well as to the SmSTRIPAK-component SCI1. To unravel mechanistic links between VAC14, PtdIns(3,5)P_2 homeostasis and developmental processes in filamentous fungi further studies are required.

Supplementary Material

Supplementary Table 1

Table S1: List of plasmids used and generated in this study.

Plasmid	Feature	Reference
pRS-nat	*amp*^{R}, *ura3*, *nat*^{R}	(Klix *et al.*, 2010)
pRS-hyg	*amp*^{R}, *ura3*, *hyg*^{R}	(Bloemendal *et al.*, 2012)
pJet_nat	*amp*^{R}, *nat*^{R}	Nordzieke, unpublished
p1783-1	*amp*^{R}, *ura3*, *hyg*^{R} *Pgpd::egfp::TtrpC*	(Pöggeler *et al.*, 2003)
pDS23	*amp*^{R}, *ura3*, *nat*^{R} *Pgpd::egfp::TtrpC*	(Teichert *et al.*, 2012)
pTagRFP-T	*amp*^{R}, *nat*^{R} *Pccg1::TagRFP-T::TtrpC*	(Werner *et al.*, 2021)
pGG-hph	*kan*^{R}*, bla* *Bsa*I*(6)::PtrpC::hph::Bsa*I*(5)* in pDrive	(Dahlmann *et al.*, 2021)
pDest-Amp	Destination vector for Golden Gate cloning; *bla* (Bsamut), *lacZ* gene with two internal *Bsa*I sites: *Bsa*I*(4)* and *Bsa*I*(7)*	(Dahlmann *et al.*, 2021)
pRH2B_nat	*amp*^{R}, *ura3*, *nat*^{R} *Pgpd::hh2b::tdTomato::TtrpC*	(Reschka *et al.*, 2018)
pHeGFPRab5_hyg	*kan*^{R}, *ura3*, *hyg*^{R} *PZttub2::egfp::Ztrab5::TZttub2*	(Kilaru *et al.*, 2015)
pHeGFPRab7_hyg	*kan*^{R}, *ura3*, *hyg*^{R} *PZttub2::egfp::Ztrab7::TZttub2*	(Kilaru *et al.*, 2015)
pnbr1-egfp	*amp*^{R}, *ura3*, *nat*^{R} *Pnbr1::nbr1::egfp::TtrpC*	(Werner *et al.*, 2019)
pegfp-atg8	*nat*^{R} *Patg8::egfp::atg8::Tatg8*	(Voigt and Pöggeler, 2013)
P5'sci1-egfp	*amp*^{R}, *ura3*, *nat*^{R} *Psci1::sci1::egfp::TtrpC*	(Reschka *et al.*, 2018)
pegfp-Ztrab5_nat	*amp*^{R}, *ura3*, *nat*^{R} *PZttub2::egfp::Ztrab5::TZttub2*	This study
pegfp-Ztrab7_nat	*amp*^{R}, *ura3*, *nat*^{R} *PZttub2::egfp::Ztrab7::TZttub2*	This study
pegfp-Ztrab5_hyg	*amp*^{R}, *ura3*, hyg^R *PZttub2::egfp::Ztrab5::TZttub2*	This study
pegfp-Ztrab7_hyg	*amp*^{R}, *ura3*, hyg^R *PZttub2::egfp::Ztrab7::TZttub2*	This study
pegfp-vma1	*amp*^{R}, *ura3*, *hyg*^{R} *Pvma1::egfp::vma1::Tvma1*	This study
pTagRFP-T-ypt1	*amp*^{R}, *ura3*, *nat*^{R} *Pccg1::TagRFP-T::ypt1::TtrpC*	This study
pvac14-KO_V3w	*amp*^{R}, first 1030bp (=5'-flank) and last 1030bp (=3'-flank) of *vac14* ORF interrupted by *hyg*^{R} in pDest-Amp	This study
pvac14-egfp	*amp*^{R}, *ura3*, *hyg*^{R} *Pvac14::vac14::egfp::TtrpC*	This study
p5'vac14-TagRFP-T	*amp*^{R}, *ura3*, *nat*^{R} *Pvac14::vac14::TagRFP-T::TtrpC*	This study
pccg1vac14-TagRFP-T_nat	*amp*^{R}, *ura3*, *nat*^{R} *Pccg1::vac14::TagRFP-T::TtrpC*	This study
pccg1vac14-TagRFP-T_hyg	*amp*^{R}, *ura3*, *hyg*^{R} *Pccg1::vac14::TagRFP-T::TtrpC*	This study
pTagRFP-T-vac14	*amp*^{R}, *nat*^{R} *Pvac14::TagRFP-T::vac14::Tvac14*	This study

nat^{R}: nourseothricin resistant, *hyg*^{R}: hygromycin resistant, *amp*^{R}: ampicillin resistance, *kan*^{R}: kanamycin resistance, *ura3*: orotidine-5′-phosphate decarboxylase gene of *Saccharomyces cerevisiae*, *hph*: hygromycin B phosphotransferase gene, 5′: represents the native promoter of the respective gene, bp: base pairs, ORF: open-reading frame, *P*: promoter, *T*: terminator, *Pgpd*: promoter of the glyceraldehyde-3-phosphate dehydrogenase gene from *A. nidulans*, *Pccg1*: promoter of the *clock-controlled gene 1* from *N. crassa*, *TtrpC*: terminator of the anthranilate synthase gene from *A. nidulans*, *egfp*: gene for green fluorescence protein enhanced green fluorescent protein (EGFP) from *Aequorea Victoria*, *TagRFP-T*: gene for red fluorescence protein TagRFP-T of *Entacmaea quadricolor*, *tdTomato*: gene for red fluorescence protein tdTomato from *Discosoma species*.

Supplementary Table 2

Table S2: List of primers used in this study.

Oligo name	Sequence (5'→3')
Vac14-ko-5f_3w	***GACTGGTCTCA AGTC*** CCTGGAGCGTACCATACGTGA
Vac14-ko-5r_3w	***CAGAGGTCTCA GCAG*** AGTCGACCTCGTCCCCATCCT
Vac14-ko-3f_3	***GTACGGTCTCG GTCA*** GTTCTTTGTAGCGCTTTTCCG
Vac14-ko-3r_3	***CTCAGGTCTCC CGTA*** TCATTGCTGGGCTCGCTTGCC
GG_KO_fw	TAGGGCGAATTGGGTACCG
GG_KO_rv	GGCCGCTCTAGAACTAGTG
Vac14-egfp-f	***GTAACGCCAGGGTTTTCCCAGTCACGACG*** AAGCAGCACGTCCAACAGTC
Vac14-egfp-r	***CGGTGAACAGCTCCTCGCCCTTGCTCACCAT*** TTGCTGGGCTCGCTTGCC
GFP-f	ATGGTGAGCAAGGGCGAGGA
pRS426GFPrev	***GCGGATAACAATTTCACACAGGAAACAGC*** TCGAGTGGAGATGTGGAGTG
Vac14-tRFP-r	***TTAATCAGCTCTTCGCCCTTAGACACCAT*** TTGCTGGGCTCGCTTGCCTC
RFP-f	ATGGTGTCTAAGGGCGAAGAG
pRSccg1	***GTAACGCCAGGGTTTTCCCAGTCACGACG*** TAGAAGGAGCAGTCCATCTG
Pccg1-r	TTTGGTTGATGTGAGGGGTT
Vac14-ccg1-f	***CACTTTCACAACCCCTCACATCAACCAAA*** ATGGACGCGAACATTCAGCG
Vac14-2v5f	TAATGAGGTGCTTCTGGCAT
Vac14-2vORF5-r	AGATTTTTCTGGCGACTGGT
tC1_o	CCTGGACGACTAAACCAAAA
Vac14-2v3r	CCGTGATCTTTTCCCCCTCC
Smku70-v1-f	CATCGAGGTGAGCAAGTCAATG
ku70-ko-v3f(R)	GCGCAACTCCAGCGTGACTG
Tub2Ztf	***GTAACGCCAGGGTTTTCCCAGTCACGACG*** GCAGTCGACGCCAGATGATG
Tub2Ztr	***GCGGATAACAATTTCACACAGGAAACAGC*** GAGGAGTCGACAGCCAAGCT
Vma1P-f	***GTAACGCCAGGGTTTTCCCAGTCACGACG*** ACGGTTCTTGCAAATGGGTT
Vma1P-EGFP-r	***GTGAACAGCTCCTCGCCCTTGCTCACCAT*** GCATGCAATCTGTCTGTTCC
Vma1-EGFP-f	***TCACTCTCGGCATGGACGAGCTGTACAAG*** CAGGCGGGATTCAGACCG
Vma1-r	***GCGGATAACAATTTCACACAGGAAACAGC*** GCAGCAGCAGCAGCAGTAGC
RFP-r	CTTGTACAGCTCGTCCATGC
Ypt1-RFP_f	***AACTTAATGGCATGGACGAGCTGTACAAG*** ATGAACCCTGAGTACGACTACC
Rek_dsred_ypt1 bw	***GTTTGATGATTTCAGTAACGTTAAGTGGA*** TTAGCAGCAGCCGCCGGAAGAG

TtrpC_F	TCCACTTAACGTTACTGAAAT
N-vac14_P-f	***GATCTTCCGGATGGC*** AAGCAGCACGTCCAACAGTC
N-vac14_P-r	GGCTCAGAAGGGTCTCGTCGG
N-tRFP-f	***AGACCCTTCTGAGCC*** ATGGTGTCTAAGGGCGAAGAG
N-tRFP-r	CTTGTACAGCTCGTCCATGCC
N-vac14-f	***GACGAGCTGTACAAG*** ATGGACGCGAACATTCAGC
N-vac14_T-r	***ATGCCCTGCCCCTGA*** GGATTAAAACGCTGACGGGAC

Bold italics = overhangs

Supplementary Figure 1

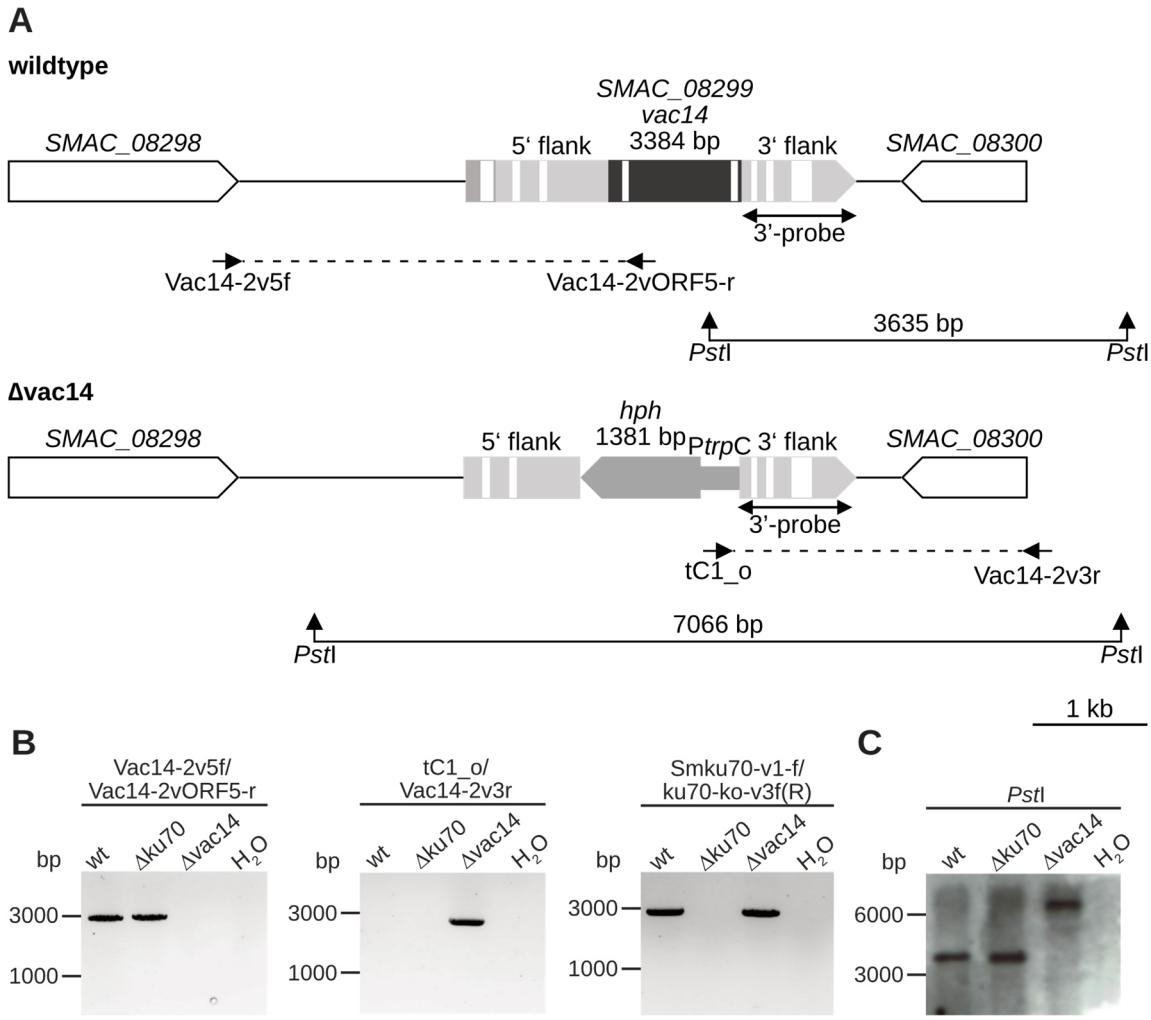

Figure S1: Verification of partial *vac14* deletion by PCR and Southern blot analyses.
A Schematic representation of the *vac14* ORF SMAC_08299 (light grey arrow) with 8 introns (white boxes). The dark grey box indicates the region of the *vac14* ORF that is partially replaced by the *hph* cassette after Golden Gate cloning. White arrows indicate adjacent ORFs. Primer combinations, probe for Southern hybridization and hybridization regions of *Pst*I including corresponding fragment sizes are indicated. **B** PCR verification of the integration of the *hph* cassette into the *vac14* locus. Genomic DNA was isolated from the wt, Δku70 and Δvac14 strain and tested with given primer combinations. Water served as negative control. **C** Confirmation of the *vac14* deletion was performed by Southern blot. The isolated genomic DNA was hydrolyzed with *Pst*I. Signals detected correspond to the fragment size of 3635 bp for the wt and Δku70 strain and 7066 bp for the Δvac14 deletion strain.

Supplementary Figure 2

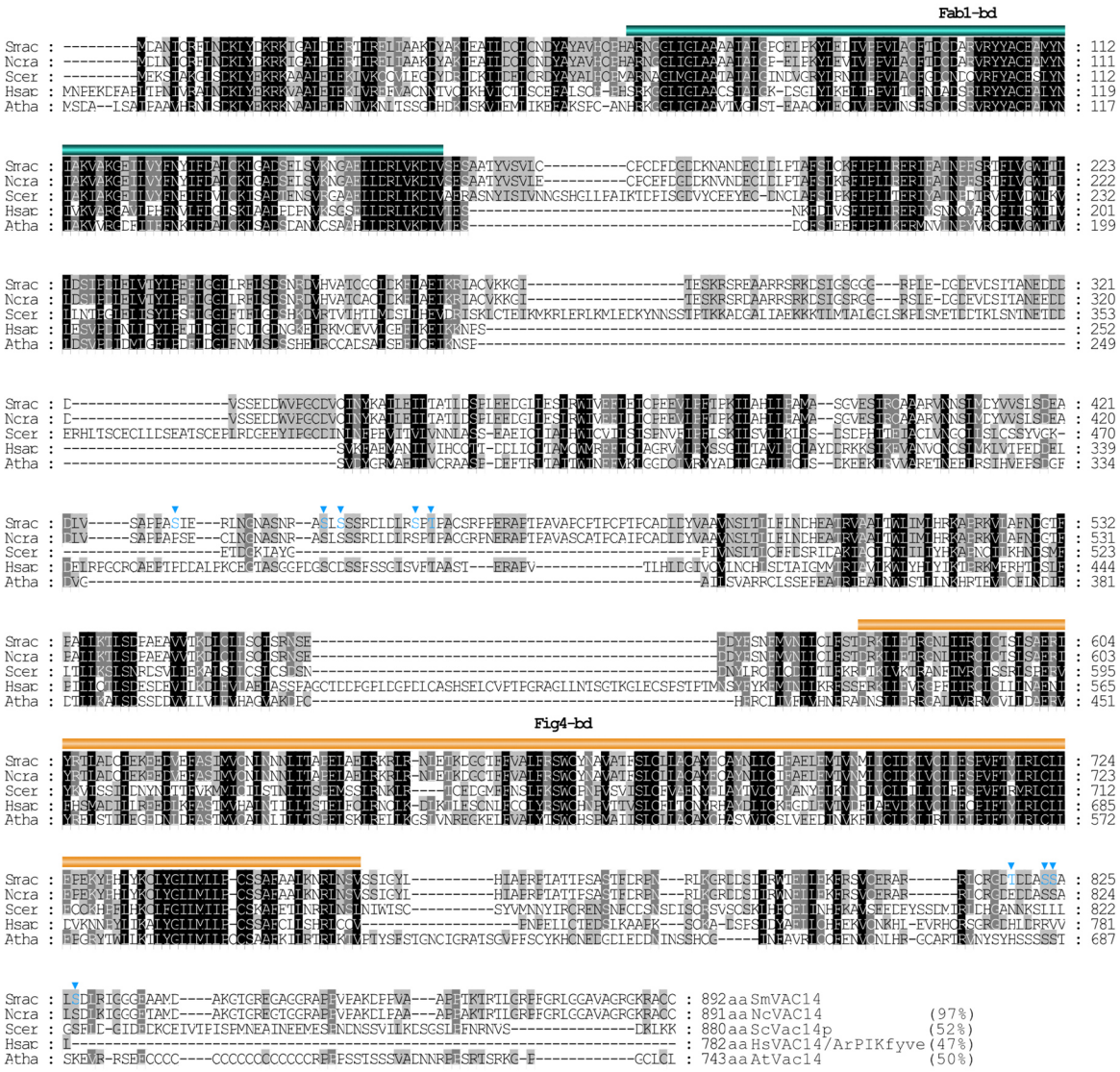

Figure S2: Multiple sequence alignment of VAC14 homologs in different species.
Alignment of full-length VAC14 homologs. Smac, *Sordaria macrospora* (SMAC_08922) taken from the *S. macrospora*-specific peptide database Smacrospora_v03 (Blank-Landeshammer *et al.*, 2019); Ncra, *Neurospora crassa* (XP_011395167.1); Scer, *Saccharomyces cerevisiae* (NP_013490.3); Hsap, *Homo sapiens* (NP_060522.3); and Atha, *Arabidopsis thaliana* (NP_565275.1). Sequence similarities to SmVAC14 of *S. macrospora* are indicated in percentage in brackets at the end of the protein sequence. Amino acids (aa) conserved in all proteins are shaded in black, in five of six sequences in dark grey and in four of six sequences in light grey. The N-terminal Fab1-binding domain (Fab1-bd) is shown in cyan, the C-terminal Fig4-bd in orange. Light blue triangles indicate potential phosphorylation sites after (Märker *et al.*, 2020)and (Stein *et al.*, 2020).

Supplementary Figure 3

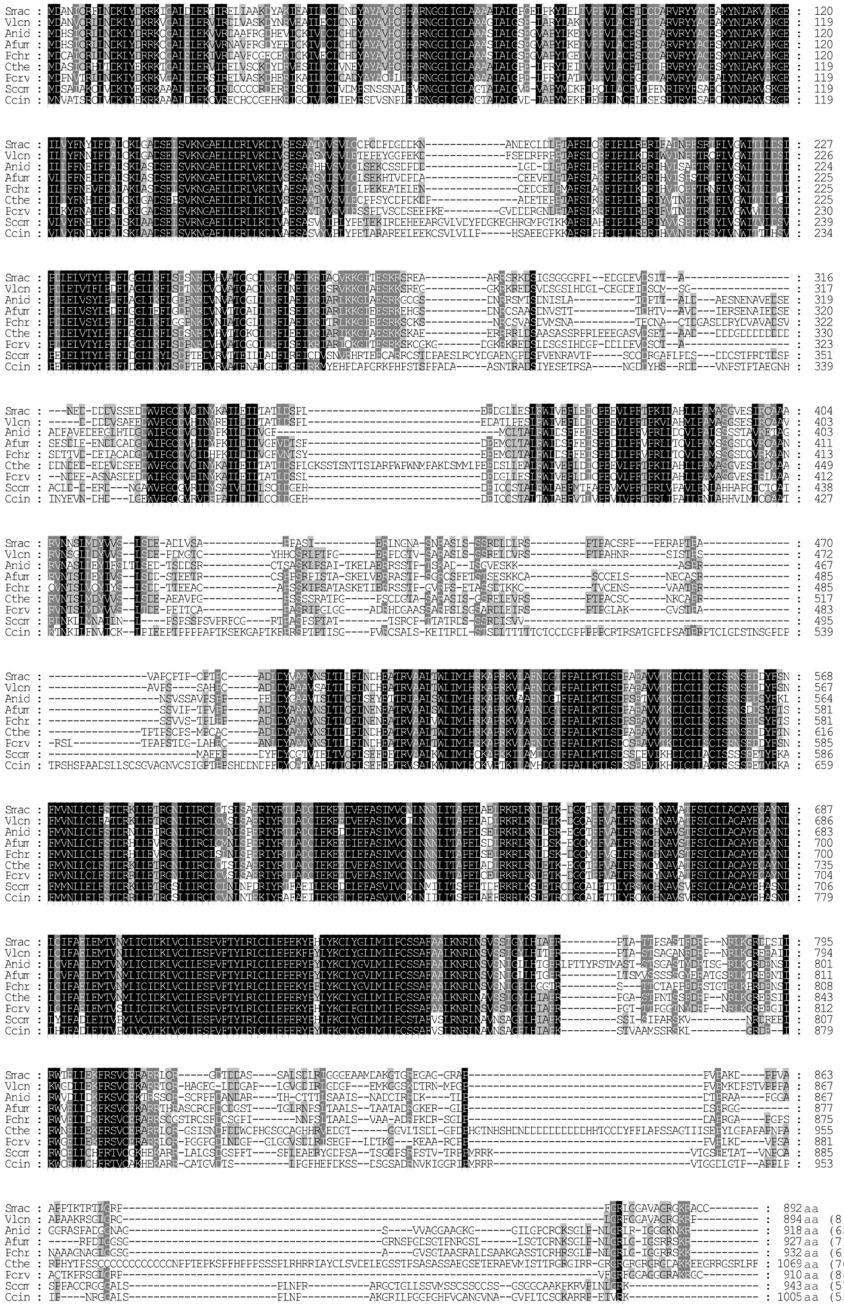

Figure S3: Multiple sequence alignment of VAC14 proteins in fungal species.
Ascomycota: Smac, *Sordaria macrospora* (SMAC_08922) taken from the *S. macrospora*-specific peptide database Smacrospora_v03 (Blank-Landeshammer *et al.*, 2019); Vlon, *Verticillium longisporum* (KAG7121875.1); Anid, *Aspergillus nidulans* (CBF81734.1); Afum, *Aspergillus fumigatus* (KAF4276542.1); Pchr, *Penicillium chrysogenum* (KZN86095.1); Cthe, *Chaetomium thermophilum* (XP_006695219.1) and Pory, *Pyricularia oryzae* (XP_003716347.1). Basidiomycota: Scom, *Schizophyllum commune* (XP_003038141.1) and Ccin, *Coprinopsis cinerea* (KAG2013354.1). Amino acids (aa) conserved in all proteins are shaded in black, in nine or eight of ten sequences in dark grey and in seven of ten sequences in light grey. Sequence similarities to SmVAC14 of *S. macrospora* are indicated in percentage in brackets at the end of the protein sequence.

Supplementary Figure 4

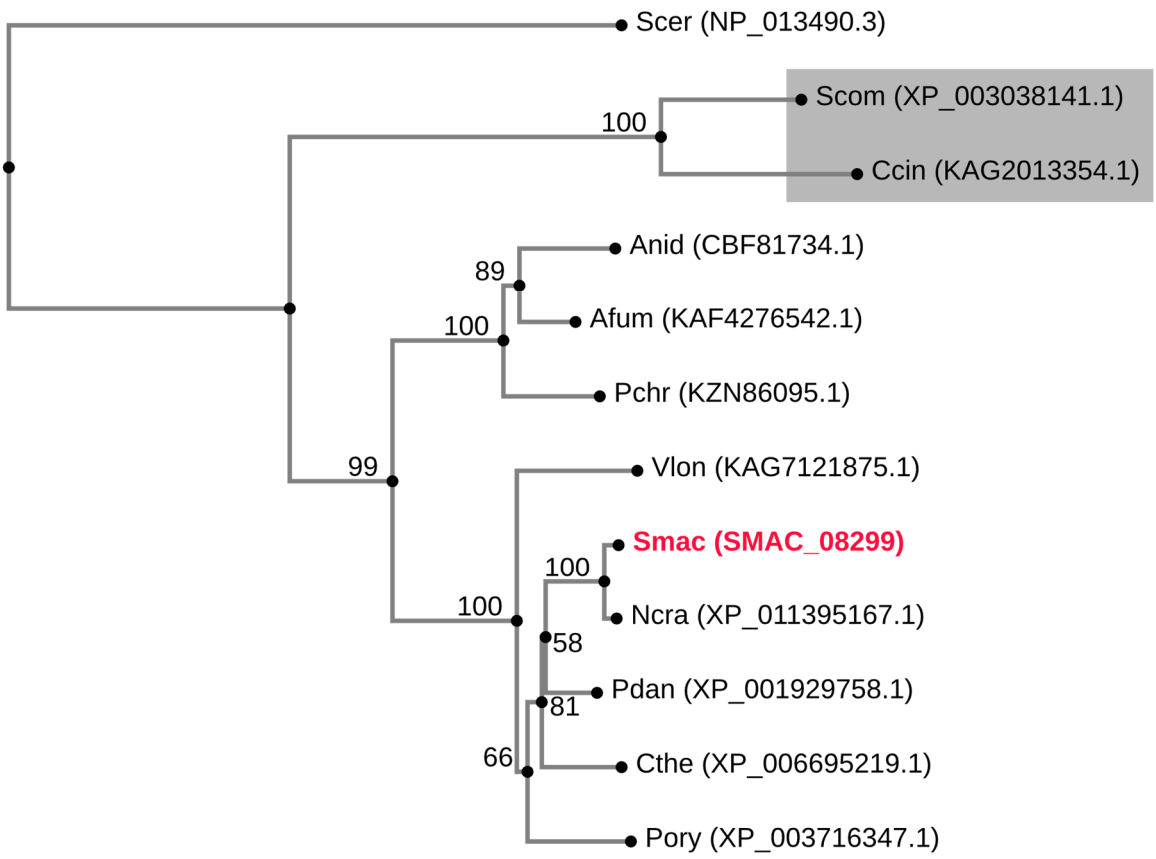

Figure S4: Phylogenetic tree of Vac14 orthologs from fungi.
The phylogenetic tree of Vac14 was generated using the Neighbor Joining method. Orthologs were identified with BLASTP search using amino acid sequences of the *Sordaria macrospora* SmVAC14 (SMAC_08299) indicated in red. The multiple sequence alignment and phylogenetic analysis was performed with MAFFT (version 7, https://mafft.cbrc.jp/alignment/server/; accessed on 24.08.2021) (Katoh *et al.*, 2019). Bootstrap values of 1000 replications are percentages rounded to whole numbers and are indicated at the nodes. Accession numbers are indicated. Ascomycota: Smac, *Sordaria macrospora* (SMAC_08922) from the *S. macrospora*-specific peptide database Smacrospora_v03 (Blank-Landeshammer *et al.*, 2019); Ncra, *Neurospora crassa* (XP_011395167.1); Vlon, *Verticillium longisporum* (KAG7121875.1); Pans, *Podospora anserina* (XP_001929758.1); Anid, *Aspergillus nidulans* (CBF81734.1); Afum, *Aspergillus fumigatus* (KAF4276542.1); Pchr, *Penicillium chrysogenum* (KZN86095.1); Cthe, *Chaetomium thermophilum* (XP_006695219.1) and Pory, *Pyricularia oryzae* (XP_003716347.1). Basidiomycota: Scom, *Schizophyllum commune* (XP_003038141.1) and Ccin, *Coprinopsis cinerea* (KAG2013354.1) are shaded in grey.

Supplementary Figure 5

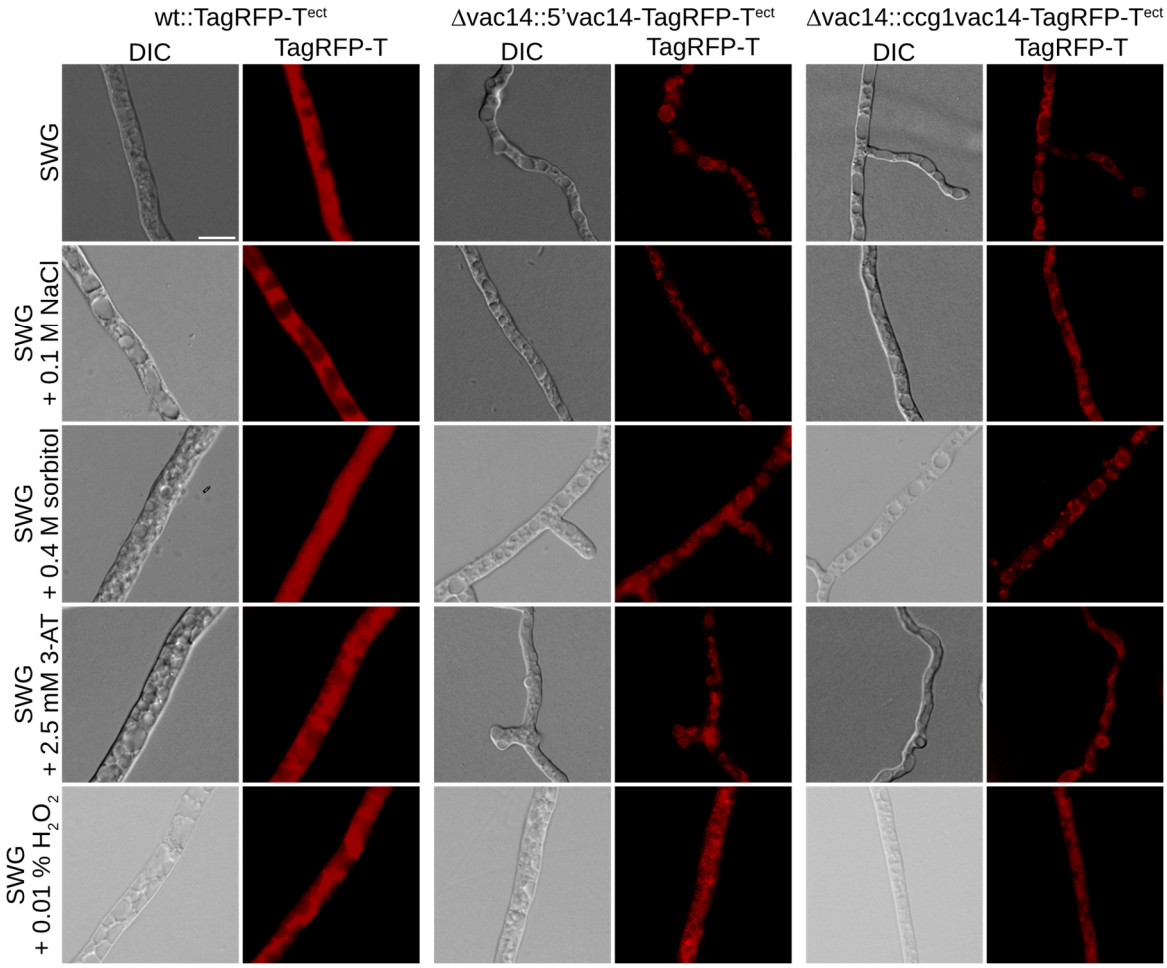

Figure S5: Localization of native and overexpressed VAC14-TagRFP-T and free TagRFP-T in *S. macrospora* wt and Δvac14 on different stress media.

The wt::TagRFP-Tect strain, expressing free TagRFP-T served as control. Strains were grown in presence of various stress conditions, such as osmotic- (0.1 M NaCl, 0.4 M sorbitol) or oxidative stress (0.01 % H_2O_2) or under amino-acid starvation (25 mM 3-AT) by adding the components to SWG + 1.5 % agarose medium. Scale bars = 10 µm, DIC: differential interference contrast.

Supplementary Figure 6

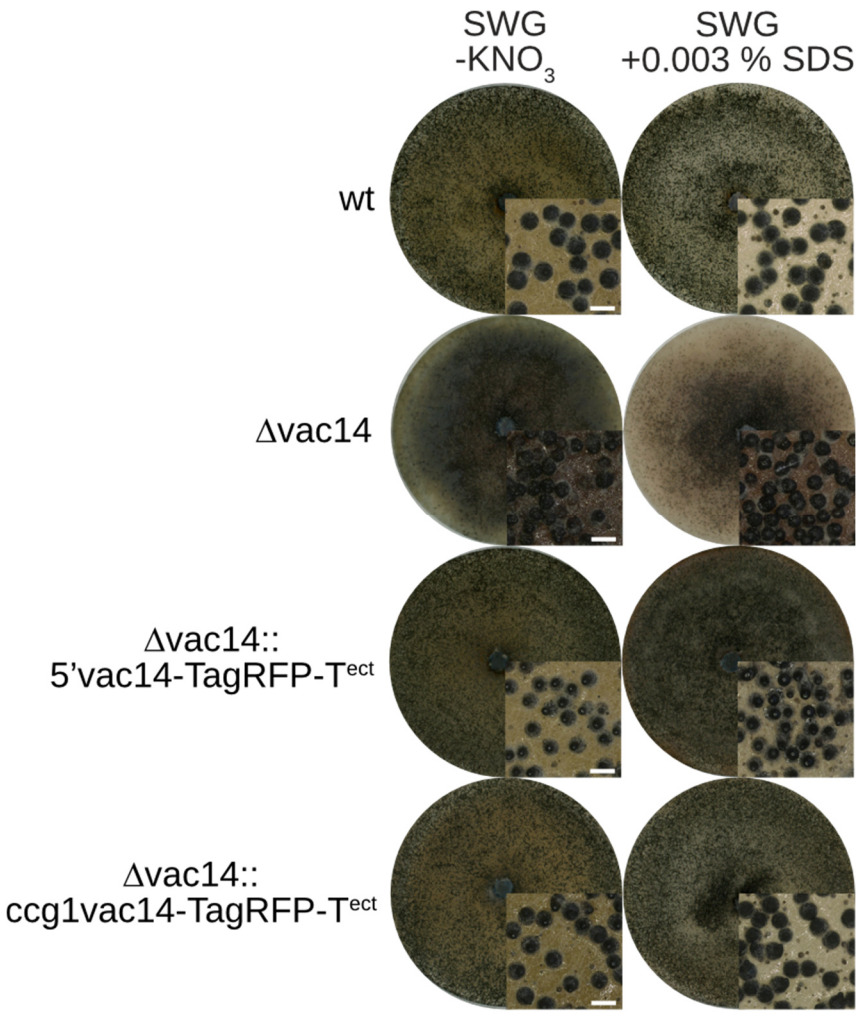

Figure S6: Sexual developmental and growth behavior of *S. macrospora* wt, Δvac14 and the complementation strains Δvac14::5'vac14-TagRFP-T^{ect} and Δvac14::ccg1vac14-TagRFP-T^{ect} on stress media.

Strains were grown on limitation of nitrogen (-KNO_3) and under cell-wall stress conditions (+0.003 % SDS) on SWG medium. Pictures of the agar plates and enlargement of perithecia by microscopic images were taken after 10 days. Scale bar of microscopic images: 0.5 mm.

Supplementary Figure 7

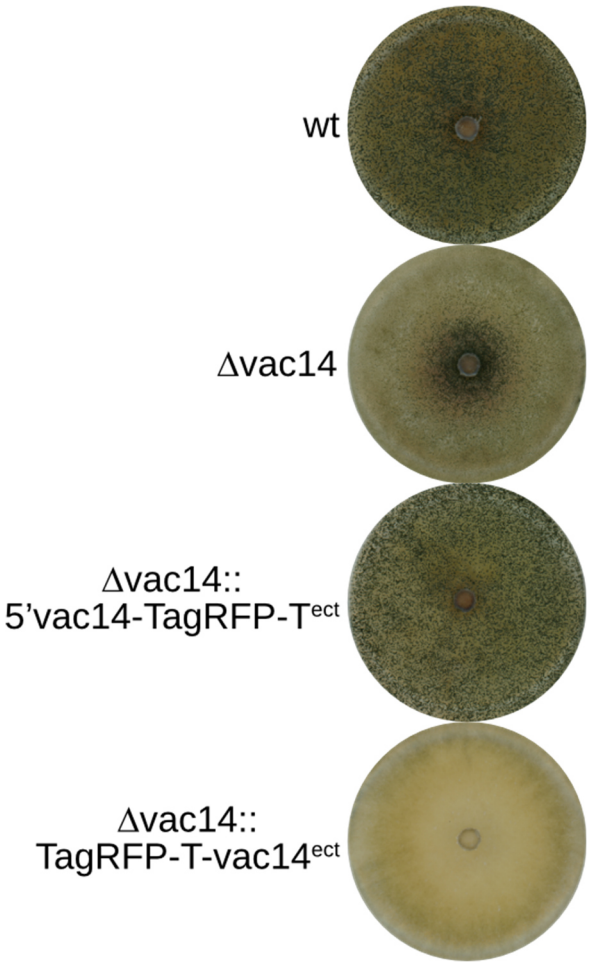

Figure S7: Sexual developmental of S. macrospora wt, Δvac14 and complementation strains. Strains were grown on SWG medium for 7 days at 27 °C under continuous light conditions. The Δvac14 mutant was complemented with SmVAC14 either C-terminally (Δvac14::5′vac14-TagRFP-T^{ect}) or N-terminally (Δvac14::TagRFP-T-vac14^{ect}) fused to TagRFP-T.

Supplementary Figure 8

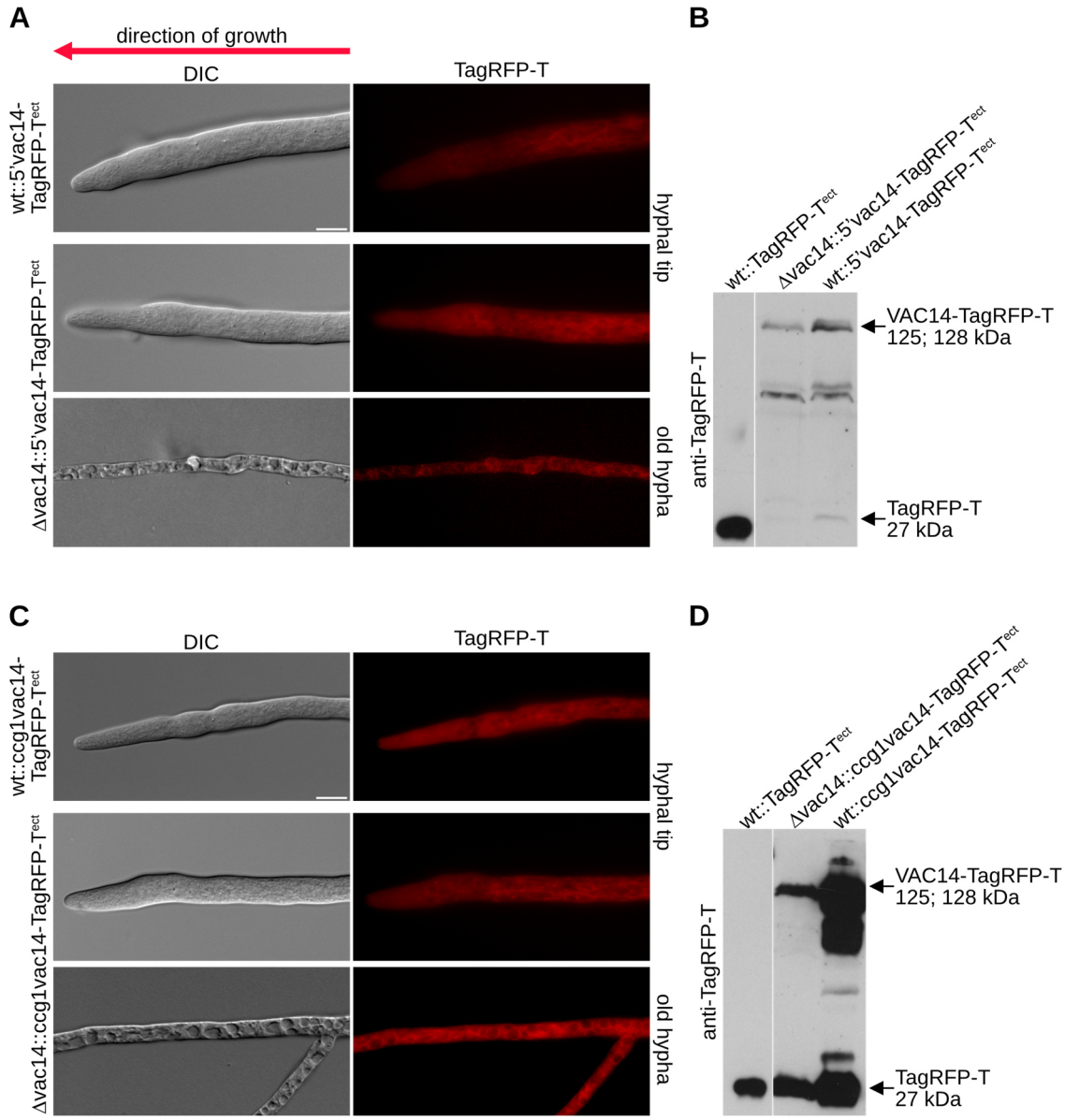

Figure S8: Localization of native and overexpressed VAC14-TagRFP-T in *S. macrospora* wt and Δvac14 strains.

For Fluorescence microscopy, strains were grown on BMM-slides for 24 h or on solid SWG + 1.5 % agarose medium for 24 h at 27 °C under continuous light to visualize young and old hyphae, respectively. **A** Localization of 5'VAC14-TagRFP-T under the control of the endogenous promoter in *S. macrospora* wt and Δvac14. **B** Corresponding Western blot analysis. **C** Localization of overexpressed ccg1VAC14-TagRFP-T, with *vac14* under the control of the overexpression promoter ccg1 of *N. crassa*, in wt and Δvac14 strains. **D** Corresponding Western blot analysis. The wt::TagRFP-T^{ect} strain expressing free TagRFP-T served as control in Western blot experiments. Protein sizes are indicated. Degradation products of the VAC14-fusion protein are visible in **B** and **D**. A putative dimerization band is visible in **D**. Scale bars = 10 µm, DIC: differential interference contrast.

Supplementary Figure 9

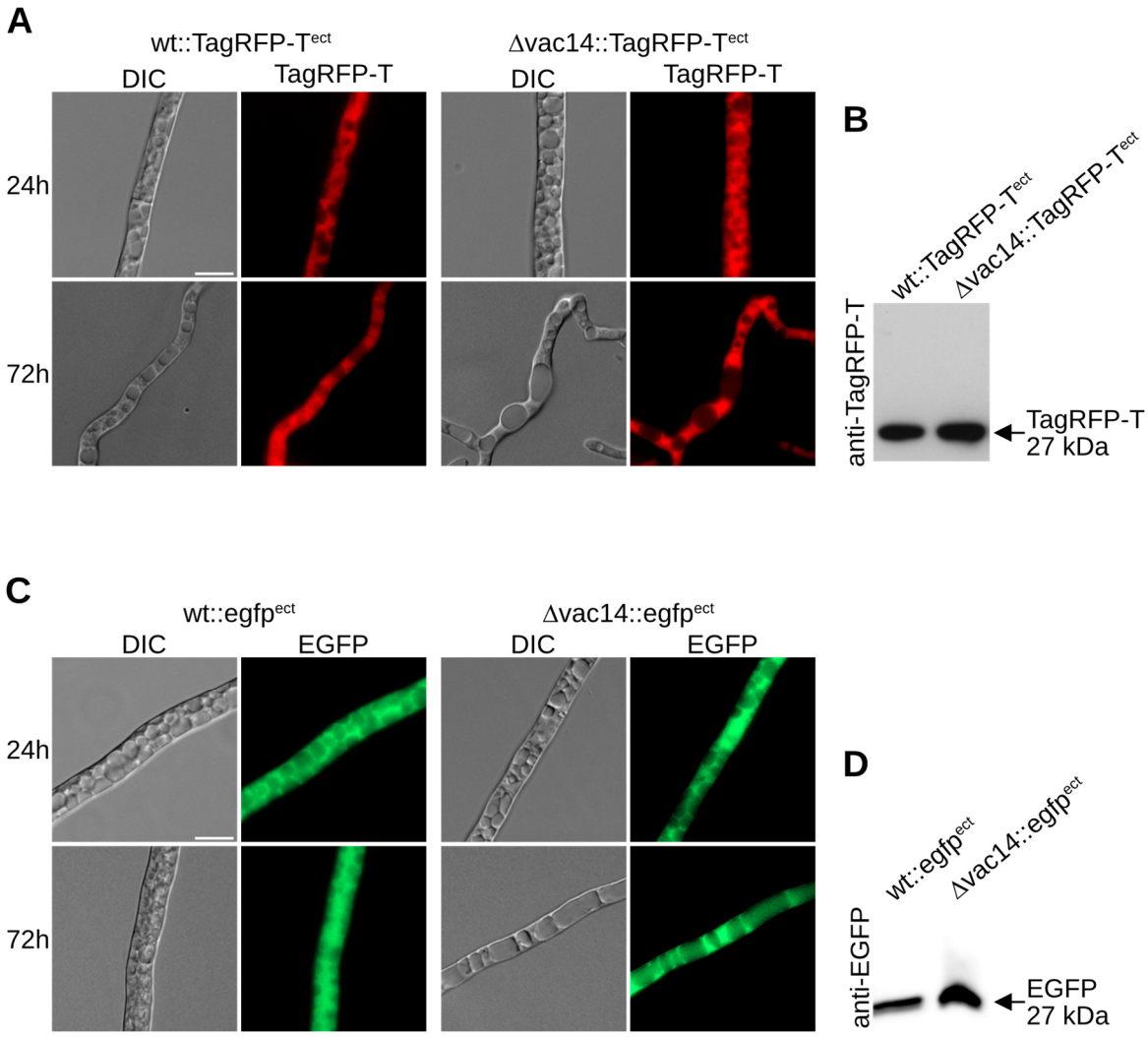

Figure S9: Localization of free TagRFP-T and EGFP in *S. macrospora* wt and Δvac14.
Strains were grown on BMM-slides for 24 h or on SWG + 1.5 % agarose for 72 h at 27 °C under continuous light for fluorescence microscopic analysis. **A** *S. macrospora* wt and Δvac14 carrying pTagRFP-T with *TagRFP-T* under the control of the *N. crassa ccg1* promoter (Werner *et al.*, 2021) and corresponding Western blot analysis (**B**) are shown. **C** *S. macrospora* wt carrying p1783-1 (Pöggeler *et al.*, 2003) and Δvac14 carrying pDS23 (Teichert *et al.*, 2012) with *egfp* under the control of the *A. nidulans gpd* promoter, respectively. Corresponding Western blot experiment is shown in **D**. Protein sizes are indicated. Scale bars = 10 µm, DIC: differential interference contrast.

Supplementary Video 1 and Video 2

Video S1 and S2: Localization of nuclei in growing hyphal tips.
Heterologous expression of pRH2B_nat (Reschka *et al.*, 2018) in *S. macrospora* wt (S1) and Δvac14 (S2) hyphae. Recording of hyphae from growing strains on BMM + agarose medium after incubation for 24 h at 27 °C, recording interval = 5 s, size bar = 20 µm.

References

Andrade, M.A.; Petosa, C.; O'Donoghue, S.I.; Müller, C.W. and Bork, P. (2001) Comparison of ARM and HEAT protein repeats. *J Mol Biol*, 309, 1–18.

Banerjee, S. and Kane, P.M. (2020) Regulation of V-ATPase Activity and Organelle pH by Phosphatidylinositol Phosphate Lipids. *Front Cell Dev Biol*, **8**, 510.

Beier, A.; Teichert, I.; Krisp, C.; Wolters, D.A. and Kück, U. (2016) Catalytic Subunit 1 of Protein Phosphatase 2A Is a Subunit of the STRIPAK Complex and Governs Fungal Sexual Development. *mBio*, **7**, e00870-16.

Bernhards, Y. and Pöggeler, S. (2011) The phocein homologue SmMOB3 is essential for vegetative cell fusion and sexual development in the filamentous ascomycete *Sordaria macrospora*. *Curr Genet*, **57**, 133–149.

Blank-Landeshammer, B.; Teichert, I.; Märker, R.; Nowrousian, M. and Kück, U.; et al. (2019) Combination of Proteogenomics with Peptide De Novo Sequencing Identifies New Genes and Hidden Posttranscriptional Modifications. *mBio*, **10**, 1–17.

Bloemendal, S.; Bernhards, Y.; Bartho, K.; Dettmann, A. and Voigt, O.; et al. (2012) A homologue of the human STRIPAK complex controls sexual development in fungi. *Mol Microbiol*, **84**, 310–323.

Blum, M.; Chang, H.-Y.; Chuguransky, S.; Grego, T. and Kandasaamy, S.; et al. (2021) The InterPro protein families and domains database: 20 years on. *Nucleic Acids Res*, **49**, D344-D354.

Bonangelino, C.J.; Catlett, N.L. and Weisman, L.S. (1997) Vac7p, a novel vacuolar protein, is required for normal vacuole inheritance and morphology. *Mol Cell Biol*, **17**, 6847–6858.

Bonangelino, C.J.; Nau, J.J.; Duex, J.E.; Brinkman, M. and Wurmser, A.E.; et al. (2002) Osmotic stress-induced increase of phosphatidylinositol 3,5-bisphosphate requires Vac14p, an activator of the lipid kinase Fab1p. *J Cell Biol*, **156**, 1015–1028.

Botelho, R.J.; Efe, J.A.; Teis, D. and Emr, S.D. (2008) Assembly of a Fab1 phosphoinositide kinase signaling complex requires the Fig4 phosphoinositide phosphatase. *Mol Biol Cell*, **19**, 4273–4286.

Chow, C.Y.; Landers, J.E.; Bergren, S.K.; Sapp, P.C. and Grant, A.E.; et al. (2009) Deleterious variants of FIG4, a phosphoinositide phosphatase, in patients with ALS. *Am J Hum Genet*, **84**, 85–88.

Chow, C.Y.; Zhang, Y.; Dowling, J.J.; Jin, N. and Adamska, M.; et al. (2007) Mutation of FIG4 causes neurodegeneration in the pale tremor mouse and patients with CMT4J. *Nature*, **448**, 68–72.

Cingolani, G.; Petosa, C.; Weis, K. and Müller, C.W. (1999) Structure of importin-beta bound to the IBB domain of importin-alpha. *Nature*, **399**, 221–229.

Cole, L.; Hyde, G.J. and Ashford, A.E. (1997) Uptake and compartmentalisation of fluorescent probes by *Pisolithus tinctorius* hyphae: evidence for an anion transport

mechanism at the tonoplast but not for fluid-phase endocytosis. *Protoplasma*, **199**, 18–29.

Cole, L.; Orlovich, D.A. and Ashford, A.E. (1998) Structure, function, and motility of vacuoles in filamentous fungi. *Fungal Genet Biol*, **24**, 86–100.

Colot, H.V.; Park, G.; Turner, G.E.; Ringelberg, C. and Crew, C.M.; et al. (2006) A high-throughput gene knockout procedure for Neurospora reveals functions for multiple transcription factors. *Proc Natl Acad Sci USA*, **103**, 10352–10357.

Dahlmann, T.A.; Terfehr, D.; Becker, K. and Teichert, I. (2021) Golden Gate vectors for efficient gene fusion and gene deletion in diverse filamentous fungi. *Curr Genet*, **67**, 317–330.

De Lartigue, J.; Polson, H.; Feldman, M.; Shokat, K. and Tooze, S.A.; et al. (2009) PIKfyve regulation of endosome-linked pathways. *Traffic*, **10**, 883–893.

Dove, S.K.; Cooke, F.T.; Douglas, M.R.; Sayers, L.G. and Parker, P.J.; et al. (1997) Osmotic stress activates phosphatidylinositol-3,5-bisphosphate synthesis. *Nature*, **390**, 187–192.

Dove, S.K.; Dong, K.; Kobayashi, T.; Williams, F.K. and Michell, R.H. (2009) Phosphatidylinositol 3,5-bisphosphate and Fab1p/PIKfyve underPPIn endo-lysosome function. *Biochem J*, **419**, 1–13.

Dove, S.K.; McEwen, R.K.; Mayes, A.; Hughes, D.C. and Beggs, J.D.; et al. (2002) Vac14 Controls PtdIns(3,5)P_2 Synthesis and Fab1-Dependent Protein Trafficking to the Multivesicular Body. *Curr Biol*, **12**, 885–893.

Duex, J.E.; Nau, J.J.; Kauffman, E.J. and Weisman, L.S. (2006a) Phosphoinositide 5-phosphatase Fig 4p is required for both acute rise and subsequent fall in stress-induced phosphatidylinositol 3,5-bisphosphate levels. *Eukaryot Cell*, **5**, 723–731.

Duex, J.E.; Tang, F. and Weisman, L.S. (2006b) The Vac14p-Fig4p complex acts independently of Vac7p and couples PI3,5P2 synthesis and turnover. *J Cell Biol*, **172**, 693–704.

Efe, J.A.; Botelho, R.J. and Emr, S.D. (2005) The Fab1 phosphatidylinositol kinase pathway in the regulation of vacuole morphology. *Curr Opin Cell Biol*, **17**, 402–408.

Efe, J.A.; Botelho, R.J. and Emr, S.D. (2007) Atg18 regulates organelle morphology and Fab1 kinase activity independent of its membrane recruitment by phosphatidylinositol 3,5-bisphosphate. *Mol Biol Cell*, **18**, 4232–4244.

Elleuche, S. and Pöggeler, S. (2009) Evolution of carbonic anhydrases in fungi. *Curr Genet*, **55**, 211–222.

Engh, I.; Nowrousian, M. and Kück, U. (2007) Regulation of melanin biosynthesis via the dihydroxynaphthalene pathway is dependent on sexual development in the ascomycete *Sordaria macrospora*. *FEMS Microbiol Lett*, **275**, 62–70.

Esser, K. (1982) *Cryptogams. Cyanobacteria, Algae, Fungi, Lichens*, CUP Archive.

Esser, K. and Straub, J. (1958) Genetische Untersuchungen an *Sordaria macrospora* Auersw., Kompensation und Induktion bei Genbedingten Entwicklungsdefekten. *Zeitschrift für Vererbungslehre*, **89**, 729–746.

Ferguson, C.J.; Lenk, G.M. and Meisler, M.H. (2009) Defective autophagy in neurons and astrocytes from mice deficient in PI(3,5)P2. *Hum Mol Genet*, **18**, 4868–4878.

Fischer-Parton, S.; Parton, R.M.; Hickey, P.C.; Dijksterhuis, J. and Atkinson, H.A.; et al. (2000) Confocal microscopy of FM4-64 as a tool for analysing endocytosis and vesicle trafficking in living fungal hyphae. *J Microsc*, **198**, 246–259.

Frey, S.; Reschka, E.J. and Pöggeler, S. (2015) Germinal Center Kinases SmKIN3 and SmKIN24 Are Associated with the *Sordaria macrospora* Striatin-Interacting Phosphatase and Kinase (STRIPAK) Complex. *PLoS One*, **10**, e0139163; 1-27.

Gary, J.D.; Sato, T.K.; Stefan, C.J.; Bonangelino, C.J. and Weisman, L.S.; et al. (2002) Regulation of Fab1 phosphatidylinositol 3-phosphate 5-kinase pathway by Vac7 protein and Fig4, a polyphosphoinositide phosphatase family member. *Mol Biol Cell*, **13**, 1238–1251.

Gary, J.D.; Wurmser, A.E.; Bonangelino, C.J.; Weisman, L.S. and Emr, S.D. (1998) Fab1p is essential for PtdIns(3)P 5-kinase activity and the maintenance of vacuolar size and membrane homeostasis. *J Cell Biol*, **143**, 65–79.

Groth, A.; Schmitt, K.; Valerius, O.; Herzog, B. and Pöggeler, S. (2021) Analysis of the Putative Nucleoporin POM33 in the Filamentous Fungus *Sordaria macrospora*. *J Fungi (Basel)*, **682**, 1–23.

Ho, C.Y.; Alghamdi, T.A. and Botelho, R.J. (2012) Phosphatidylinositol-3,5-bisphosphate: no longer the poor PIP2. *Traffic*, **13**, 1–8.

Ho, C.Y.; Choy, C.H.; Wattson, C.A.; Johnson, D.E. and Botelho, R.J. (2015) The Fab1/PIKfyve phosphoinositide phosphate kinase is not necessary to maintain the pH of lysosomes and of the yeast vacuole. *J Biol Chem*, **290**, 9919–9928.

Hwang, J. and Pallas, D.C. (2014) STRIPAK complexes: structure, biological function, and involvement in human diseases. *Int J Biochem Cell Biol*, **47**, 118–148.

Ikonomov, O.C.; Sbrissa, D.; Fenner, H. and Shisheva, A. (2009a) PIKfyve-ArPIKfyve-Sac3 core complex: contact sites and their consequence for Sac3 phosphatase activity and endocytic membrane homeostasis. *J Biol Chem*, **284**, 35794–35806.

Ikonomov, O.C.; Sbrissa, D.; Ijuin, T.; Takenawa, T. and Shisheva, A. (2009b) Sac3 is an insulin-regulated phosphatidylinositol 3,5-bisphosphate phosphatase: gain in insulin responsiveness through Sac3 down-regulation in adipocytes. *J Biol Chem*, **284**, 23961–23971.

Ikonomov, O.C.; Sbrissa, D. and Shisheva, A. (2001) Mammalian cell morphology and endocytic membrane homeostasis require enzymatically active phosphoinositide 5-kinase PIKfyve. *J Biol Chem*, **276**, 26141–26147.

James, P.; Halladay, J. and Craig, E.A. (1996) Genomic libraries and a host strain designed for highly efficient two-hybrid selection in yeast. *Genetics*, **144**, 1425–1436.

Jin, N.; Chow, C.Y.; Liu, L.; Zolov, S.N. and Bronson, R.; et al. (2008) VAC14 nucleates a protein complex essential for the acute interconversion of PI3P and PI(3,5)P(2) in yeast and mouse. *EMBO J*, **27**, 3221–3234.

Jin, N.; Jin, Y. and Weisman, L.S. (2017) Early protection to stress mediated by CDK-dependent PI3,5P2 signaling from the vacuole/lysosome. *J Cell Biol*, **216**, 2075–2090.

Katoh, K.; Rozewicki, J. and Yamada, K.D. (2019) MAFFT online service: multiple sequence alignment, interactive sequence choice and visualization. *Brief Bioinform*, **20**, 1160–1166.

Kilaru, S.; Schuster, M.; Latz, M.; Guo, M. and Steinberg, G. (2015) Fluorescent markers of the endocytic pathway in *Zymoseptoria tritici*. *Fungal Genet Biol*, **79**, 150–157.

Klix, V.; Nowrousian, M.; Ringelberg, C.; Loros, J.J. and Dunlap, J.C.; et al. (2010) Functional characterization of MAT1-1-specific mating-type genes in the homothallic ascomycete *Sordaria macrospora* provides new insights into essential and nonessential sexual regulators. *Eukaryot Cell*, **9**, 894–905.

Kück, U.; Beier, A.M. and Teichert, I. (2016) The composition and function of the striatin-interacting phosphatases and kinases (STRIPAK) complex in fungi. *Fungal Genet Biol*, **90**, 31–38.

Kück, U. and Hoff, B. (2006) Application of the nourseothricin acetyltransferase gene (nat1) as dominant marker for the transformation of filamentous fungi. *Fungal Genet Rep*, **53**, 9–11.

Kück, U.; Pöggeler, S.; Nowrousian, M.; Nolting, N. and Engh, I. (2009) *Sordaria macrospora*, a Model System for Fungal Development. In *Physiology and Genetics (*Anke, T. and Weber, D., eds). The Mycota (A Comprehensive Treatise on Fungi as Experimental Systems for Basic and Applied Research), Springer, Berlin, Heidelberg, Vol. 15, pp. 17–39.

Kück, U.; Radchenko, D. and Teichert, I. (2019) STRIPAK, a highly conserved signaling complex, controls multiple eukaryotic cellular and developmental processes and is linked with human diseases. *Biol Chem*, **400**, 1005–1022.

Lees, J.A.; Li, P.; Kumar, N.; Weisman, L.S. and Reinisch, K.M. (2020) Insights into Lysosomal PI(3,5)P2 Homeostasis from a Structural-Biochemical Analysis of the PIKfyve Lipid Kinase Complex. *Mol Cell*, **80**, 736-743.e4.

Lemaire, J.-F. and McPherson, P.S. (2006) Binding of Vac14 to neuronal nitric oxide synthase: Characterisation of a new internal PDZ-recognition motif. *FEBS Letters*, **580**, 6948–6954.

Li, S.C.; Diakov, T.T.; Xu, T.; Tarsio, M. and Zhu, W.; et al. (2014) The signaling lipid PI(3,5)P_2 stabilizes V_1-V(o) sector interactions and activates the V-ATPase. *Mol Biol Cell*, **25**, 1251–1262.

Lupas, A.; van Dyke, M. and Stock, J. (1991) Predicting coiled coils from protein sequences. *Science*, **252**, 1162–1164.

Malik, H.S.; Eickbush, T.H. and Goldfarb, D.S. (1997) Evolutionary specialization of the nuclear targeting apparatus. *Proc Natl Acad Sci USA*, **94**, 13738–13742.

Märker, R.; Blank-Landeshammer, B.; Beier-Rosberger, A.; Sickmann, A. and Kück, U. (2020) Phosphoproteomic analysis of STRIPAK mutants identifies a conserved serine

phosphorylation site in PAK kinase CLA4 to be important in fungal sexual development and polarized growth. *Mol Microbiol*, **113**, 1053–1069.

Nicholas, K. and Nicholas, H. (1997) GeneDoc: a tool for editing and annotating multiple sequence alignments.

Nicot, A.-S.; Fares, H.; Payrastre, B.; Chisholm, A.D. and Labouesse, M.; et al. (2006) The phosphoinositide kinase PIKfyve/Fab1p regulates terminal lysosome maturation in *Caenorhabditis elegans*. *Mol Biol Cell*, **17**, 3062–3074.

Nowrousian, M.; Ringelberg, C.; Dunlap, J.C.; Loros, J.J. and Kück, U. (2005) Cross-species microarray hybridization to identify developmentally regulated genes in the filamentous fungus *Sordaria macrospora*. *Zeitschrift für Vererbungslehre*, **273**, 137–149.

Nowrousian, M.; Teichert, I.; Masloff, S. and Kück, U. (2012) Whole-Genome Sequencing of *Sordaria macrospora* Mutants Identifies Developmental Genes. *G3 (Bethesda)*, **2**, 261–270.

Peñalva, M.A. (2005) Tracing the endocytic pathway of *Aspergillus nidulans* with FM4-64. *Fungal Genet Biol*, **42**, 963–975.

Pöggeler, S. and Kück, U. (2004) A WD40 repeat protein regulates fungal cell differentiation and can be replaced functionally by the mammalian homologue striatin. *Eukaryot Cell*, **3**, 232–240.

Pöggeler, S. and Kück, U. (2006) Highly efficient generation of signal transduction knockout mutants using a fungal strain deficient in the mammalian ku70 ortholog. *Gene*, **378**, 1–10.

Pöggeler, S.; Masloff, S.; Hoff, B.; Mayrhofer, S. and Kück, U. (2003) Versatile EGFP reporter plasmids for cellular localization of recombinant gene products in filamentous fungi. *Curr Genet*, **43**, 54–61.

Pöggeler, S.; Nowrousian, M. and Kück, U. (2006) Fruiting-Body Development in Ascomycetes. In *Growth, Differentiation and Sexuality* (Kües, U. and Fischer, R., eds). The Mycota (A Comprehensive Treatise on Fungi as Experimental Systems for Basic and Applied Research), Springer, Berlin, Heidelberg, Vol. 1, pp. 325–355.

Qiu, S.; Lavallée-Adam, M. and Côté, M. (2021) Proximity Interactome Map of the Vac14-Fig4 Complex Using BioID. *J Proteome Res*, **20**, 4959–4973.

Reschka, E.J.; Nordzieke, S.; Valerius, O.; Braus, G.H. and Pöggeler, S. (2018) A novel STRIPAK complex component mediates hyphal fusion and fruiting-body development in filamentous fungi. *Mol Microbiol*, **110**, 513–532.

Robinson, O.; Dylus, D. and Dessimoz, C. (2016) Phylo.io: Interactive Viewing and Comparison of Large Phylogenetic Trees on the Web. *Mol Biol Evol*, **33**, 2163–2166.

Rudge, S.A.; Anderson, D.M. and Emr, S.D. (2004) Vacuole size control: regulation of PtdIns(3,5)P2 levels by the vacuole-associated Vac14-Fig4 complex, a PtdIns(3,5)P2-specific phosphatase. *Mol Biol Cell*, **15**, 24–36.

Rusten, T.E.; Rodahl, L.M.W.; Pattni, K.; Englund, C. and Samakovlis, C.; et al. (2006) Fab1 phosphatidylinositol 3-phosphate 5-kinase controls trafficking but not silencing of endocytosed receptors. *Mol Biol Cell*, **17**, 3989–4001.

Rusten, T.E.; Vaccari, T.; Lindmo, K.; Rodahl, L.M.W. and Nezis, I.P.; et al. (2007) ESCRTs and Fab1 regulate distinct steps of autophagy. *Curr Biol*, **17**, 1817–1825.

Rutherford, A.C.; Traer, C.; Wassmer, T.; Pattni, K. and Bujny, M.V.; et al. (2006) The mammalian phosphatidylinositol 3-phosphate 5-kinase (PIKfyve) regulates endosome-to-TGN retrograde transport. *J Cell Sci*, **119**, 3944–3957.

Sambrook, J., Fritsch, E. and Maniatis, T. (2001) *Molecular Cloning: A Laboratory Manual,* Laboratory Press, Cold Spring Harbor, NY, USA.

Sbrissa, D.; Ikonomov, O.C.; Fenner, H. and Shisheva, A. (2008) ArPIKfyve homomeric and heteromeric interactions scaffold PIKfyve and Sac3 in a complex to promote PIKfyve activity and functionality. *J Mol Biol*, **384**, 766–779.

Sbrissa, D.; Ikonomov, O.C.; Fu, Z.; Ijuin, T. and Gruenberg, J.; et al. (2007) Core protein machinery for mammalian phosphatidylinositol 3,5-bisphosphate synthesis and turnover that regulates the progression of endosomal transport. Novel Sac phosphatase joins the ArPIKfyve-PIKfyve complex. *J Biol Chem*, **282**, 23878–23891.

Sbrissa, D.; Ikonomov, O.C.; Strakova, J.; Dondapati, R. and Mlak, K.; et al. (2004) A mammalian ortholog of *Saccharomyces cerevisiae* Vac14 that associates with and up-regulates PIKfyve phosphoinositide 5-kinase activity. *Mol Cell Biol*, **24**, 10437–10447.

Schulze, U.; Vollenbröker, B.; Braun, D.A.; van Le, T. and Granado, D.; et al. (2014) The Vac14-interaction network is linked to regulators of the endolysosomal and autophagic pathway. *Mol Cell Proteomics*, **13**, 1397–1411.

Schulze, U.; Vollenbröker, B.; Kühnl, A.; Granado, D. and Bayraktar, S.; et al. (2017) Cellular vacuolization caused by overexpression of the PIKfyve-binding deficient Vac14L156R is rescued by starvation and inhibition of vacuolar-ATPase. *Biochim Biophys Acta Mol Cell Res*, **1864**, 749–759.

Shi, Z.; Jiao, S. and Zhou, Z. (2016) STRIPAK complexes in cell signaling and cancer. *Oncogene*, **35**, 4549–4557.

Shisheva, A. (2008) PIKfyve: Partners, significance, debates and paradoxes. *Cell Biol Int*, **32**, 591–604.

Stein, V.; Blank-Landeshammer, B.; Müntjes, K.; Märker, R. and Teichert, I.; et al. (2020) The STRIPAK signaling complex regulates dephosphorylation of GUL1, an RNA-binding protein that shuttles on endosomes. *PLoS Genet*, **16**, 1-32.

Teichert, I.; Nowrousian, M.; Pöggeler, S. and Kück, U. (2014) The filamentous fungus *Sordaria macrospora* as a genetic model to study fruiting body development. *Adv Genet*, **87**, 199–244.

Teichert, I.; Pöggeler, S. and Nowrousian, M. (2020) *Sordaria macrospora*: 25 years as a model organism for studying the molecular mechanisms of fruiting body development. *Appl Microbiol Biotechnol*, **104**, 3691–3704.

Teichert, I.; Wolff, G.; Kück, U. and Nowrousian, M. (2012) Combining laser microdissection and RNA-seq to chart the transcriptional landscape of fungal development. *BMC Genomics*, **511**, 1–18.

Towbin, H.; Staehelin, T. and Gordon, J. (1979) Electrophoretic transfer of proteins from polyacrylamide gels to nitrocellulose sheets: procedure and some applications. *Proc Natl Acad Sci USA*, **76**, 4350–4354.

Tusnády, G.E. and Simon, I. (2001) The HMMTOP transmembrane topology prediction server. *Bioinformatics*, **17**, 849–850.

Vicinanza, M.; D'Angelo, G.; Di Campli, A. and Matteis, M.A. de (2008) Function and dysfunction of the PI system in membrane trafficking. *EMBO J*, **27**, 2457–2470.

Voigt, O. and Pöggeler, S. (2013) Autophagy genes Smatg8 and Smatg4 are required for fruiting-body development, vegetative growth and ascospore germination in the filamentous ascomycete *Sordaria macrospora*. *Autophagy*, **9**, 33–49.

Walz, M. and Kück, U. (1995) Transformation of *Sordaria macrospora* to hygromycin B resistance: characterization of transformants by electrophoretic karyotyping and tetrad analysis. *Curr Genet*, **29**, 88–95.

Werner, A.; Herzog, B.; Voigt, O.; Valerius, O. and Braus, G.H.; et al. (2019) NBR1 is involved in selective pexophagy in filamentous ascomycetes and can be functionally replaced by a tagged version of its human homolog. *Autophagy*, **15**, 78–97.

Werner, A.; Otte, K.; Stahlhut, G.; Hanke, L.M. and Pöggeler, S. (2021) The Glyoxysomal Protease LON2 Is Involved in Fruiting-Body Development, Ascosporogenesis and Stress Resistance in *Sordaria macrospora*. *J Fungi (Basel)*, **82**, 1–17.

Wilson, Z.N.; Scott, A.L.; Dowell, R.D. and Odorizzi, G. (2018) PI(3,5)P2 controls vacuole potassium transport to support cellular osmoregulation. *Mol Biol Cell*, **29**, 1718–1731.

Zhang, X.; Chow, C.Y.; Sahenk, Z.; Shy, M.E. and Meisler, M.H.; et al. (2008) Mutation of FIG4 causes a rapidly progressive, asymmetric neuronal degeneration. *Brain*, **131**, 1990–2001.

Zhang, Y.; Zolov, S.N.; Chow, C.Y.; Slutsky, S.G. and Richardson, S.C.; et al. (2007) Loss of Vac14, a regulator of the signaling lipid phosphatidylinositol 3,5-bisphosphate, results in neurodegeneration in mice. *Proc Natl Acad Sci USA*, **104**, 17518–17523.

5. Additional Result: Localization of VAC14 in the Δsci1 Strain

In this chapter, obtained result not included in the manuscript "The Vacuolar Morphology Protein VAC14 Plays an Important Role in Sexual Development in the Filamentous Ascomycete *Sordaria macrospora*" is presented. For the manuscript, we focused on the role of SmVAC14 regarding sexual development and localization without reference to localization in SmSTRIPAK mutants. Therefore, we investigated the localization of SmVAC14 in the Δsci1 deletion mutant via fluorescence microscopy.

Contribution

The additional result was performed by A. Groth.

Result

The Δsci1 strain was transformed with pccg1vac14-TagRFP-T_nat to ectopically express VAC14-TagRFP-T. After incubation of the strain together with the complementation strain vac14::ccg1vac14-TagRFP-T^{ect} for 72 h at 27 °C continuous light, strains were stained with CMAC to visualize acidic vacuoles. In both strains, VAC14-TagRFP-T localizes in a ring-like structure at membranes of the vacuoles. However, the signal of the fluorescently tagged protein also appears in the vacuolar lumen of the complementation strain. Therefore, the overlapping signal of the red fluorescent protein and the blue dye result in a purple signal which can not be observed in the Δsci1 mutant. Here, VAC14-TagRFP-T showed no signal inside vacuoles and was localized more prominently at vacuolar membranes.

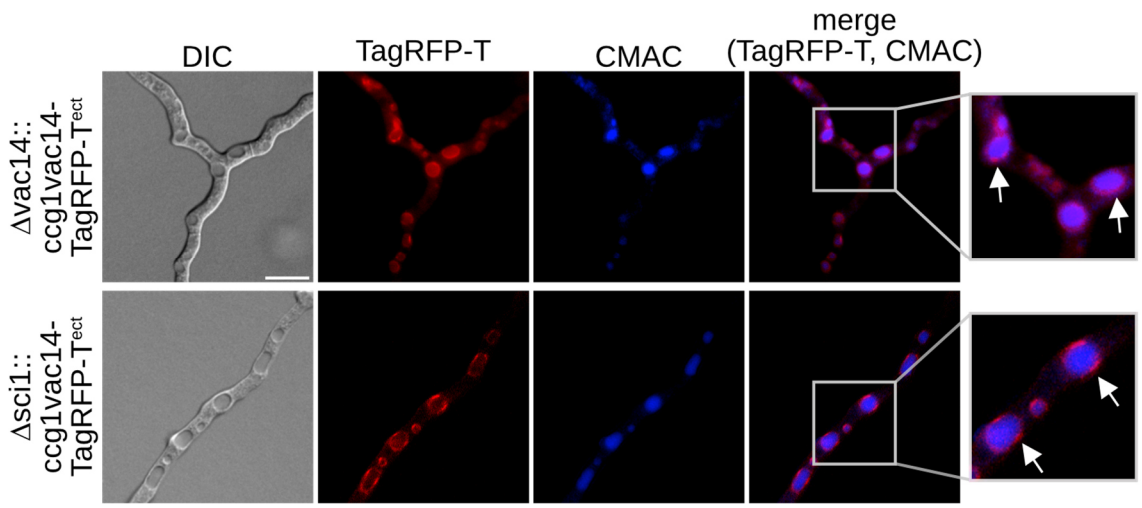

Figure 8: Localization of VAC14-TagRFP-T around vacuoles in Δvac14 and Δsci1.
S. macrospora Δvac14 and Δsci1 strains were transformed to overexpress VAC14-TagRFPT by setting *vac14* under the control of the overexpression promoter ccg1 of the *clock-controlled gene 1* of *N. crassa*. Strains were grown on solid SWG + 1.5 % agarose medium for 72 h under continuous light. Vacuoles of the hyphae were stained with CMAC (1:400 of 10 mM stock solution) and incubated for 30 min at 37 °C. White arrows indicate localization of the fusion protein in a ring-like structure around vacuoles. Scale bars = 10 μm, DIC: differential interference contrast. Detailed two-fold enlargements of the merge pictures are indicated by a grey frame and shown at the right margin.

6. Discussion

In the present thesis, the three proteins ARP1, POM33 and VAC14 of *S. macrospora*, pulled-down with SmSTRIPAK, were analyzed. In the following, the results of the individual proteins are discussed independently. It will begin with ARP1, continue with POM33, and conclude with VAC14. Afterwards, a possible connection of the SmSTRIPAK-complex with these proteins and other proteins pulled-down with SmSTRIPAK functioning in similar pathways is discussed.

6.1 Dynamic localization of ARP1 correlates with active growth of fungal hyphae

In article I, we showed that the dynactin compound ARP1 localizes at distinct sites of germlings and mature hyphae in the ascomycetous fungi *S. macrospora* and *Colletotrichum graminicola*. Fluorescence microscopy of C-terminally fluorescently labeled Arp1 revealed that it localizes dynamically to the subapical part of the hyphal tip (Figure 1 of Article I). Moreover, we provide evidence that the localization of ARP1 correlates with active growth of fungal hyphae (Figure 1 and Figure 2 of Article I). In *A. nidulans*, the dynein-heavy chain (NUDA) fused to GFP was shown to localize similarly at hyphal tips (Xiang *et al.*, 2000). Moreover, it could be shown that this localization pattern was disrupted in the temperature sensitive *A. nidulans* ARP1 mutant *nudK317*. The targeting of GFP-NUDA as comet-like structures to microtubule plus ends required the ARP1 protein NUDK. However, the loss of dynein targeting was discussed to be caused by the impairment of the dynactin-complex functionality rather than being a specific ARP1 effect. Consistent with this assumption, the p150 subunit of the dynactin shoulder domain is unstable when ARP1 is mutated in *N. crassa* (Minke *et al.*, 2000; Xiang *et al.*, 2000). Furthermore, during wound healing mammalian ARP1 is enriched in the leading edge of polar growing cells like axons and moving fibroblasts (Baas and Lin, 2011; Dujardin *et al.*, 2003).

Consequently, the accumulation of ARP1 is related to polarity establishment in these mammalian cells and thus it was proposed that the dynein-dynactin complex is not only a motor on microtubules but also is being involved in the orientation and transport of MTs

(Baas *et al.*, 2006). Moreover, in the unicellular budding yeast ARP1 was identified in yeast-two-hybrid screens to be involved in cell-polarity development (Drees *et al.*, 2001). These finding implement that ARP1 is not only necessary for polarity establishment but may also function in organizing microtubules together with the dynein-complex.

6.2 The dynein-dynactin machinery is involved in microtubule organization

It has been shown that in filamentous fungi, the dynein-dynactin complex is directly involved in organizing the microtubular cytoskeleton by connecting the machinery to hyphal expansion, polar growth and SPK positioning (Riquelme *et al.*, 2000). In our article, we used the dye FM4-64 to demonstrate that ARP1 localizes behind the SPK and seems to be embedded in this VSC (Figure 3 and Figure S6 of Article I). Consistent with this observation is that dynein and dynactin are involved in the retrograde transport of endosomal vesicles from microtubule plus ends at the hyphal apex to subapical nuclei (Lenz *et al.*, 2006; Schuster *et al.*, 2011; Steinberg, 2007). Moreover, dynein mutants of *N. crassa* showed defects in SPK organization and stability (Riquelme *et al.*, 2002). In the maize pathogen *U. maydis*, the organization of microtubules was shown to be a dynein-dependent process (Fink and Steinberg, 2006). Moreover, dynein functions in ER-organization and transport of endosomes in *U. maydis* (Wedlich-Söldner *et al.*, 2002b; Wedlich-Söldner *et al.*, 2002a).

In animal fibroblasts, ARP1 and other components of dynactin were shown to localize at centrosomes, microtubule plus ends and on membranes including endosomes, lysosomes and Gogli vesicles (Clark and Meyer, 1992; Habermann *et al.*, 2001; Schafer and Schroer, 1999; Valetti *et al.*, 1999; Vaughan *et al.*, 1999). Thus, suggesting a role for dynactin in vesicle motility. Moreover, dynactin localizes at SPBs, along microtubules and at chromosome kinetochores in dividing mammalian cells (Pfarr *et al.*, 1990; Steuer *et al.*, 1990).

A recently published study revealed that dynein-dynactin clusters were formed at MT minus ends to reorganize microtubules thus showing the role of the complex-association in mitotic spindle assembly (Tan *et al.*, 2018).

6.3 ARP1 functions in movement of nuclei and retrograde transport of many other diverse cargoes

In our study, we were able to show that the deletion of *Smarp1* also results in drastically reduced and curled hyphal growth (Figure S4 of Article I). In addition, we showed the dynamic association of ARP1 with nuclei in fungal hyphae and germlings (Figure 1 and Figure 4 of Article I).

In fungi, cytoplasmic dynein has many roles including nuclear migration and organelle transport (Xiang and Fischer, 2004; Yamamoto and Hiraoka, 2003). For example, deletion of *N. crassa* heavy chain of cytoplasmic dynein (Ro-1) or the ARP1 homolog Ro-4 resulted in defects of polarized growth, sexual development, and unevenly distributed nuclei along the fungal hyphae. Both *N. crassa* mutants revealed segmented accumulation of nuclei leaving other hyphal segments nuclei free (Plamann *et al.*, 1994). Additionally, mutations in the *S. cerevisiae Act5p* gene defective for nuclear migration proposed a role for Arp1 during mitosis and organelle transport (Muhua *et al.*, 1994).

The mammalian Arp1 was shown to link dynactin to intracellular organelles by associating or directly interacting with spectrin (Holleran *et al.*, 1996; Holleran *et al.*, 2001). Thereby, the dynein-dynactin complex transports many other cargoes on MTs, including nuclei, in an ARP1-dependent manner (Reck-Peterson *et al.*, 2018). The transport is facilitated by various adaptors connecting the dynein-dynactin complex with the cargo and by activating dynein motility. These so-called activating adaptors share the feature of coiled-coil domains. Among them, the Hook homolog proteins 1 and 3 (HOOK1 an HOOK3) binding to Rab5 on early endosomes for their transport (Guo *et al.*, 2016). Besides activating adaptors, other adaptors are known to link dynein-dynactin with cargoes. For example, c-Jun N-terminal kinase-interacting proteins (JIPs) are implicated in autophagosomal transport, co-localize with dynein and dynactin and also contain CC motifs (Cavalli *et al.*, 2005; Fu *et al.*, 2014; Reck-Peterson *et al.*, 2018). Interestingly, JIP3 is not only composed of two short CC stretches but also of a WD40-repeat domain (Reck-Peterson *et al.*, 2018). The presence of these adaptors linking the dynein-dynactin complex to its cargos raises the hypothesis that other proteins with CC motifs and WD40-repeats may act as such adaptors. Since the ARP1 protein was found in *S. macrospora* pulldown

experiments with PRO11 as bait (Reschka *et al.*, 2018), both the WD40-containing PRO11 striatin homolog as well as its interaction partner, the CC protein SCI1, could be considered adaptors for ARP1. To verify this assumption, further studies including direct interaction analysis should be performed.

6.4 SmPOM33 is rather an ER-marker protein than a component of the NPC

In article II, we illustrated that POM33 is rather an ER-marker protein than a component of the NPC. In order to verify the subcellular localization of SmPOM33, fluorescence microscopy was performed using different organelle marker proteins as well as labeled histones (Figure 2 of Article II). For example, the *S. macrospora* homolog of the *N. crassa* SERCA-type Ca^{2+}-ATPase NCA-1, SmNCA1, was used as marker protein for the ER/NE since fluorescently labeled NCA-1-GFP localized to these cellular compartments (Bowman *et al.*, 2009; Monnerjahn *et al.*, 2001). In our study we showed that SmPOM33 co-localizes with SmNCA1 and only partially with the TM-Nup SmPOM152, which was previously used to co-localize SCI1 and PRO11 at the NE (Reschka *et al.*, 2018), suggesting that SmPOM33 is an ER/NE protein, rather than an NPC building block. In *S. cerevisiae*, ScPom33p acts as dynamic TM-Nup because it shuttles between the NPC and the ER with major fractions localizing at the membranes of the NE (Chadrin *et al.*, 2010). However, beyond this localization ScPom33p was shown to be involved in assembly, distribution, and stabilization of NPCs. Interestingly, the ScPom33p paralog, ScPer33p, can associate with NPCs but was mainly localized to the ER and the NE (Floch *et al.*, 2015). The subcellular localization of the mammalian ScPom33p/ScPer33p ortholog, HsTMEM33, was determined at the ER, and demonstrated to be enriched at the NE, lacking the presence at NPCs (Floch *et al.*, 2015; Sakabe *et al.*, 2015). Similarly to HsTMEM33, the *S. pombe* Tts1p was only partially localized to NPCs and mainly enriched at the tubular ER network and the NE (Zhang *et al.*, 2010; Zhang and Oliferenko, 2014).

In addition to localization studies, we performed pulldown experiments coupled to LC-MS analysis to identify potential interaction partners of SmPOM33 to gain more insights in the function of the protein. These experiments confirmed that mainly ER membrane proteins were enriched in SmPOM33 pulldowns (Figure 5 and Table S4 of Article II). In

total, 33 candidates could be identified as putative interactors of SmPOM33. Among them, the ER-shaping and organization component SEY1 and a reticulon-like protein homologous to the *S. cerevisiae* Rtn2p protein were identified with high significance. ER-membrane proteins, like members of the reticulon (RTN) and the DP1/Yop1p family actively shape and stabilize highly curved ER tubules thus maintaining their form and structure (Hu *et al.*, 2008; Oertle *et al.*, 2003; Shibata *et al.*, 2008; Voeltz *et al.*, 2006). In our experiments, we could identify the homolog of the yeast Yop1p, SMAC_06633, but without high significance. RTNs are restricted to the tubular ER network and are absent from ER sheets and peripheral ER in yeast and mammals (Voeltz *et al.*, 2006). Due to the membrane-bending properties of RTNs and DP1/Yop1p, they were proposed to function in *de novo* nuclear-pore formation and NE assembly (Anderson and Hetzer, 2008; Dawson *et al.*, 2009). For example, the mammalian reticulon Rtn4a/NogoA is located to highly curved membrane regions where it maintains formation of ER tubules *in vitro* (Kiseleva *et al.*, 2007) and HsTMEM33 was shown to bind reticulons thus suppressing their membrane-bending activity to regulate the structure of ER tubules (Urade *et al.*, 2014). In *S. pombe*, Tts1p co-localizes and interacts, via its C-terminal α-helix, with Rtn1p and Yop1p at curved ER membranes and the NE to sustain the bended ER domains (Zhang *et al.*, 2010; Zhang and Oliferenko, 2014). Interestingly, α-helices were also predicted for SmPOM33 and in the pulldowns a RTN2 homolog (SMAC_00989) was detected hinting to a possible interaction between the SmPOM33 helices and SmRTN2. In addition, for the dynamin-like GTPase atlastin/Sey1p, cooperation between their TMDs and C-terminal helices to maintain ER morphology has been reported (Hu *et al.*, 2009; Liu *et al.*, 2012; Orso *et al.*, 2009). The homolog of yeast Sey1p, SMAC_08906, was also identified as a potential interactor of SmPOM33, further classifying SmPOM33 as ER protein. Mammalian atlastins are located to the tubular ER network where they interact with proteins shaping the ER tubules (Hu *et al.*, 2009). In *S. cerevisiae*, the functional ortholog of atlastin, Sey1p, interacts with other ER-shaping proteins to mediate the fusion of ER tubules at three-way junctions (Chen *et al.*, 2013; Hu *et al.*, 2009).

In addition to ER-shaping proteins, candidates with functions at the ER have been identified as putative interactors of SmPOM33. For example, SmNCA1 occurred among the best hits hinting to a possible interaction with SmPOM33, which matched their co-

localization. Furthermore, homologs of *S. cerevisiae* proteins involved in tethering cER to the PM to regulate PtdIns(4)P levels were detected. These include *S. macrospora* homologs of tricalbin Tcb3p (SMAC_02980), the phosphatidylinositol-phosphate phosphatase Sac1p (SMAC_01583) and the cER protein Ist2p (SMAC_000943) (Manford *et al.*, 2012). In *S. cerevisiae*, a regulatory connection between ScPer33p and the tricalbin Tcb3p was proposed since they genetically interact with each other (Costanzo *et al.*, 2016). In addition, putative homologs of the Sec61- and Sec63-complex were identified, Sec61p (SMAC_05120) and Sec63p (SMAC_02255), as well as a signal-recognition particle (SRP) receptor beta subunit (SMAC_09603). The interaction of both Sec-complexes mediates SRP-independent protein import into the ER, whereas when acting alone the Sec61-complex is responsible for SRP-dependent import (Deshaies and Schekman, 1987; Plath *et al.*, 2004). In *S. macrospora* homologs of yeast proteins that function in protein O-glycosylation and are putatively located in the ER membrane were enriched in the SmPOM33 pulldown (Gentzsch *et al.*, 1995; Gentzsch and Tanner, 1996; Strahl-Bolsinger *et al.*, 1993). These include the homologs of Pmt1p (SMAC_06805), Pmt2p (SMAC_02375) and Pmt4p (SMAC_08483). Apart from these ER-membrane proteins, a homolog of the *S. cerevisiae* COPII-coated vesicle protein Erv46p (SMAC_04901) was pulled down. COPII-coated vesicles are formed at specialized regions of the smooth tubular ER, known as ER-exit sites (ERES), and mediate the transport from the ER to the Golgi (Watanabe and Riezman, 2004). In addition, several *S. macrospora* homologs of the ergosterol-biosynthetic pathway were enriched.

The results of the performed fluorescence microscopic localization studies in combination with the pulldown experiments coupled to LC-MS analysis indicate that SmPOM33 behaves similarly to the human homolog HsTMEM33 that is also found absent from the NPC and abundant in the ER and NE (Chadrin *et al.*, 2010; Floch *et al.*, 2015). Therefore, it can be concluded that SmPOM33 is an ER/NE protein rather than a component of the NPC. Another indication for this conclusion is that no components of the NPC or any nuclear import factors could be identified in the pulldowns. In yeast, Scpom33p is bound to the NPC by interaction with its C-terminal amphipathic α-helices and the karyopherin Kap123 (Floch *et al.*, 2015). Interestingly, the C-terminal domain of ScPom33p is not highly

conserved in SmPOM33 and therefore no binding site for direct interaction with nuclear import factors is present in SmPOM33.

6.5 *S. macrospora* proper sexual development and stress response is dependent on VAC14

In the manuscript prepared for submission, we focused on the vacuolar morphology protein VAC14. This protein has exclusively been studied in mammalian cells, including mice or human cell lines, and yeast (Jin *et al.*, 2008; Schulze *et al.*, 2014). Here, we highlighted the importance of VAC14 for correct sexual development and stress response in *S. macrospora*. Phenotypic analysis of the Δvac14 mutant strain revealed that deletion of the *Smvac14* gene resulted in reduced formation of mature ascospores and enlarged vacuoles compared to the wt (Figure 2 and Figure 3 of the manuscript). Moreover, the deletion of *Smvac14* caused deformed and less melanized perithecia (Figure 2 of the manuscript). Interestingly, a similar pigmentation-deficient phenotype was observed in Vac14 mice mutants. More precisely, a point mutant, $Vac14^{L156R}$, that is unable to bind the kinase PIKfyve, was shown to induce the infantile gliosis (*ingls*) phenotype that is characterized by small size and less pigmented coat color (Jin *et al.*, 2008).

Moreover, we showed that the Δvac14 mutant strain is more sensitive to hyperosmotic stress (0.4 M sorbitol and 0.1 M NaCl) and amino-acid starvation (2.5 mM 3-AT) (Figure 4 of the manuscript) than the wt. Under these conditions, perithecia formation was restricted to a small area around the agar-piece and the Δvac14 deletion strain showed significantly slower growth rates. In *Arabidopsis thaliana*, the VAC14 protein mediates vacuolar organization and is thus critical for pollen development (Zhang *et al.*, 2018). An increased sensitivity against hyperosmotic stress has also been described in yeast. Here, individual mutants of the Fab1p-complex components, Δfab1, Δfig4 and Δvac14, respond to hyperosmotic stress by a short increase of PtdIns(3,5)P_2 levels that returned to its native state within few minutes after shocking the cells (Bonangelino *et al.*, 2002; Dove *et al.*, 1997; Duex *et al.*, 2006b). The increase of PtdIns(3,5)P_2 during stress conditions was shown to require Vac14p which is therefore known as osmoregulator of the Fab1p activity (Bonangelino *et al.*, 2002). PtdIns(3,5)P_2 in turn plays a major role in osmotic stress response by regulating the vacuolar morphology (Bonangelino *et al.*, 2002). Interestingly,

in mammalian podocytes, amino-acid starvation was shown to rescue the hyper-vacuolization phenotype of $Vac14^{L156R}$ overexpression mutant cells, indicating that autophagy might be affected (Schulze *et al.*, 2017). Together with our observations in *S. macrospora*, it can be concluded, that the VAC14-dependent osmotic regulation of PtdIns(3,5)P_2 levels might be important for stress response and thus proper development in eukaryotes.

6.6 SmVAC14 is important for controlling vacuolar and endosomal morphology but not autophagy

Besides the Δvac14 impairments in sexual development, FM4-64 and CMAC staining illustrated that the Δvac14 mutant strain is characterized by enlarged and visually poorly acidified vacuolar compartments (Figure 3A and Figure 3B of the manuscript). Interestingly, an altered vacuolar phenotype had been described previously for Δsci1 showing vacuoles already present in young hyphae (Reschka *et al.*, 2018). Our studies revealed that enlarged vacuoles also appear in young growing hyphal tips of *S. macrospora* Δvac14 strains (Figure 3C of the manuscript). Moreover, VAC14 was identified as potential interactor of SCI1 in recently performed pulldown experiments (Reschka *et al.*, 2018). In our study we showed that VAC14 could be co-localized with SCI1 in fluorescence microscopy (Figure 5 of the manuscript). These similar characteristics of both strains and same localizations of the proteins hint to a possible connection of components of both multiprotein complexes, SmSTRIPAK and the SmFAB1-complex, in *S. macrospora*.

Fluorescence microscopic investigation of *S. macrospora* strains revealed a co-localization of VAC14 with the early and late endosomal marker proteins RAB5 and RAB7, respectively (Figure 5 of the manuscript). Therefore, irregular enlarged structures might be the result of fusions of vacuoles and endolysosomes in the *S. macrospora* Δvac14 mutant. To determine if the subcellular localization of early and late endosomes is altered in Δvac14 compared to the wt, we performed fluorescence microscopy of the fluorescently tagged EE and LE markers RAB5 and RAB7, respectively (Figure 6 of the manuscript). RAB5 localized already after 24 h in large vacuoles in Δvac14, whereas after 72 h in the wt. This observation hints to a faster degradation of early endosomes into vacuoles when *Smvac14* is deleted. On the other hand, the late endosomal marker RAB7 localized in

deformed mixed structures of vacuoles and endosomes after 24 h and as a ring-like structure at vacuolar membranes after 72 h in Δvac14. Contrary to early endosomes, late endosomes seem to accumulate at vacuolar membranes in *Smvac14* deletion strains. Notably, RAB7 localized also to bigger and irregular vacuoles in the Δsci1 deletion background. These observations give another hint for the SmSTRIPAK and the SmFAB1-complex being somehow involved in similar cellular pathways such as endosome trafficking. Additionally, SmSTRIPAK mutants were used in recently performed global phosphoproteomic study which revealed that SmVAC14 is differentially phosphorylated at T455 and S429 in SmSTRIPAK mutants (Märker *et al.*, 2020; Stein *et al.*, 2020). This suggests another connection between the scaffolding protein SmVAC14 and the SmSTRIPAK-complex. Furthermore, recent studies showed that inhibition of mammalian PIKfyve with its potent and selective inhibitor YM201636 results in the accumulation of late endosomal compartments (Jefferies *et al.*, 2008). Taken together, the *S. macrospora* homolog of the Fab1p/PIKfyve-complex has an impact on the endosomal pathway and is possibly connected with the SmSTRIPAK-complex.

The results of our fluorescent microscopic studies of SmVAC14 are consistent with those made in yeast an mammals, where Vac14p/ArPIKfyve was shown to localize to vacuolar membranes and endolysosomes, respectively (Bonangelino *et al.*, 2002; Dove *et al.*, 2002; Jin *et al.*, 2008). Moreover, dilated vacuoles and lysosomes were also described for deletions of *fab1* and *vac14* in yeast and mammals (Gary *et al.*, 1998; Ikonomov *et al.*, 2001). In human cell lines and podocytes, swollen vacuoles upon $Vac14^{L156R}$ or $Vac14^{wt}$ overexpression were marked with the late endosomal marker proteins Rab7, CD63, and Lamp2 (Schulze *et al.*, 2014; Schulze *et al.*, 2017). Therefore, Schulze and co-workers proposed that the vacuolization is based on a defect in trafficking from endosomes to the vacuole/lysosome. On the other hand, subunits of the vacuolar proton pump V-ATPase were identified as Vac14 interaction partners, proposing the theory that the vacuolization phenotype is pH dependent (Schulze *et al.*, 2014). In our studies, we visualized vacuoles of *S. macrospora* hyphae with the blue dye CMAC and observed a weaker staining of Δvac14 vacuoles compared to the wt (Figure 3B of the manuscript). Therefore, we assumed that the deletion of *Smvac14* caused less acidified vacuolar compartments. Interestingly, poorly acidified vacuoles and lysosomes of yeast and mammals were described for Δfab1

and Δvac14 deletion mutants accompanied by lower levels of PtdIns(3,5)P_2 (Gary *et al.*, 1998; Ikonomov *et al.*, 2001; Rusten *et al.*, 2006). In his context, is was assumed that PtdIns(3,5)P_2 is required to sustain the acidic lumen of the vacuole and, to an as yet unclear extent of lysosomes (Ho *et al.*, 2015). However, these observations were made based on qualitative analyses with acidotrophic dyes. Accordingly, Ho and co-workers performed assays to quantitatively measure the pH of vacuoles and lysosomes. Whit this, they showed that yeast vacuoles of Δfab1 and Δvac14 deletion mutants as well as lysosomes of PIKfyve-inhibited cells remain as acidic as wt cells. Moreover, PtdIns(3,5)P_2 was proposed to maintain the vacuolar pH during salt stress. Interestingly, in this context PtdIns(3,5)P_2 was shown to activate the V-ATPase hinting to a connection between this signaling lipid and vacuolar proton pumps (Li *et al.*, 2014). However, PtdIns(3,5)P_2 might control the activity of the V-ATPase rather in response to salt stress than under steady-state conditions (Li *et al.*, 2014). In this regard, vacuolization of $Vac14^{L156R}$ overexpressing podocytes and mammalian cells that were treated with the PIKfyve-inhibitor YM201636, could be rescued by treatment with the V-ATPase inhibitor Bafilomycin A (Compton *et al.*, 2016; Schulze *et al.*, 2017). Since Δfab1 and Δvac14 deletions show no acidification defects in yeast, but lower levels of PtdIns(3,5)P_2 are associated with lower V-ATPase activity, the hypothesis arose that another regulator might be present at the vacuolar membrane that regulate the luminal pH (Banerjee and Kane, 2020; Ho *et al.*, 2015; Li *et al.*, 2014). In plants, V-ATPase activity is not increased by PtdIns(3,5)P_2. Here, PtdIns(3,5)P_2 rather decreases the H^+-efflux from the vacuole by acting as negative regulator of CLC-a, an H^+-exchanger (Banerjee and Kane, 2020; Carpaneto *et al.*, 2017). These studies indicate a connection of PtdIns(3,5)P_2 with vacuolar acidification in a V-ATPase-dependent manner. However, it is not clear if in a parallel or anti-parallel way. In his context, it should be noted that using fluorescence microscopy we could co-localize VAC14 with the V-ATPase catalytic subunit A, VMA1 (Figure 2 of the manuscript). Therefore, a possible interaction of both proteins or components of their corresponding complexes cannot be excluded for *S. macrospora*. In mammalian endolysosomes, PtdIns(3,5)P_2 was shown to activate transient receptor potential of Ca^{2+}-channels of the mucolipin subfamily (TRPML) (Dong *et al.*, 2010). In this context, the authors analyzed the yeast TRPML1 homolog Yvc1p and showed that Ca^{2+}-release from the vacuole was reduced in Δfab1, Δvac7, Δfig4 and

Δvac14 yeast mutants correlating with lower levels of PtdIns(3,5)P_2. Since Ca^{2+} is a key transmitter in vesicle fusion, loss of PtdIns(3,5)P_2 thus loss of Ca^{2+}-release might explain the fusion defects of vacuolar and endolysosomal structures in Fab1p/PIKfyve-complex mutant strains. The exact correlation of PtdIns(3,5)P_2 in association with pH and ion channel regulation needs to be further analyzed. However, it can be stated that the vacuolar and endolysosomal enlargements are a result of disturbed osmotic regulation (Banerjee and Kane, 2020; Wilson *et al.*, 2018).

Interestingly, besides subunits of the V-ATPase, proteins of the endolysosomal and autophagic pathway were identified as mammalian Vac14 interactors including the late endosomal protein Rab9, the Rab7 activator TBC1D15 that binds to LC3/Atg8 protein family members and the Rab5-interacting protein Sun2 (Schulze *et al.*, 2014; Schulze *et al.*, 2017). These analyses link the mammalian Vac14 protein to the endosomal and autophagic pathways. Therefore, and together with the strong Δvac14 phenotype under amino-acid starvation, we analyzed if autophagy might be affected by deletion of *Smvac14*. For this, localization of the autophagic marker proteins SmATG8 and SmNBR1 were analyzed in the Δvac14 strain using fluorescence microscopy (Figure 7C-E of the manuscript). However, our analyses revealed that the subcellular localization of NBR1 and ATG8 in vacuoles and autophagosomes and their degradation is not altered compared to the wt. In contrast, the autophagosomal marker proteins LC3 and p62 accumulated in mammalian $Vac14^{wt}$ and $Vac14^{L156R}$ overexpressing cells and accumulation of autophagosomes was also detected in *vac14* deletion mutants of *ingls* mice, *D. melanogaster* and *C. elegans* (De Lartigue *et al.*, 2009; Ferguson *et al.*, 2009; Ho *et al.*, 2012; Nicot *et al.*, 2006; Rusten *et al.*, 2007). However, in $Vac14^{wt}$ and $Vac14^{L156R}$ overexpressing cells, LC3 was not present at the membranes of enlarged vacuoles and the autophagic flux was also not impaired suggesting that the observed accumulation is an indirect effect due to dysfunctional maturation of endosomes (Schulze *et al.*, 2014; Schulze *et al.*, 2017).

In conclusion, SmVAC14 is important for *S. macrospora* sexual development, stress resistance, and vacuolar as well as endosomal morphology. The link of the SmVAC14 impact on the vacuolar and endosomal pH and associated levels of PtdIns(3,5)P_2, as well as potential interplay of SmVAC14 and the SmSTRIPAK-complex need to be evaluated though.

6.7 Indications of possible connections of the SmSTRIPAK-complex with other multiprotein complexes

In the present thesis, the *S. macrospora* proteins ARP1, POM33, and VAC14 were analyzed. They are all components of large individual multiprotein complexes and were enriched using the SmSTRIPAK-components PRO11 or SCI1 in pulldown experiments as baits. All of these complexes function in different cellular signaling pathways within the cell. It is therefore reasonable to assume that the SmSTRIPAK-complex is highly dynamic and plays a crucial role in various signaling pathways by probably cooperating with multiprotein complexes or possibly regulating their function by phosphorylation and de-phosphorylation of individual components of the complexes. However, further analyses and experiments are required to clarify this suggested link. In Figure 7, a schematic overview of the localizations of the addressed complexes in *S. macrospora* hyphae together with the potential localization of the SmSTRIPAK is given.

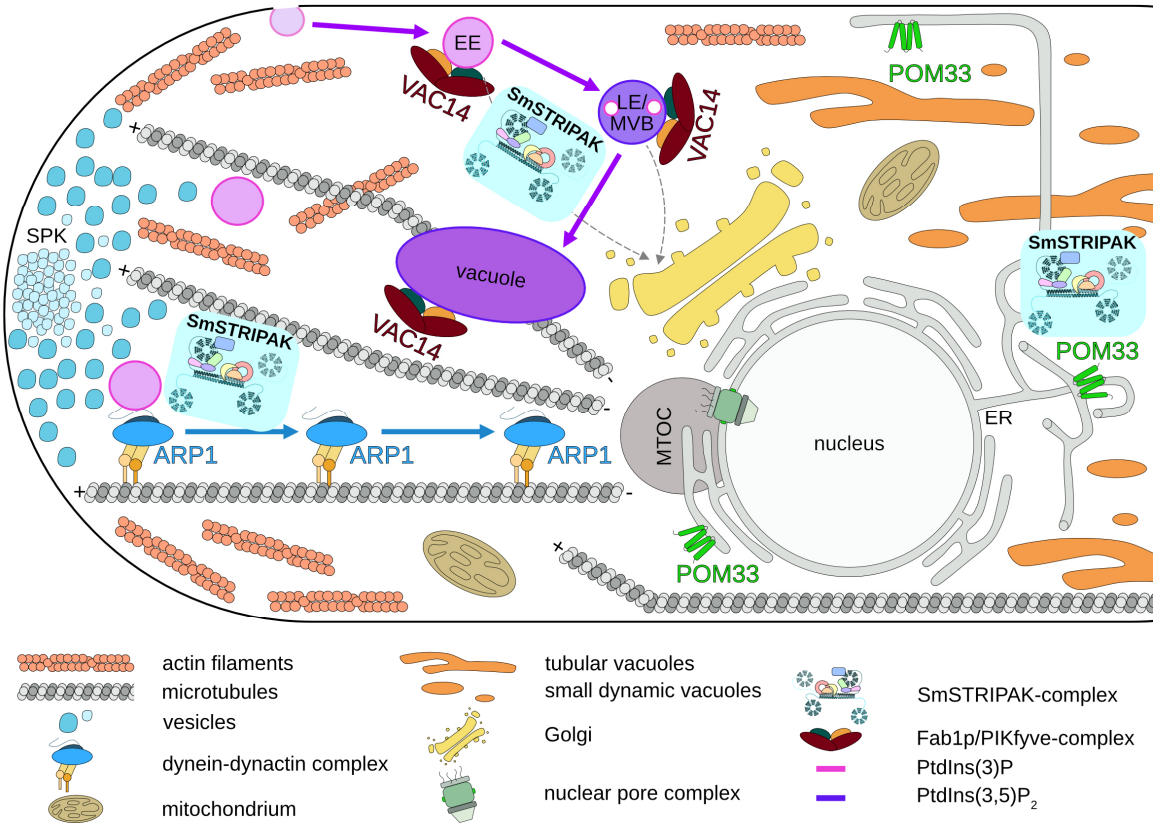

Figure 7: Schematic overview of multiprotein complexes in *S. macrospora* hyphae.
Shown is a model of *S. macrospora* hypha with accumulated vesicles at the Spitzenkörper (SPK) near the tip, several organelles, the location of the analyzed components (ARP1, POM33 and VAC14)

together with their individual multiprotein complexes, and the potential localization of the SmSTRIPAK-complex. In pulldown experiments with SCI1 as bait, POM33 (green) was identified, which localizes to the endoplasmic reticulum (ER). Also pulled down with SCI1 was VAC14 (dark red), which is a component of the Fab1p/PIKfyve-complex. This localizes to early endosomes (EE), late endosomes (LE) or multivesicular bodies (MVBs), which are transported to lysosomes or vacuoles for degradation (endocytic pathway is indicated by purple arrows). ARP1 (blue) is part of the dynein-dynactin complex and was pulled-down with PRO11. This complex mediates retrograde transport (indicated with a blue arrow) of various cargos on microtubules originating from the microtubule organizing center (MTOC) near the nucleus.

In the previously performed SmSTRIPAK-pulldown experiments coupled to LC-MS analysis with either PRO11, SCI1 or SmMOB3 as bait, several proteins were enriched pointing out that the SmSTRIPAK-complex might be a highly dynamic signaling structure within hyphae (Reschka *et al.*, 2018). Among these candidates, proteins were found that are connected with long-distance vesicle transport along microtubules or actin filaments. Besides ARP1, a putative MT motor protein of the kinesin superfamily, KIF4-like protein (SMAC_04212), was identified. Kinesins were shown to be involved in intracellular organelle transport and play further roles in chromosome aggregation, spindle assembly, as well as cell division and -motility (Hirokawa, 1998; Miki *et al.*, 2005; Sheng *et al.*, 2018; Vale and Milligan, 2000). KIF4 is highly conserved among eukaryotes and functions in cell division by interacting with chromatin during mitosis and is therefore known as chromokinesin (Almeida and Maiato, 2018). It interacts with DNA and aligns chromosomes to maintain their structure throughout the cell cycle (Almeida and Maiato, 2018; Sheng *et al.*, 2018). Furthermore, another protein involved in intracellular transport was enriched in the PRO11 and SmMOB3 pulldowns, namely a putative myosin-5 (SMAC_05008). Myosin-5 is a conserved member of the myosin family of molecular motors that transport cargoes moving towards the plus ends of actin filaments via ATP-hydrolysis (Mehta *et al.*, 1999; Reck-Peterson *et al.*, 2000). In addition to the molecular motors, kinesin KIF4 and myosin-5, and the dynactin-component ARP1, the dynein-heavy chain (DHC) (SMAC_00761) was identified using SCI1 as bait protein. DHC is the major core of cytoplasmic dynein, a large multisubunit-motor complex. Together with dynactin, the dynein-dynactin complex is formed that facilitates long-distance transport of diverse cargoes on microtubules (Figure 4 of the introduction) (Reck-Peterson *et al.*, 2018). Due to the fact that diverse motor proteins or components of such complexes have been pulled-

down with SmSTRIPAK-components, it can be assumed that this complex is associated with cellular transport and hyphal growth. However, additional experiments should be performed to determine the exact connection of SmSTRIPAK and motor proteins.

In addition to the pulldowns, Reschka *et al.* (2018) used fluorescence microscopy to reveal that SCI1 and PRO11 were co-localized around the nucleus. Furthermore, the SmSTRIPAK-components SmMOB3 and the SLMAP homolog PRO45 were localized to the NE, ER, and mitochondria (Nordzieke *et al.*, 2015). Therefore, the question arose which proteins are responsible for anchoring the SmSTRIPAK to the NE. To address this, we investigated the pulled-down potential nucleoporin POM33 in this thesis. However, this protein is not the only one identified that can be associated with nuclear-anchoring of the SmSTRIPAK. Another pulled-down candidate to potentially fulfill this function was the putative nucleoporin-interacting protein of 96 kDa (NIC96; SMAC_02409) (Reschka *et al.*, 2018). As shown in Figure 5 of the introduction, yeast Nic96p is a major component of NPCs. It contributes to the formation of nuclear pores, the biogenesis of NPCs, and is involved in nucleocytoplasmic transport by forming stable associations with FG-Nups (Alber *et al.*, 2007; Grandi *et al.*, 1993; Grandi *et al.*, 1995; Zabel *et al.*, 1996). Due to the fact that the *S. macrospora* NIC96 protein was enriched in pulldowns using PRO11 as well as SmMOB3 as bait, makes it a promising candidate as potential interactor at the NE. However, NIC96 might be an essential protein so deletion of *nic96* would be lethal and thus knockout strains will be impossible to generate.

Furthermore, using SCI1 as bait, another protein was enriched that might also affect vacuolar morphology and is distinct from VAC14 (Reschka *et al.*, 2018). The putative *S. macrospora* homolog of a yeast phosphatidylinositol 4-kinase Stt4p, SMAC_04234, was identified as potential interaction partner of SCI1. In yeast, Stt4p is required for cell wall integrity, organization of the actin cytoskeleton, normal vacuole morphology, and fusion of autophagosomes with vacuoles during autophagy (Audhya *et al.*, 2000; Kurokawa *et al.*, 2019). Moreover, an Arf-like protein (SMAC_04918) was identified in the PRO11 pulldown. In mammals, ADP ribosylation factors (ARFs) are members of Ras-GTPases regulating vesicular traffic and functioning in actin remodeling (Donaldson and Honda, 2005). On the other hand, members of the related ARF-like (ARL) GTPases were shown to play roles in β-tubulin folding, tethering of endosome-derived vesicles at the TGN, and

are localized at diverse sites of the cell including the cytosol, nucleus, mitochondria and the cytoskeleton (Burd *et al.*, 2004; Panic *et al.*, 2003). Interestingly, the Arl1 protein was also identified as potential interactor of Vac14 in human cell lines (Schulze *et al.*, 2014). In this context, Arf1 involved in the COPI-assembly was found in proximity to human Vac14 using proximity-dependent biotin identification (BioID) experiments and both proteins were validated to interact with each other (Qiu *et al.*, 2021). The fact that homologs of these proteins have been pulled-down with SmSTRIPAK suggests that SmSTRIPAK might regulate vesicle transport and fusion events in hyphae. To verify this, direct interaction studies of the referred proteins with SmSTRIPAK-components should be performed. This would provide further insights into potential interaction partners and the diverse functions of the SmSTRIPAK-complex.

Concluding remarks

The aim of this thesis was to give insights into individual proteins from the filamentous ascomycete *S. macrospora* that were pulled-down with SmSTRIPAK. These include the cytoskeletal protein ARP1, the putative nucleoporin POM33, and the vacuolar protein VAC14. They are all components of individual multiprotein complexes, which are involved in different signaling pathways and localize to distinct sites in the cell. In order to determine their functions and localizations in *S. macrospora*, different molecular methods were applied.

Fluorescence microscopic analyses showed that ARP1 localizes at hyphal tips subapical to the SPK and in close proximity to nuclei. Its localization is therefore a dynamic process. With respect to POM33, the same method demonstrated that this putative nucleoporin co-localizes with proteins of the ER as well as around the nucleus in *S. macrospora*. Furthermore, pulldown experiments following LC-MS analysis showed that mainly ER proteins could be enriched with SmPOM33. Also by fluorescence microscopy, VAC14 was shown to localize to the membranes of vacuoles and endosomes. Furthermore, this protein also co-localizes with vacuolar membrane proteins and the SmSTRIPAK-component SCI1. Phenotypic analyses of knockout mutants showed that ARP1 is required for correct hyphal growth and development in *S. macrospora*. For the knockout of *pom33*, however, no developmental defect could be detected even under various stress conditions. On the contrary, analysis of VAC14 showed that this protein is required for the normal morphology of vacuoles and endolysosomes. In addition, VAC14 plays a crucial role in the proper development of fruiting bodies and in hyphal growth. Further experiments revealed that VAC14 is also important for the stress response during hyperosmotic chock and amino-acid deficiency. With the results obtained, ARP1 could be successfully established as a marker for hyphal growth and polarity establishment in filamentous fungi. Future research could benefit from this by using this marker to study the event of hyphal fusion in more detail or even apply it in other organisms. With the results gained from the analysis of POM33, this protein could be classified as an ER and NE resident, rather than being a component of the NPC. This findings are more consistent with the analyses of human HsTMEM33 and are different from analysis of yeast Scpom33p.

Therefore, the analysis of *S. macrospora* POM33 contributes to a better understanding of this ER/NE protein in fungi. However, further studies are required to clarify the POM33 function in more detail. These should for example include interaction studies with individual candidates from the LC-MS analysis as well as high-resolution microscopy procedures. The analysis of VAC14 showed that this protein is important for the morphology of cell organelles such as the vacuole or the endolysosomes. Furthermore, it plays an important role in the proper sexual development of *S. macrospora*. Since VAC14 and the components of its associated complex have so far only been investigated in mammals and yeasts, the results of this work can serve as basis for analyses of the link between vacuolar morphology and developmental processes in filamentous fungi.

The pulled-down proteins analyzed in this work suggest a link of the SmSTRIPAK-complex to various signaling pathways at distinct sites within the cell. Accordingly, the SmSTRIPAK is a dynamic multiprotein complex that may cooperate with other multiprotein complexes or even regulate their functions. However, the precise mode in which this is accomplished has yet to be clarified.

References

Alber, F.; Dokudovskaya, S.; Veenhoff, L.M.; Zhang, W. and Kipper, J.; et al. (2007) The molecular architecture of the nuclear pore complex. *Nature*, **450**, 695–701.

Alberts, B. (2008) *Molecular biology of the cell.* 5th ed., Garland Science, NY.

Almeida, A.C. and Maiato, H. (2018) Chromokinesins. *Curr Biol*, **28**, R1131-R1135.

Anderson, D.J. and Hetzer, M.W. (2008) Reshaping of the endoplasmic reticulum limits the rate for nuclear envelope formation. *J Cell Biol*, **182**, 911–924.

Andrade, M.A.; Petosa, C.; O'Donoghue, S.I.; Müller, C.W. and Bork, P. (2001) Comparison of ARM and HEAT protein repeats. *J Mol Biol*, **309**, 1–18.

Antonin, W.; Ellenberg, J. and Dultz, E. (2008) Nuclear pore complex assembly through the cell cycle: regulation and membrane organization. *FEBS Letters*, **582**, 2004–2016.

Audhya, A.; Foti, M. and Emr, S.D. (2000) Distinct roles for the yeast phosphatidylinositol 4-kinases, Stt4p and Pik1p, in secretion, cell growth, and organelle membrane dynamics. *Mol Biol Cell*, **11**, 2673–2689.

Baas, P.W. and Lin, S. (2011) Hooks and comets: The story of microtubule polarity orientation in the neuron. *Dev Neurobiol*, **71**, 403–418.

Baas, P.W.; Vidya Nadar, C. and Myers, K.A. (2006) Axonal transport of microtubules: the long and short of it. *Traffic*, **7**, 490–498.

Backer, J.M. (2008) The regulation and function of Class III PI3Ks: novel roles for Vps34. *Biochem J*, **410**, 1–17.

Bai, S.W.; Herrera-Abreu, M.T.; Rohn, J.L.; Racine, V. and Tajadura, V.; et al. (2011) Identification and characterization of a set of conserved and new regulators of cytoskeletal organization, cell morphology and migration. *BMC Biol*, **9**, 1–18.

Baillat, G.; Gaillard, S.; Castets, F. and Monneron, A. (2002) Interactions of phocein with nucleoside-diphosphate kinase, Eps15, and Dynamin I. *J Biol Chem*, **277**, 18961–18966.

Baillat, G.; Moqrich, A.; Castets, F.; Baude, A. and Bailly, Y.; et al. (2001) Molecular cloning and characterization of phocein, a protein found from the Golgi complex to dendritic spines. *Mol Biol Cell*, **12**, 663–673.

Banerjee, S. and Kane, P.M. (2020) Regulation of V-ATPase Activity and Organelle pH by Phosphatidylinositol Phosphate Lipids. *Front Cell Dev Biol*, **8**, 510.

Bartlett, K. and Kim, K. (2014) Insight into Tor2, a budding yeast microdomain protein. *Eur J Cell Biol*, **93**, 87–97.

Bartoli, M.; Monneron, A. and Ladant, D. (1998) Interaction of calmodulin with striatin, a WD-repeat protein present in neuronal dendritic spines. *J Biol Chem*, **273**, 22248–22253.

Baumann, O. and Walz, B. (2001) Endoplasmic reticulum of animal cells and its organization into structural and functional domains. *Int Rev Cytol*, **205**, 149–214.

Bayliss, R.; Littlewood, T. and Stewart, M. (2000) Structural Basis for the Interaction between FxFG Nucleoporin Repeats and Importin-β in Nuclear Trafficking. *Cell*, **102**, 99–108.

Bazzi, H.; Soroka, E.; Alcorn, H.L. and Anderson, K.V. (2017) STRIP1, a core component of STRIPAK complexes, is essential for normal mesoderm migration in the mouse embryo. *Proc Natl Acad Sci USA*, **114**, e10928-36.

Beck, M. and Hurt, E. (2017) The nuclear pore complex: understanding its function through structural insight. *Nat Rev Mol Cell Biol*, **18**, 73–89.

Beier, A.; Teichert, I.; Krisp, C.; Wolters, D.A. and Kück, U. (2016) Catalytic Subunit 1 of Protein Phosphatase 2A Is a Subunit of the STRIPAK Complex and Governs Fungal Sexual Development. *mBio*, **7**, e00870-16.

Belanger, K.D.; Gupta, A.; MacDonald, K.M.; Ott, C.M. and Hodge, C.A.; et al. (2005) Nuclear pore complex function in *Saccharomyces cerevisiae* is influenced by glycosylation of the transmembrane nucleoporin Pom152p. *Genetics*, **171**, 935–947.

Benoist, M.; Gaillard, S. and Castets, F. (2006) The striatin family: a new signaling platform in dendritic spines. *J Physiol Paris*, **99**, 146–153.

Bernhards, Y. and Pöggeler, S. (2011) The phocein homologue SmMOB3 is essential for vegetative cell fusion and sexual development in the filamentous ascomycete *Sordaria macrospora*. *Curr Genet*, **57**, 133–149.

Bingham, J.B. and Schroer, T.A. (1999) Self-regulated polymerization of the actin-related protein Arp1. *Curr Biol*, **9**, 223–228.

Blank-Landeshammer, B.; Teichert, I.; Märker, R.; Nowrousian, M. and Kück, U.; et al. (2019) Combination of Proteogenomics with Peptide De Novo Sequencing Identifies New Genes and Hidden Posttranscriptional Modifications. *mBio*, **10**, 1–17.

Bloemendal, S.; Bernhards, Y.; Bartho, K.; Dettmann, A. and Voigt, O.; et al. (2012) A homologue of the human STRIPAK complex controls sexual development in fungi. *Mol Microbiol*, **84**, 310–323.

Bloemendal, S.; Lord, K.M.; Rech, C.; Hoff, B. and Engh, I.; et al. (2010) A mutant defective in sexual development produces aseptate ascogonia. *Eukaryot Cell*, **9**, 1856–1866.

Blum, M.; Chang, H.-Y.; Chuguransky, S.; Grego, T. and Kandasaamy, S.; et al. (2021) The InterPro protein families and domains database: 20 years on. *Nucleic Acids Res*, **49**, D344-D354.

Bonangelino, C.J.; Catlett, N.L. and Weisman, L.S. (1997) Vac7p, a novel vacuolar protein, is required for normal vacuole inheritance and morphology. *Mol Cell Biol*, **17**, 6847–6858.

Bonangelino, C.J.; Nau, J.J.; Duex, J.E.; Brinkman, M. and Wurmser, A.E.; et al. (2002) Osmotic stress-induced increase of phosphatidylinositol 3,5-bisphosphate requires Vac14p, an activator of the lipid kinase Fab1p. *J Cell Biol*, **156**, 1015–1028.

Botelho, R.J.; Efe, J.A.; Teis, D. and Emr, S.D. (2008) Assembly of a Fab1 phosphoinositide kinase signaling complex requires the Fig4 phosphoinositide phosphatase. *Mol Biol Cell*, **19**, 4273–4286.

Botstein, D. and Fink, G.R. (1988) Yeast: an experimental organism for modern biology. *Science*, **240**, 1439–1443.

Bowman, B.J.; Draskovic, M.; Freitag, M. and Bowman, E.J. (2009) Structure and distribution of organelles and cellular location of calcium transporters in *Neurospora crassa*. *Eukaryot Cell*, **8**, 1845–1855.

Brown, J.T.; Haraczy, A.J.; Wilhelm, C.M. and Belanger, K.D. (2021) Characterization of nuclear pore complex targeting domains in Pom152 in *Saccharomyces cerevisiae*. *Biol Open*, **10**, 1–8.

Burd, C.G.; Strochlic, T.I. and Setty, S.R.G. (2004) Arf-like GTPases: not so Arf-like after all. *Trends Cell Biol*, **14**, 687–694.

Byers, J.T.; Guzzo, R.M.; Salih, M. and Tuana, B.S. (2009) Hydrophobic profiles of the tail anchors in SLMAP dictate subcellular targeting. *BMC Cell Biol*, **10**, 1–18.

Carpaneto, A.; Boccaccio, A.; Lagostena, L.; Di Zanni, E. and Scholz-Starke, J. (2017) The signaling lipid phosphatidylinositol-3,5-bisphosphate targets plant CLC-a anion/H+ exchange activity. *EMBO Rep*, **18**, 1100–1107.

Carter, A.P.; Diamant, A.G. and Urnavicius, L. (2016) How dynein and dynactin transport cargos: a structural perspective. *Curr Opin Struct Biol*, **37**, 62–70.

Castets, F.; Bartoli, M.; Barnier, J.V.; Baillat, G. and Salin, P.; et al. (1996) A novel calmodulin-binding protein, belonging to the WD-repeat family, is localized in dendrites of a subset of CNS neurons. *J Cell Biol*, **134**, 1051–1062.

Castets, F.; Rakitina, T.; Gaillard, S.; Moqrich, A. and Mattei, M.G.; et al. (2000) Zinedin, SG2NA, and striatin are calmodulin-binding, WD repeat proteins principally expressed in the brain. *J Biol Chem*, **275**, 19970–19977.

Cavalli, V.; Kujala, P.; Klumperman, J. and Goldstein, L.S.B. (2005) Sunday Driver links axonal transport to damage signaling. *J Cell Biol*, **168**, 775–787.

Chadrin, A.; Hess, B.; San Roman, M.; Gatti, X. and Lombard, B.; et al. (2010) Pom33, a novel transmembrane nucleoporin required for proper nuclear pore complex distribution. *J Cell Biol*, **189**, 795–811.

Chen, H.-W.; Marinissen, M.J.; Oh, S.-W.; Chen, X. and Melnick, M.; et al. (2002) CKA, a novel multidomain protein, regulates the JUN N-terminal kinase signal transduction pathway in Drosophila. *Mol Cell Biol*, **22**, 1792–1803.

Chen, S.; Novick, P. and Ferro-Novick, S. (2013) ER structure and function. *Curr Opin Cell Biol*, **25**, 428–433.

Chial, H.J.; Rout, M.P.; Giddings, T.H. and Winey, M. (1998) *Saccharomyces cerevisiae* Ndc1p is a shared component of nuclear pore complexes and spindle pole bodies. *J Cell Biol*, **143**, 1789–1800.

Cho, U.S. and Xu, W. (2007) Crystal structure of a protein phosphatase 2A heterotrimeric holoenzyme. *Nature*, **445**, 53–57.

Chow, C.Y.; Landers, J.E.; Bergren, S.K.; Sapp, P.C. and Grant, A.E.; et al. (2009) Deleterious variants of FIG4, a phosphoinositide phosphatase, in patients with ALS. *Am J Hum Genet*, **84**, 85–88.

Chow, C.Y.; Zhang, Y.; Dowling, J.J.; Jin, N. and Adamska, M.; et al. (2007) Mutation of FIG4 causes neurodegeneration in the pale tremor mouse and patients with CMT4J. *Nature*, **448**, 68–72.

Cingolani, G.; Petosa, C.; Weis, K. and Müller, C.W. (1999) Structure of importin-beta bound to the IBB domain of importin-alpha. *Nature*, **399**, 221–229.

Clark, S.W. and Meyer, D.I. (1992) Centractin is an actin homologue associated with the centrosome. *Nature*, **359**, 246–250.

Clark, S.W.; Staub, O.; Clark, I.B.; Holzbaur, E.L. and Paschal, B.M.; et al. (1994) Beta-centractin: characterization and distribution of a new member of the centractin family of actin-related proteins. *Mol Biol Cell*, **5**, 1301–1310.

Cohen, M.; Feinstein, N.; Wilson, K.L. and Gruenbaum, Y. (2003) Nuclear pore protein gp210 is essential for viability in HeLa cells and *Caenorhabditis elegans*. *Mol Biol Cell*, **14**, 4230–4237.

Cole, L.; Hyde, G.J. and Ashford, A.E. (1997) Uptake and compartmentalisation of fluorescent probes by *Pisolithus tinctorius* hyphae: evidence for an anion transport mechanism at the tonoplast but not for fluid-phase endocytosis. *Protoplasma*, **199**, 18–29.

Cole, L.; Orlovich, D.A. and Ashford, A.E. (1998) Structure, function, and motility of vacuoles in filamentous fungi. *Fungal Genet Biol*, **24**, 86–100.

Colot, H.V.; Park, G.; Turner, G.E.; Ringelberg, C. and Crew, C.M.; et al. (2006) A high-throughput gene knockout procedure for Neurospora reveals functions for multiple transcription factors. *Proc Natl Acad Sci USA*, **103**, 10352–10357.

Compton, L.M.; Ikonomov, O.C.; Sbrissa, D.; Garg, P. and Shisheva, A. (2016) Active vacuolar H^+ ATPase and functional cycle of Rab5 are required for the vacuolation defect triggered by PtdIns(3,5)P_2 loss under PIKfyve or Vps34 deficiency. *Am J Physiol Cell Physiol*, **311**, C366-77.

Costanzo, M.; VanderSluis, B.; Koch, E.N.; Baryshnikova, A. and Pons, C.; et al. (2016) A global genetic interaction network maps a wiring diagram of cellular function. *Science*, **353**, aaf14201-aaf142014.

Couzens, A.L.; Knight, J.D.R.; Kean, M.J.; Teo, G. and Weiss, A.; et al. (2013) Protein interaction network of the mammalian Hippo pathway reveals mechanisms of kinase-phosphatase interactions. *Sci Signal*, **6**, 1-13.

Craig, H.D.; Günel, M.; Cepeda, O.; Johnson, E.W. and Ptacek, L.; et al. (1998) Multilocus linkage identifies two new loci for a mendelian form of stroke, cerebral cavernous malformation, at 7p15-13 and 3q25.2-27. *Hum Mol Genet*, **7**, 1851–1858.

Dadgostar, H.; Doyle, S.E.; Shahangian, A.; Garcia, D.E. and Cheng, G. (2003) T3JAM, a novel protein that specifically interacts with TRAF3 and promotes the activation of JNK 1. *FEBS Letters*, **553**, 403–407.

Dahlmann, T.A.; Terfehr, D.; Becker, K. and Teichert, I. (2021) Golden Gate vectors for efficient gene fusion and gene deletion in diverse filamentous fungi. *Curr Genet*, **67**, 317–330.

Dan, I.; Watanabe, N.M.; Kobayashi, T.; Yamashita-Suzuki, K. and Fukagaya, Y.; et al. (2000) Molecular cloning of MINK, a novel member of mammalian GCK family kinases, which is up-regulated during postnatal mouse cerebral development. *FEBS Letters*, **469**, 19–23.

Dawson, T.R.; Lazarus, M.D.; Hetzer, M.W. and Wente, S.R. (2009) ER membrane-bending proteins are necessary for de novo nuclear pore formation. *J Cell Biol*, **184**, 659–675.

De Lartigue, J.; Polson, H.; Feldman, M.; Shokat, K. and Tooze, S.A.; et al. (2009) PIKfyve regulation of endosome-linked pathways. *Traffic*, **10**, 883–893.

De Magistris, P. and Antonin, W. (2018) The Dynamic Nature of the Nuclear Envelope. *Curr Biol*, **28**, R487-R497.

De Souza, C.P.C.; Osmani, A.H.; Hashmi, S.B. and Osmani, S.A. (2004) Partial nuclear pore complex disassembly during closed mitosis in *Aspergillus nidulans*. *Curr Biol*, **14**, 1973–1984.

Deshaies, R.J. and Schekman, R. (1987) A yeast mutant defective at an early stage in import of secretory protein precursors into the endoplasmic reticulum. *J Cell Biol*, **105**, 633–645.

Dettmann, A.; Heilig, Y.; Ludwig, S.; Schmitt, K. and Illgen, J.; et al. (2013) HAM-2 and HAM-3 are central for the assembly of the Neurospora STRIPAK complex at the nuclear envelope and regulate nuclear accumulation of the MAP kinase MAK-1 in a MAK-2-dependent manner. *Mol Microbiol*, **90**, 796–812.

Di Paolo, G. and Camilli, P. de (2006) Phosphoinositides in cell regulation and membrane dynamics. *Nature*, **443**, 651–657.

Dickmanns, A.; Kehlenbach, R.H. and Fahrenkrog, B. (2015) Nuclear Pore Complexes and Nucleocytoplasmic Transport: From Structure to Function to Disease. *Int Rev Cell Mol Biol*, **320**, 171–233.

Donaldson, J.G. and Honda, A. (2005) Localization and function of Arf family GTPases. *Biochem Soc Trans*, **33**, 639–642.

Dong, X.; Shen, D.; Wang, X.; Dawson, T. and Li, X.; et al. (2010) PI(3,5)P(2) controls membrane trafficking by direct activation of mucolipin Ca(2+) release channels in the endolysosome. *Nat Commun*, **1**, 38.

Donnaloja, F.; Jacchetti, E.; Soncini, M. and Raimondi, M.T. (2019) Mechanosensing at the Nuclear Envelope by Nuclear Pore Complex Stretch Activation and Its Effect in Physiology and Pathology. *Front Physiol*, **10**, 1–15.

Doucet, C.M. and Hetzer, M.W. (2010) Nuclear pore biogenesis into an intact nuclear envelope. *Chromosoma*, **119**, 469–477.

Doucet, C.M.; Talamas, J.A. and Hetzer, M.W. (2010) Cell cycle-dependent differences in nuclear pore complex assembly in metazoa. *Cell*, **141**, 1030–1041.

Dove, S.K.; Cooke, F.T.; Douglas, M.R.; Sayers, L.G. and Parker, P.J.; et al. (1997) Osmotic stress activates phosphatidylinositol-3,5-bisphosphate synthesis. *Nature*, **390**, 187–192.

Dove, S.K.; Dong, K.; Kobayashi, T.; Williams, F.K. and Michell, R.H. (2009) Phosphatidylinositol 3,5-bisphosphate and Fab1p/PIKfyve underPPIn endo-lysosome function. *Biochem J*, **419**, 1–13.

Dove, S.K.; McEwen, R.K.; Mayes, A.; Hughes, D.C. and Beggs, J.D.; et al. (2002) Vac14 Controls PtdIns(3,5)P_2 Synthesis and Fab1-Dependent Protein Trafficking to the Multivesicular Body. *Curr Biol*, **12**, 885–893.

Dove, S.K.; Piper, R.C.; McEwen, R.K.; Yu, J.W. and King, M.C.; et al. (2004) Svp1p defines a family of phosphatidylinositol 3,5-bisphosphate effectors. *EMBO J*, **23**, 1922–1933.

Doye, V. and Hurt, E. (1997) From nucleoporins to nuclear pore complexes. *Curr Opin Cell Biol*, **9**, 401–411.

Drees, B.L.; Sundin, B.; Brazeau, E.; Caviston, J.P. and Chen, G.C.; et al. (2001) A protein interaction map for cell polarity development. *J Cell Biol*, **154**, 549–571.

Du, Y.; Ferro-Novick, S. and Novick, P. (2004) Dynamics and inheritance of the endoplasmic reticulum. *J Cell Sci*, **117**, 2871–2878.

Duex, J.E.; Nau, J.J.; Kauffman, E.J. and Weisman, L.S. (2006a) Phosphoinositide 5-phosphatase Fig 4p is required for both acute rise and subsequent fall in stress-induced phosphatidylinositol 3,5-bisphosphate levels. *Eukaryot Cell*, **5**, 723–731.

Duex, J.E.; Tang, F. and Weisman, L.S. (2006b) The Vac14p-Fig4p complex acts independently of Vac7p and couples PI3,5P2 synthesis and turnover. *J Cell Biol*, **172**, 693–704.

Dujardin, D.L.; Barnhart, L.E.; Stehman, S.A.; Gomes, E.R. and Gundersen, G.G.; et al. (2003) A role for cytoplasmic dynein and LIS1 in directed cell movement. *J Cell Biol*, **163**, 1205–1211.

Dultz, E. and Ellenberg, J. (2010) Live imaging of single nuclear pores reveals unique assembly kinetics and mechanism in interphase. *J Cell Biol*, **191**, 15–22.

Efe, J.A.; Botelho, R.J. and Emr, S.D. (2005) The Fab1 phosphatidylinositol kinase pathway in the regulation of vacuole morphology. *Curr Opin Cell Biol*, **17**, 402–408.

Efe, J.A.; Botelho, R.J. and Emr, S.D. (2007) Atg18 regulates organelle morphology and Fab1 kinase activity independent of its membrane recruitment by phosphatidylinositol 3,5-bisphosphate. *Mol Biol Cell*, **18**, 4232–4244.

Egan, M.J.; McClintock, M.A. and Reck-Peterson, S.L. (2012) Microtubule-based transport in filamentous fungi. *Curr Opin Microbiol*, **15**, 637–645.

Elleuche, S. and Pöggeler, S. (2009) Evolution of carbonic anhydrases in fungi. *Curr Genet*, **55**, 211–222.

Elramli, N.; Karahoda, B.; Sarikaya-Bayram, Ö.; Frawley, D. and Ulas, M.; et al. (2019) Assembly of a heptameric STRIPAK complex is required for coordination of light-dependent multicellular fungal development with secondary metabolism in *Aspergillus nidulans*. *PLoS Genet*, **15**, e1008053.

Engh, I.; Nowrousian, M. and Kück, U. (2007) Regulation of melanin biosynthesis via the dihydroxynaphthalene pathway is dependent on sexual development in the ascomycete *Sordaria macrospora*. *FEMS Microbiol Lett*, **275**, 62–70.

Engh, I.; Nowrousian, M. and Kück, U. (2010) *Sordaria macrospora*, a model organism to study fungal cellular development. *Eur J Cell Biol*, **89**, 864–872.

Esser, K. (1982) *Cryptogams. Cyanobacteria, Algae, Fungi, Lichens*, CUP Archive.

Esser, K. and Straub, J. (1958) Genetische Untersuchungen an *Sordaria macrospora* Auersw., Kompensation und Induktion bei Genbedingten Entwicklungsdefekten. *Zeitschrift für Vererbungslehre*, **89**, 729–746.

Fahrenkrog, B. and Aebi, U. (2003) The nuclear pore complex: nucleocytoplasmic transport and beyond. *Nat Rev Mol Cell Biol*, **4**, 757–766.

Farrell, J.A. and O'Farrell, P.H. (2014) From egg to gastrula: how the cell cycle is remodeled during the Drosophila mid-blastula transition. *Annu Rev Genet*, **48**, 269–294.

Ferguson, C.J.; Lenk, G.M. and Meisler, M.H. (2009) Defective autophagy in neurons and astrocytes from mice deficient in PI(3,5)P2. *Hum Mol Genet*, **18**, 4868–4878.

Fidalgo, M.; Fraile, M.; Pires, A.; Force, T. and Pombo, C.; et al. (2010) CCM3/PDCD10 stabilizes GCKIII proteins to promote Golgi assembly and cell orientation. *J Cell Sci*, **123**, 1274–1284.

Fink, G. and Steinberg, G. (2006) Dynein-dependent motility of microtubules and nucleation sites supports polarization of the tubulin array in the fungus *Ustilago maydis*. *Mol Biol Cell*, **17**, 3242–3253.

Fischer, R.; Zekert, N. and Takeshita, N. (2008) Polarized growth in fungi-interplay between the cytoskeleton, positional markers and membrane domains. *Mol Microbiol*, **68**, 813–826.

Fischer-Parton, S.; Parton, R.M.; Hickey, P.C.; Dijksterhuis, J. and Atkinson, H.A.; et al. (2000) Confocal microscopy of FM4-64 as a tool for analysing endocytosis and vesicle trafficking in living fungal hyphae. *J Microsc*, **198**, 246–259.

Fletcher, D.A. and Mullins, R.D. (2010) Cell mechanics and the cytoskeleton. *Nature*, **463**, 485–492.

Floch, A.G.; Tareste, D.; Fuchs, P.F.J.; Chadrin, A. and Naciri, I.; et al. (2015) Nuclear pore targeting of the yeast Pom33 nucleoporin depends on karyopherin and lipid binding. *J Cell Sci*, **128**, 305–316.

Frey, S.; Lahmann, Y.; Hartmann, T.; Seiler, S. and Pöggeler, S. (2015a) Deletion of *Smgpi1* encoding a GPI-anchored protein suppresses sterility of the STRIPAK mutant

ΔSmmob3 in the filamentous ascomycete *Sordaria macrospora*. *Mol Microbiol*, **97**, 676–697.

Frey, S.; Reschka, E.J. and Pöggeler, S. (2015b) Germinal Center Kinases SmKIN3 and SmKIN24 Are Associated with the *Sordaria macrospora* Striatin-Interacting Phosphatase and Kinase (STRIPAK) Complex. *PLoS One*, **10**, e0139163; 1-27.

Frost, A.; Elgort, M.G.; Brandman, O.; Ives, C. and Collins, S.R.; et al. (2012) Functional repurposing revealed by comparing *S. pombe* and *S. cerevisiae* genetic interactions. *Cell*, **149**, 1339–1352.

Fu, M.-M.; Nirschl, J.J. and Holzbaur, E.L.F. (2014) LC3 binding to the scaffolding protein JIP1 regulates processive dynein-driven transport of autophagosomes. *Dev Cell*, **29**, 577–590.

Fuller, S.J.; Edmunds, N.S.; McGuffin, L.J.; Hardyman, M.A. and Cull, J.J.; et al. (2021) MAP4K4 expression in cardiomyocytes: multiple isoforms, multiple phosphorylations and interactions with striatins. *Biochem J*, **478**, 2121–2143.

Funakoshi, T.; Maeshima, K.; Yahata, K.; Sugano, S. and Imamoto, F.; et al. (2007) Two distinct human POM121 genes: requirement for the formation of nuclear pore complexes. *FEBS Letters*, **581**, 4910–4916.

Gaillard, S.; Bartoli, M.; Castets, F. and Monneron, A. (2001) Striatin, a calmodulin-dependent scaffolding protein, directly binds caveolin-1. *FEBS Letters*, **508**, 49–52.

Gary, J.D.; Sato, T.K.; Stefan, C.J.; Bonangelino, C.J. and Weisman, L.S.; et al. (2002) Regulation of Fab1 phosphatidylinositol 3-phosphate 5-kinase pathway by Vac7 protein and Fig4, a polyphosphoinositide phosphatase family member. *Mol Biol Cell*, **13**, 1238–1251.

Gary, J.D.; Wurmser, A.E.; Bonangelino, C.J.; Weisman, L.S. and Emr, S.D. (1998) Fab1p is essential for PtdIns(3)P 5-kinase activity and the maintenance of vacuolar size and membrane homeostasis. *J Cell Biol*, **143**, 65–79.

Gentzsch, M.; Immervoll, T. and Tanner, W. (1995) Protein O-glycosylation in *Saccharomyces cerevisiae* : the protein O-mannosyltransferases Pmt1p and Pmt2p function as heterodimer. *FEBS Letters*, **377**, 128–130.

Gentzsch, M. and Tanner, W. (1996) The PMT gene family: protein O-glycosylation in *Saccharomyces cerevisiae* is vital. *EMBO J*, **15**, 5752–5759.

Gill, S.R.; Schroer, T.A.; Szilak, I.; Steuer, E.R. and Sheetz, M.P.; et al. (1991) Dynactin, a conserved, ubiquitously expressed component of an activator of vesicle motility mediated by cytoplasmic dynein. *J Cell Biol*, **115**, 1639–1650.

Gillooly, D.J.; Morrow, I.C.; Lindsay, M.; Gould, R. and Bryant, N.J.; et al. (2000) Localization of phosphatidylinositol 3-phosphate in yeast and mammalian cells. *EMBO J*, **19**, 4577–4588.

Glatter, T.; Wepf, A.; Aebersold, R. and Gstaiger, M. (2009) An integrated workflow for charting the human interaction proteome: insights into the PP2A system. *Mol Syst Biol*, **5**, 1–14.

Goudreault, M.; D'Ambrosio, L.M.; Kean, M.J.; Mullin, M.J. and Larsen, B.G.; et al. (2009) A PP2A phosphatase high density interaction network identifies a novel striatin-interacting phosphatase and kinase complex linked to the cerebral cavernous malformation 3 (CCM3) protein. *Mol Cell Proteomics*, **8**, 157–171.

Grallert, A.; Boke, E.; Hagting, A.; Hodgson, B. and Connolly, Y.; et al. (2015) A PP1-PP2A phosphatase relay controls mitotic progression. *Nature*, **517**, 94–98.

Grandi, P.; Doye, V. and Hurt, E.C. (1993) Purification of NSP1 reveals complex formation with 'GLFG' nucleoporins and a novel nuclear pore protein NIC96. *EMBO J*, **12**, 3061–3071.

Grandi, P.; Schlaich, N.; Tekotte, H. and Hurt, E.C. (1995) Functional interaction of Nic96p with a core nucleoporin complex consisting of Nsp1p, Nup49p and a novel protein Nup57p. *EMBO J*, **14**, 76–87.

Groth, A.; Schmitt, K.; Valerius, O.; Herzog, B. and Pöggeler, S. (2021) Analysis of the Putative Nucleoporin POM33 in the Filamentous Fungus *Sordaria macrospora*. *J Fungi (Basel)*, **682**, 1–23.

Guo, X.; Farías, G.G.; Mattera, R. and Bonifacino, J.S. (2016) Rab5 and its effector FHF contribute to neuronal polarity through dynein-dependent retrieval of somatodendritic proteins from the axon. *PNAS*, **113**, E5318-27.

Habermann, A.; Schroer, T.A.; Griffiths, G. and Burkhardt, J.K. (2001) Immunolocalization of cytoplasmic dynein and dynactin subunits in cultured macrophages: enrichment on early endocytic organelles. *J Cell Sci*, **114**, 229–240.

Hampoelz, B.; Andres-Pons, A.; Kastritis, P. and Beck, M. (2019) Structure and Assembly of the Nuclear Pore Complex. *Annu Rev Biophys*, **48**, 515–536.

Harris, S.D. (2011) Cdc42/Rho GTPases in fungi: variations on a common theme. *Mol Microbiol*, **79**, 1123–1127.

Harris, S.D.; Read, N.D.; Roberson, R.W.; Shaw, B. and Seiler, S.; et al. (2005) Polarisome meets spitzenkörper: microscopy, genetics, and genomics converge. *Eukaryot Cell*, **4**, 225–229.

Hauri, S.; Wepf, A.; van Drogen, A.; Varjosalo, M. and Tapon, N.; et al. (2013) Interaction proteome of human Hippo signaling: modular control of the co-activator YAP1. *Mol Syst Biol*, **9**, 1–16.

Hawksworth, D.L. (2001) The magnitude of fungal diversity: the 1.5 million species estimate revisited. *Mycol Res*, **105**, 1422–1432.

Herrmann, H.; Bär, H.; Kreplak, L.; Strelkov, S.V. and Aebi, U. (2007) Intermediate filaments: from cell architecture to nanomechanics. *Nat Rev Mol Cell Biol*, **8**, 562–573.

Hetzer, M.W.; Walther, T.C. and Mattaj, I.W. (2005) Pushing the envelope: structure, function, and dynamics of the nuclear periphery. *Annu Rev Cell Dev Biol*, **21**, 347–380.

Higuchi, Y.; Ashwin, P.; Roger, Y. and Steinberg, G. (2014) Early endosome motility spatially organizes polysome distribution. *J Cell Biol*, **204**, 343–357.

Hirokawa, N. (1998) Kinesin and dynein superfamily proteins and the mechanism of organelle transport. *Science*, **279**, 519–526.

Ho, C.Y.; Alghamdi, T.A. and Botelho, R.J. (2012) Phosphatidylinositol-3,5-bisphosphate: no longer the poor PIP2. *Traffic*, **13**, 1–8.

Ho, C.Y.; Choy, C.H.; Wattson, C.A.; Johnson, D.E. and Botelho, R.J. (2015) The Fab1/PIKfyve phosphoinositide phosphate kinase is not necessary to maintain the pH of lysosomes and of the yeast vacuole. *J Biol Chem*, **290**, 9919–9928.

Holleran, E.A.; Ligon, L.A.; Tokito, M.; Stankewich, M.C. and Morrow, J.S.; et al. (2001) beta III spectrin binds to the Arp1 subunit of dynactin. *J Biol Chem*, **276**, 36598–36605.

Holleran, E.A.; Tokito, M.K.; Karki, S. and Holzbaur, E.L. (1996) Centractin (ARP1) associates with spectrin revealing a potential mechanism to link dynactin to intracellular organelles. *J Cell Biol*, **135**, 1815–1829.

Hu, J.; Shibata, Y.; Voss, C.; Shemesh, T. and Li, Z.; et al. (2008) Membrane proteins of the endoplasmic reticulum induce high-curvature tubules. *Science*, **319**, 1247–1250.

Hu, J.; Shibata, Y.; Zhu, P.-P.; Voss, C. and Rismanchi, N.; et al. (2009) A class of dynamin-like GTPases involved in the generation of the tubular ER network. *Cell*, **138**, 549–561.

Huang, T.; Kim, C.K.; Alvarez, A.A.; Pangeni, R.P. and Wan, X.; et al. (2017) MST4 Phosphorylation of ATG4B Regulates Autophagic Activity, Tumorigenicity, and Radioresistance in Glioblastoma. *Cancer Cell*, **32**, 840-855.e8.

Hurt, E. and Beck, M. (2015) Towards understanding nuclear pore complex architecture and dynamics in the age of integrative structural analysis. *Curr Opin Cell Biol*, **34**, 31–38.

Hwang, J. and Pallas, D.C. (2014) STRIPAK complexes: structure, biological function, and involvement in human diseases. *Int J Biochem Cell Biol*, **47**, 118–148.

Hyodo, T.; Ito, S.; Hasegawa, H.; Asano, E. and Maeda, M.; et al. (2012) Misshapen-like kinase 1 (MINK1) is a novel component of striatin-interacting phosphatase and kinase (STRIPAK) and is required for the completion of cytokinesis. *J Biol Chem*, **287**, 25019–25029.

Ikonomov, O.C.; Sbrissa, D.; Fenner, H. and Shisheva, A. (2009a) PIKfyve-ArPIKfyve-Sac3 core complex: contact sites and their consequence for Sac3 phosphatase activity and endocytic membrane homeostasis. *J Biol Chem*, **284**, 35794–35806.

Ikonomov, O.C.; Sbrissa, D.; Ijuin, T.; Takenawa, T. and Shisheva, A. (2009b) Sac3 is an insulin-regulated phosphatidylinositol 3,5-bisphosphate phosphatase: gain in insulin responsiveness through Sac3 down-regulation in adipocytes. *J Biol Chem*, **284**, 23961–23971.

Ikonomov, O.C.; Sbrissa, D. and Shisheva, A. (2001) Mammalian cell morphology and endocytic membrane homeostasis require enzymatically active phosphoinositide 5-kinase PIKfyve. *J Biol Chem*, **276**, 26141–26147.

Ikonomov, O.C.; Sbrissa, D. and Shisheva, A. (2006) Localized PtdIns 3,5-P2 synthesis to regulate early endosome dynamics and fusion. *Am J Physiol Cell Physiol*, **291**, C393-404.

Irniger, S.; Sarikaya-Bayram, Ö. and Bayram, Ö. (2016) 6 Fungal MAP-Kinase-Mediated Regulatory Pathways. In *Biochemistry and Molecular Biology (*Hoffmeister, D., ed). The Mycota (A Comprehensive Treatise on Fungi as Experimental Systems for Basic and Applied Research), Springer, Cham, Vol. III, pp. 97–117.

Ito, M.; Masumi, A.; Mochida, K.; Kukihara, H. and Moriishi, K.; et al. (2010) Peripheral B cells may serve as a reservoir for persistent hepatitis C virus infection. *J Innate Immun*, **2**, 607–617.

James, P.; Halladay, J. and Craig, E.A. (1996) Genomic libraries and a host strain designed for highly efficient two-hybrid selection in yeast. *Genetics*, **144**, 1425–1436.

Janssens, V. and Goris, J. (2001) Protein phosphatase 2A: a highly regulated family of serine/threonine phosphatases implicated in cell growth and signalling. *Biochem J*, **353**, 417–439.

Janssens, V.; Longin, S. and Goris, J. (2008) PP2A holoenzyme assembly: in cauda venenum (the sting is in the tail). *Trends Biochem Sci*, **33**, 113–121.

Jefferies, H.B.J.; Cooke, F.T.; Jat, P.; Boucheron, C. and Koizumi, T.; et al. (2008) A selective PIKfyve inhibitor blocks PtdIns(3,5)P_2 production and disrupts endomembrane transport and retroviral budding. *EMBO Rep*, **9**, 164–170.

Jeong, B.-C.; Bae, S.J.; Ni, L.; Zhang, X. and Bai, X.-C.; et al. (2021) Cryo-EM structure of the Hippo signaling integrator human STRIPAK. *Nat Struct Mol Biol*, **28**, 290–299.

Jin, N.; Chow, C.Y.; Liu, L.; Zolov, S.N. and Bronson, R.; et al. (2008) VAC14 nucleates a protein complex essential for the acute interconversion of PI3P and PI(3,5)P(2) in yeast and mouse. *EMBO J*, **27**, 3221–3234.

Jin, N.; Jin, Y. and Weisman, L.S. (2017) Early protection to stress mediated by CDK-dependent PI3,5P2 signaling from the vacuole/lysosome. *J Cell Biol*, **216**, 2075–2090.

Joly, M.; Kazlauskas, A. and Corvera, S. (1995) Phosphatidylinositol 3-kinase activity is required at a postendocytic step in platelet-derived growth factor receptor trafficking. *J Biol Chem*, **270**, 13225–13230.

Jones, A.T. and Clague, M.J. (1995) Phosphatidylinositol 3-kinase activity is required for early endosome fusion. *Biochem J*, **311**, 31–34.

Jones, D.R.; González-García, A.; Díez, E.; Martinez-A, C. and Carrera, A.C.; et al. (1999) The identification of phosphatidylinositol 3,5-bisphosphate in T-lymphocytes and its regulation by interleukin-2. *J Biol Chem*, **274**, 18407–18413.

Kapinos, L.E.; Huang, B.; Rencurel, C. and Lim, R.Y.H. (2017) Karyopherins regulate nuclear pore complex barrier and transport function. *J Cell Biol*, **216**, 3609–3624.

Kardon, J.R.; Reck-Peterson, S.L. and Vale, R.D. (2009) Regulation of the processivity and intracellular localization of *Saccharomyces cerevisiae* dynein by dynactin. *PNAS*, **106**, 5669–5674.

Katoh, K.; Rozewicki, J. and Yamada, K.D. (2019) MAFFT online service: multiple sequence alignment, interactive sequence choice and visualization. *Brief Bioinform*, **20**, 1160–1166.

Kean, M.J.; Ceccarelli, D.F.; Goudreault, M.; Sanches, M. and Tate, S.; et al. (2011) Structure-function analysis of core STRIPAK Proteins: a signaling complex implicated in Golgi polarization. *J Biol Chem*, **286**, 25065–25075.

Keating, T.J. and Borisy, G.G. (1999) Centrosomal and non-centrosomal microtubules. *Biol Cell*, **91**, 321–329.

Kemp, H.A. and Sprague, G.F. (2003) Far3 and five interacting proteins prevent premature recovery from pheromone arrest in the budding yeast *Saccharomyces cerevisiae*. *Mol Cell Biol*, **23**, 1750–1763.

Kilaru, S.; Schuster, M.; Latz, M.; Guo, M. and Steinberg, G. (2015) Fluorescent markers of the endocytic pathway in *Zymoseptoria tritici*. *Fungal Genet Biol*, **79**, 150–157.

Kim, J.W.; Berrios, C.; Kim, M.; Schade, A.E. and Adelmant, G.; et al. (2020) STRIPAK directs PP2A activity toward MAP4K4 to promote oncogenic transformation of human cells. *Elife*, **9**, e53003.

Kim, S.J.; Fernandez-Martinez, J.; Nudelman, I.; Shi, Y. and Zhang, W.; et al. (2018) Integrative structure and functional anatomy of a nuclear pore complex. *Nature*, **555**, 475–482.

Kiseleva, E.; Morozova, K.N.; Voeltz, G.K.; Allen, T.D. and Goldberg, M.W. (2007) Reticulon 4a/NogoA locates to regions of high membrane curvature and may have a role in nuclear envelope growth. *J Struct Biol*, **160**, 224–235.

Klix, V.; Nowrousian, M.; Ringelberg, C.; Loros, J.J. and Dunlap, J.C.; et al. (2010) Functional characterization of MAT1-1-specific mating-type genes in the homothallic ascomycete *Sordaria macrospora* provides new insights into essential and nonessential sexual regulators. *Eukaryot Cell*, **9**, 894–905.

Kück, U.; Beier, A.M. and Teichert, I. (2016) The composition and function of the striatin-interacting phosphatases and kinases (STRIPAK) complex in fungi. *Fungal Genet Biol*, **90**, 31–38.

Kück, U. and Hoff, B. (2006) Application of the nourseothricin acetyltransferase gene (nat1) as dominant marker for the transformation of filamentous fungi. *Fungal Genet Rep*, **53**, 9–11.

Kück, U.; Pöggeler, S.; Nowrousian, M.; Nolting, N. and Engh, I. (2009) *Sordaria macrospora*, a Model System for Fungal Development. In *Physiology and Genetics* (Anke, T. and Weber, D., eds). The Mycota (A Comprehensive Treatise on Fungi as Experimental Systems for Basic and Applied Research), Springer, Berlin, Heidelberg, Vol. 15, pp. 17–39.

Kück, U.; Radchenko, D. and Teichert, I. (2019) STRIPAK, a highly conserved signaling complex, controls multiple eukaryotic cellular and developmental processes and is linked with human diseases. *Biol Chem*, **400**, 1005–1022.

Kurokawa, Y.; Konishi, R.; Yoshida, A.; Tomioku, K. and Futagami, T.; et al. (2019) Essential and distinct roles of phosphatidylinositol 4-kinases, Pik1p and Stt4p, in yeast autophagy. *Biochim Biophys Acta Mol Cell Biol Lipids*, **1864**, 1214–1225.

Lai, F.; Wu, R.; Wang, J.; Li, C. and Zou, L.; et al. (2011) Far3p domains involved in the interactions of Far proteins and pheromone-induced cell cycle arrest in budding yeast. *FEMS Yeast Res*, **11**, 72–79.

Lant, B.; Yu, B.; Goudreault, M.; Holmyard, D. and Knight, J.D.R.; et al. (2015) CCM-3/STRIPAK promotes seamless tube extension through endocytic recycling. *Nat Commun*, **6**, 1–13.

Lasser, M.; Tiber, J. and Lowery, L.A. (2018) The Role of the Microtubule Cytoskeleton in Neurodevelopmental Disorders. *Front Cell Neurosci*, **12**, 1–18.

Lee, C. and Chen, L.B. (1988) Dynamic behavior of endoplasmic reticulum in living cells. *Cell*, **54**, 37–46.

Lees, J.A.; Li, P.; Kumar, N.; Weisman, L.S. and Reinisch, K.M. (2020) Insights into Lysosomal PI(3,5)P2 Homeostasis from a Structural-Biochemical Analysis of the PIKfyve Lipid Kinase Complex. *Mol Cell*, **80**, 736-743.e4.

Lemaire, J.-F. and McPherson, P.S. (2006) Binding of Vac14 to neuronal nitric oxide synthase: Characterisation of a new internal PDZ-recognition motif. *FEBS Letters*, **580**, 6948–6954.

Lemmon, M.A. (2008) Membrane recognition by phospholipid-binding domains. *Nat Rev Mol Cell Biol*, **9**, 99–111.

Lenz, J.H.; Schuchardt, I.; Straube, A. and Steinberg, G. (2006) A dynein loading zone for retrograde endosome motility at microtubule plus-ends. *EMBO J*, **25**, 2275–2286.

Li, S.C.; Diakov, T.T.; Xu, T.; Tarsio, M. and Zhu, W.; et al. (2014) The signaling lipid PI(3,5)P_2 stabilizes V_1-V(o) sector interactions and activates the V-ATPase. *Mol Biol Cell*, **25**, 1251–1262.

Liang, Y.; Franks, T.M.; Marchetto, M.C.; Gage, F.H. and Hetzer, M.W. (2013) Dynamic association of NUP98 with the human genome. *PLoS Genet*, **9**, e1003308.

Lichius, A. and Lord, K.M. (2014) Chemoattractive Mechanisms in Filamentous Fungi. *TOMYCJ*, **8**, 28–57.

Lin, A.; Hokugo, A.; Choi, J. and Nishimura, I. (2010) Small cytoskeleton-associated molecule, fibroblast growth factor receptor 1 oncogene partner 2/wound inducible transcript-3.0 (FGFR1OP2/wit3.0), facilitates fibroblast-driven wound closure. *Am J Pathol*, **176**, 108–121.

Lin, D.H.; Stuwe, T.; Schilbach, S.; Rundlet, E.J. and Perriches, T.; et al. (2016) Architecture of the symmetric core of the nuclear pore. *Science*, **352**, aaf1015.

Lindmo, K. and Stenmark, H. (2006) Regulation of membrane traffic by phosphoinositide 3-kinases. *J Cell Sci*, **119**, 605–614.

Lipka, J.; Kuijpers, M.; Jaworski, J. and Hoogenraad, C.C. (2013) Mutations in cytoplasmic dynein and its regulators cause malformations of cortical development and neurodegenerative diseases. *Biochem Soc Trans*, **41**, 1605–1612.

Lisa-Santamaría, P.; Jiménez, A. and Revuelta, J.L. (2012) The protein factor-arrest 11 (Far11) is essential for the toxicity of human caspase-10 in yeast and participates in the regulation of autophagy and the DNA damage signaling. *J Biol Chem*, **287**, 29636–29647.

Liu, H.-L.; De Souza, C.P.C.; Osmani, A.H. and Osmani, S.A. (2009) The three fungal transmembrane nuclear pore complex proteins of *Aspergillus nidulans* are dispensable in the presence of an intact An-Nup84-120 complex. *Mol Biol Cell*, **20**, 616–630.

Liu, T.Y.; Bian, X.; Sun, S.; Hu, X. and Klemm, R.W.; et al. (2012) Lipid interaction of the C terminus and association of the transmembrane segments facilitate atlastin-mediated homotypic endoplasmic reticulum fusion. *PNAS*, **109**, E2146-54.

Lupas, A.; van Dyke, M. and Stock, J. (1991) Predicting coiled coils from protein sequences. *Science*, **252**, 1162–1164.

Ma, X.; Zhao, H.; Shan, J.; Long, F. and Chen, Y.; et al. (2007) PDCD10 interacts with Ste20-related kinase MST4 to promote cell growth and transformation via modulation of the ERK pathway. *Mol Biol Cell*, **18**, 1965–1978.

Madrid, A.S.; Mancuso, J.; Cande, W.Z. and Weis, K. (2006) The role of the integral membrane nucleoporins Ndc1p and Pom152p in nuclear pore complex assembly and function. *J Cell Biol*, **173**, 361–371.

Madsen, C.D.; Hooper, S.; Tozluoglu, M.; Bruckbauer, A. and Fletcher, G.; et al. (2015) STRIPAK components determine mode of cancer cell migration and metastasis. *Nat Cell Biol*, **17**, 68–80.

Makhnevych, T.; Lusk, C.; Anderson, A.M.; Aitchison, J.D. and Wozniak, R.W. (2003) Cell Cycle Regulated Transport Controlled by Alterations in the Nuclear Pore Complex. *Cell*, **115**, 813–823.

Makio, T.; Stanton, L.H.; Lin, C.-C.; Goldfarb, D.S. and Weis, K.; et al. (2009) The nucleoporins Nup170p and Nup157p are essential for nuclear pore complex assembly. *J Cell Biol*, **185**, 459–473.

Malik, H.S.; Eickbush, T.H. and Goldfarb, D.S. (1997) Evolutionary specialization of the nuclear targeting apparatus. *Proc Natl Acad Sci USA*, **94**, 13738–13742.

Manford, A.G.; Stefan, C.J.; Yuan, H.L.; Macgurn, J.A. and Emr, S.D. (2012) ER-to-plasma membrane tethering proteins regulate cell signaling and ER morphology. *Dev Cell*, **23**, 1129–1140.

Mansfeld, J.; Güttinger, S.; Hawryluk-Gara, L.A.; Panté, N. and Mall, M.; et al. (2006) The conserved transmembrane nucleoporin NDC1 is required for nuclear pore complex assembly in vertebrate cells. *Mol Cell*, **22**, 93–103.

Märker, R.; Blank-Landeshammer, B.; Beier-Rosberger, A.; Sickmann, A. and Kück, U. (2020) Phosphoproteomic analysis of STRIPAK mutants identifies a conserved serine phosphorylation site in PAK kinase CLA4 to be important in fungal sexual development and polarized growth. *Mol Microbiol*, **113**, 1053–1069.

McEwen, R.K.; Dove, S.K.; Cooke, F.T.; Painter, G.F. and Holmes, A.B.; et al. (1999) Complementation analysis in PtdInsP kinase-deficient yeast mutants demonstrates that

Schizosaccharomyces pombe and murine Fab1p homologues are phosphatidylinositol 3-phosphate 5-kinases. *J Biol Chem*, **274**, 33905–33912.

Mehta, A.D.; Rock, R.S.; Rief, M.; Spudich, J.A. and Mooseker, M.S.; et al. (1999) Myosin-V is a processive actin-based motor. *Nature*, **400**, 590–593.

Mela, A.P.; Rico-Ramírez, A.M. and Glass, N.L. (2020) Syncytia in Fungi. *Cells*, **2255**, 1–14.

Miki, H.; Okada, Y. and Hirokawa, N. (2005) Analysis of the kinesin superfamily: insights into structure and function. *Trends Cell Biol*, **15**, 467–476.

Miller, K.E.; Kang, P.J. and Park, H.-O. (2020) Regulation of Cdc42 for polarized growth in budding yeast. *Microb Cell*, **7**, 175–189.

Minke, P.F.; Lee, I.H.; Tinsley, J.H. and Plamann, M. (2000) A *Neurospora crassa* Arp1 mutation affecting cytoplasmic dynein and dynactin localization. *Mol Gen Genet*, **264**, 433–440.

Momany, M. (2002) Polarity in filamentous fungi: establishment, maintenance and new axes. *Curr Opin Microbiol*, **5**, 580–585.

Monnerjahn, C.; Techel, D.; Meyer, U. and Rensing, L. (2001) The grp78 promoter of Neurospora crassa: constitutive, stress and differentiation-dependent protein-binding patterns. *Curr Genet*, **39**, 319–326.

Moreno, C.S.; Park, S.; Nelson, K.; Ashby, D. and Hubalek, F.; et al. (2000) WD40 repeat proteins striatin and S/G(2) nuclear autoantigen are members of a novel family of calmodulin-binding proteins that associate with protein phosphatase 2A. *J Biol Chem*, **275**, 5257–5263.

Mouriño-Pérez, R.R.; Roberson, R.W. and Bartnicki-García, S. (2006) Microtubule dynamics and organization during hyphal growth and branching in *Neurospora crassa*. *Fungal Genet Biol*, **43**, 389–400.

Mudumbi, K.C.; Czapiewski, R.; Ruba, A.; Junod, S.L. and Li, Y.; et al. (2020) Nucleoplasmic signals promote directed transmembrane protein import simultaneously via multiple channels of nuclear pores. *Nat Commun*, **11**, 1–14.

Muhua, L.; Karpova, T.S. and Cooper, J.A. (1994) A yeast actin-related protein homologous to that in vertebrate dynactin complex is important for spindle orientation and nuclear migration. *Cell*, **78**, 669–679.

Muro, Y.; Chan, E.K.; Landberg, G. and Tan, E.M. (1995) A cell-cycle nuclear autoantigen containing WD-40 motifs expressed mainly in S and G2 phase cells. *Biochem Biophys Res Commun*, **207**, 1029–1037.

Neal, S.J.; Zhou, Q. and Pignoni, F. (2020) STRIPAK-PP2A regulates Hippo-Yorkie signaling to suppress retinal fate in the Drosophila eye disc peripodial epithelium. *J Cell Sci*, **133**, 1–11.

Neer, E.J.; Schmidt, C.J.; Nambudripad, R. and Smith, T.F. (1994) The ancient regulatory-protein family of WD-repeat proteins. *Nature*, **371**, 297–300.

Neisch, A.L.; Neufeld, T.P. and Hays, T.S. (2017) A STRIPAK complex mediates axonal transport of autophagosomes and dense core vesicles through PP2A regulation. *J Cell Biol*, **216**, 441–461.

Nicholas, K. and Nicholas, H. (1997) GeneDoc: a tool for editing and annotating multiple sequence alignments.

Nicot, A.-S.; Fares, H.; Payrastre, B.; Chisholm, A.D. and Labouesse, M.; et al. (2006) The phosphoinositide kinase PIKfyve/Fab1p regulates terminal lysosome maturation in *Caenorhabditis elegans*. *Mol Biol Cell*, **17**, 3062–3074.

Nordzieke, S.; Zobel, T.; Fränzel, B.; Wolters, D.A. and Kück, U.; et al. (2015) A fungal sarcolemmal membrane-associated protein (SLMAP) homolog plays a fundamental role in development and localizes to the nuclear envelope, endoplasmic reticulum, and mitochondria. *Eukaryot Cell*, **14**, 345–358.

Nowrousian, M.; Ringelberg, C.; Dunlap, J.C.; Loros, J.J. and Kück, U. (2005) Cross-species microarray hybridization to identify developmentally regulated genes in the filamentous fungus *Sordaria macrospora*. *Zeitschrift für Vererbungslehre*, **273**, 137–149.

Nowrousian, M.; Stajich, J.E.; Chu, M.; Engh, I. and Espagne, E.; et al. (2010) De novo assembly of a 40 Mb eukaryotic genome from short sequence reads: *Sordaria macrospora*, a model organism for fungal morphogenesis. *PLoS Genet*, **6**, e1000891.

Nowrousian, M.; Teichert, I.; Masloff, S. and Kück, U. (2012) Whole-Genome Sequencing of *Sordaria macrospora* Mutants Identifies Developmental Genes. *G3 (Bethesda)*, **2**, 261–270.

Oertle, T.; Klinger, M.; Stuermer, C.A.O. and Schwab, M.E. (2003) A reticular rhapsody: phylogenic evolution and nomenclature of the RTN/Nogo gene family. *FASEB J*, **17**, 1238–1247.

Orso, G.; Pendin, D.; Liu, S.; Tosetto, J. and Moss, T.J.; et al. (2009) Homotypic fusion of ER membranes requires the dynamin-like GTPase atlastin. *Nature*, **460**, 978–983.

Osmani, A.H.; Davies, J.; Liu, H.-L.; Nile, A. and Osmani, S.A. (2006) Systematic deletion and mitotic localization of the nuclear pore complex proteins of *Aspergillus nidulans*. *Mol Biol Cell*, **17**, 4946–4961.

Pace, N.R. (2009) Mapping the tree of life: progress and prospects. *Microbiol Mol Biol Rev*, **73**, 565–576.

Panatala, R.; Barbato, S.; Kozai, T.; Luo, J. and Kapinos, L.E.; et al. (2019) Nuclear Pore Membrane Proteins Self-Assemble into Nanopores. *Biochemistry*, **58**, 484–488.

Pandey, S.; Talukdar, I.; Jain, B.P.; Tanti, G.K. and Goswami, S.K. (2017) GSK3β and ERK regulate the expression of 78 kDa SG2NA and ectopic modulation of its level affects phases of cell cycle. *Sci Rep*, **7**, 1–12.

Panic, B.; Whyte, J.R. and Munro, S. (2003) The ARF-like GTPases Arl1p and Arl3p Act in a Pathway that Interacts with Vesicle-Tethering Factors at the Golgi Apparatus. *Curr Biol*, **13**, 405–410.

Park, H.-O. and Bi, E. (2007) Central roles of small GTPases in the development of cell polarity in yeast and beyond. *Microbiol Mol Biol Rev*, **71**, 48–96.

Peñalva, M.A. (2005) Tracing the endocytic pathway of *Aspergillus nidulans* with FM4-64. *Fungal Genet Biol*, **42**, 963–975.

Peñalva, M.Á. (2010) Endocytosis in filamentous fungi: Cinderella gets her reward. *Curr Opin Microbiol*, **13**, 684–692.

Pfarr, C.M.; Coue, M.; Grissom, P.M.; Hays, T.S. and Porter, M.E.; et al. (1990) Cytoplasmic dynein is localized to kinetochores during mitosis. *Nature*, **345**, 263–265.

Plamann, M.; Minke, P.F.; Tinsley, J.H. and Bruno, K.S. (1994) Cytoplasmic dynein and actin-related protein Arp1 are required for normal nuclear distribution in filamentous fungi. *J Cell Biol*, **127**, 139–149.

Plath, K.; Wilkinson, B.M.; Stirling, C.J. and Rapoport, T.A. (2004) Interactions between Sec complex and prepro-alpha-factor during posttranslational protein transport into the endoplasmic reticulum. *Mol Biol Cell*, **15**, 1–10.

Pöggeler, S. and Kück, U. (2004) A WD40 repeat protein regulates fungal cell differentiation and can be replaced functionally by the mammalian homologue striatin. *Eukaryot Cell*, **3**, 232–240.

Pöggeler, S. and Kück, U. (2006) Highly efficient generation of signal transduction knockout mutants using a fungal strain deficient in the mammalian ku70 ortholog. *Gene*, **378**, 1–10.

Pöggeler, S.; Masloff, S.; Hoff, B.; Mayrhofer, S. and Kück, U. (2003) Versatile EGFP reporter plasmids for cellular localization of recombinant gene products in filamentous fungi. *Curr Genet*, **43**, 54–61.

Pöggeler, S.; Nowrousian, M. and Kück, U. (2006) Fruiting-Body Development in Ascomycetes. In *Growth, Differentiation and Sexuality* (Kües, U. and Fischer, R., eds). The Mycota (A Comprehensive Treatise on Fungi as Experimental Systems for Basic and Applied Research), Springer, Berlin, Heidelberg, Vol. 1, pp. 325–355.

Pracheil, T. and Liu, Z. (2013) Tiered assembly of the yeast Far3-7-8-9-10-11 complex at the endoplasmic reticulum. *J Biol Chem*, **288**, 16986–16997.

Pruyne, D. and Bretscher, A. (2000) Polarization of cell growth in yeast. I. Establishment and maintenance of polarity states. *J Cell Sci*, **113**, 365–375.

Qiu, S.; Lavallée-Adam, M. and Côté, M. (2021) Proximity Interactome Map of the Vac14-Fig4 Complex Using BioID. *J Proteome Res*, **20**, 4959–4973.

Radchenko, D.; Teichert, I.; Pöggeler, S. and Kück, U. (2018) A Hippo Pathway-Related GCK Controls Both Sexual and Vegetative Developmental Processes in the Fungus *Sordaria macrospora*. *Genetics*, **210**, 137–153.

Reck-Peterson, S.L.; Provance, D.; Mooseker, M.S. and Mercer, J.A. (2000) Class V myosins. *Biochim Biophys Acta Mol Cell Res*, **1496**, 36–51.

Reck-Peterson, S.L.; Redwine, W.B.; Vale, R.D. and Carter, A.P. (2018) The cytoplasmic dynein transport machinery and its many cargoes. *Nat Rev Mol Cell Biol*, **19**, 382–398.

Reschka, E.J.; Nordzieke, S.; Valerius, O.; Braus, G.H. and Pöggeler, S. (2018) A novel STRIPAK complex component mediates hyphal fusion and fruiting-body development in filamentous fungi. *Mol Microbiol*, **110**, 513–532.

Ribeiro, P.S.; Josué, F.; Wepf, A.; Wehr, M.C. and Rinner, O.; et al. (2010) Combined functional genomic and proteomic approaches identify a PP2A complex as a negative regulator of Hippo signaling. *Mol Cell*, **39**, 521–534.

Riquelme, M. (2013) Tip growth in filamentous fungi: a road trip to the apex. *Annu Rev Microbiol*, **67**, 587–609.

Riquelme, M.; Aguirre, J.; Bartnicki-García, S.; Braus, G.H. and Feldbrügge, M.; et al. (2018) Fungal Morphogenesis, from the Polarized Growth of Hyphae to Complex Reproduction and Infection Structures. *Microbiol Mol Biol Rev*, **82**, e00068-17.

Riquelme, M.; Fischer, R. and Bartnicki-García, S. (2003) Apical growth and mitosis are independent processes in *Aspergillus nidulans*. *Protoplasma*, **222**, 211–215.

Riquelme, M.; Gierz, G. and Bartnicki-Garcı A, S. (2000) Dynein and dynactin deficiencies affect the formation and function of the Spitzenkörper and distort hyphal morphogenesis of *Neurospora crassa*. *Microbiology (Reading)*, **146**, 1743–1752.

Riquelme, M.; Roberson, R.W.; McDaniel, D.P. and Bartnicki-García, S. (2002) The effects of ropy-1 mutation on cytoplasmic organization and intracellular motility in mature hyphae of *Neurospora crassa*. *Fungal Genet Biol*, **37**, 171–179.

Robinson, O.; Dylus, D. and Dessimoz, C. (2016) Phylo.io: Interactive Viewing and Comparison of Large Phylogenetic Trees on the Web. *Mol Biol Evol*, **33**, 2163–2166.

Rout, M.P.; Aitchison, J.D.; Suprapto, A.; Hjertaas, K. and Zhao, Y.; et al. (2000) The yeast nuclear pore complex: composition, architecture, and transport mechanism. *J Cell Biol*, **148**, 635–651.

Rudge, S.A.; Anderson, D.M. and Emr, S.D. (2004) Vacuole size control: regulation of PtdIns(3,5)P2 levels by the vacuole-associated Vac14-Fig4 complex, a PtdIns(3,5)P2-specific phosphatase. *Mol Biol Cell*, **15**, 24–36.

Rusten, T.E.; Rodahl, L.M.W.; Pattni, K.; Englund, C. and Samakovlis, C.; et al. (2006) Fab1 phosphatidylinositol 3-phosphate 5-kinase controls trafficking but not silencing of endocytosed receptors. *Mol Biol Cell*, **17**, 3989–4001.

Rusten, T.E.; Vaccari, T.; Lindmo, K.; Rodahl, L.M.W. and Nezis, I.P.; et al. (2007) ESCRTs and Fab1 regulate distinct steps of autophagy. *Curr Biol*, **17**, 1817–1825.

Rutherford, A.C.; Traer, C.; Wassmer, T.; Pattni, K. and Bujny, M.V.; et al. (2006) The mammalian phosphatidylinositol 3-phosphate 5-kinase (PIKfyve) regulates endosome-to-TGN retrograde transport. *J Cell Sci*, **119**, 3944–3957.

Sakabe, I.; Hu, R.; Jin, L.; Clarke, R. and Kasid, U.N. (2015) TMEM33: a new stress-inducible endoplasmic reticulum transmembrane protein and modulator of the unfolded protein response signaling. *Breast Cancer Res Treat*, **153**, 285–297.

Sambrook, J., Fritsch, E. and Maniatis, T. (2001) *Molecular Cloning: A Laboratory Manual*, Laboratory Press, Cold Spring Harbor, NY, USA.

Sbrissa, D.; Ikonomov, O.C.; Fenner, H. and Shisheva, A. (2008) ArPIKfyve homomeric and heteromeric interactions scaffold PIKfyve and Sac3 in a complex to promote PIKfyve activity and functionality. *J Mol Biol*, **384**, 766–779.

Sbrissa, D.; Ikonomov, O.C.; Fu, Z.; Ijuin, T. and Gruenberg, J.; et al. (2007) Core protein machinery for mammalian phosphatidylinositol 3,5-bisphosphate synthesis and turnover that regulates the progression of endosomal transport. Novel Sac phosphatase joins the ArPIKfyve-PIKfyve complex. *J Biol Chem*, **282**, 23878–23891.

Sbrissa, D.; Ikonomov, O.C.; Strakova, J.; Dondapati, R. and Mlak, K.; et al. (2004) A mammalian ortholog of *Saccharomyces cerevisiae* Vac14 that associates with and up-regulates PIKfyve phosphoinositide 5-kinase activity. *Mol Cell Biol*, **24**, 10437–10447.

Schafer, D.A.; Gill, S.R.; Cooper, J.A.; Heuser, J.E. and Schroer, T.A. (1994) Ultrastructural analysis of the dynactin complex: an actin-related protein is a component of a filament that resembles F-actin. *J Cell Biol*, **126**, 403–412.

Schafer, D.A. and Schroer, T.A. (1999) Actin-related proteins. *Annu Rev Cell Dev Biol*, **15**, 341–363.

Schroer, T.A.; Fyrberg, E.; Cooper, J.A.; Waterston, R.H. and Helfman, D.; et al. (1994) Actin-related protein nomenclature and classification. *J Cell Biol*, **127**, 1777–1778.

Schroer, T.A. and Sheetz, M.P. (1991) Two activators of microtubule-based vesicle transport. *J Cell Biol*, **115**, 1309–1318.

Schulze, U.; Vollenbröker, B.; Braun, D.A.; van Le, T. and Granado, D.; et al. (2014) The Vac14-interaction network is linked to regulators of the endolysosomal and autophagic pathway. *Mol Cell Proteomics*, **13**, 1397–1411.

Schulze, U.; Vollenbröker, B.; Kühnl, A.; Granado, D. and Bayraktar, S.; et al. (2017) Cellular vacuolization caused by overexpression of the PIKfyve-binding deficient Vac14L156R is rescued by starvation and inhibition of vacuolar-ATPase. *Biochim Biophys Acta Mol Cell Res*, **1864**, 749–759.

Schuster, M.; Kilaru, S.; Ashwin, P.; Lin, C. and Severs, N.J.; et al. (2011) Controlled and stochastic retention concentrates dynein at microtubule ends to keep endosomes on track. *EMBO J*, **30**, 652–664.

Schwartz, T.U. (2005) Modularity within the architecture of the nuclear pore complex. *Curr Opin Struct Biol*, **15**, 221–226.

Schwartz, T.U. (2016) The Structure Inventory of the Nuclear Pore Complex. *J Mol Biol*, **428**, 1986–2000.

Sents, W.; Ivanova, E.; Lambrecht, C.; Haesen, D. and Janssens, V. (2013) The biogenesis of active protein phosphatase 2A holoenzymes: a tightly regulated process creating phosphatase specificity. *FEBS J*, **280**, 644–661.

Shaw, B.D.; Chung, D.-W.; Wang, C.-L.; Quintanilla, L.A. and Upadhyay, S. (2011) A role for endocytic recycling in hyphal growth. *Fungal Biol*, **115**, 541–546.

Sheng, L.; Hao, S.-L.; Yang, W.-X. and Sun, Y. (2018) The multiple functions of kinesin-4 family motor protein KIF4 and its clinical potential. *Gene*, **678**, 90–99.

Shi, Z.; Jiao, S. and Zhou, Z. (2016) STRIPAK complexes in cell signaling and cancer. *Oncogene*, **35**, 4549–4557.

Shibata, Y.; Voeltz, G.K. and Rapoport, T.A. (2006) Rough sheets and smooth tubules. *Cell*, **126**, 435–439.

Shibata, Y.; Voss, C.; Rist, J.M.; Hu, J. and Rapoport, T.A.; et al. (2008) The reticulon and DP1/Yop1p proteins form immobile oligomers in the tubular endoplasmic reticulum. *J Biol Chem*, **283**, 18892–18904.

Shisheva, A. (2008) PIKfyve: Partners, significance, debates and paradoxes. *Cell Biol Int*, **32**, 591–604.

Singh, N.S.; Shao, N.; McLean, J.R.; Sevugan, M. and Ren, L.; et al. (2011) SIN-inhibitory phosphatase complex promotes Cdc11p dephosphorylation and propagates SIN asymmetry in fission yeast. *Curr Biol*, **21**, 1968–1978.

Sontag, E. (2001) Protein phosphatase 2A: the Trojan Horse of cellular signaling. *Cell Signal*, **13**, 7–16.

Stauffer, T.P.; Ahn, S. and Meyer, T. (1998) Receptor-induced transient reduction in plasma membrane PtdIns(4,5)P2 concentration monitored in living cells. *Curr Biol*, **8**, 343–346.

Stavru, F.; Hülsmann, B.B.; Spang, A.; Hartmann, E. and Cordes, V.C.; et al. (2006) NDC1: a crucial membrane-integral nucleoporin of metazoan nuclear pore complexes. *J Cell Biol*, **173**, 509–519.

Stein, V.; Blank-Landeshammer, B.; Müntjes, K.; Märker, R. and Teichert, I.; et al. (2020) The STRIPAK signaling complex regulates dephosphorylation of GUL1, an RNA-binding protein that shuttles on endosomes. *PLoS Genet*, **16**, 1-32.

Steinberg, G. (2007) On the move: endosomes in fungal growth and pathogenicity. *Nat Rev Microbiol*, **5**, 309–316.

Steinberg, G. (2014) Endocytosis and early endosome motility in filamentous fungi. *Curr Opin Microbiol*, **20**, 10–18.

Steinberg, G.; Peñalva, M.A.; Riquelme, M.; Wösten, H.A. and Harris, S.D. (2017) Cell Biology of Hyphal Growth. *Microbiol Spectr*, **5**, 1–34.

Stenmark, H.; Aasland, R. and Driscoll, P.C. (2002) The phosphatidylinositol 3-phosphate-binding FYVE finger. *FEBS Letters*, **513**, 77–84.

Steuer, E.R.; Wordeman, L.; Schroer, T.A. and Sheetz, M.P. (1990) Localization of cytoplasmic dynein to mitotic spindles and kinetochores. *Nature*, **345**, 266–268.

Strahl-Bolsinger, S.; Immervoll, T.; Deutzmann, R. and Tanner, W. (1993) PMT1, the gene for a key enzyme of protein O-glycosylation in *Saccharomyces cerevisiae*. *Proc Natl Acad Sci USA*, **90**, 8164–8168.

Sugden, P.H.; McGuffin, L.J. and Clerk, A. (2013) SOcK, MiSTs, MASK and STicKs: the GCKIII (germinal centre kinase III) kinases and their heterologous protein-protein interactions. *Biochem J*, **454**, 13–30.

Suh, B.-C. and Hille, B. (2008) PIP2 is a necessary cofactor for ion channel function: how and why? *Annu Rev Biophys*, **37**, 175–195.

Tan, R.; Foster, P.J.; Needleman, D.J. and McKenney, R.J. (2018) Cooperative Accumulation of Dynein-Dynactin at Microtubule Minus-Ends Drives Microtubule Network Reorganization. *Dev Cell*, **44**, 233-247.

Tang, Y.; Chen, M.; Zhou, L.; Ma, J. and Li, Y.; et al. (2019) Architecture, substructures, and dynamic assembly of STRIPAK complexes in Hippo signaling. *Cell Discov*, **5**, 1–21.

Teichert, I.; Nowrousian, M.; Pöggeler, S. and Kück, U. (2014) The filamentous fungus *Sordaria macrospora* as a genetic model to study fruiting body development. *Adv Genet*, **87**, 199–244.

Teichert, I.; Pöggeler, S. and Nowrousian, M. (2020) *Sordaria macrospora*: 25 years as a model organism for studying the molecular mechanisms of fruiting body development. *Appl Microbiol Biotechnol*, **104**, 3691–3704.

Teichert, I.; Wolff, G.; Kück, U. and Nowrousian, M. (2012) Combining laser microdissection and RNA-seq to chart the transcriptional landscape of fungal development. *BMC Genomics*, **511**, 1–18.

Towbin, H.; Staehelin, T. and Gordon, J. (1979) Electrophoretic transfer of proteins from polyacrylamide gels to nitrocellulose sheets: procedure and some applications. *Proc Natl Acad Sci USA*, **76**, 4350–4354.

Tusnády, G.E. and Simon, I. (2001) The HMMTOP transmembrane topology prediction server. *Bioinformatics*, **17**, 849–850.

Urade, T.; Yamamoto, Y.; Zhang, X.; Ku, Y. and Sakisaka, T. (2014) Identification and characterization of TMEM33 as a reticulon-binding protein. *Kobe J Med Sci*, **60**, E57-65.

Vale, R.D. and Milligan, R.A. (2000) The way things move: looking under the hood of molecular motor proteins. *Science*, **288**, 88–95.

Valetti, C.; Wetzel, D.M.; Schrader, M.; Hasbani, M.J. and Gill, S.R.; et al. (1999) Role of dynactin in endocytic traffic: effects of dynamitin overexpression and colocalization with CLIP-170. *Mol Biol Cell*, **10**, 4107–4120.

Van der Klei, I.J. and Veenhuis, M. (2006) Yeast and filamentous fungi as model organisms in microbody research. *Biochim Biophys Acta*, **1763**, 1364–1373.

Vaughan, K.T.; Tynan, S.H.; Faulkner, N.E.; Echeverri, C.J. and Vallee, R.B. (1999) Colocalization of cytoplasmic dynein with dynactin and CLIP-170 at microtubule distal ends. *J Cell Sci*, **112**, 1437–1447.

Vicinanza, M.; D'Angelo, G.; Di Campli, A. and Matteis, M.A. de (2008) Function and dysfunction of the PI system in membrane trafficking. *EMBO J*, **27**, 2457–2470.

Voeltz, G.K.; Prinz, W.A.; Shibata, Y.; Rist, J.M. and Rapoport, T.A. (2006) A class of membrane proteins shaping the tubular endoplasmic reticulum. *Cell*, **124**, 573–586.

Voigt, O.; Herzog, B.; Jakobshagen, A. and Pöggeler, S. (2014) Autophagic kinases SmVPS34 and SmVPS15 are required for viability in the filamentous ascomycete *Sordaria macrospora*. *Microbiol Res*, **169**, 128–138.

Voigt, O. and Pöggeler, S. (2013) Autophagy genes Smatg8 and Smatg4 are required for fruiting-body development, vegetative growth and ascospore germination in the filamentous ascomycete *Sordaria macrospora*. *Autophagy*, **9**, 33–49.

Von Appen, A. and Beck, M. (2016) Structure Determination of the Nuclear Pore Complex with Three-Dimensional Cryo electron Microscopy. *J Mol Biol*, **428**, 2001–2010.

Walz, M. and Kück, U. (1995) Transformation of *Sordaria macrospora* to hygromycin B resistance: characterization of transformants by electrophoretic karyotyping and tetrad analysis. *Curr Genet*, **29**, 88–95.

Wang, C.-L.; Shim, W.-B. and Shaw, B.D. (2010) *Aspergillus nidulans* striatin (StrA) mediates sexual development and localizes to the endoplasmic reticulum. *Fungal Genet Biol*, **47**, 789–799.

Wang, N. and Rapoport, T.A. (2019) Reconstituting the reticular ER network - mechanistic implications and open questions. *J Cell Sci*, **132**, 1–7.

Watanabe, R. and Riezman, H. (2004) Differential ER exit in yeast and mammalian cells. *Curr Opin Cell Biol*, **16**, 350–355.

Waterman-Storer, C.M.; Karki, S. and Holzbaur, E.L. (1995) The p150Glued component of the dynactin complex binds to both microtubules and the actin-related protein centractin (Arp-1). *Proc Natl Acad Sci USA*, **92**, 1634–1638.

Wedlich-Söldner, R.; Schulz, I.; Straube, A. and Steinberg, G. (2002a) Dynein supports motility of endoplasmic reticulum in the fungus *Ustilago maydis*. *Mol Biol Cell*, **13**, 965–977.

Wedlich-Söldner, R.; Straube, A.; Friedrich, M.W. and Steinberg, G. (2002b) A balance of KIF1A-like kinesin and dynein organizes early endosomes in the fungus *Ustilago maydis*. *EMBO J*, **21**, 2946–2957.

Wendland, J. and Philippsen, P. (2001) Cell polarity and hyphal morphogenesis are controlled by multiple rho-protein modules in the filamentous ascomycete *Ashbya gossypii*. *Genetics*, **157**, 601–610.

Werner, A.; Herzog, B.; Voigt, O.; Valerius, O. and Braus, G.H.; et al. (2019) NBR1 is involved in selective pexophagy in filamentous ascomycetes and can be functionally replaced by a tagged version of its human homolog. *Autophagy*, **15**, 78–97.

Werner, A.; Otte, K.; Stahlhut, G.; Hanke, L.M. and Pöggeler, S. (2021) The Glyoxysomal Protease LON2 Is Involved in Fruiting-Body Development, Ascosporogenesis and Stress Resistance in *Sordaria macrospora*. *J Fungi (Basel)*, **82**, 1–17.

West, R.R.; Vaisberg, E.V.; Ding, R.; Nurse, P. and McIntosh, J.R. (1998) cut11(+): A gene required for cell cycle-dependent spindle pole body anchoring in the nuclear envelope and bipolar spindle formation in *Schizosaccharomyces pombe*. *Mol Biol Cell*, **9**, 2839–2855.

Wilson, Z.N.; Scott, A.L.; Dowell, R.D. and Odorizzi, G. (2018) PI(3,5)P2 controls vacuole potassium transport to support cellular osmoregulation. *Mol Biol Cell*, **29**, 1718–1731.

Winey, M.; Hoyt, M.A.; Chan, C.; Goetsch, L. and Botstein, D.; et al. (1993) NDC1: a nuclear periphery component required for yeast spindle pole body duplication. *J Cell Biol*, **122**, 743–751.

Wolf, K.W. and Böhm, J.K. (1997) Organisation von Mikrotubuli in der Zelle. In *Biologie in unserer Zeit 2 (*VBiO e.V, ed), Wiley-VCH, Weinheim, Vol. 27, pp. 87–95.

Woods, B. and Lew, D.J. (2019) Polarity establishment by Cdc42: Key roles for positive feedback and differential mobility. *Small GTPases*, **10**, 130–137.

Wozniak, R.W.; Blobel, G. and Rout, M.P. (1994) POM152 is an integral protein of the pore membrane domain of the yeast nuclear envelope. *J Cell Biol*, **125**, 31–42.

Xiang, X. and Fischer, R. (2004) Nuclear migration and positioning in filamentous fungi. *Fungal Genet Biol*, **41**, 411–419.

Xiang, X.; Han, G.; Winkelmann, D.A.; Zuo, W. and Morris, N. (2000) Dynamics of cytoplasmic dynein in living cells and the effect of a mutation in the dynactin complex actin-related protein Arp1. *Curr Biol*, **10**, 603–606.

Yamamoto, A. and Hiraoka, Y. (2003) Cytoplasmic dynein in fungi: insights from nuclear migration. *J Cell Sci*, **116**, 4501–4512.

Yao, X.; Zhang, J.; Zhou, H.; Wang, E. and Xiang, X. (2012) In vivo roles of the basic domain of dynactin p150 in microtubule plus-end tracking and dynein function. *Traffic*, **13**, 375–387.

Zabel, U.; Doye, V.; Tekotte, H.; Wepf, R. and Grandi, P.; et al. (1996) Nic96p is required for nuclear pore formation and functionally interacts with a novel nucleoporin, Nup188p. *J Cell Biol*, **133**, 1141–1152.

Zhang, D. and Oliferenko, S. (2014) Tts1, the fission yeast homologue of the TMEM33 family, functions in NE remodeling during mitosis. *Mol Biol Cell*, **25**, 2970–2983.

Zhang, D.; Vjestica, A. and Oliferenko, S. (2010) The cortical ER network limits the permissive zone for actomyosin ring assembly. *Curr Biol*, **20**, 1029–1034.

Zhang, H.; Ma, X.; Deng, X.; Chen, Y. and Mo, X.; et al. (2012) PDCD10 interacts with STK25 to accelerate cell apoptosis under oxidative stress. *Front Biosci (Landmark Ed)*, **17**, 2295–2305.

Zhang, J.; Li, S.; Fischer, R. and Xiang, X. (2003) Accumulation of cytoplasmic dynein and dynactin at microtubule plus ends in *Aspergillus nidulans* is kinesin dependent. *Mol Biol Cell*, **14**, 1479–1488.

Zhang, K.; Foster, H. and Carter, A. (2017) The Structure of Complete Human Dynein-1 and its Mechanism of Activation. *Biophys J*, **112**, 44a.

Zhang, W.-T.; Li, E.; Guo, Y.-K.; Yu, S.-X. and Wan, Z.-Y.; et al. (2018) Arabidopsis VAC14 Is Critical for Pollen Development through Mediating Vacuolar Organization. *Plant Physiol*, **177**, 1529–1538.

Zhang, X.; Chow, C.Y.; Sahenk, Z.; Shy, M.E. and Meisler, M.H.; et al. (2008) Mutation of FIG4 causes a rapidly progressive, asymmetric neuronal degeneration. *Brain*, **131**, 1990–2001.

Zhang, Y.; Tang, W.; Zhang, H.; Niu, X. and Xu, Y.; et al. (2013) A network of interactions enables CCM3 and STK24 to coordinate UNC13D-driven vesicle exocytosis in neutrophils. *Dev Cell*, **27**, 215–226.

Zhang, Y.; Zolov, S.N.; Chow, C.Y.; Slutsky, S.G. and Richardson, S.C.; et al. (2007) Loss of Vac14, a regulator of the signaling lipid phosphatidylinositol 3,5-bisphosphate, results in neurodegeneration in mice. *Proc Natl Acad Sci USA*, **104**, 17518–17523.

Zheng, P.; Nguyen, T.A.; Wong, J.Y.; Lee, M. and Nguyen, T.-A.; et al. (2020) Spitzenkörper assembly mechanisms reveal conserved features of fungal and metazoan polarity scaffolds. *Nat Commun*, **11; 2830**, 1–13.

Zheng, Y.; Liu, B.; Wang, L.; Lei, H. and Pulgar Prieto, K.D.; et al. (2017) Homeostatic Control of Hpo/MST Kinase Activity through Autophosphorylation-Dependent Recruitment of the STRIPAK PP2A Phosphatase Complex. *Cell Rep*, **21**, 3612–3623.

Danksagung

Mein erster und besonderer Dank gilt meiner Doktormutter Prof. Dr. Stefanie Pöggeler. Liebe Stefanie, vielen Dank für das entgegengebrachte Vertrauen mich in deine Arbeitsgruppe aufgenommen und mir damit die Möglichkeit gegeben zu haben, an deinen Forschungsprojekten wissenschaftlich mitzuarbeiten. Ohne zu zögern hast du mir stets Hilfestellung gegeben, wenn ich sie brauchte. Deine Worte „Nicht aufgeben!“ haben mich ermutigt und motivierend durch die Promotion getragen. Du warst jederzeit ansprechbar bei Anliegen und Problemen und hast mir immer geholfen eine Lösung zu finden. Der gemeinsame Gedankenaustausch und deine hilfreichen Anregungen haben diese Arbeit vorangetrieben und zu deren Erfolg beigetragen. Vielen lieben Dank dafür!

Als nächstes möchte ich mich bei den Mitgliedern meines „Thesis Advisory Committee“: Prof. Dr. Heike Krebber, Prof. Dr. Kai Heimel und Dr. Oliver Valerius, bedanken. Danke, dass ihr Euch meine Vorträge angehört und mir konstruktives Feedback zu meinen Projekten gegeben habt. Ihr habt mir während meiner Promotion durch eure wissenschaftliche Betreuung zur Seite gestanden und mit neuen Anregungen und Anmerkungen sowie kritischer Betrachtung zu hilfreichen Diskussionen beigetragen.

Darüber hinaus gilt mein weiterer Dank Dr. Kerstin Schmitt für die Kommunikation und Hilfestellung zu jeder Zeit hinsichtlich der LC-MS Auswertungen und den zugehörigen Programmen. Lieben Dank dir zusammen mit Dr. Oliver Valerius auch für das Korrekturlesen meines Pom33-Papers. Vielen Dank für die tolle Zusammenarbeit!

Ebenfalls danken möchte ich der ehemaligen Doktorandin Dr. Eva Reschka und den Postdocs Dr. Antonia Werner und Dr. Daniela Nordzieke. Vielen Dank, Eva für die Möglichkeit das STRIPAK-Projekt dank deiner LC-MS Listen weiterzuführen und dein offenes Ohr bezüglich meines Themas zu Beginn meiner Promotionszeit. Liebe Antonia, du warst für mich während meiner Promotion wie eine große Schwester. Ich danke dir für die Ratschläge und die Hilfe wenn es um experimentelle Fragen ging, aber auch für die vielen privaten Gespräche und Momente. Liebe Daniela, danke für die gute

Zusammenarbeit, die Unterstützung und deine Geduld mit mir bei unserem Arp1-Paper. Dein wissenschaftlicher Input und deine Tipps und Anregungen zu einzelnen Experimenten haben mir neue Sichtweisen eröffnet und zum Erfolg dieser Arbeit beigetragen. Danke auch für das Korrekturlesen und die kritische Betrachtung meiner Dissertation. Du warst mir in meiner Zeit als Doktorandin ein wertvoller Ruhepol. Vielen Dank dafür!

Des Weiteren bedanke ich mich bei den technischen Assistentinnen Gertrud Stahlhut, Gabriele Beyer und Silvia Castellón. Liebe Gertrud, danke für deine ehrliche, hilfsbereite Art sowie die Mithilfe an den Experimenten, die diese Arbeit vorangebracht haben. Danke auch für deine uneingeschränkte Bereitschaft dein Laborwissen und Geschick weiterzugeben und den Mut, Dinge auch mal abweichend vom Protokoll, aber dennoch ergebnisorientiert, durchzuführen. Außerdem bedanke ich mich bei dir ganz herzlich für die Hilfe bei mathematischen Rechnungsaufgaben. Als „Labormutti“ warst du immer Ansprechpartnerin, wenn es um private Themen oder einfach nur menschlichen Halt ging. Danke dir auch dafür! Liebe Gabriele, dir möchte ich neben experimentellen Ratschlägen für den moralischen Beistand, die tiefen Gespräche und gegenseitige Hilfestellung in privaten Angelegenheiten danken. Liebe Silvia, du bist die einzige Person, die sich darüber gefreut hat, wenn wir viel Müll gemacht haben. Bei dir bedanke ich mich für die schnelle Versorgung mit ausreichenden Labormaterialien, vor allem wenn wir wieder mal das BMM „getrunken“ hatten.

Ich möchte mich außerdem bei meinen Mitdoktorandinnen Sabrina Erb und Anina Rudolph bedanken. Liebe Sabrina, danke für die schönen Gespräche. Gemeinsam haben wir die Doktorzeit mit all ihren Höhen und Tiefen durchlebt. Vielen Dank auch für deine Tipps bei Laborfragen und das ruhige Arbeiten in angenehmer „Dunkelheit“ in unserem Büro. Liebe Anina, danke für die vielen Gespräche im Mikroskopierraum und die gute Laune, die du verbreitest. Deine lebendige Art, die man bisweilen bis in unser Labor hören konnte, hat mir immer ein Lächeln ins Gesicht gezaubert.

Außerdem möchte ich mich bei allen ehemaligen Bachelor-, Master- und Labrotation-Studenten bedanken, die während meiner Promotionszeit in unserer Abteilung waren. Vielen Dank für die gute Stimmung und die nette Arbeitsatmosphäre. Dazu zählen insbesondere Svenja Ahlmann und Lucas Hollstein. Liebe Svenja, vielen Dank für den Gedankenaustausch hinsichtlich deines Projektes, deine eifrige Mitarbeit sowie zielbringende Leistung während deiner Bachelorarbeit (auch wenn es eigentlich nicht so lief, wie wir es gebraucht hätten). Es war mir ein Vergnügen und eine Freude mit dir zu Arbeiten! Lieber Lucas, danke, dass du für meinen ersten Besuch im Forstbotanischen Garten gesorgt hast und für die vielen Spaziergänge – egal bei welchem Wetter. Danke für die schönen Gespräche über Gott und die Welt und die gegenseitige Unterstützung in unseren gleichzeitigen Schreibphasen und ähnlichen Lebenslagen.

Neben meiner Arbeitsgruppe möchte ich auch meinen Freunden und meiner Familie danken. Danke an die „Göttinger“ für das Verständnis und die Aufheiterungen in stressigen Phasen. Ein besonderer Dank gilt hier meiner Mutter, die mir immer zur Seite stand und in allen Lebenslagen immer ein offenes Ohr für mich hat. Danke für deine aufmunternden Worte und Gespräche, die mir Motivation und Durchhaltevermögen geschenkt haben. An dieser Stelle möchte ich mich auch bei meiner Schwieger-Familie bedanken. Vielen lieben Dank für euer Interesse an meiner Arbeit und den Rückhalt.

Ein ganz besonderer Dank gilt meinem Ehemann Mike Groth. Danke für deine Unterstützung, deinen seelischen Beistand und dein Verständnis besonders in schweren Zeiten. Danke für deine grenzenlose Geduld, deine Hilfe, deinen Rückhalt und deine Bemühungen für Ruhe und Entspannung zu sorgen – gerade in der erschöpfenden Endphase meiner Dissertation. Danke für dein „Ja“! Du erfüllst mein Leben mit Sinn und Freude. Ich freue mich auf die Zukunft mit dir an meiner Seite.